**Thermodynamics of salt system: $Li^+$, $K^+$, $Na^+$ // $Cl^-$, $CO_3^{2-}$**

Von der Fakultät für Georessourcen und Materialtechnik der
Rheinisch-Westfälischen Technischen Hochschule Aachen

zur Erlangung des akademischen Grades einer

**Doktorin der Ingenieurwissenschaften**

genehmigte Dissertation

vorgelegt von

**Jia Qi, Master of Engineering**

**Berichtende:** **Univ.-Prof. Dr. rer. nat. Robert Spatschek**
**Univ.-Prof. Dr. h.c. Jochen Michael Schneider, Ph.D.**
**Univ.-Doz. Dr. rer. nat. Michael Müller**

Tag der mündlichen Prüfung: 14.03.2024

# Abstract

In this work, a new thermodynamic database of the $Li^+$, $Na^+$, $K^+//Cl^-$, $CO_3^{2-}$ system was generated using the Calphad method with FactSage. After collecting and analyzing the available thermodynamic data in the literature, experiments were designed to improve the comprehensiveness of the new database. Differential Thermal Analysis (DTA) and high temperature X-ray diffraction (HTXRD) were used to determine the phase transition temperatures. Different types of Differential Scanning Calorimetry (DSC) were used to investigate the heat capacity of pure salts and intermediate compounds. The controversial solid-solid phase transition of $Li_2CO_3$ was proved to be caused by impurities. The accuracy of the heat capacity of $Li_2CO_3$, $LiKCO_3$ was improved, the heat capacity of $LiNaCO_3$ was measured for the first time. The eutectic temperature of the $K_2CO_3$-KCl system was measured, the solid solubility in the $K_2CO_3$-$Li_2CO_3$ system based on $K_2CO_3$ was checked. The phase diagram of the subsystem $Li_2CO_3$-$Na_2CO_3$ was further completed, three solid solution phases based on the three solid modifications of pure $Na_2CO_3$ were determined. For the reciprocal systems $Li^+$, $K^+//Cl^-$, $CO_3^{2-}$ and $Li^+$, $Na^+//Cl^-$, $CO_3^{2-}$, phase diagrams of diagonal systems $Li_2CO_3$-$K_2Cl_2$, $K_2CO_3$-$Li_2Cl_2$, $Li_2Cl_2$-$Na_2CO_3$ and $Li_2CO_3$-$Na_2Cl_2$ were measured.

The Gibbs energy data of stoichiometric compounds ($Li_2CO_3$, $LiKCO_3$ and $LiNaCO_3$) and the Gibbs energy functions of the solutions (liquid and solid solutions) of the mentioned systems were reassessed according to the literature and own experimental data for the new database. Mainly based on the literature data, the Gibbs energy of pure salt LiCl, the Gibbs energy of the liquid phase of binary LiCl-NaCl, LiCl-KCl, LiCl-$Li_2CO_3$, KCl-$K_2CO_3$, NaCl-$Na_2CO_3$ systems and the reciprocal system $Na^+$, $K^+//Cl^-$, $CO_3^{2-}$ and the ternary systems $Li^+$, $K^+$, $Na^+//Cl^-$ and $Li^+$, $K^+$, $Na^+//CO_3^{2-}$ were reassessed. A new database was developed, which can calculate and predict the thermodynamic properties of the whole system more precisely and reliably.

# Kurzfassung

In dieser Arbeit wurde eine neue thermodynamische Datenbank für das $Li^+$, $Na^+$, $K^+//Cl^-$, $CO_3^{2-}$ System mit Hilfe der Calphad-Methode mit FactSage erstellt. Nach dem Sammeln und Analysieren der in der Literatur verfügbaren thermodynamischen Daten wurden Experimente entworfen, um den Umfang der neuen Datenbank zu verbessern. Zur Bestimmung der Phasenübergangstemperaturen wurden die Differenzthermoanalyse (DTA) und die Hochtemperatur-Röntgenbeugung (HTXRD) eingesetzt. Zur Untersuchung der Wärmekapazität von reinen Salzen und Zwischenverbindungen wurden verschiedene Arten der Wärmestromkalorimetrie (DSC) eingesetzt. Es wurde nachgewiesen, dass der umstrittene Festkörper-Phasenübergang von $Li_2CO_3$ durch Verunreinigungen verursacht wird. Die Genauigkeit der Wärmekapazität von $Li_2CO_3$ und $LiKCO_3$ wurde verbessert, die Wärmekapazität von $LiNaCO_3$ wurde zum ersten Mal gemessen. Die eutektische Temperatur des $K_2CO_3$-KCl-Systems wurde gemessen, die Feststofflöslichkeit im $K_2CO_3$-$Li_2CO_3$-System auf der Basis von $K_2CO_3$ wurde überprüft. Das Phasendiagramm des Teilsystems $Li_2CO_3$-$Na_2CO_3$ wurde weiter vervollständigt, drei Mischkristallphasen auf der Grundlage der drei festen Modifikationen von reinem $Na_2CO_3$ wurden bestimmt. Für die reziproken Systeme $Li^+$, $K^+//Cl^-$, $CO_3^{2-}$ und $Li^+$, $Na^+//Cl^-$, $CO_3^{2-}$ wurden Phasendiagramme der Diagonalsysteme $Li_2CO_3$-$K_2Cl_2$, $K_2CO_3$-$Li_2Cl_2$, $Li_2Cl_2$-$Na_2CO_3$ und $Li_2CO_3$-$Na_2Cl_2$ gemessen.

Die Gibbs-Energiedaten der stöchiometrischen Verbindungen ($Li_2CO_3$, $LiKCO_3$ und $LiNaCO_3$) und die Gibbs-Energiefunktionen der Lösungen (flüssige und feste Lösungen) der genannten Systeme wurden anhand der Literatur und eigener experimenteller Daten für die neue Datenbank neu ausgewertet. Die Gibbs-Energie des reinen Salzes LiCl, die Gibbs-Energie der flüssigen Phase der binären Systeme LiCl-NaCl, LiCl-KCl, LiCl-$Li_2CO_3$, KCl-$K_2CO_3$, NaCl-$Na_2CO_3$ und des reziproken Systems $Na^+$, $K^+//Cl^-$, $CO_3^{2-}$ sowie der ternären Systeme $Li^+$, $K^+$, $Na^+//Cl^-$ und $Li^+$, $K^+$, $Na^+//CO_3^{2-}$ wurden neu ausgewertet, wobei man sich hauptsächlich auf die Literaturdaten stützte. Es wurde eine neue Datenbank entwickelt, mit der die thermodynamischen Eigenschaften des gesamten Systems genauer und zuverlässiger berechnet und vorhergesagt werden können.

# Contents

Abstract ..... I
Kurzfassung ..... II
Contents ..... III
List of figures ..... VI
List of tables ..... X
1. Introduction ..... 1
2. Literature review ..... 3
2.1 Applications of molten salts ..... 3
2.2 Thermodynamic properties of salt systems ..... 6
2.2.1 Pure salts ..... 6
2.2.2 Binary systems ..... 8
2.2.3 Ternary systems ..... 21
2.2.4 Reciprocal system ..... 26
2.3 Aims of this work based on the literature review ..... 29
3. Experimental ..... 31
3.1 Samples ..... 31
3.2 Instruments ..... 32
3.2.1 Thermogravimetry/Differential Thermal Analysis (TG/DTA) ..... 32
3.2.2 Differential Scanning Calorimetry (DSC) ..... 34
3.2.3 X-Ray Diffractometry/High Temperature X-Ray Diffractometry (XRD/HTXRD) ..... 36
3.2.4 Knudsen Effusion Mass Spectrometry (KEMS) ..... 37
4. Thermodynamic modelling ..... 39
4.1 Thermodynamic background ..... 39
4.2 Gibbs energy description ..... 41
4.2.1 Stoichiometric compounds ..... 41
4.2.2 Solution phases ..... 43
4.3 Calphad method ..... 46
4.4 Factsage ..... 47
4.5 Optimization process ..... 49
4.5.1 Stoichiometric compounds assessment ..... 49

4.5.2 Solution phase assessment ..... 50
5. Experimental results ..... 52
5.1 $Li_2CO_3$ ..... 52
5.1.1 Phase change temperature ..... 52
5.1.2 Heat capacity ..... 57
5.2 System $K_2CO_3$-KCl ..... 58
5.3 System $Na_2CO_3$-NaCl ..... 58
5.4 System $Li_2CO_3$-$Na_2CO_3$ ..... 67
5.4.1 XRD/HTXRD of $LiNaCO_3$ ..... 68
5.4.2 HTXRD of 0.975$Na_2CO_3$-0.025$Li_2CO_3$ mixture ..... 72
5.4.3 DTA results ..... 74
5.4.4 Heat capacity of $LiNaCO_3$ ..... 76
5.5 System $Li_2CO_3$-$K_2CO_3$ ..... 77
5.6 Reciprocal system $Li^+$, $K^+$ // $Cl^-$, $CO_3^{2-}$ ..... 81
5.7 Reciprocal system $Li^+$, $Na^+$ // $Cl^-$, $CO_3^{2-}$ ..... 84
5.8 Reciprocal system $Na^+$, $K^+$ // $Cl^-$, $CO_3^{2-}$ ..... 85
6. Modelling results ..... 87
6.1 Pure substances ..... 87
6.1.1 $Li_2CO_3$ ..... 87
6.1.2 LiCl ..... 91
6.2 Binary systems ..... 95
6.2.1 System LiCl-KCl ..... 95
6.2.2 System LiCl-NaCl ..... 100
6.2.3 System $Li_2CO_3$-LiCl ..... 104
6.2.4 System $Na_2CO_3$-NaCl ..... 105
6.2.5 System $K_2CO_3$-KCl ..... 108
6.2.6 System $Li_2CO_3$-$Na_2CO_3$ ..... 109
6.2.7 System $Li_2CO_3$- $K_2CO_3$ ..... 117
6.3 Ternary systems ..... 123
6.3.1 System LiCl-NaCl-KCl ..... 123
6.3.2 System $Li_2CO_3$-$Na_2CO_3$-$K_2CO_3$ ..... 125

6.4 Reciprocal systems ..... 129
6.4.1 System $Li^+$, $Na^+$//$Cl^-$, $CO_3^{2-}$ ..... 129
6.4.2 System $Li^+$, $K^+$//$Cl^-$, $CO_3^{2-}$ ..... 132
6.4.3 System $Na^+$, $K^+$//$Cl^-$, $CO_3^{2-}$ ..... 135
6.5 Entire System $Li^+$, $Na^+$, $K^+$//$Cl^-$, $CO_3^{2-}$ ..... 138
7. Conclusion and outlook ..... 141
8. Acknowledgement ..... 143
9. Reference ..... 144
Appendix ..... 158

# List of figures

Figure 1-1. Salt system $Li^+$, $Na^+$, $K^+$//$Cl^-$, $CO_3^{2-}$ represented by a prism (a) and by an open prism (b). ..... 1
Figure 2-1. Thermal storage system integrated in the CSP plant with solar field and power block [12]: (a) direct heat storage and (b) indirect heat storage. ..... 3
Figure 2-2. Demonstration of sensible heat storage and latent heat storage. [14] ..... 4
Figure 2-3. Physical model of a cascaded shell-and-tube PCM storage system. [11] ..... 4
Figure 2-4. The phase diagram of binary system NaCl-KCl [33]. ..... 8
Figure 2-5. The phase diagram of binary system $Na_2CO_3$-$K_2CO_3$ calculated with PCM database. . 9
Figure 2-6. Phase diagram of the LiCl-NaCl system measured by Zhemchuzhnui and Rambach [44] ..... 10
Figure 2-7. Phase diagram of the LiCl-NaCl system measured by Chesnokov et al. [79] ..... 11
Figure 2-8 Liquidus line of the LiCl-NaCl system detected by Bukhalova and Arabadzhan [79] .. 12
Figure 2-9 Heat capacity of the intermediate compound $LiKCO_3$ from the literature. ..... 16
Figure 2-10. The phase diagram of the $Li_2CO_3$-$Na_2CO_3$ system measured by Burmistrova and Volozhanina. [131] . ..... 17
Figure 2-11. The phase diagram of the $Li_2CO_3$-$Na_2CO_3$ system measured by Janz and Lorenz [120]. ..... 18
Figure 2-12. The phase diagram of $Li_2CO_3$-$Na_2CO_3$ system reported by Cairns and Macdonald [134]. ..... 19
Figure 2-13. The phase diagram of the $Li_2CO_3$-$Na_2CO_3$ system from the literature and calculated with FTsalt. ..... 20
Figure 2-14. The liquidus surface of the ternary system $Li^+$, $Na^+$, $K^+$// $Cl^-$ reported by Akopov [87] and Akopov and Bergman [83], temperature is in °C and composition is in mole fraction. ..... 22
Figure 2-15. The liquidus surface of the ternary system of $Li^+$, $Na^+$, $K^+$// $Cl^-$ reported by Storonkin et al. [147], temperature is in °C and composition is in mole fraction. ..... 22
Figure 2-16. The liquidus surface of the ternary system of $Li^+$, $Na^+$, $K^+$// $CO_3^{2-}$ reported by by Volkova [119], temperature is in °C and composition is in mole fraction. ..... 23
Figure 2-17. The liquidus surface of the ternary system $Li^+$, $Na^+$, $K^+$// $CO_3^{2-}$ measured by Janz and Lorenz [120], temperature is in °C and composition is in mole fraction. ..... 24
Figure 2-18. The liquidus surface of the ternary system $Li^+$, $Na^+$, $K^+$// $CO_3^{2-}$ reported by Rolin and Recapet [121] , temperature is in °C and composition is in mass faction. ..... 25
Figure 2-19. The liquidus surface of the reciprocal system $Na^+$, $K^+$//$Cl^-$, $CO_3^{2-}$ reported by Nyankovskaya [156], temperature is in °C and composition is in mole fraction. ..... 27
Figure 2-20. The liquidus surface of the ternary part NaCl-$Na_2CO_3$-KCl in the reciprocal system $Na^+$, $K^+$//$Cl^-$, $CO_3^{2-}$ reported by a) Busse- Machukas et al. [157] and b) Sato [115], temperature is in °C. ..... 27
Figure 2-21. The liquidus surface of the reciprocal system $Li^+$, $K^+$//$Cl^-$, $CO_3^{2-}$ reported by Volkov and Zakhvalinskii [103] ..... 28

Figure 2-22. The liquidus surface of the reciprocal system $Li^+$, $Na^+//Cl^-$, $CO_3^{2-}$ calculated using FTsalt. ..... 29
Figure 3-1. Schematic diagram of DTA, A and B denote the different legs of thermocouples. [160] ..... 33
Figure 3-2. Schematic diagram of KEMS [166]..... 37
Figure 4-1. The variation of the Gibbs energy with the temperature is determined by the entropy [167]. ..... 40
Figure 4-2. The relationship of phase diagram and Gibbs energy curves of different phases. [168] ..... 41
Figure 4-3. Three geometric models for estimating ternary thermodynamic properties from optimized binary data: a) Kohler model, b) Kohler/Toop model and c) Muggianu model [178]. 45
Figure 5-1. DTA curve of a) raw material $Li_2CO_3$ in open Pt crucible, b) $Li_2CO_3$ in closed Pt crucible after heating at 923 K in $CO_2$ atmosphere for 1 h..... 53
Figure 5-2. High temperature XRD of the raw material $Li_2CO_3$..... 54
Figure 5-3. a) Comparison of the weight change of raw material $Li_2CO_3$ in Ar and $CO_2$ gas and b) corresponding DTA signal of $Li_2CO_3$ in Ar and $CO_2$ gas. ..... 55
Figure 5-4. Temperature dependence of lattice parameters for $Li_2CO_3$. ..... 57
Figure 5-5. Literature values of the heat capacity of $Li_2CO_3$ and measured in this work..... 58
Figure 5-6. Heating and cooling DTA curve of $0.38K_2CO_3$-0.62KCl. ..... 59
Figure 5-7. Melting temperature of the eutectic composition in the system NaCl-$Na_2CO_3$ measured by KEMS (a) and DTA (b). ..... 60
Figure 5-8. Ion species of eutectic composition in the system NaCl-$Na_2CO_3$ (a) and NaCl (b) determined by KEMS at 580 °C. ..... 61
Figure 5-9. Isothermal results of ion species of eutectic composition in the NaCl-$Na_2CO_3$ (a) and NaCl (b) determined by KEMS at 580 °C. ..... 63
Figure 5-10. Isothermal results of ion species of eutectic composition in the NaCl-$Na_2CO_3$ (a) and NaCl (b) determined by KEMS at 665 °C. ..... 65
Figure 5-11. Composition change of the liquid phase demonstrated in the phase diagram. ..... 66
Figure 5-12. $J_{(Na_2Cl^+)}/J_{(NaCl^+)}$ at 665 °C (a) and $J_{(Na_3Cl_2^+)}/J_{(NaCl^+)}$ at 665 °C (b). ..... 67
Figure 5-13. HTXRD of the composition $0.5Na_2CO_3$-$0.5Li_2CO_3$. ..... 68
Figure 5-14. HTXRD of $LiNaCO_3$ in the temperature range of 25-100 °C. ..... 69
Figure 5-15. XRD patterns of $LiNaCO_3$ a) in initial state and b) after HTXRD measurement..... 70
Figure 5-16. Temperature dependence of lattice parameters of $LiNaCO_3$. ..... 71
Figure 5-17. Lattice parameters of $LiNaCO_3$ in the temperature range of 25-100 °C. ..... 71
Figure 5-18. HTXRD of the composition $0.975Na_2CO_3$-$0.025Li_2CO_3$. ..... 73
Figure 5-19. Lattice parameters and unit cell volume dependence on temperature for the composition $0.975Na_2CO_3$-$0.025Li_2CO_3$ compared with those of pure $Na_2CO_3$..... 74
Figure 5-20. Heating DTA-curves for various compositions in the $Li_2CO_3$-$Na_2CO_3$ system ..... 75
Figure 5-21. Heat capacity of $LiNaCO_3$ determined by three different types of DSC..... 77
Figure 5-22. DTA results of 0.85, 0.9, 0.95 molar fraction of $K_2CO_3$ in the system $Li_2CO_3$-$K_2CO_3$. 78
Figure 5-23. Heat capacity of $LiKCO_3$ measured by three types of DSC. ..... 79

Figure 5-24. High temperature XRD of $LiKCO_3$. ..... 80
Figure 5-25. Temperature dependence of lattice parameters for $LiKCO_3$ ..... 81
Figure 5-26. a) Heating DTA curves and b) cooling DTA curves with heating and cooling rate of 5 K/min for different compositions of the $Li_2CO_3$-$(KCl)_2$ binary system. ..... 82
Figure 5-27. Heating DTA curves for different compositions of $K_2CO_3$-$(LiCl)_2$ binary system. ..... 83
Figure 5-28. Comparison of the DTA results of the compositions $0.5Li_2CO_3$-$0.5(KCl)_2$ and $0.5K_2CO_3$-$0.5(LiCl)_2$. ..... 83
Figure 5-29. Heating and cooling DTA-curves for various compositions in the $Li_2CO_3$-$(NaCl)_2$ system ..... 84
Figure 5-30. Heating and cooling DTA-curves for various compositions in the $Na_2CO_3$-$(LiCl)_2$ system ..... 85
Figure 5-31. DSC measurement of the eutectic composition ($0.428KCl$-$0.359Na_2CO_3$-$0.213K_2CO_3$ in molar fraction) in the reciprocal system ..... 86
Figure 6-1. Calculated heat capacity of $Li_2CO_3$ along with the experimental and reference data (This work, Brown and Latimer [43], Janz et al. [39] and Kourkova and Sadovska [44]). ..... 89
Figure 6-2. Calculated heat content of $Li_2CO_3$ along with the experimental data. ..... 91
Figure 6-3. Heat capacity for solid and liquid phases of LiCl ..... 93
Figure 6-4. Enthalpy increment of LiCl ..... 94
Figure 6-5. Phase diagram of the LiCl-KCl system. ..... 95
Figure 6-6. Comparison of the experimental data with the calculated enthalpy increment ($H_T$-$H_{298.15}$) of the LiCl-KCl system at the eutectic composition. ..... 97
Figure 6-7. Heat of solution of solid KCl in liquid LiCl at 740 °C ..... 98
Figure 6-8. Calculated mixing enthalpy of liquid KCl and liquid LiCl at 740 °C. ..... 99
Figure 6-9. Activity of LiCl in the liquid phase at 722 °C. ..... 99
Figure 6-10. Phase diagram of the LiCl-NaCl system. ..... 101
Figure 6-11. Heat of solution of solid NaCl in liquid LiCl at 740 °C. ..... 103
Figure 6-12. Calculated mixing enthalpy of liquid LiCl and liquid NaCl at 740 °C. ..... 103
Figure 6-13. Phase diagram of the $Li_2CO_3$-LiCl system. ..... 104
Figure 6-14. Phase diagram of $Na_2CO_3$-NaCl system. ..... 106
Figure 6-15. The activity of $Na_2CO_3$ in NaCl-$Na_2CO_3$ system. ..... 107
Figure 6-16. Phase diagram of the $K_2CO_3$-KCl system. ..... 108
Figure 6-17. Comparison of the phase diagram calculated by the current database with experimental data in the $Li_2CO_3$-$Na_2CO_3$ system. ..... 110
Figure 6-18. Heat capacity of the intermediate compound $LiNaCO_3$. ..... 113
Figure 6-19. Mixing enthalpy of the $Li_2CO_3$-$Na_2CO_3$ system. ..... 116
Figure 6-20. Phase diagram of the $Li_2CO_3$- $K_2CO_3$ system. ..... 118
Figure 6-21. Calculated mixing enthalpy of the $Li_2CO_3$- $K_2CO_3$ system at 905 °C compared with experimental results [128]. ..... 120
Figure 6-22. Calculated temperature dependence of the heat capacity of $LiKCO_3$ compared with several studies (Janz and Perano [125], Jo and Banerjee [22], Liu et al. [127], Araki et al. [126]) ..... 121

Figure 6-23. Calculated enthalpy increment ($H_T$-$H_{298.15}$) of $LiKCO_3$ compared with experimental data from Janz and Perano [125]. ..... 122
Figure 6-24. The phase diagram of the ternary system LiCl-NaCl-KCl. ..... 123
Figure 6-25. Comparison between calculated cross sections in the ternary system LiCl-NaCl-KCl with reference data [87]: a) KCl-$Na_{0.8}Li_{0.2}Cl$, b) NaCl-$Li_{0.6}K_{0.4}Cl$, and c) LiCl-$Na_{0.7}K_{0.3}Cl$. ..... 124
Figure 6-26. Calculated liquidus surface of the ternary system $Li_2CO_3$-$Na_2CO_3$-$K_2CO_3$. ..... 125
Figure 6-27. Comparison between calculated cross section in the ternary system $Li_2CO_3$-$Na_2CO_3$-$K_2CO_3$ with reference data [39]: a) $Na_2CO_3$-$Li_{1.218}K_{0.782}CO_3$, b) $Na_2CO_3$-$Li_{0.862}K_{1.138}CO_3$, c) $Li_2CO_3$-$Na_{1.2}K_{0.8}CO_3$, d) $Li_2CO_3$-$Na_{1.446}K_{0.554}CO_3$, e) $K_2CO_3$-$Li_{1.16}Na_{0.84}CO_3$ and f) $K_2CO_3$-$Li_{0.974}Na_{1.026}CO_3$.126
Figure 6-28. Isothermal section of the ternary system $Li_2CO_3$-$Na_2CO_3$-$K_2CO_3$ at 25 °C. ..... 127
Figure 6-29. Enthalpy increment of the eutectic composition in ternary system $Li_2CO_3$-$Na_2CO_3$-$K_2CO_3$. ..... 127
Figure 6-30. Heat capacity of eutectic composition in ternary system $Li_2CO_3$-$Na_2CO_3$-$K_2CO_3$... 129
Figure 6-31. Phase diagram of the system $Li_2CO_3$-$(NaCl)_2$. ..... 130
Figure 6-32.Phase diagram of the $(LiCl)_2$-$Na_2CO_3$ system. ..... 130
Figure 6-33. Liquidus surface of the reciprocal system $Li^+$, $Na^+$//$Cl^-$, $CO_3^{2-}$ ..... 131
Figure 6-34. Phase diagram of the $Li_2CO_3$-$(KCl)_2$ system. ..... 132
Figure 6-35. Phase diagram of the $K_2CO_3$-$(LiCl)_2$ system. ..... 133
Figure 6-36. Liquidus surface of the reciprocal system $Li^+$, $K^+$//$Cl^-$, $CO_3^{2-}$: a) proposed by Volkov and Zakhvalinskii [103] and b) calculated with the new dataset. ..... 134
Figure 6-37. Phase diagram of the $(KCl)_2$-$Na_2CO_3$ system. ..... 136
Figure 6-38. Phase diagram of the $(NaCl)_2$-$K_2CO_3$ system. ..... 136
Figure 6-39. Liquidus surface of the reciprocal system $Na^+$, $K^+$//$Cl^-$, $CO_3^{2-}$: a) measured by Volkov and Bergman [215] and b) calculated with the new database..... 138

# List of tables

Table 3-1. Information on different samples. 31
Table 3-2. Parameters of the differential scanning calorimeters. 35
Table 5-1. The gas species activity calculated with PCM and SGPS database at 5 Pa. 64
Table 5-2. Comparison of lattice parameters of $\alpha_1$ and $\alpha_2$ at room temperature. 70
Table 5-3. Phase transition temperatures in the system $Li_2CO_3$-$Na_2CO_3$ obtained by DTA, HTXRD and DSC 75
Table 6-1. Transition data of $Li_2CO_3$. 87
Table 6-2. Thermodynamic data of $Li_2CO_3$. 90
Table 6-3. Phase transition data of LiCl. 92
Table 6-4. Thermodynamic properties of LiCl. 94
Table 6-5. Experimental and calculated eutectic points in the system LiCl-KCl. 96
Table 6-6. Experimental and calculated melting enthalpy of the LiCl-KCl system at the eutectic composition. 97
Table 6-7. Experimental and calculated invariant points in the system LiCl-NaCl. 102
Table 6-8. Melting enthalpy of the azeotropic composition in the system LiCl-NaCl. 102
Table 6-9. Experimental and calculated eutectic points in the system $Li_2CO_3$-LiCl. 105
Table 6-10. Experimental and calculated eutectic points in the system $Na_2CO_3$-NaCl. 106
Table 6-11. Melting enthalpy of eutectic composition in the $Na_2CO_3$-NaCl system. 107
Table 6-12. Experimental and calculated temperature and composition of the eutectic point in the system $K_2CO_3$-KCl. 109
Table 6-13. Melting enthalpy of the eutectic composition in the system $K_2CO_3$-KCl. 109
Table 6-14. Experimental and calculated phase transitions in the system $Li_2CO_3$-$Na_2CO_3$. 111
Table 6-15. Thermodynamic parameters of $LiNaCO_3$. 114
Table 6-16. Melting enthalpy at certain compositions in the $Li_2CO_3$-$Na_2CO_3$ system. 116
Table 6-17. Experimental and calculated invariant points in the system $Li_2CO_3$- $K_2CO_3$. 119
Table 6-18. Thermodynamic data of $LiKCO_3$. 121
Table 6-19. Experimental and calculated melting enthalpy of $LiKCO_3$. 122
Table 6-20. The eutectic point in the ternary system LiCl-NaCl-KCl. 124
Table 6-21. Melting temperature and melting enthalpy of compositions in the ternary system $Li_2CO_3$-$Na_2CO_3$-$K_2CO_3$. 128
Table 6-22. Information on the lowest temperatures in the liquidus surface of the reciprocal system $Li^+$, $Na^+$//$Cl^-$, $CO_3^{2-}$ 131
Table 6-23. Experimental and calculated eutectic points in the reciprocal system $Li^+$, $K^+$//$Cl^-$, $CO_3^{2-}$. 134
Table 6-24. Eutectic information in the $(KCl)_2$-$Na_2CO_3$ system. 137
Table 6-25. Minimum in the liquidus in the $(NaCl)_2$-$K_2CO_3$ system. 137
Table 6-26. Experimental and calculated eutectic points or lowest temperatures in the liquidus surface in the reciprocal system $Na^+$, $K^+$//$Cl^-$, $CO_3^{2-}$ 138

Table 6-27. Thermodynamic description of the liquid and solid solution phases in the $Li^+$, $Na^+$, $K^+//Cl^-$, $CO_3^{2-}$ system..... 139

# 1 Introduction

The salt mixtures in the $Li^+$, $Na^+$, $K^+$//$Cl^-$, $CO_3^{2-}$ system have many applications in different fields such as molten carbonate fuel cells [1–3], die casting processes [4], electrochemical deposition of carbon materials [5,6] and molten salt oxidation [7] etc. They gain increasing attention as PCMs (phase change materials) for thermal energy storage, especially in the application of concentrated solar power (CSP) [8]. Thermodynamic calculations can be used to predict the phase equilibria and thermodynamic properties for different systems. Therefore, it plays a significant role in the corresponding application fields. A complete reliable database, appropriate models, software, etc. are essential for performing thermodynamic calculations properly. The thermodynamic calculations performed using the commercial database, e.g., FTsalt [9] is rough for prediction, therefore, a new database based on more reliable experimental data is necessary to reduce the undesirable discrepancy between the calculated and experimental results. In this work, a new database for the PCM salt systems (PCM database [10]) is developed for a better utilization of the salt systems.

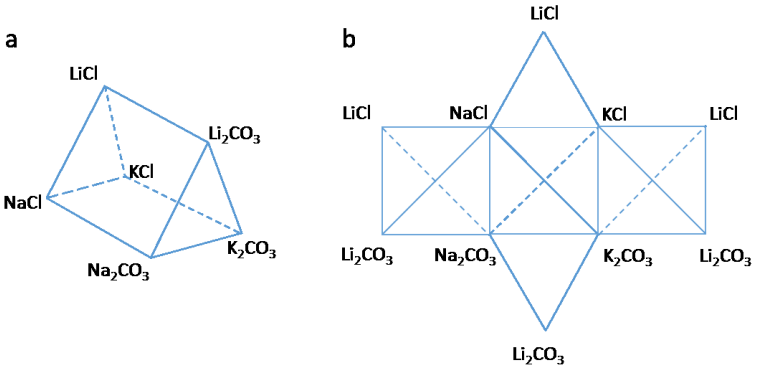


Figure 1-1. Salt system $Li^+$, $Na^+$, $K^+$//$Cl^-$, $CO_3^{2-}$ represented by a prism (a) and by an open prism (b).

A schematic representation of the $Li^+$, $Na^+$, $K^+$//$Cl^-$, $CO_3^{2-}$ salt system is shown in Figure 1-1. The combination of different anions and cations gives possibility to consider different subsystems. The whole system includes

- Six pure salts: LiCl, NaCl, KCl, $Li_2CO_3$, $Na_2CO_3$, $K_2CO_3$,

- Nine binary systems: LiCl-NaCl, LiCl-KCl, NaCl-KCl, $Li_2CO_3$-$Na_2CO_3$, $Li_2CO_3$-$K_2CO_3$, $Na_2CO_3$-$K_2CO_3$, LiCl-$Li_2CO_3$, NaCl-$Na_2CO_3$, KCl-$K_2CO_3$,
- Two ternary systems: LiCl-NaCl-KCl, $Li_2CO_3$-$Na_2CO_3$-$K_2CO_3$
- Three reciprocal systems: ($Li^+$, $K^+$//$Cl^-$, $CO_3^{2-}$), ($Li^+$, $Na^+$//$Cl^-$, $CO_3^{2-}$), ($Na^+$, $K^+$//$Cl^-$, $CO_3^{2-}$).

The present work was a part of the PCM-Screening project (FKZ 03ET1441D and 03EN6005D) funded by the Federal Ministry for Economic Affairs and Climate Action (Bundesministerium für Wirtschaft und Klimaschutz), which focuses on identifying phase change materials (PCM) that can be used in thermal energy storage systems. The goal of the work is to establish a thermodynamic database, which can improve the accuracy of the calculation and prediction of the thermodynamic properties of the mixtures in the whole system. To achieve this goal, the literature data on thermodynamic properties of the salt systems were collected and critically analyzed, then according to the literature data, experimental work was designed and carried out using appropriate experimental techniques. Finally, based on all available experimental data, a new thermodynamic dataset was generated including the Gibbs energies for all phases (stoichiometric compounds, the molten salt and the solid solutions). The optimization of the corresponding thermodynamic parameters in the system was performed using FactSage software [9].

For the framework of this thesis, a literature review is given in chapter 2, the experimental methods and modelling method are introduced in chapter 3 and chapter 4. The experimental and modelling results and corresponding discussions are given in chapters 5 and 6, respectively. Finally, the conclusions and outlook are given in chapter 7. Additional figures are presented in the Appendix.

# 2 Literature review

In this chapter, various applications of molten salts are introduced, and the status of the thermodynamic data for each subsystem in the $Li^+$, $Na^+$, $K^+//Cl^-$, $CO_3^{2-}$ system are summarized for the experimental design and the modelling work on the thermodynamic database.

## 2.1 Applications of molten salts

Nowadays, the energy consumption is a big issue in the development of the economy. Compared to the conventional energy based on fossil fuel, the renewable energy such as wind, solar and tidal energy has drawn great attention. Concentrated solar power (CSP) systems convert sunlight into heat that can be used in conventional power plants [11]. Stekli et al. [12] reported a thermal storage system integrated in the CSP plant with solar field and power block with direct and indirect heat storage, which is shown in Figure 2-1. Thermal Energy Storage (TES) improves the dispatchability of CSP power plants.

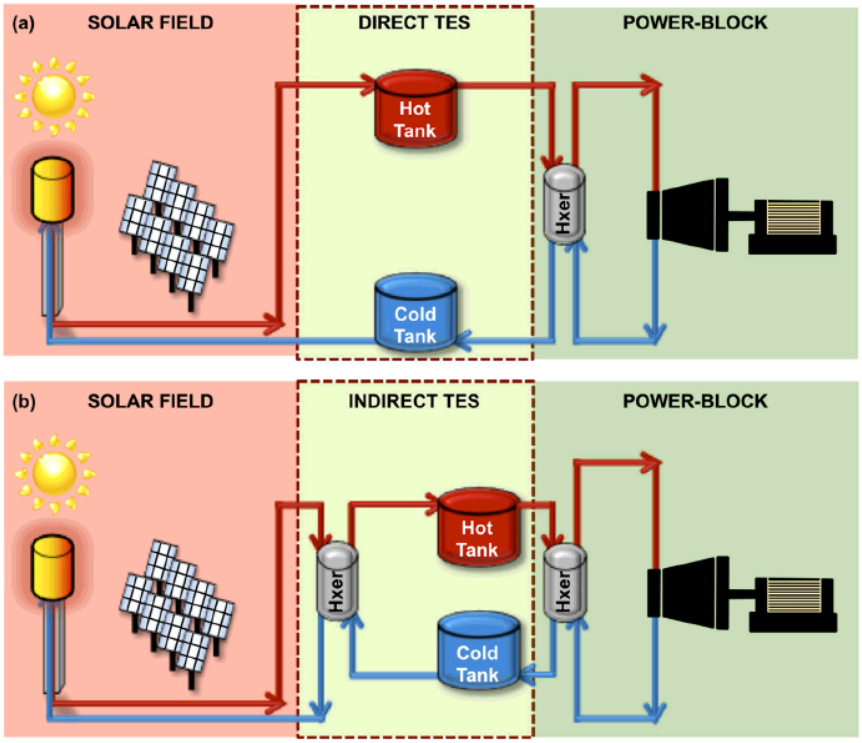


Figure 2-1. Thermal storage system integrated in the CSP plant with solar field and power block [12]: (a) direct heat storage and (b) indirect heat storage.

There are three methods for thermal energy storage: sensible heat storage (using heat capacity), latent heat storage (using heat of phase change) and chemical reaction [13]. While the sensible heat storage and latent heat storage are most widely used and shown in Figure 2-2. It is obvious that the phase change materials (PCM) for thermal energy storage in the CSP power plant use the latent heat storage.

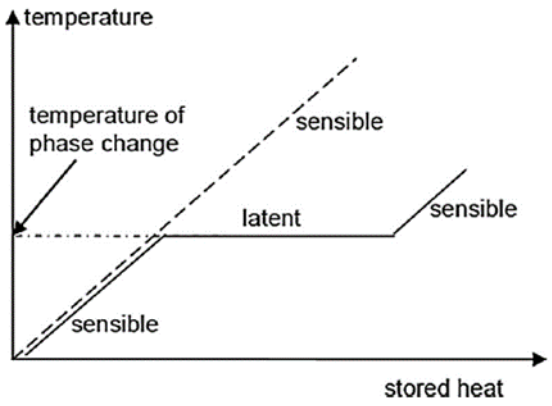


Figure 2-2. Demonstration of sensible heat storage and latent heat storage. [14]

A cascaded latent heat storage is shown in Figure 2-3, where different PCMs with different melting temperatures are connected to each other, in order to obtain high energy and exergy efficiency [11,15–19]. The selection of suitable salts or salt mixtures is crucial for building a cascaded heat storage system.

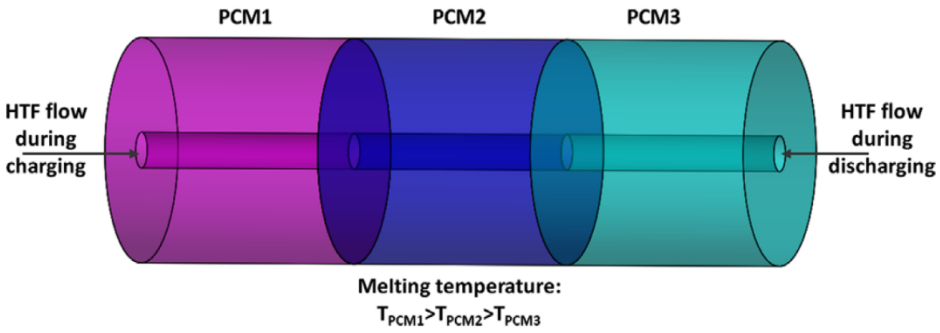


Figure 2-3. Physical model of a cascaded shell-and-tube PCM storage system. [11]

The requirements for a material to become a PCM are suitable phase transition temperature, high energy density, low volatility, low viscosity, and high heat conductivity, etc. Organic materials such as paraffins and fatty acids, inorganic materials like salts, salt hydrates, saline

composites and metallic alloys can be used as PCM [13]. Due to the wide range of available melting temperatures, high latent heat of fusion and density in solid state, inorganic salts and their eutectic compositions are considered to be promising potential candidates as PCM.

Now, the nitrate salts are used commonly as PCM in the CSP applications, but they are limited in application to temperatures below 600 °C due to the decomposition of the salts at higher temperature [20,21].

Compared with the nitrate salts, carbonate salts and chloride salts have higher melting temperature. Therefore, they can be applied in high temperature thermal energy storage applications. Sodium salts and Potassium salts are readily available and cheap. Thus, they are good candidates as PCM. Since it was reported that enhancement in specific heat can dramatically decrease the costs by improving the energy efficiency [22], lithium salts with high latent and sensible heat are also promising candidates for the use in CSP plants.

In this work, the salt mixtures in the $Li^+$, $Na^+$, $K^+//Cl^-$, $CO_3^{2-}$ system are selected to be investigated. The pure salts have relatively high melting temperature ($Li_2CO_3$ - 726 °C, $Na_2CO_3$ - 858 °C, $K_2CO_3$ - 900 °C, LiCl - 610 °C, NaCl - 803 °C and KCl - 771 °C) [10,23–25] and high fusion enthalpy, they have potential as PCMs for thermal energy storage. While the eutectic compositions with various melting temperature and fusion enthalpy inside this salt system provide potential candidates for the cascaded latent heat storage (Figure 2-3) mentioned above.

Chloride salts are reported as potential candidates for the thermal energy storage in the next generation of CSP plants [8]. The eutectic compositions of the NaCl-$Na_2CO_3$ and KCl-$K_2CO_3$ systems have been reported by Raud et al. [26] as potential high temperature PCM materials. Thermophysical properties of the salts $Li_2CO_3$, $Na_2CO_3$ and $K_2CO_3$, and their mixtures for high temperature application were reviewed by Nunes et al. [27]. Besides the investigation of the carbonate system itself, other salts or nanomaterials are used to improve the properties (heat capacity, thermal conductivity, etc.) for the application in thermal energy storage. For example, Shin et al. [28] added silica nanoparticles into the $Li_2CO_3$-$K_2CO_3$ eutectic, Ge et al. [29] added carbon nanotubes and MgO to $LiNaCO_3$, while Zhang et al. [30] combined ZnO with the ternary eutectic of $Li_2CO_3$-$K_2CO_3$-$Na_2CO_3$.

Besides the application as PCM in CSP, the salt mixtures in the $Li^+$, $Na^+$, $K^+//Cl^-$, $CO_3^{2-}$ system have many other applications. The carbonate salts $Li_2CO_3$, $Na_2CO_3$ and $K_2CO_3$, and their mixtures are used widely in molten carbonate fuel cell [1–3], die casting process [4], Electrochemical Deposition of Carbon Materials [5,6] and Molten Salt Oxidation [7] etc. Chloride salts can be used in nuclear power plants [31]. Besides, the eutectics of the $Li_2CO_3$-$K_2CO_3$ and $Li_2CO_3$-$K_2CO_3$-$Na_2CO_3$ systems were reported as catalysts for the gasification of coal by Sheth et al. [32]. The binary systems NaCl–$Na_2CO_3$, KCl–$K_2CO_3$, KCl–NaCl and $K_2CO_3$–$Na_2CO_3$ were reported by Yaokawa [4] as expendable salt cores for high pressure die casting processes.

Therefore, the development of a thermodynamic database for the salt system $Li^+$, $Na^+$, $K^+//Cl^-$, $CO_3^{2-}$ is significant for the calculation and prediction of thermodynamic properties in the different applications.

## 2.2 Thermodynamic properties of salt systems

The salt system $Li^+$, $Na^+$, $K^+//Cl^-$, $CO_3^{2-}$ is divided into 6 pure salts, 9 binary systems, 2 ternary systems, and 3 reciprocal systems for the establishment of the thermodynamic database. Thermodynamic data for each subsystem are collected.

### 2.2.1 Pure salts

Thermodynamic data of NaCl, KCl, $Na_2CO_3$ and $K_2CO_3$ are already investigated many times and their data are already collected in the FTsalt database. In the framework of the salt-screening project, the salts NaCl, KCl, $Na_2CO_3$ and $K_2CO_3$ have already been assessed in the PCM database [10,23,24,33], so they are introduced briefly here. The assessment of the pure substances in this work focuses on $Li_2CO_3$ and LiCl.

The Gibbs energy function of the pure salts KCl and NaCl above 298 K has been assessed previously by Sergeev et al. [33], and the thermodynamic data below 298 K has been assessed by Reis [10], both of these data have been included into the PCM database and both salts have one solid phase only. $K_2CO_3$ has also been assessed based on the previous literature data and DSC, DTA and HTXRD measurements [23,24]. The Gibbs energy of the three solid phases $K_2CO_3$ (LT), $K_2CO_3$ (MT), $K_2CO_3$ (HT) and the liquid phase are described in the new database from 0-1200 K.

The three solid phases $Na_2CO_3$ (LT). $Na_2CO_3$ (MT), $Na_2CO_3$ (HT) and the liquid phase of $Na_2CO_3$ have also been assessed previously in the PCM database [34].

***$Li_2CO_3$***

$Li_2CO_3$ was extensively investigated in the past. The results of DTA experiments by Reisman [35] reveal solid-solid phase transition at 683 K, and those of Otsubo and Yamaguchi [36] show it at 688 K. The results of DTA experiments by Klement and Cohen [37] also show solid-solid phase transitions at 693 K on heating and at 680 K on cooling. Furthermore, high temperature XRD result of Khlapova and Kovaleva [38] shows that there are three different solid phases of $Li_2CO_3$, i.e. the stable phase α below 681 K, the metastable phase β below 681 K and the γ phase transformed from β phase above 681 K. In contrast, the experimental results of Janz et al. [39] and Rolin and Recapet [40] indicate no solid-solid phase transition. Besides, no solid-solid transition was found (e.g., by Dissanayake and Mellander [41] and Brown and Boryta [42]) when the measurements have been conducted under $CO_2$ atmosphere to prevent the decomposition of $Li_2CO_3$. To verify whether the solid phase transition really exists or not, in the present work the phase transformation of $Li_2CO_3$ was investigated using DTA and high temperature XRD.

Brown and Latimer [43] measured the $C_p$ of $Li_2CO_3$ from 16-300 K with low temperature calorimetry, while Kourkova and Sadovska [44] obtained the $C_p$ values in the temperature range of 303-563 K with a C80 calorimeter. Janz et al. [39] derived the equation of $C_p$ (560-1150 K) from the measured heat content data. A 20 J/(mol·K) difference at 563 K between results of Janz et al. [39] and Kourkova and Sadovska [44] is noticed, where actually no phase transition occurs. The heat capacity of $Li_2CO_3$ presented in the commercial database FTsalt [45] was based on the previous literature experimental data and adopted the 20 J/(mol·K) difference at 563 K, which is not sufficiently reliable. Therefore, a detailed experimental study of the $C_p$ is necessary in the wide temperature range to provide reliable $C_p$ data.

***LiCl***

The phase change temperatures of LiCl were investigated in previous works [46–63] and no solid-solid phase transition was reported. The heat capacity of LiCl was measured by Shirley [60] in the temperature range 15-325 K with a copper calorimeter, by Rodigina et al. [57] with a

calorimeter at 300-1100 K and by Douglas and Victor [50] at 298-1200 K. The data below 298 K are not included in the current commercial database FTsalt and SGPS [25,45].

### 2.2.2 Binary systems

The Gibbs energy of the different solution phases in the binary NaCl-KCl and $Na_2CO_3$-$K_2CO_3$ systems have been described in the PCM database [10,33,34]. The systems $Na_2CO_3$- $K_2CO_3$ and NaCl-KCl are not a part of the present work. They are just briefly introduced here.

***NaCl-KCl***

The binary NaCl-KCl system was previously assessed [10,33] and introduced into the PCM database. The assessment was performed based on the experimental data of the phase diagram [64–67], the mixing enthalpy measured by Hersh and Kleppa [68] and the recent measurements using DSC, DTA, DROP and XRD from Sergeev et al. [69]. A continuous solid solution phase is formed in this system, and a miscibility gap shows up at low temperatures. The Gibbs energy of the liquid and solid solution has been described in the PCM database and the calculated phase diagram is shown in Figure 2-4.

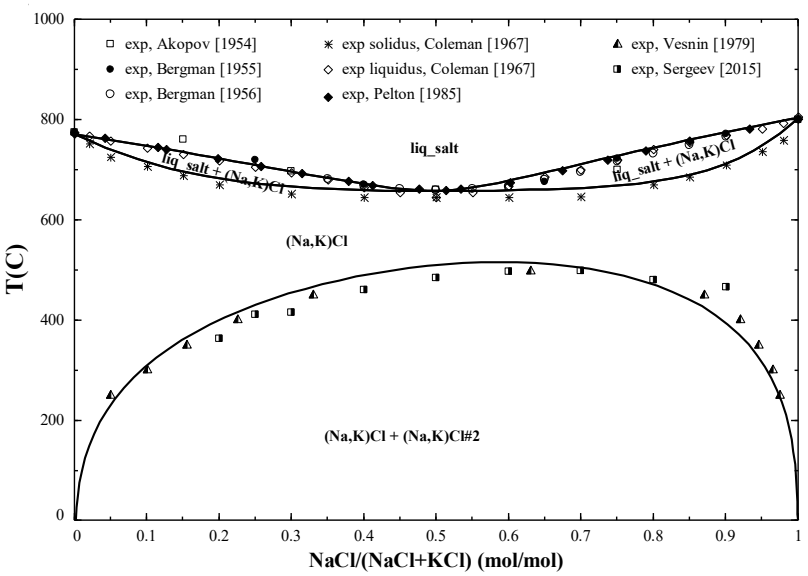


Figure 2-4. The phase diagram of binary system NaCl-KCl [33].

***$Na_2CO_3$- $K_2CO_3$***

The preliminary assessment of the $Na_2CO_3$- $K_2CO_3$ system was done [34] (Figure 2-5) based on the phase equilibria data and thermodynamic properties from the literature [70–72] along with a recent experimental study [24]. In the work of Sergeev et al. [24], the existence of the solid-solid phase transition between the solid solution phases HEXA and HEX2 in this system was confirmed by DTA and HTXRD.

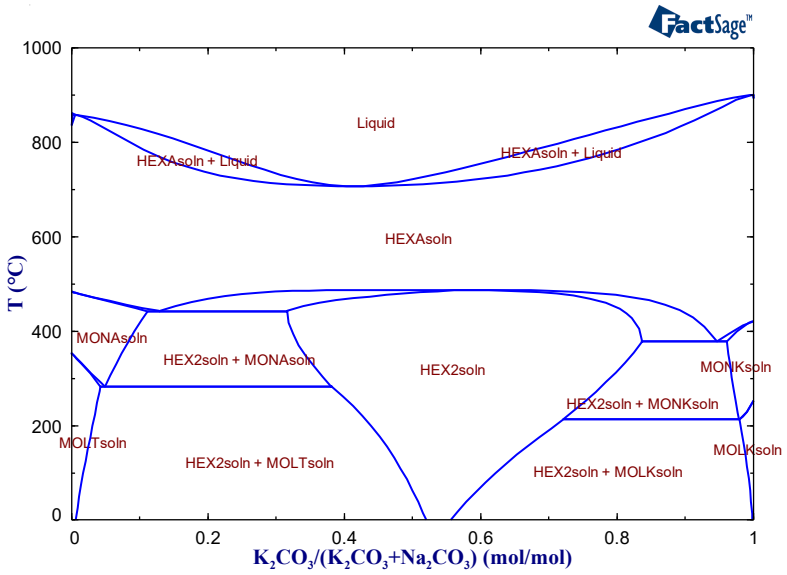


Figure 2-5. The phase diagram of binary system $Na_2CO_3$-$K_2CO_3$ calculated with PCM database.

As shown in Figure 2-5, six solid solutions are formed in this system: HEXA, HEX2, MONA, MOLT, MONK and MOLK. HEXA is the unlimited solid solution between the high temperature modification of the alkali carbonates, $Na_2CO_3$ (HT) and $K_2CO_3$ (HT). HEX2 is the low temperature phase of HEXA. The solid solutions based on the medium (MT) and low temperature modification (LT) are MONA, MOLT, MONK and MOLK, which are based on $Na_2CO_3$ (MT), $Na_2CO_3$ (LT), $K_2CO_3$ (MT) and $K_2CO_3$ (LT), respectively. The Gibbs energy of these six solid solutions and the liquid phase was described in the PCM database.

***LiCl-NaCl***

The phase diagram of LiCl-NaCl system was studied experimentally many times. There are contradictory data on phase equilibria, namely on the presence of solid solubility and the intermediate compound. Some authors claimed that a complete solid solution exists in the

system [46,73–76]. The temperature of the miscibility gap of the solid solution was detected in some references [46,73,75]. Some authors claimed two limited solid solutions formed in this system [77–79], while some authors considered the system as a eutectic system with intermediate compounds [80–88]. Sangster and Pelton [89] calculated the phase diagram of this system with a continuous solid solution, which was described with a sub-regular model, while the liquid solution was described with a regular model. In 2012, Guo et al. [90] assessed this system and described the liquid and solid solutions with the two-sublattice model.

This system was measured for the first time by Zhemchuzhnui and Rambach [46] using thermal analysis method in 1910 (shown in Figure 2-6). In their work, the solid solution was found to formed in the whole composition range, and the miscibility gap was detected in x(NaCl) = 0.23-0.54 mole fraction. The minimum temperature of the liquidus line was 552 °C at the composition x(NaCl) = 0.27. The maximum temperature of the miscibility gap appeared at 314 °C and the composition x(NaCl) = 0.35. Later, the liquidus line and the miscibility gap were detected by Schaefer [73] with thermal analysis and the maximum temperature of miscibility gap was 271 °C at the composition x(NaCl) = 0.43.

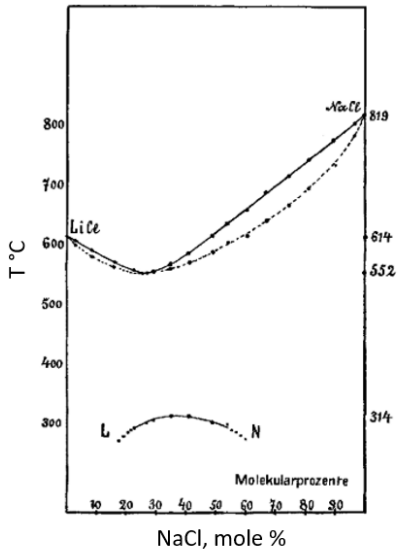


Figure 2-6. Phase diagram of the LiCl-NaCl system measured by Zhemchuzhnui and Rambach [44]

Limited solid solutions based on both LiCl and NaCl were detected by Storonkin et al. [78] and Chesnokov et al. [79] by XRD. While Chesnokov et al. [79] also reported the miscibility gap in the range of x(NaCl) = 0.2-0.63 with the maximum point at 280 °C and the composition x(NaCl) = 0.40 and x(NaCl) = 0.42 (see Figure 2-7). Tian et al. [76] confirmed the formation of a complete solid solution in the system by XRD analysis of the samples quenched from 250 °C and 400 °C, where a continuous change of lattice parameter with compositions was reported for the samples quenched from 400 °C.

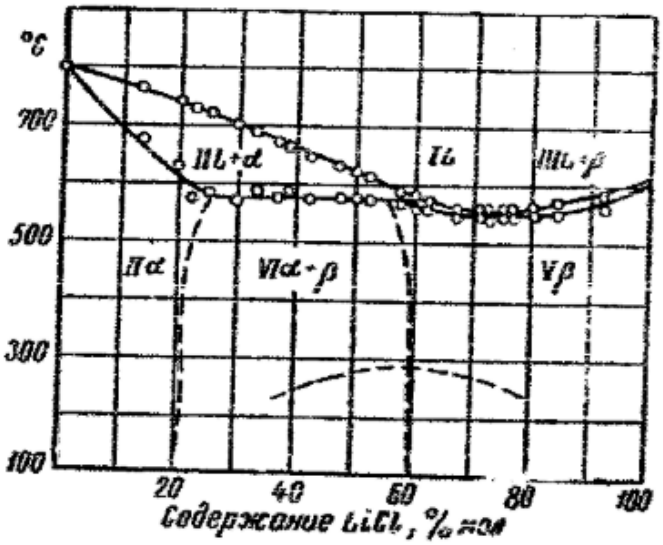


Figure 2-7. Phase diagram of the LiCl-NaCl system measured by Chesnokov et al. [79]

Bergman and Akopov [88] measured the liquidus line and obtained the minimum temperature 556 °C for the composition x(NaCl) = 0.28. In their work, a compound $LiNaCl_2$ was mentioned. Bukhalova and Arabadzhan [86] also detected the liquidus line and mentioned two compounds $LiNaCl_2$ and $LiNa_2Cl_3$ (see Figure 2-8). The assumptions that this system is a eutectic system are only based on the liquidus measurement, and the determination of compounds was based on the break of the liquidus curve. In the study of Akopov and Korobka [77], this system was considered to be an eutectic system. The thermal effects of those are assumed to be caused by the two compounds, $LiNaCl_2$ and $LiNa_2Cl_3$, detected in the heating process, while the cooling curves measurement showed a complete solid solution formed in this system. These unstable thermal effects make their existence questionable. In addition, the XRD results of Smits et al. [91]

did not show the formation of these intermediate compounds. Therefore, they were not considered in the present assessment. Only the measured liquidus data are selected for the optimization. Comparing the liquidus and solidus data from different studies, the solidus temperature measured by Klochko [75] and Zhemchuzhnui and Rambach [46] are much higher than others, so they are excluded in the optimization process.

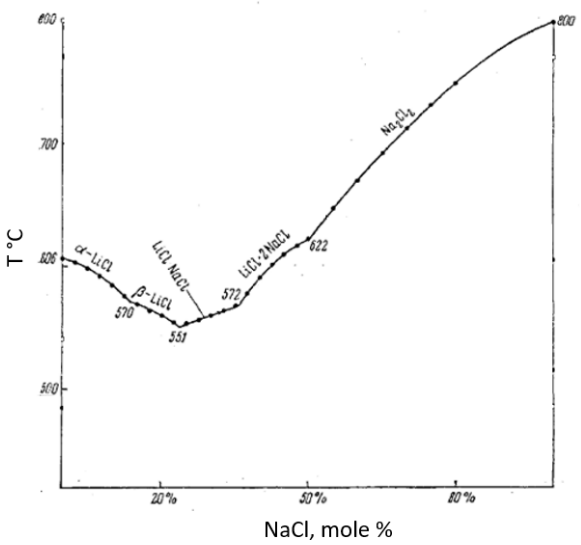


Figure 2-8 Liquidus line of the LiCl-NaCl system detected by Bukhalova and Arabadzhan [79]

The mixing enthalpy between the solid NaCl and liquid LiCl at 740 °C was measured by Hersh and Kleppa [68], and according to these results the equation of the mixing enthalpy between the liquid phases was derived.

***LiCl-KCl***

The studies of Richards and Meldrum [47], Aukrust et al. [92], Zhemchuzhnui and Rambach [46], Korin and Soifer [93] and Elchardus and Laffitte [94] concluded that the LiCl-KCl system is a simple eutectic system. However, after measuring the DTA curves for four terminal compositions ($x_{KCl}$ = 0.03, 0.05, 0.95 and 0.97), Ghosh et al. [95] concluded that solid solutions based on both KCl and LiCl exist in this system. This system was first assessed by Sangster and Pelton [89] as a simple eutectic system and mentioned that there is a limited solid solubility less than 0.05 at either side of the phase diagram from the limiting liquidus slopes from the result of Zhemchuzhnui and Rambach [46]. Later, the system LiCl-KCl was assessed by Zhou and Zhang [96]

considering the experimental results of Ghosh et al. [95]. In that assessment, the two-sublattice model was applied for the liquid phase and the compound energy formalism was applied for the solid solutions. Zhou and Zhang [96] showed the formation of solid solutions based on both chlorides with the limit of solubility of 0.05 mole fraction.

In addition to the phase equilibria, the thermodynamic properties were reported in the literature. Powers and Blalock [97] measured $H-H_{0^{\circ}c}$ using a Bunsen ice-calorimeter. Solomons et al. [98] measured $H_T-H_{298}$ with cryoscopic measurement in the temperature range 592-656 K. Then, Markov et al. [99] and Clark [100] obtained their data using the more reliable measurement, namely drop calorimetry. The mixing enthalpy of solid KCl and liquid LiCl at 740 °C was measured by Hersh and Kleppa [68]. Markov et al. [99] measured the mixing enthalpy of the eutectic composition at 770 °C as -4.02 kJ/mol. In addition, Aukrust et al. [92] investigated the mixing enthalpy of this system at 775 °C. The activity of LiCl in the liquid mixture at 722 °C was measured by Thulin et al. [101] using electromotive force (EMF) method. In addition, the activity data of LiCl and KCl in the liquid phase at 640 °C were measured by Behl [102] using EMF method.

***$Li_2CO_3$-LiCl***

The phase diagram of the $Li_2CO_3$-LiCl system was studied by Volkov and Zakhvalinskii [103] and the measured eutectic temperature is 517 °C. While Reshetnikov and Diogenov [104] and Levin et al. [105] have studied it using the visual-polythermal method and TA method and obtained an eutectic temperature of 507 °C and 506 °C, respectively. All results indicate the absence of a solid solution in this system. This binary system was assessed firstly by Dessureault et al. [106] with the modified quasi-chemical model for the description of the liquid phase.

***$K_2CO_3$-KCl***

The liquidus temperature of the $K_2CO_3$-KCl system was widely investigated in the past [107–112], and the experimental results show that it is a simple eutectic system. The liquidus line was firstly studied by Sackur [110] in dilute liquid solutions in 1910. Then, the eutectic line was measured by Amadori [109] in the composition range of x(NaCl) = 0.09-0.94. These experimental results were firstly reviewed and assessed by Dessurealt et al. [106]. Then, this system was also assessed by Yaokawa et al. [113] using the two-sublattice model for the description of the liquid

phase. In their work, the activity of $K_2CO_3$ and KCl in the liquid phase at 950 °C was predicted. It is noticed that the largest difference in the measured eutectic temperature is 13 °C, i.e. the difference between that of Amadori, 636 °C [109] and Radishchev, 623 °C [108]. Therefore, the DTA measurement of the sample $0.38K_2CO_3$-0.62KCl should be carried out to verify the exact eutectic temperature.

***$Na_2CO_3$-NaCl***

The phase diagram of the $Na_2CO_3$-NaCl system has been investigated in the past for many times [108,109,114–116] and it is a simple eutectic system, the eutectic temperature was proved for the entire composition range. The activity of $Na_2CO_3$ in the compositions $x(Na_2CO_3)$=0.2, 0.4, 0.5 and 0.7 was tested by Iwasawa et al. [116] using EMF method. The fusion enthalpy of the eutectic composition of this system has been reported to be 24.1 ± 1.4 kJ/mol by Jiang et al. [117] and 22.5 kJ/mol by Raud et al. [26]. However, the fusion enthalpy was measured to be 7.9 kJ/mol by Ye et al. [118], the deviation is too large from other literature, therefore it is not considered for the assessment work. Additional measurements on the thermal stability was also done by KEMS (this method can provide precise information of the equilibrium between the condensed phase and gas phase) in this work.

***$Li_2CO_3$-$K_2CO_3$***

The phase diagram of the $Li_2CO_3$-$K_2CO_3$ system has been studied experimentally by many authors [22,119–124]. All the experimental results reach a consensus regarding the existence of the congruently melting intermediate compound $LiKCO_3$. The melting point of $K_2CO_3$ and the liquidus line on the $K_2CO_3$ side measured by Le Chatelier [123] deviate by around 40-50 °C from the other results, so it is not taken into account for the optimization in the present work. The eutectic temperatures and melting temperature obtained by Reshetnikov and Perfil'eva [124] were about 20 °C lower than those measured by others, which was also excluded from the optimization in the present work.

The heat capacity data of the intermediate compound $LiKCO_3$ obtained by different authors [22,125–127] are not consistent (see Figure 2-9). Janz and Perano [125] determined the heat capacity of $LiKCO_3$ from the enthalpy increment measurement and obtained 186.8 J/K·mol (778-

1200 K) and 141.5 J/K·mol (457-778 K) for the liquid and solid phase, respectively. It was also measured by Jo and Banerjee [22] using DSC method with the result of 124.2 J/K·mol for the solid phase at 250 °C and 400 °C and 163.6 J/K·mol for the liquid phase in the temperature range 525-555 °C. For the $C_p$ of the solid phase, both results of Janz and Perano [125] and Jo and Banerjee [22] are unreasonable because the temperature dependence coefficient of $C_p$ is not supposed to be zero. The measured $C_p$ of the solid phase by Araki et al. [126] and Liu et al. [127] increases with temperature, which makes more sense compared to the constant $C_p$. However, the data points are scattered in a wide range, therefore, the accuracy of the data is under question. The heat capacity of the solid phase measured by Araki et al. [126] was 164.4 J/K·mol (800-1066 K), which is close to the result of Jo and Banerjee [22] but around 20 J/K·mol lower than the results of Janz and Perano [125]. The Cp of the liquid phase measured by Liu et al. [127] at 833-908 K first increases and then stabilizes at 183.3 J/K·mol, which is close to the result of Janz and Perano [125]. For the $C_p$ of the solid phase, both results of Janz and Perano [125] and Jo and Banerjee [22] are unreasonable because the temperature dependence coefficient of $C_p$ is not supposed to be zero. The measured $C_p$ of the solid phase by Araki et al. [126] and Liu et al. [127] increases with temperature, which makes more sense compared to the constant $C_p$. However, they are not consist with each other. The data points by Araki et al. [126] are scattered in a wide range, while the data points by Liu et al. [127] are limited within a small temperature range of 634-753 K. Therefore, the accuracy and completeness of the data is under question. The $C_p$ data from FTsalt are calculated using the Neumann-Kopp relation of the pure substances $Li_2CO_3$ and $K_2CO_3$. The heat capacity of the pure substances cannot be applied directly because the solid-solid phase transition of $K_2CO_3$ will affect the $C_p$ curve of $LiKCO_3$. In this work, the heat capacity of the solid phase $LiKCO_3$ was measured in detail using the DSC method.

The enthalpy increment ($H_T$-$H_{298.15}$) of $LiKCO_3$ was investigated by Janz and Perano [125] using drop calorimetry, and the melting enthalpy of $LiKCO_3$ was measured to be 36.4 ± 0.4 kJ/mol. While Jo and Banerjee [22] measured the melting enthalpy as 40 ± 2 kJ/mol and Liu et al. [127] measured it as 31.27 kJ/mol.

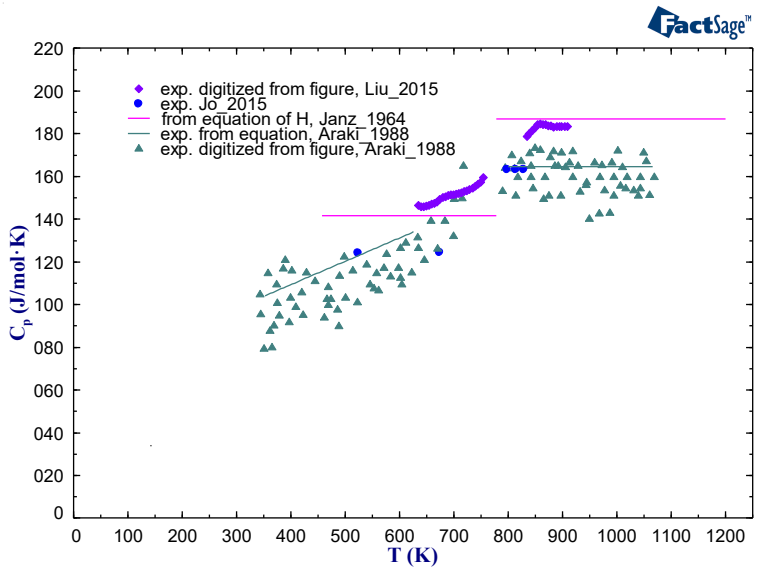


Figure 2-9 Heat capacity of the intermediate compound $LiKCO_3$ from the literature.

Moreover, the mixing enthalpy of the $Li_2CO_3$-$K_2CO_3$ system at 1178 K was measured by Andersen and Kleppa [128] by calorimetry in dry $CO_2$ atmosphere. Chen et al. [129] assessed the $Li_2CO_3$-$K_2CO_3$ system with the cell model for the liquid phase.

***$Li_2CO_3$-$Na_2CO_3$***

The $Li_2CO_3$-$Na_2CO_3$ system was extensively investigated in the past. The literature phase diagrams are shown in Figure 2-10, Figure 2-11 and Figure 2-12. The literature data and calculation of the phase diagram with the FTsalt database are summarized in Figure 2-13. There are controversial opinions concerning the formation of the intermediate compound $LiNaCO_3$ and its melting behavior. In the literature, the congruent melting and peritectic decomposition are still discussed. Moreover, various temperatures of the structure phase transition of the intermediate compound $LiNaCO_3$ were also reported by different authors. Besides, the existence of the solid solution in the phase diagram is under question.

The phase diagram of the $Li_2CO_3$-$Na_2CO_3$ system was firstly reported by Eitel and Skaliks [130]. In their work, the intermediate compound $LiNaCO_3$ was detected by XRD, and its congruent melting was reported since the melting point of $x(Na_2CO_3)$=0.5 (514 °C) was measured 4 °C higher than that of the other compositions (510 °C, eutectic temperature).

Burmistrova and Volozhanina [131] studied the phase diagram of the $Li_2CO_3$-$Na_2CO_3$ system by DTA method and electrical conductivity measurement (Figure 2-10). According to their work, $LiNaCO_3$ melts congruently at 510 °C and the two eutectic temperatures for the sub-systems $Li_2CO_3$-$LiNaCO_3$ and $Na_2CO_3$-$LiNaCO_3$ were found at 496 °C and 510 °C, respectively. Besides, the thermal effects at 340 °C and 360 °C were detected (Figure 2-10), and the authors assumed that they were caused by the solid-solid phase transitions of $Na_2CO_3$, $Li_2CO_3$ or $LiNaCO_3$.

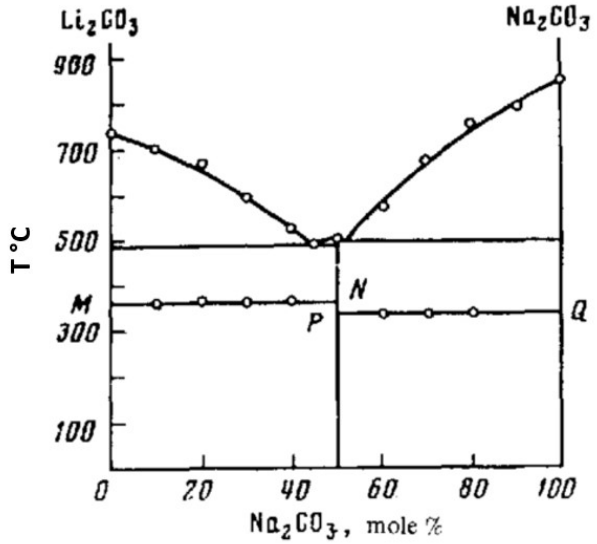


Figure 2-10. The phase diagram of the $Li_2CO_3$-$Na_2CO_3$ system measured by Burmistrova and Volozhanina. [131] .

The liquidus line of $LiNaCO_3$ was also reported by Volkov and Volkova [132], its crystallisation line intersects with $Li_2CO_3$ and $Na_2CO_3$ at 0.47 and 0.53 mole fraction of $Na_2CO_3$ at 497 and 510 °C, respectively, these points correspond to the eutectics and it means $LiNaCO_3$ melts congruently. The phase diagram of this system was also reported by Volkov and Shvab [133], where the crystallization lines of $LiNaCO_3$ intersects with $Li_2CO_3$ and $Na_2CO_3$ at 0.45 (496 °C) and 0.50 (501 °C, maximum) of $Na_2CO_3$. According to Volkova [119], the liquidus lines of the intermediate compound extend from 497 to 501°C in the concentration range 0.44 to 0.499 of $Na_2CO_3$. Therefore, $LiNaCO_3$ was detected melting incongruently in both references [119] and [133].

Janz and Lorenz [120] concluded that this system is a simple eutectic system, as shown in Figure 2-11. According to the measurements of Rolin and Recapet [121], this system was also thought to be a simple eutectic system.

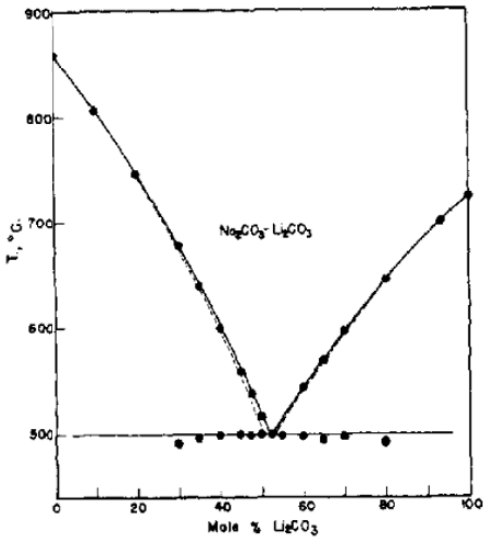


Figure 2-11. The phase diagram of the $Li_2CO_3$-$Na_2CO_3$ system measured by Janz and Lorenz [120].

Cairns and Macdonald [134] measured this system by a highly sensitive (± 0.003 °C) thermal analysis equipment in the composition range of 0.45-0.52 mole fraction of $Na_2CO_3$ and confirmed that the intermediate compound $LiNaCO_3$ melts incongruently at 500.757± 0.005 °C, the eutectic temperature between $LiNaCO_3$ and $Li_2CO_3$ was 499.757 ± 0.057 °C (Figure 2-12). D'yakov et al. [135] measured this system in the composition range of 0.4 to 0.54 of $Na_2CO_3$ with DTA and found that $LiNaCO_3$ melts incongruently at 493 °C while the eutectic temperature between $LiNaCO_3$ and $Li_2CO_3$ is 485 °C.

Regarding solid solution in the $Li_2CO_3$-$Na_2CO_3$ system, Khlapova and Elenevskaya [136] reported that $Na_2CO_3$ (LT) can be solved into $LiNaCO_3$ in the composition range x($Na_2CO_3$)=0.5-0.56 through XRD investigation of different compositions in this system at room temperature.

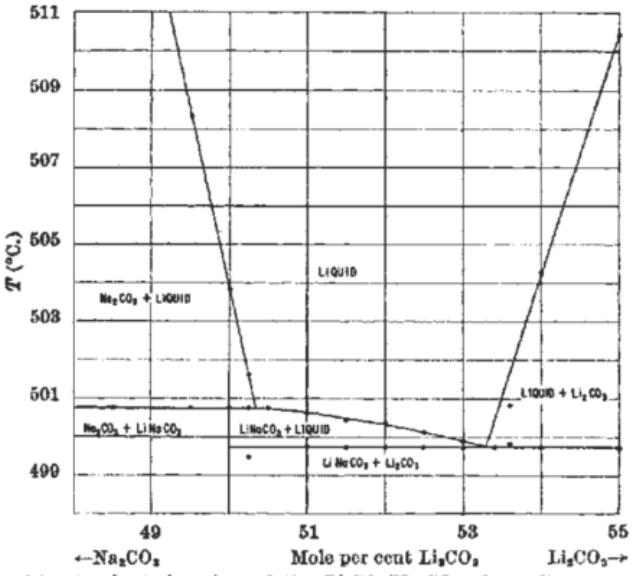


Figure 2-12. The phase diagram of $Li_2CO_3$-$Na_2CO_3$ system reported by Cairns and Macdonald [134].

Dessureault et al. [137] assessed the $Li_2CO_3$-$Na_2CO_3$ system with the quasi-chemical model for the liquid and the sub-lattice model for the solid solution. In their assessment, the existence of $LiNaCO_3$ was not considered due to the uncertainty of the XRD data obtained before. A solid solution based on $Na_2CO_3$ (HT) with maximum solubility at 0.88 mole fraction of $Na_2CO_3$ was introduced by the analysis of the slope of liquidus line near $Na_2CO_3$ and the experimental data of Khlapova and Elenevskaya [136], in which the solubility of $Li_2CO_3$ in $Na_2CO_3$ was actually not mentioned. Chen et al. [129] assessed the $Li_2CO_3$-$Na_2CO_3$ system as an eutectic system with the cell model for the liquid phase according to the experimental results from Janz and Lorenz [120] and Rolin and Recapet [121], and in this assessment the solid solubility was not considered. Similar to the assessment of Dessureault et al. [137], in the commercial database FTsalt, the intermediate compound $LiNaCO_3$ is not included. Besides, the calculated result suggests a solid solution based on $Na_2CO_3$ (HT) with maximum solubility at 0.84 mole fraction of $Na_2CO_3$.

When comparing the calculated results using the commercial database FTsalt with the literature data (Figure 2-13), some uncertainties in both experimental data and the calculated results were found. For example, the lack of experimental description of the solid solution phase based on $Na_2CO_3$ (HT), which might be caused by the lower precision of the previous instruments.

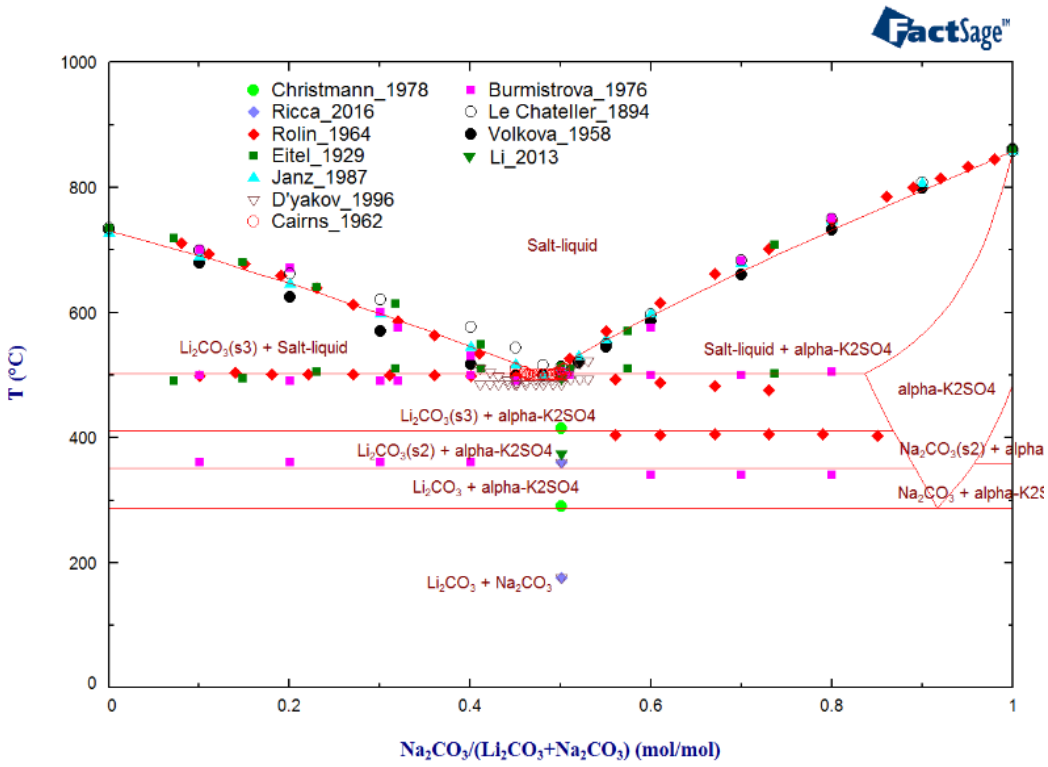


Figure 2-13. The phase diagram of the $Li_2CO_3$-$Na_2CO_3$ system from the literature and calculated with FTsalt.

In more detail, the points shown at around 350 °C measured by Burmistrova and Burmistrova [131] as well as the points at around 400 °C measured by Rolin and Recapet [121] (see Figure 2-13) can be explained as the two solid-solid phase transitions of $Li_2CO_3$ in the FTsalt database. If that is true, the points at around 400 °C measured by Rolin and Recapet [121] should be shown when the composition is close to the pure $Li_2CO_3$. There is a noticeable temperature difference split by $x(Na_2CO_3)=0.5$ for points shown at around 350 °C measured by Burmistrova and Burmistrova [131], which means that they are not raised by the same reaction or phase transition in the phase diagram. According to analysis of the pure $Li_2CO_3$, the solid-solid phase transition was also under question, so that these phase transition temperatures need to be analyzed further. There is only one solid solution based on $Na_2CO_3$ (HT) introduced in the FTsalt database. Besides $Na_2CO_3$ (HT) modification, there is also $Na_2CO_3$ (MT) and $Na_2CO_3$ (LT). It is reasonable, that the solubility based on the low temperature modifications of $Na_2CO_3$ can also exist along with the

solid solution based on $Na_2CO_3$ (HT). Therefore, the solubility of $Li_2CO_3$ in $Na_2CO_3$ (MT) and $Na_2CO_3$ (LT) should be checked.

The structure of $LiNaCO_3$ at room temperature was measured by Eitel and Skaliks [130] by XRD. Due to the poor formation of the crystal faces it was assumed probably to be hexagonal. Christmann et al. [138] measured $LiNaCO_3$ with high temperature XRD and reported three solid phases from low temperature to high temperature: α phase (monoclinic, 25-290 °C), β phase (hexagonal, 290-415 °C) and γ phase (hexagonal, 415-500 °C). Yatsenko et al. [139,140] investigated the crystal structures of α phase (triclinic, 25-175 °C) and β phase (hexagonal, 175-360 °C) by XRD with single crystal samples. Zhukov et al. [141] confirmed the crystal structures of γ phase (hexagonal, 360-500 °C). D'yakov et al. [135] detected two solid-solid phase transitions of $LiNaCO_3$ at 175 °C and 360 °C by DTA. Li and Zhang [142] measured one solid-solid transition at 373 °C. These results are close to the results from Yatsenko et al. [139,140], Zhukov et al. [141] and D'yakov et al.[135] and significantly deviate from Christmann et al. [138] (290 °C and 415 °C).

No heat capacity values of $LiNaCO_3$ were found in the literature. The fusion enthalpy of $LiNaCO_3$ was measured to be 32.87 kJ/mol by Li and Zhang [142] using DSC. The fusion enthalpy of the eutectic composition was measured by Li et al. [143], Jiang et al. [144], Ge et al. [29], Janz et al. [145] and Petri et al. [146], the results were in a range from 29.9 to 35.5 kJ/mol

In addition, the mixing enthalpy of the $Li_2CO_3$-$Na_2CO_3$ system at 1178 K was measured by Andersen and Kleppa [128] by calorimetry in dry $CO_2$ atmosphere.

### 2.2.3 Ternary systems

***LiCl-NaCl-KCl***

The liquidus surface of the ternary system $Li^+$, $Na^+$, $K^+//Cl^-$ was investigated by Akopov [87] with visual-polythermal method, as shown in Figure 2-14a. As mentioned before, the intermediate compound $LiNaCl_2$ was observed in the LiCl-NaCl system and reflected in the liquidus surface of the ternary system as a crystallization field. Later, Akopov and Bergman [83] proposed the liquidus projection again considering another intermediate compound $LiNa_2Cl_3$, as

shown in Figure 2-14b. The temperature of the ternary eutectic point obtained was 346 °C.

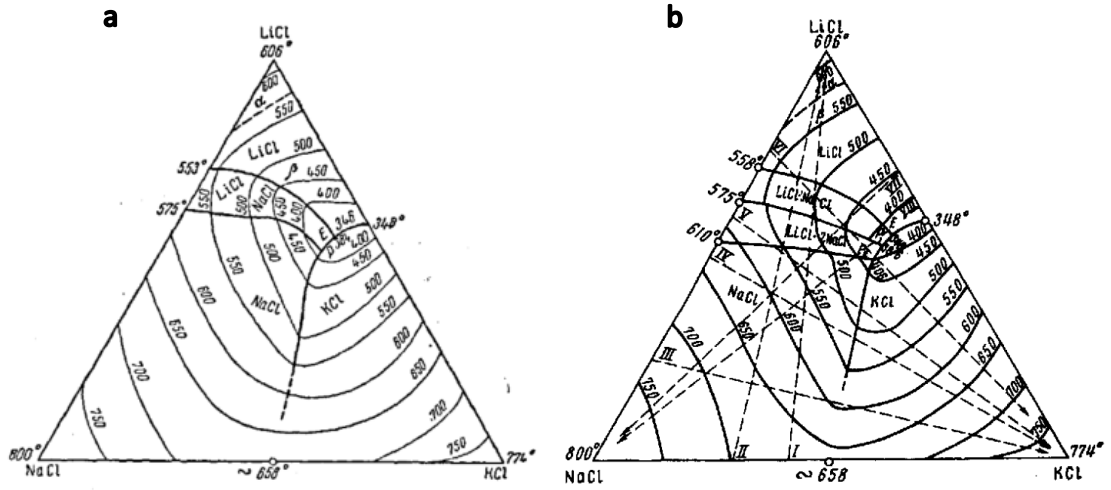


Figure 2-14. The liquidus surface of the ternary system $Li^+$, $Na^+$, $K^+$// $Cl^-$ reported by Akopov [87] and Akopov and Bergman [83], temperature is in °C and composition is in mole fraction.

The ternary system $Li^+$, $Na^+$, $K^+$//$Cl^-$ was investigated by Storonkin et al. [147] by thermal analysis. The liquidus surface is shown in Figure 2-15. The temperature of the ternary eutectic was found at 350 °C. The peritectic reaction measured in the binary system LiCl- NaCl influenced the liquidus of the ternary system, which is marked as $P_{12}$ point in the bottom line $A_1A_2$ (Figure 2-15), and extends into the point c in the ternary system.

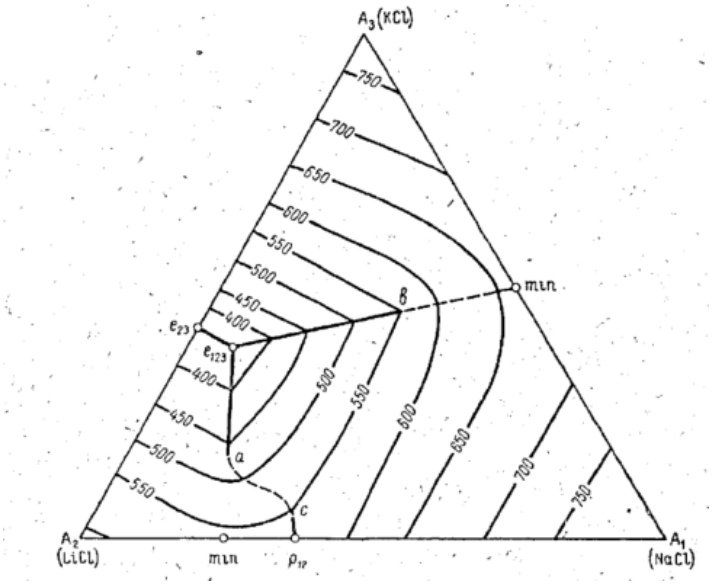


Figure 2-15. The liquidus surface of the ternary system of $Li^+$, $Na^+$, $K^+$// $Cl^-$ reported by Storonkin et al. [147], temperature is in °C and composition is in mole fraction.

Then, this ternary system was thermodynamically assessed by Sangster and Pelton [148]. As it is mentioned, the intermediate compound $LiNaCl_2$ was not considered in the binary system LiCl-NaCl and this binary system was assessed as a system with continuous solid solution. This effect was reflected in the ternary liquidus surface and the eutectic temperature of system was calculated to be 343 °C [148].

***$Li_2CO_3$-$Na_2CO_3$-$K_2CO_3$***

The ternary system $Li_2CO_3$-$Na_2CO_3$-$K_2CO_3$ was extensively investigated due to its wide applications (molten carbonate fuel cell [1–3], die casting process [4], Electrochemical Deposition of Carbon Materials [5,6], etc.). The liquidus surface has been investigated by Volkova [119], Janz and Lorenz [120] as well as Rolin and Recapet [121]. The ternary eutectic points in the liquidus surface are close to each other, whereas the liquidus surface from the different authors are not identical.

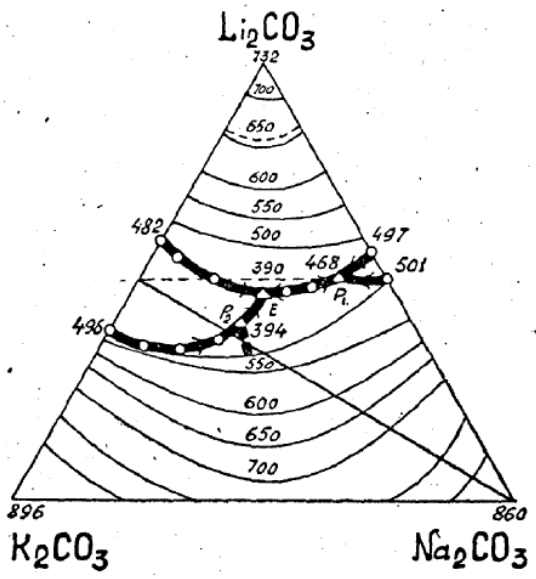


Figure 2-16. The liquidus surface of the ternary system of $Li^+$, $Na^+$, $K^+$// $CO_3^{2-}$ reported by by Volkova [119], temperature is in °C and composition is in mole fraction.

The liquidus surface of the ternary system $Li^+$, $Na^+$, $K^+$// $CO_3^{2-}$ was obtained by Volkova [119] through the measurement of the binary systems and 10 quasi-binary sections with visual-polythermal method (Figure 2-16). In their work, four primary crystallization fields were found in the liquidus surface: $Li_2CO_3$, $LiKCO_3$, $LiNaCO_3$ and solid solution (between $Na_2CO_3$ and $K_2CO_3$). The

eutectic E lies in the intersections of 3 fields ($Li_2CO_3$, $LiKCO_3$, solid solution) at 390 °C with a composition of 0.27 $Li_2CO_3$, 0.45 $K_2CO_3$ and 0.28 $Na_2CO_3$ mole fraction(Figure 2-16).

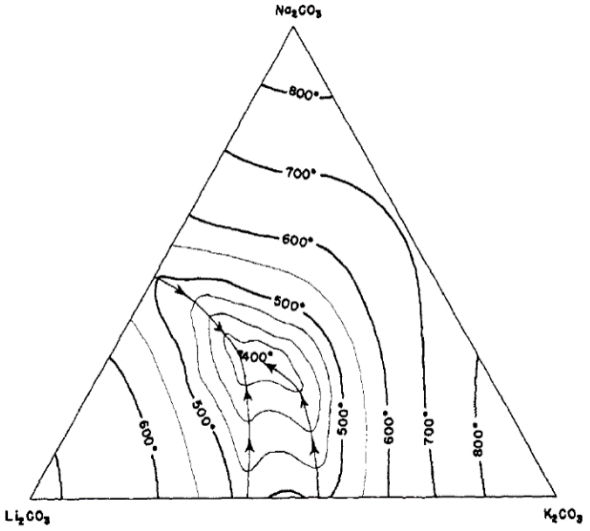


Figure 2-17. The liquidus surface of the ternary system $Li^+$, $Na^+$, $K^+$// $CO_3^{2-}$ measured by Janz and Lorenz [120], temperature is in °C and composition is in mole fraction.

Later, this system was studied by Janz and Lorenz [120] by thermal analyses method. Because the $Li_2CO_3$-$Na_2CO_3$ system was considered as simple eutectic system in their work, only three crystallization fields were found in the liquidus surface: $Li_2CO_3$, $LiKCO_3$ and solid solution (between $Na_2CO_3$ and $K_2CO_3$). The simple ternary eutectic lies in the intersections at 397±1 °C, the composition (mole fraction) is 0.435 $Li_2CO_3$-0.315 $Na_2CO_3$-0.25 $K_2CO_3$ (Figure 2-17).

Rolin and Recapet [121] obtained the liquidus surface of this system by measuring 171 compositions inside the ternary system as well as the binary systems, as shown in Figure 2-18. Besides the crystallization fields $Li_2CO_3$, $LiKCO_3$ and solid solution (between $Na_2CO_3$ and $K_2CO_3$), an additional field $K_2CO_3$ was shown in the liquidus surface. The reason why this phase shows up is that in the binary system $Na_2CO_3$-$K_2CO_3$ a transformation of $K_2CO_3$ was mentioned and caused the discontinuity of liquidus line, but its reproducibility is under question. The eutectic is located at 393 °C with a composition of 0.325 $Li_2CO_3$, 0.36 $K_2CO_3$ and 0.315 $Na_2CO_3$ mass fraction (Figure 2-18), which corresponds to 0.437 $Li_2CO_3$, 0.259 $K_2CO_3$ and 0.305 $Na_2CO_3$ mole fraction.

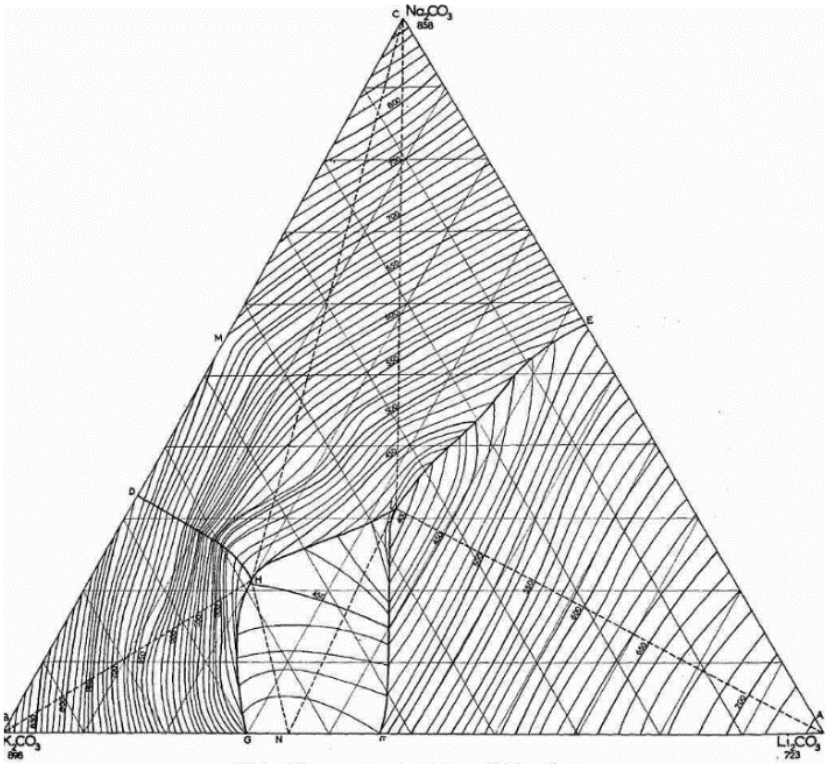


Figure 2-18. The liquidus surface of the ternary system $Li^+$, $Na^+$, $K^+$// $CO_3^{2-}$ reported by Rolin and Recapet [121] , temperature is in °C and composition is in mass faction.

Pelton et al. [149] assessed this system, where the $Li_2CO_3$-$Na_2CO_3$ system was considered to be a simple eutectic system. Chen et al. [129] assessed the liquid phase of this ternary system with the cell model.

Yan et al. [150] measured the phase change temperature of different compositions in the ternary system by DTA. Sang et al. [151] did XRD measurements for the compositions 0.531 $Li_2CO_3$-0.284 $K_2CO_3$ -0.185 $Na_2CO_3$ and 0.5 $Li_2CO_3$-0.25 $K_2CO_3$ -0.25 $Na_2CO_3$, for both compositions $LiNaCO_3$, $LiKCO_3$ and $Li_2CO_3$ were detected coexisting in the system.

The enthalpy increment of the eutectic composition was measured by Janz et al.[39] and Rolin and Recapet [40]. Both of them used drop calorimetry. Janz et al. [39] determined the fusion enthalpy for the eutectic composition to be 27.6 kJ/mol. Olivares et al. [152] studied the thermal stability of the eutectic salt with a melting point of 401 °C and fusion enthalpy of 22.12 kJ/mol. Janz et al. [39] obtained the heat capacity of the eutectic composition based on the equation of enthalpy increment. An et al. [153] measured the heat capacity of the eutectic composition in

the temperature range of 450-600 °C with 161±8 J/(mol·K). Wu et al. [154] measured the heat capacity of the eutectic composition in the temperature range 450-830 °C and the fusion enthalpy of three different compositions. Liao et al. [155] measured the fusion enthalpy (16.0 kJ/mol) and heat capacity of the eutectic composition. Liu et al. [127] also measured the fusion enthalpy (27.95 kJ/mol) and heat capacity of the eutectic composition.

To assess the ternary system, reliable information about binary subsystems should be well known. Instead of only one hexagonal solid solution formed between $Na_2CO_3$ and $K_2CO_3$, another hexagonal solid solution below around 500 °C was reported by Sergeev et al. [24], which is confirmed by HTXRD method and DTA measurements.

As it is mentioned before, the solid solution of the $Li_2CO_3$ -$Na_2CO_3$ system has also hexagonal structure, which belong to the same phase as the high temperature hexagonal solid solution between $Na_2CO_3$ and $K_2CO_3$ in the ternary system. Therefore, the solubility of $Li_2CO_3$ in the low temperature hexagonal solution is reasonable and should be checked experimentally.

### 2.2.4 Reciprocal system

The phase diagrams of the reciprocal systems are based on the corresponding binary systems. In this section, the thermodynamic information on the three reciprocal systems are collected.

***$Na^+$, $K^+$//$Cl^-$, $CO_3^{2-}$***

The projection of the liquidus surface of the reciprocal system $Na^+$, $K^+$//$Cl^-$, $CO_3^{2-}$ was studied by Radishchev [108] and Nyankovskaya [156] (Figure 2-19).

The liquidus surface of the ternary part NaCl-$Na_2CO_3$-KCl was measured by Busse-Machukas et al. [157] (Figure 2-20 a) and Sato [115] (Figure 2-20 b). In the ternary part measured by Sato [115], the curve connecting the two eutectic points and the minimum occurs at 660 °C with 0.29 $Na_2CO_3$, 0.32 NaCl and 0.39 KCl mole fraction. In the work of Radishchev [108], the phase diagrams of the diagonal systems $K_2CO_3$-$(NaCl)_2$ and $(KCl)_2$-$Na_2CO_3$ and other sections were measured. In the work of Sato [115], the phase diagrams of the diagonal system $(KCl)_2$-$Na_2CO_3$ and other sections were measured. According to the measurement of Sato [115], the binary system KCl-$Na_2CO_3$ forms a eutectic mixture at 660 °C with 0.425 $Na_2CO_3$. Recently, the phase

diagram of the diagonal section KCl-$Na_2CO_3$ was reported by Haseli et al. [158], and the fusion enthalpy of the eutectic composition was measured to be 32.28 ± 1 kJ/mol. Moreover, the fusion enthalpy of four different compositions inside this reciprocal system was reported by Liu et al. [159].

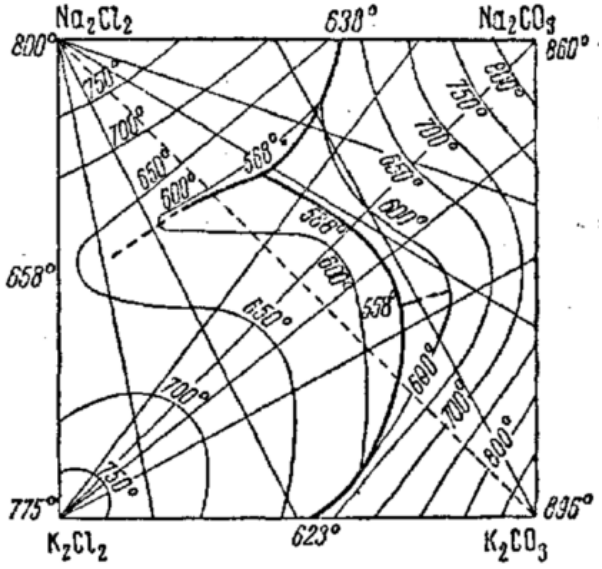


Figure 2-19. The liquidus surface of the reciprocal system $Na^+$, $K^+$//$Cl^-$, $CO_3^{2-}$ reported by Nyankovskaya [156], temperature is in °C and composition is in mole fraction.

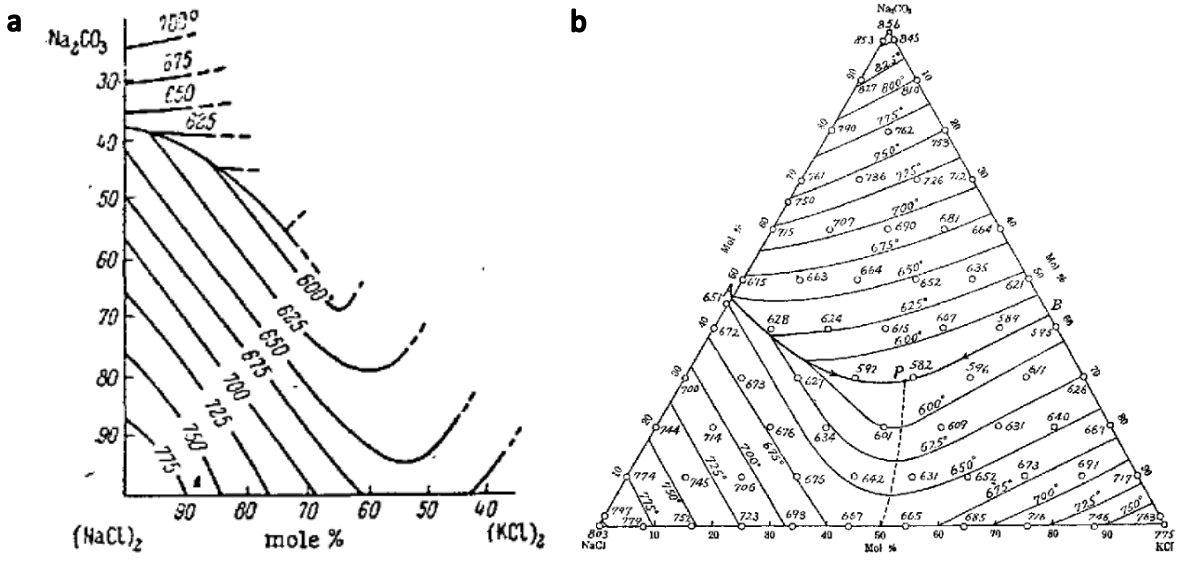


Figure 2-20. The liquidus surface of the ternary part NaCl-$Na_2CO_3$-KCl in the reciprocal system $Na^+$, $K^+$//$Cl^-$, $CO_3^{2-}$ reported by a) Busse- Machukas et al. [157] and b) Sato [115], temperature is in °C.

***$Li^+, K^+//Cl^-, CO_3^{2-}$***

The reciprocal system $Li^+$, $K^+//Cl^-$, $CO_3^{2-}$ was published by Volkov and Zakhvalinskii [103], whereas the phase relations in the diagonals are not studied experimentally, but they were derived from those of the binary systems. In their work, the eutectic point of the $Li_2CO_3$-$(KCl)_2$ system was reported and the liquidus surface of the reciprocal system was plotted, as shown in Figure 2-21.

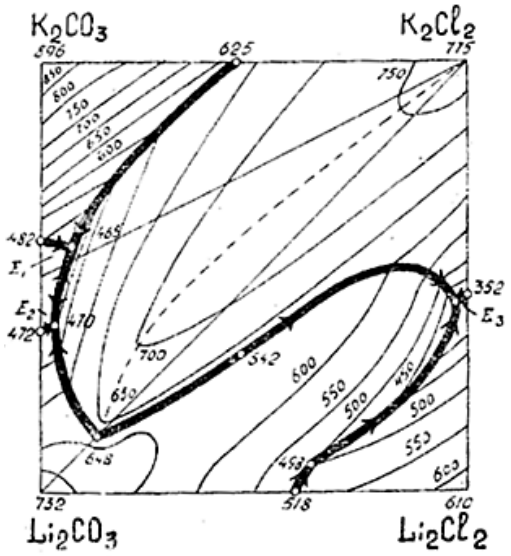


Figure 2-21. The liquidus surface of the reciprocal system $Li^+$, $K^+//Cl^-$, $CO_3^{2-}$ reported by Volkov and Zakhvalinskii [103]

***$Li^+, Na^+//Cl^-, CO_3^{2-}$***

No experimental data of the reciprocal system $Li^+$, $Na^+//Cl^-$, $CO_3^{2-}$ have been published so far. The prediction based on the FTsalt database (Figure 2-22) shows three crystallization fields: $Li_2CO_3$ (S3), Rocksalt (solid solution between alkali chloride salts) and alpha-$K_2SO_4$ (solid solution based on $Na_2CO_3$ (HT) and $K_2CO_3$ (HT)). These phases correspond to those used in the present work: $Li_2CO_3$, Alk_chlorides, and HEXAsoln, respectively.

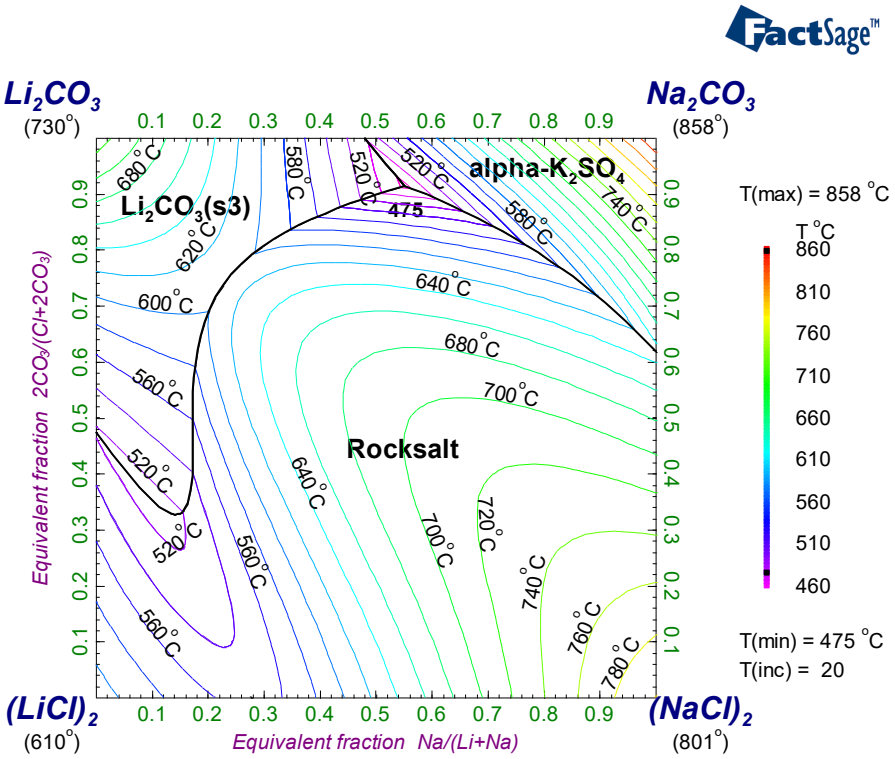


Figure 2-22. The liquidus surface of the reciprocal system $Li^+$, $Na^+$//$Cl^-$, $CO_3^{2-}$ calculated using FTsalt.

## 2.3 Aims of this work based on the literature review

The literature data on the thermodynamic properties and phase equilibria of the salt system $Li^+$, $Na^+$, $K^+$//$Cl^-$, $CO_3^{2-}$ were collected and critically analyzed. In accordance with these data, the aims of the work are:

1. The thermodynamic information and transition data for $Li_2CO_3$ is not complete in the literature, therefore, a detailed study on thermal behavior and structure of $Li_2CO_3$ was performed and its Gibbs energy was modelled in accordance with this data. The thermodynamic data of LiCl below room temperature was assessed according to the literature data.
2. The controversial information on the binary $Li_2CO_3$-$K_2CO_3$, $Na_2CO_3$-NaCl, $K_2CO_3$-KCl and $Li_2CO_3$-$Na_2CO_3$ systems and the reciprocal systems was verified by experimental studies

on phase equilibria. The thermal behavior of $LiNaCO_3$ and $LiKCO_3$ was checked. The solid solution phases in the $Li_2CO_3$-$Na_2CO_3$ were measured.

3. Since the commercial databases for the salt system are not accurate enough (For example, the thermodynamic information of $LiNaCO_3$ is absent), a new database is necessary. The Gibbs energy of all phases in the system $Li^+$, $Na^+$, $K^+$//$Cl^-$, $CO_3^{2-}$ was generated using both literature and own experimental data, and a new thermodynamic database was developed. The reciprocal system $Li^+$, $Na^+$//$Cl^-$, $CO_3^{2-}$ was evaluated using the present experimental results, while the other systems (binary systems LiCl-KCl and NaCl-LiCl, ternary systems LiCl-NaCl-KCl and $Li_2CO_3$-$Na_2CO_3$-$K_2CO_3$, and reciprocal system $K^+$, $Na^+$//$Cl^-$, $CO_3^{2-}$) are mainly optimized according to the experimental data in the literature.

The relevant details of experiments and modelling results will be introduced in the following chapters.

# 3 Experimental

In this chapter, the selection and preparation of samples are described to have an overview of the applied materials in the whole experiments. Four devices, Thermogravimetry/Differential Thermal Analysis (TG/DTA), Differential Scanning Calorimetry (DSC), X-Ray Diffractometry/High Temperature X-Ray Diffractometry (XRD/HTXRD) and Knudsen Effusion Mass Spectrometry (KEMS) were used for the measurement of thermodynamic properties of the salt mixtures in this work.

## 3.1 Samples

The pure salts LiCl (Alfa Aesar, ultra-dry, 99.995%), NaCl (Fluka, 99.999%), KCl (Alfa Aesar, ultra-dry, 99.95%), $Li_2CO_3$ (Acros Organics, 99.999%), $Na_2CO_3$ (Fluka, 99.9999%) and $K_2CO_3$ (Alfa Aesar, 99.997%) were used to prepare different mixtures. The $Li_2CO_3$ raw material was measured by DTA and XRD. According to the results, which are explained in Chapter 5, the $Li_2CO_3$ raw material was heated in $CO_2$ gas at 650 °C for 1 h to remove the impurity LiOH before the heat capacity measurement. The intermediate compound $LiKCO_3$ was prepared by melting $Li_2CO_3$ and $K_2CO_3$ together in 1:1 molar ratio in a tube furnace (Prüfer) at 550 °C for 4 h under $CO_2$ atmosphere (gas flow rate 100 ml/min). The intermediate compound $LiNaCO_3$ was prepared in the same way with $Li_2CO_3$ and $Na_2CO_3$ in 1:1 molar ratio. However, the XRD test always shows extra $Li_2CO_3$ in the samples of $LiNaCO_3$ (marked as sample 1), therefore, more samples were prepared with extra $Na_2CO_3$ with the molar ratio 0.51:0.49 ($Na_2CO_3$:$Li_2CO_3$) (marked as sample 2) for heat capacity measurement. All samples were weighed in a glove box under a dry argon atmosphere and the composition of different samples and their measurements are summarized in Table 3-1.

Table 3-1. Information on different samples.

| Salt system | Composition | Measurement |
|---|---|---|
| $Li_2CO_3$ | $Li_2CO_3$ | DTA, DSC, HTXRD |
| $LiKCO_3$ | $LiKCO_3$ | DSC, HTXRD |
| $LiNaCO_3$ | $LiNaCO_3$ (sample 1 and sample 2) | DTA, DSC, HTXRD |
| $K_2CO_3$-KCl | Molar fraction ($K_2CO_3$)=0.38 | DTA |
| $Na_2CO_3$-NaCl | Molar fraction ($Na_2CO_3$)=0.53 | DTA, KEMS |

| | | |
|---|---|---|
| $Li_2CO_3$- $K_2CO_3$ | Molar fraction ($K_2CO_3$)=0.85, 0.9, 0.95 | DTA |
| $Li_2CO_3$-$Na_2CO_3$ | Molar fraction ($Na_2CO_3$)=0.975 | DTA, HTXRD |
| | Molar fraction ($Na_2CO_3$)=0.4, 0.6, 0.7, 0.75, 0.8, 0.85, 0.9, 0.95 | DTA |
| $Li_2CO_3$-$(KCl)_2$ | Molar fraction ($Li_2CO_3$)=0.1, 0.2, 0.3, 0.4, 0.5, 0.6, 0.7, 0.8, 0.9 | DTA |
| $K_2CO_3$-$(LiCl)_2$ | Molar fraction ($(LiCl)_2$)=0.07, 0.16, 0.18, 0.19, 0.20, 0.24, 0.29, 0.33, 0.38, 0.40, 0.43, 0.48, 0.50, 0.53, 0.60, 0.64, 0.69, 0.71, 0.75, 0.82, 0.84, 0.87, 0.93 | DTA |
| $(LiCl)_2$-$Na_2CO_3$ | Molar fraction ($Na_2CO_3$)=0.1, 0.2, 0.3, 0.4, 0.5, 0.6, 0.7, 0.8, 0.9 | DTA |
| $Li_2CO_3$-$(NaCl)_2$ | Molar fraction ($Li_2CO_3$)=0.3, 0.5, 0.7, 0.8, 0.9, 0.95 | DTA |
| $Na^+$, $K^+$//$Cl^-$, $CO_3^{2-}$ | 0.428KCl–0.359$Na_2CO_3$–0.213$K_2CO_3$ (in molar fraction) | DSC |

## 3.2 Instruments

### 3.2.1 Thermogravimetry/Differential Thermal Analysis (TG/DTA)

TG/DTA (Netzsch) was used to measure the phase transition temperature and weight change during the heating/cooling process. The results were analyzed using the Netzsch software. Normally, the phase transition temperatures are taken from the heating curves because the supercooling effect should be taken into consideration in the cooling process. For the determination of melting temperature and eutectic temperature, the onset temperatures in the heating curves were taken, while the liquidus temperatures were taken from the peak temperature on the heating curves.

The schematic diagram of a DTA is shown in Figure 3-1. During the measurement two crucibles are used, one is filled with the sample and the other is empty as reference.

Netzsch STA449C device was used to measure the phase transition temperature of various mixtures in different salt systems. The sample mass was between 150 and 200 mg. A SiC furnace was used, which allows to reach 1600 °C. The thermal couple of the DTA is type S (Pt-Pt/Rh). For each sample, at least 3 heating-cooling cycles of measurements were conducted with heating and cooling rate of 5 K/min. In the first cycle, there was a gap between the salt powders and the crucible wall, which caused a bad contact and influenced the heat transfer. Besides, the mixing enthalpy of two components also influenced the slope of the curve. Therefore, the results

obtained from the first cycle are usually different from that of the second and third ones. After the salt is molten in the first cycle, the aforementioned influences disappear and usually the second and third cycle are reproducible and used for determination of the phase diagram, otherwise an additional cycle is necessary to get a reproducible and reliable result.

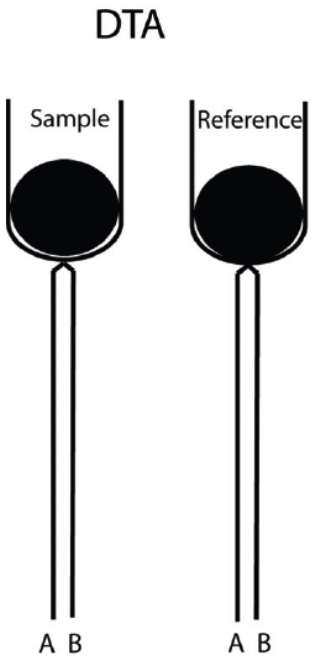


Figure 3-1. Schematic diagram of DTA, A and B denote the different legs of thermocouples. [160]

As for the selection of the crucible, it was taken into account that chloride salts have relatively high vapor pressure compared with the carbonate salts. For the $(LiCl)_2$-$K_2CO_3$ and $(LiCl)_2$-$Na_2CO_3$ system, the reciprocal reaction will occur after melting towards the stable phases. For example, if the molar fraction of $(LiCl)_2$ is larger than 0.5, the binary $(LiCl)_2$-$K_2CO_3$ system will become the ternary LiCl-KCl-$Li_2CO_3$ system after reaction. If the measurement is done in open crucibles, the weight loss is mainly due to the vaporization of LiCl and KCl. Their proportion is hard to be determined for further calculation. Therefore, closed platinum crucibles were selected for the measurement of the samples in the $(LiCl)_2$-$K_2CO_3$ and $(LiCl)_2$-$Na_2CO_3$ system to avoid mass loss. Some preliminary measurements were carried out in closed Pt crucibles for the $Li_2CO_3$-$(KCl)_2$ system, but unexpected results were observed. Besides, it was reported that $Li_2CO_3$ can react with Pt and $O_2$ to form $LiPtO_4$ [161]. Therefore, instead of Pt closed crucibles, $Al_2O_3$ crucibles were

used for the measurement of the $(KCl)_2$-$Li_2CO_3$, $K_2CO_3$-$Li_2CO_3$ and $Li_2CO_3$-$Na_2CO_3$ systems. Graphite crucibles were used for the measurement of the $(NaCl)_2$-$Li_2CO_3$ system and one composition $0.5(LiCl)_2$-$0.5K_2CO_3$. Crucibles from different materials were calibrated separately. The reference materials $RbNO_3$, $KClO_4$, $Ag_2SO_4$, CsCl, $K_2CrO_4$, and $BaCO_3$ were used for the calibration of the Pt crucible and graphite crucibles, while the pure metals In, Sn, Bi, Zn, Al, and Ag were used for the calibration of the $Al_2O_3$ crucibles.

### 3.2.2 Differential Scanning Calorimetry (DSC)

The heat capacity of $Li_2CO_3$, $LiKCO_3$ and $LiNaCO_3$ salts was measured with different types of DSC instruments, i.e., Netzsch DSC 404C_low_T, Netzsch DSC 404C_high_T and Setaram mHTC 96. For each device, several samples were measured to ensure the reproducibility of the results. The parameters of these devices and experimental conditions are summarized in Table 3-2. It can be seen that the main difference between the DSC 404C_low_T and the other two devices is the temperature range, which allows the measurement of the heat capacity below room temperature by the use of liquid $N_2$. The DSC sample holder of the Setaram mHTC 96 device is equipped with a 3D-Calvet type thermopile, which can measure the heat capacity in 3-dimensions more precisely.

Besides, the selection of crucible is essential for the measurement. As mentioned, Pt can react with $Li_2CO_3$, which was confirmed in our pretest. When the salt $Li_2CO_3$ was tested with a Pt crucible in Helium atmosphere, it was found that the color of the bottom of the crucible became brown, which means that a reaction occurred between Pt and $Li_2CO_3$. Therefore, Pt crucibles were not used. When the salt $Li_2CO_3$ was tested with an $Al_2O_3$ crucible, the results from the different devices showed obvious discrepancy (see Figure A-1 in the Appendix), which is probably due to the fact that the thermal conductivity of the used $Al_2O_3$ crucible was not good enough for the heat capacity measurement. Finally, a Pt crucible with alumina liner was selected, which avoids the reaction between Pt crucible and $Li_2CO_3$ and also ensured thermal conductivity. The results obtained are shown in the next chapter.

The specific heat was determined with the three-step method according to the American Standard Test Method (ASTM E1269) [162]. A Pt crucible with alumina liner was used to measure the $C_p$. The heat flows of the empty crucible and the crucible containing sapphire were measured separately in the same heating process, before the DSC test was conducted on the sample. The heat flow of the sample was then obtained from the DSC for 3 thermal cycles. The heat capacity $C_p(T)$ was obtained according to the following Eq. (1):

$$C_p(T) = \frac{HF_{sample} - HF_{blank}}{HF_{ref} - HF_{blank}} \cdot \frac{Mass_{ref}}{Mass_{sample}} \cdot C_{p_{ref}}(T), \quad (1)$$

where $HF_{sample}$ is the heat flow of the sample, $HF_{blank}$ is the heat flow of the empty crucible as baseline, $HF_{ref}$ is the heat flow of the reference material sapphire, $Mass_{ref}$is the mass of the reference material sapphire, $Mass_{sample}$ is the mass of the sample and $C_{p_{ref}}(T)$ is the heat capacity of the reference material sapphire.

Table 3-2. Parameters of the differential scanning calorimeters.

| Instrument | DSC 404C_low_T | DSC 404C_high_T | mHTC 96 |
|---|---|---|---|
| Company | Netzsch | Netzsch | Setaram |
| Thermocouple | Type K | Type S | Type S- HFDSC |
| Temperature range | -180-650 °C | 25-1600 °C | 25-1400 °C |
| Oven (heating element) | Ag | Pt-Rh | Graphite |
| Atmosphere | He, 10 ml/min | He, 10 ml/min | He, 10 ml/min |
| Heating rate | 20 K/min | 20 K/min | 4 K/min |
| Crucible | Pt with $Al_2O_3$ liner | Pt with $Al_2O_3$ liner | Pt with $Al_2O_3$ liner |
| Sample weight | 20-50 mg | 20-50 mg | 300-400 mg |

DSC (404_F1 Pegasus®, Netzsch) was used to measure the phase-change temperature and melting enthalpy of the sample 0.428KCl–0.359$Na_2CO_3$–0.213$K_2CO_3$ (in molar fraction) with graphite crucible. This experiment was carried out in the lab of the Barbara Hardy Institute, University of South Australia.

### 3.2.3 X-Ray Diffractometry/High Temperature X-Ray Diffractometry (XRD/HTXRD)

The wavelength of X-rays is similar to the distance between the atoms in the crystal. Therefore, diffraction occurs when the X-rays light is scattered by periodic arrays of atoms in a crystal with long-range order, producing constructive interference at specific angles. The scattering of X-rays by atoms produces a diffraction pattern that contains information about the arrangement of atoms within the crystal [163].

X-Ray Diffractometry (XRD) is used for determination of crystal structure and phase ratio of the samples. The purity of the raw material and prepared samples at room temperature can be studied. High Temperature X-Ray Diffractometry (HTXRD) can measure the crystal structure and phase composition of the samples from room temperature to high temperature. Therefore, it can also be used to observe the phase transition of samples. Moreover, the temperature dependence of the lattice parameters can be determined.

Measurements were performed with an EMPYREAN diffractometer (Malvern Panalytical, Almelo, The Netherlands) equipped with a Cu LFF X-ray tube (operated at 40 kV and 40 mA), a Bragg BrentanoHD mirror, a PIXcel3D detector in 1D mode and a HTK 1200N oven chamber (Anton Paar, Austria). Lattice parameters were determined through Rietveld refinement using the profile fitting software TOPAS (version 6, Bruker AXS) and structure data was retrieved from the ICSD database (FIZ Karlsruhe) [164].

In this work, commercially available $Li_2CO_3$ was heated and cooled in the temperature range of 25-650 °C. Temperature steps were 50 K (from 50 °C and higher), with 2 min dwell time and 21 min measurement time. Heating and cooling rate was 5 K/min and atmosphere was synthetic air (continuous flow of 10 ml/min). Samples of $LiKCO_3$ and $LiNaCO_3$ were heated and cooled in the temperature range of 25-450 °C. Temperature steps were 25 K for 25-400 °C and 50 K for 400-450 °C, with 21 min measurement time. Heating and cooling rate was 5 K/min and atmosphere was $CO_2$ with continuous gas flow of 2 ml/min.

### 3.2.4 Knudsen Effusion Mass Spectrometry (KEMS)

Knudsen Effusion Mass Spectrometry (KEMS) can be used to determine gaseous species present above the condensed phase and measure their partial pressures [165].

In this work, the gas phase composition of the eutectic mixture in the $Na_2CO_3$-NaCl system was measured by KEMS. The schematic diagram of KEMS is shown in Figure 3-2.

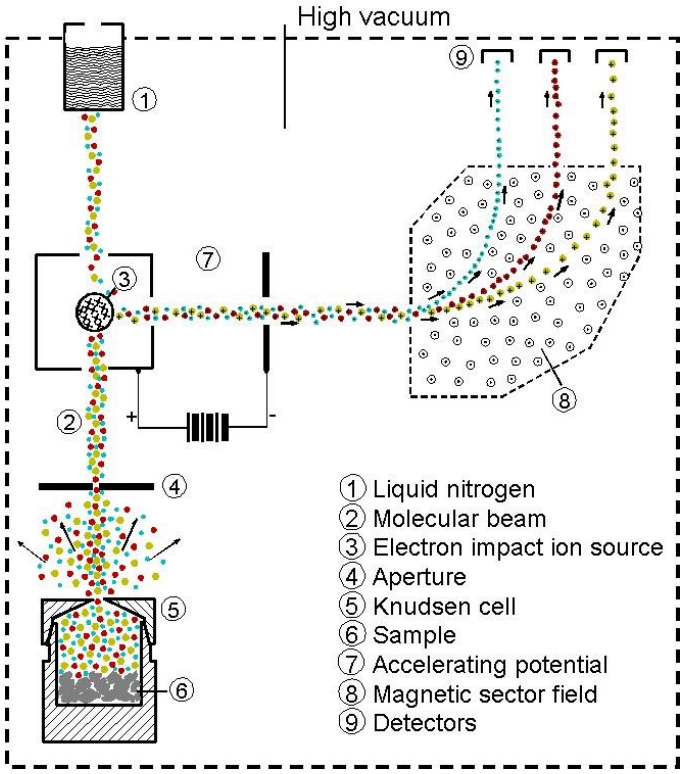


Figure 3-2. Schematic diagram of KEMS [166]

There is an effusion orifice (typical diameter 0.2 to 1 mm) in the Knudsen cell, which allows the effusion of gas species out of the cell, while inside the cell, an equilibrium state is considered to be maintained during the measurement process. After effusing from the cell, only the molecules along the vertical direction can get through the aperture and form a molecular beam. Then, the molecules are ionized by electron impact, and the produced ions are accelerated by an accelerating potential and then separated according to m/z, i.e., the mass over charge ratio in the magnetic field. The sample was heated up by a tungsten wire with radiation and electron bombardment mode. During the experiments, temperature and intensity of ions are recorded.

The temperature was measured by thermocouple and pyrometer. The Knudsen cell (inner diameter and height approximately 9 mm) is made of Ir, inside the cell a graphite liner was used to avoid the creeping problem after melting. The partial pressure can be determined in the range of $10^{-5}$ -10 Pa. For each measurement, the ion counts are detected when the shutter is opened and closed and the difference between these two values is taken as the final result. After loading the sample, the KEMS was evacuated to the pressure of $10^{-6}$ -$10^{-7}$ mbar before the measurement. The sample first was heated up to 580 °C and the ion species were detected by a preliminary test, then the isothermal signals of the species were measured at 580 °C. Then, the samples were heated from 580-680 °C to check the melting temperature. Finally, the sample was heated up to 665 °C (above the melting temperature) to get the isothermal results of the liquid phase, the signals were measured every 1 h. The pure NaCl was measured as a reference.

# 4 Thermodynamic modelling

The aim of this work is to develop an accurate thermodynamic database for the calculation and prediction of thermodynamic properties of salt mixtures in the $Li^+$, $Na^+$, $K^+//Cl^-$, $CO_3^{2-}$ system. For the development of the database, the assessment of the Gibbs energy of different phases is done with the Calphad method by the software FactSage, in particular the *OptiSage* module. In this chapter, the theoretical background of the thermodynamic calculation, corresponding models of Gibbs energy description and the process of the thermodynamic optimization are introduced.

## 4.1 Thermodynamic background

The basic theory of the thermodynamic equilibria is minimization of Gibbs energy of a system, while the Gibbs energy $G$ is a function of temperature, pressure and composition. How the Gibbs energy $G$ changes with these factors is shown in Eq. 4.1, where $V$ is the volume, $S$ is the entropy, $\mu_i$ and $n_i$ are the chemical potential and molar number of components $i$, respectively.

$$dG = Vdp - SdT + \sum \mu_i dn_i \qquad 4.1$$

The stoichiometric compounds (pure substances, e.g., $O_2$, NaCl or intermediate compounds e.g., $KLiCO_3$) have only one component, the Gibbs energy of each phase (gas, liquid, solid phase α1, solid phase α2…) is only a function of temperature $T$ and pressure $p$. When a solution phase (gas solution, liquid solution or solid solution) forms in a multicomponent system, in addition to temperature and pressure, its Gibbs energy also depends on composition $x_i$ ($x_i = {}^{n_i}/_{n}$, $n$ is the total molar number of different components). Generally speaking, the pressure has limited effect on the condensation phase (liquid and solid phase), therefore, the influence of pressure on the Gibbs energy of solid and liquid phase is not considered. Hence, the phase equilibria can be calculated at standard pressure (1 atm) using most of the available thermodynamic databases. Only in case of available data at high pressure, the phase equilibria can be predicted at non-standard pressure.

When the pressure is fixed, for the pure substance, intermediate compounds, or at a certain composition in a solution, the Gibbs energy of each phase is only a function of temperature, as

shown in Eq. 4.2. The change rate of Gibbs energy with temperature is the negative entropy, $-S$, as shown in Eq. 4.1, which depends on the characteristics of the phase itself and differs from phase to phase. At a certain temperature, the Gibbs energy of each phase can be calculated, and the phase or phase combination with the lowest Gibbs energy is the stable one. One simplified example is shown in Figure 4-1. In the real case, the entropy $S$ can be the function of temperature, which means that the lines in Figure 4-1 become curves, which does not influence the comparison.

$$dG = -SdT \tag{4.2}$$

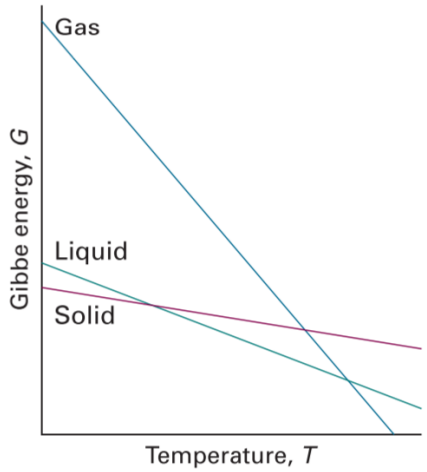


Figure 4-1. The variation of the Gibbs energy with the temperature is determined by the entropy [167].

On the other hand, at a certain pressure, when the temperature is fixed, the Gibbs energy of solution phases is only a functions of composition $x_i$. One example is the G-composition graph at temperatures T1 and T2 in Figure 4-2. For a certain composition, the phase with the minimum Gibbs energy is the stable phase shown in the phase diagram. When the common tangent line has the minimum Gibbs energy, there is a two-phase equilibria in the phase diagram. Accordingly, the composition on the line R1R2 at T2 is the two-phase equilibrium between the phases fcc and hcp.

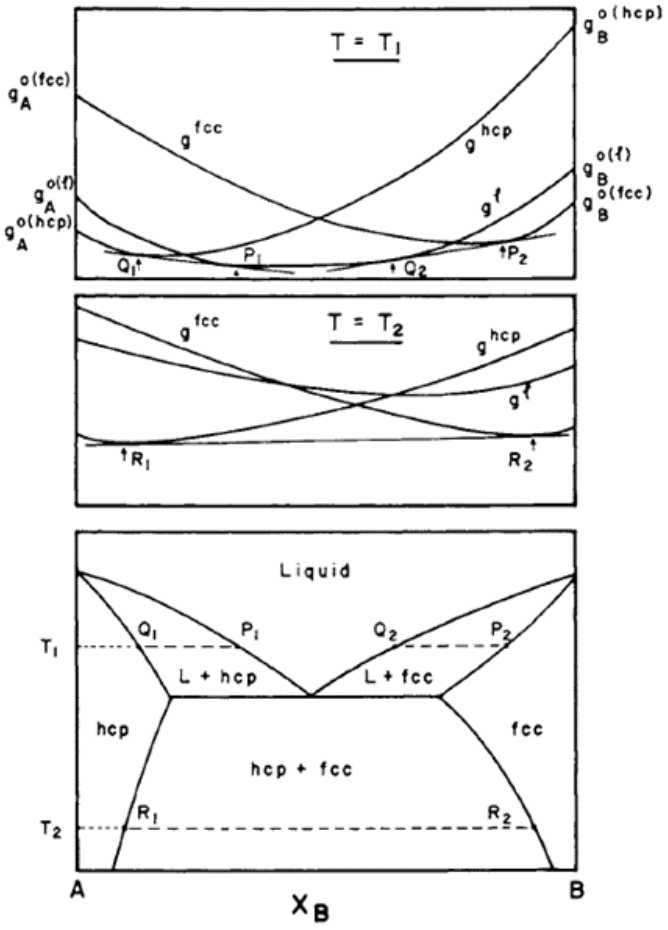


Figure 4-2. The relationship of phase diagram and Gibbs energy curves of different phases. [168]

Therefore, in order to determine the minimum Gibbs energy of the whole system at certain conditions, it is essential to know the Gibbs energy of each phase.

## 4.2 Gibbs energy description

### 4.2.1 Stoichiometric compounds

At constant pressure, the Gibbs energy $G$ of a pure substance is described by Eq. 4.3.

$$G = H - TS \tag{4.3}$$

While enthalpy $H$ and entropy $S$ can be expressed with $C_p$ according to Eq. 4.4 and Eq. 4.5, where $\Delta H^0_{f,298}$ and $S^0_{298}$ are the standard formation enthalpy and entropy at standard conditions

(298 K, 1 atm), respectively. $\Delta H_{298}$ is the formation enthalpy of the compound calculated based on the standard element reference state, which is defined at 1 atm and room temperature (298.15 K). When the heat capacity $C_p$ in the temperature range of 0-298 K is known, the value of $S_{298}$ can be obtained from Eq. 4.6

$$H = H_{298} + \int_{298}^{T} C_p \cdot dT \quad 4.4$$

$$S = S_{298} + \int_{298}^{T} \frac{C_p}{T} \cdot dT \quad 4.5$$

$$S_{298} = \int_{0}^{298} \frac{C_p}{T} \cdot dT \quad 4.6$$

After combining the Eq. 4.3, 4.4 and 4.5 into Eq. 4.7, it can be seen that $\Delta H_{298}$, $S_{298}$, and $C_p$ are the necessary information to complete the Gibbs energy function for the stoichiometric compounds.

$$G = H_{298} - TS_{298} + \int_{298}^{T} C_p \cdot dT + T \int_{298}^{T} \frac{C_p}{T} \cdot dT \quad 4.7$$

$C_p$ can be described as a polynomial of temperature, as shown in Eq. 4.8.

$$C_p = A + B \cdot T + C \cdot T^{-2} + C \cdot T^2 + C \cdot T^3 + \cdots \quad 4.8$$

When substituting the $C_p$ in Eq. 4.4, 4.5 and 4.7 with Eq. 4.8, it can be seen that $G$, $H$ and $S$ can all be described as polynomial of temperature, and their coefficients are related to the coefficients in Eq. 4.8. Therefore, the coefficients in Eq. 4.8 are essential for the determination of the Gibbs energy function for pure substances.

Meanwhile, the phase change temperatures and phase change enthalpy are significant information to recognize the Gibbs energy between different phases. The phase change enthalpy information influences the entropy of a phase, which is the negative slope of $G - T$ curves. Therefore, the Gibbs energy between different phases becomes distinguished and comparable even if the $C_p$ expression for different phases of a substance are the same in the database. For example, the enthalpy $H'$ and entropy $S'$ of the second solid phase is shown in Eq. 4.9 and Eq. 4.10, where $T_{tr}$ and $\Delta_{tr}H$ mean the phase change temperature and phase change enthalpy. $H'_{298}$

and $S'_{298}$ are the standard enthalpy and entropy for the second phase. Generalizing this to other phases, different phases have different standard enthalpy and entropy.

$$H' = H'_{298} + \int_{298}^{T_{tr}} C_p \cdot dT + \Delta_{tr}H + \int_{T_{tr}}^{T} C_p \cdot dT \quad 4.9$$

$$S' = S'_{298} + \int_{298}^{T_{tr}} \frac{C_p}{T} \cdot dT + \frac{\Delta_{tr}H}{T_{tr}} + \int_{T_{tr}}^{T} \frac{C_p}{T} \cdot dT \quad 4.10$$

### 4.2.2 Solution phases

For the solution phases, the coefficients of the Gibbs energy function $G(T, x_i)$ should be defined, the form of the G energy of a solution depends on the model used. The ideal solution model is the model for an ideal mixing, where the species are randomly mixing and the interactions between them are not considered. For a real solution, the interaction between solution species and the structure effect cannot be ignored. Therefore, variant solution models were developed for the description of the Gibbs energy of a solution phase. The regular solution is the simplest case of a non-ideal solution model. Moreover, there are sub-lattice model described using compound-energy formalism (CEF) [169], modified quasichemical model (MQM) [170–174] and modified associate species model (MAM) [175], cell model [176], ionic model, etc. The sub-lattice model/ CEF [169] is applied when considering the sublattice structure of the solutions. The MQM [170–174] and MAM [175] are widely used for the description of the liquid solution phase with strong interactions, like the molten oxides or salts, both of them consider the short-range order in the liquid solution.

The general description of the Gibbs energy of a solution is given in Eq. 4.11 and 4.12, where $x_i$ means the mole fraction of component $i$, $G_i^0$ means the Gibbs energy of the pure component $i$, $T$ is the temperature in K and $R$ is the gas constant, $G^E$ is the excess Gibbs energy, $\Delta_{mix}G$ is the mixing Gibbs energy between the species.

$$G = \sum x_i G_i^0 + \sum RT(x_i \ln x_i) + G^E \quad 4.11$$

$$\Delta_{mix}G = \sum RT(x_i \ln x_i) + G^E \quad 4.12$$

$G^E$ is zero for the ideal solution, the driving force of solution formation comes only from the entropy effect $R(x_i \ln x_i)$. $G^E$ of the regular solution is given in Eq.4.13, the influence of the mixing enthalpy is introduced. The $\alpha$, a dimensionless parameter, indicates the comparison of energy between interaction $ii$, $jj$ and $ij$. If $\alpha > 0$, the mixing is endothermal, which means that the interaction of $ii$ and $jj$ are more favorable than $ij$. If $\alpha < 0$, the mixing is exothermal, which means the interaction of $ij$ is more favorable than $ii$, $jj$.

$$G^E = H^E = \sum_i \sum_{j>i} \alpha x_i x_j \qquad 4.13$$

In the regular solution model, the $\alpha$ parameter in Eq. 4.13 is a constant. In the real solutions, the temperature influence is introduced in the excess Gibbs energy. This makes sense because the ratio of interaction energy between different species $ij$ relative to that of the same species $ii$, $jj$ in the solution can change with temperature. When $\alpha$ is described in the polynomial form of the temperature $Q_{ij}(T)$, the expression of the excess Gibbs energy can be written in the simple polynomial form.

$$G^E = H^E = \sum_i \sum_{j>i} Q_{ij}(T)\, x_i x_j \qquad 4.14$$

Besides the simple polynomial form, the Legendre and Redlich-Kister polynomial [177] can be used to describe the excess Gibbs energy. The Redlich-Kister polynomial (shown in Eqs. 4.15 and 4.16) is used especially for the expansion series, where $L_{ij}^{(v)}(T)$ is the empirical coefficient between phase components $i$ and $j$. When only parameter $L_{ij}^{(0)}$ and coefficient $A$ are included, the Eq. 4.15 is the same as Eq. 4.13.

$$G^E(T, x_i) = \sum_i \sum_{j>i} x_i x_j \sum_v^{n_{ij}} L_{ij}^{(v)}(T)\left(x_i - x_j\right)^v, v = 0, 1, 2 \ldots \qquad 4.15$$

$$L_{ij}^{(v)} = A + BT + CT\ln(T) + DT^2 + ET^3 + F/T \qquad 4.16$$

There are three different ways to extrapolate the Gibbs energy from three binary systems to a ternary system: Kohler model, Kohler/Toop model and Muggianu model, as shown in Figure 4-3. The comparison of these models was described by Pelton [178] in detail.

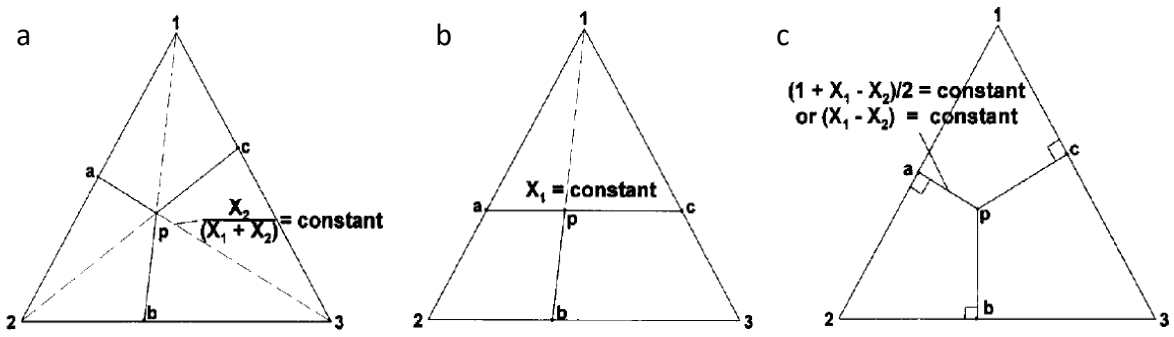


Figure 4-3. Three geometric models for estimating ternary thermodynamic properties from optimized binary data: a) Kohler model, b) Kohler/Toop model and c) Muggianu model [178].

If necessary, ternary and quaternary excess Gibbs energy may also be modelled, as Eqs. 4.17 and 4.18, $L_{ijk}(T)$ and $L_{ijkl}(T)$ are expressed in the same way as $L_{ij}^{(v)}$ in 4.16.

$$G^E = \sum_i \sum_{j>i} \sum_{k>j} x_i x_j x_k \, L_{ijk}(T) \qquad 4.17$$

$$G^E = \sum_i \sum_{j>i} \sum_{k>j} \sum_{l>k} x_i x_j x_k x_l \; L_{ijkl}(T) \qquad 4.18$$

***Sub-lattice model/compound-energy formalism (CEF)***

In this work, the sub-lattice model/compound-energy formalism (CEF) [169] is used for the description of solid solutions, where the structure of the solid solutions is taken into consideration. The random mixing of species on each lattice is assumed for the sub-lattice model/CEF [169]. A two-sublattice solution $(A,B)_k(C,D)_l$ is taken for the explanation of the Gibbs energy description, where ions A and B are in the same sublattice, ions C and D are in another sublattice, k and l are the stoichiometric coefficients of the different sublattices equivalent to that in a pure substance formula. The end-members of this solution are $A_kC_l$, $B_kC_l$, $A_kD_l$, $B_kD_l$. The site fractions of the ions in each sublattice are shown in Eq 4.19 [179].

$$x_A = \frac{n_A}{n_A+n_B}, x_B = \frac{n_B}{n_A+n_B}, x_C = \frac{n_C}{n_C+n_D}, x_D = \frac{n_D}{n_C+n_D} \qquad 4.19$$

The Gibbs energy of the solution is described in Eqs. 4.204.21 and 4.22 [179]. The random mixing of the ions in each sublattice is reflected in $G^{conf}$ in Eq. 4.21. The interaction of the ions in the same sublattice plays an important role in the description of the excess Gibbs energy $G^E$.

$$G = x_A x_C G^0_{A_kC_l} + x_A x_D G^0_{A_kD_l} + x_B x_C G^0_{B_kC_l} + x_B x_D G^0_{B_kD_l} + G^{conf} + G^E \qquad 4.20$$

$$G^{conf} = RT[k(x_A lnx_A + x_B lnx_B) + l(x_C lnx_C + x_D lnx_D)] \quad 4.21$$

$$G^E = \sum_a \sum_{b\neq a} \sum_c x_a^i x_b^j x_c L_{a,b//c}^{ij} + \sum_a \sum_c \sum_{d\neq c} x_a x_c^i x_d^j L_{a//c,d}^{ij} + \sum_a \sum_{b\neq a} \sum_c \sum_{d\neq c} x_a^i x_b^j x_c^k x_d^l L_{a,b//c,d}^{ijkl} \quad 4.22$$

***Modified associate species model***

In this work, the modified associate species model [175] is used to describe the liquid solution phase, which is basically an one-lattice substitutional model with end-members and associate species. The short-range order is considered in this model by introducing the associate species. Due to agglomerations of the ions in a certain composition, associate species are considered to be formed in the liquid phase. Interaction parameters between the species are introduced for description of the non-ideal mixing properties of the solution.

The associate species approach accurately represents the thermodynamic behavior of very complex chemical systems, and it accurately predicts the activities of components in metastable equilibrium glass phases [175]. It was successfully applied for oxide [180] and salt melts [10,33].

In the present work, this model will be applied for the liquid phase. The Gibbs energy of the solution phase is described using Eq. 4.11, where the excess molar Gibbs energy $G^E$ is described with Redlich-Kister polynomial mentioned in Eq. 4.15 and 4.16. For the assessment of the ternary systems in this work, the Muggianu model was taken.

## 4.3 Calphad method

Calphad (Calculation of Phase Diagrams) method is widely used for the development of thermodynamic databases and for the calculation and prediction of the phase equilibria and other thermodynamic properties. It was first introduced by Kaufmann and Bernstein [181]. The Calphad approach can be performed using different software, such as Thermo-Calc [182], Pandat [183], FactSage [9], etc. In this work, the assessment was performed with FactSage [9].

The thermodynamic database is a collection of Gibbs energy functions for each phase present in different systems. All other thermodynamic properties, such as enthalpy (H), entropy (S), activity (a), etc. are related to the Gibbs energy or its derivatives. Therefore, using the thermodynamic database, one can get the map of the whole system (phase diagram and other

thermodynamic properties) with several keywords (thermodynamic parameters). There are many different thermodynamic databases for various systems, such as SGTE (Scientific Group Thermodata Europe) [184] for metallic systems (alloys), FTsalt database [9] for salt system, etc. For thermodynamic calculations of different systems, the selection of proper databases is quite essential. In different databases, the solution description might be based on different models.

For the calculation of some systems, the commercial databases are not complete and accurate enough, which will affect the accuracy of calculations and predictions. For example, in case a phase is not defined in the database, it will be absent in the comparison of Gibbs energy between different phases, and it will not be calculated, for instance, the phase will not appear in the phase diagram. During the development of the new database, once a phase is detected experimentally, the Gibbs energy of this phase should be added into the database. In this case, the improvement of the Gibbs energy description enhances the accuracy of calculation and prediction of the phase diagram and other properties. The enrichment and accuracy of experimental data will drive the integrity of the database.

According to the Calphad method, the Gibbs energy functions of all phases in the system will be determined using appropriate models for all solution phases and stoichiometric compounds. The corresponding Gibbs energy coefficients discussed in the previous chapters are optimized using appropriate thermodynamic programs. The assessment is performed using all available experimental information on the system (phase equilibria, thermodynamic properties). Agreement between the measured and calculated values should be achieved.

## 4.4 Factsage

FactSage 8.1 [9] is the software used for calculation and prediction of the thermodynamic properties of the various systems (e.g. oxide and salt mixtures, alloys, intermetallic compounds, gases, etc.) depending on the chemical composition, temperature, pressure. It is operated in the MS Windows operation system. There are many different modules within the software, while in this work, *Compound*, *Solution*, *Equilib*, *Phase diagram* and *OptiSage* are mainly used. *Equilib* and *Phase diagram* are suitable for thermodynamic calculations, while *OptiSage* is used for the database development.

The thermodynamic information of the pure compounds (LiCl, NaCl, KCl, $Li_2CO_3$, $Na_2CO_3$ and $K_2CO_3$) and intermediate compounds ($LiKCO_3$ and $LiNaCO_3$) are stored in the *Compound* module. Thermodynamic information of the liquid and solid solution phases is stored in the *Solution* module. The solution model can be selected for the building of the solution. The solution end-members are defined and their thermodynamic properties are related with those on the pure substance stored in the *Compound* module. The extrapolation ways from the binary systems to the ternary system can also be selected.

Through the Gibbs energy minimization algorithm, the *Phase diagram* module can calculate various types of phase diagrams, the *Equilib* module is able to predict the thermodynamic properties of the system under defined conditions ($x_i$, T, p). In both modules, the phases from different databases (if available) can be selected by the users, also the states of the phase can be selected, like standard state or possible miscibility gap. In the *Equilib* module, the initial conditions can be set in different ways according to the calculation requirement. Many thermodynamic properties can be calculated, for example, the composition dependence of mixing enthalpy at certain temperature, enthalpy increment of the mixture and activity of the component in the solution. In the *Phase diagram* module, the various types of the phase diagram can be chosen, for example, the most used temperature-composition phase diagram, the projection of the liquidus surface, and isothermal cross sections of the ternary and reciprocal system.

*OptiSage* is used to optimize the Gibbs energy parameters. Firstly, a ChemSage file (.dat) is created in the *Phase diagram* module or the *Equilib* module, which includes the initial dataset of Gibbs energies for all phases. Then, this file is read in the *OptiSage* module. The experimental data from the literature and our own experiments are created in form of a dataset in OptiSage. After selecting the parameters, those will be optimized, the optimization is performed with the Bayesian optimization approach until a converged solution is obtained and a good agreement between the experimental and calculated data is achieved.

## 4.5 Optimization process

### 4.5.1 Stoichiometric compounds assessment

For the Gibbs energy of pure substances and intermediate compounds, the assessment work is to find proper coefficients of the function $G(T)$ (see Eq. 4.7).

In this work, the standard values $\Delta H^0_{f,298}$ and $S^0_{298}$ of the pure substances are normally taken from the SGPS database [25]. These values of the intermediate compounds are modified along with the assessment of the corresponding salt system.

The heat capacity, $C_p$, can be measured experimentally. However, for some substances, there is no experimental data available, especially in the low temperature range. In this case, ab initio calculated data can also be taken as a reference.

The coefficients in temperature polynomial of $C_p$ (Eq. 4.8) can be obtained by non-linear fitting of the experimental data or ab initio data ($C_v$) by using Origin software. Generally, it is not practical to describe the $C_p$ of one phase in the whole temperature range by one function, therefore, it was always described in different temperature ranges with different functions. However, in the assessment of the polynomial, the $C_p$ curve should be smoothly connected at breakpoints of different temperature ranges.

In a temperature range where no experimental data are available, the $C_p$ of the intermediate compound can be calculated by Neumann-Kopp rule [185]. The Neumann-Kopp $C_p$ calculation of $LiKCO_3$ and $LiNaCO_3$ are shown in Eqs. 4.23 and 4.24, which is used for the comparison with the experimental data and as reference for the low temperature estimation.

$$C_{p_{LiKCO_3}} = 0.5\, C_{p_{K_2CO_3}} + 0.5\, C_{p_{Li_2CO_3}} \quad 4.23$$

$$C_{p_{LiNaCO_3}} = 0.5\, C_{p_{Na_2CO_3}} + 0.5\, C_{p_{Li_2CO_3}} \quad 4.24$$

For pure substances, polynomials of $C_p$ in different temperature ranges for all phases (solid modifications and liquid phase) need to be described. For the intermediate compounds, the $C_p$ of the solid modifications need to be described, the liquid phase is described only if it is assumed as associate species in the liquid phase. In the database, for all stoichiometric compounds, the

$C_p$ information for the different solid modifications are kept the same (if there are more than one solid modification).

It is impossible to measure the heat capacity of the solid phase after melting and of the liquid phase before melting. However, if for example an intermediate compound has a higher melting point than its constituents, $C_p$ of the solid constituents above their melting points is needed. Analogously, calculation of $C_p$ for a molten eutectic composition requires data on $C_p$ of molten constituents below their melting point. Therefore, in the database, the $C_p$ of a solid phase above the melting point is considered to be the extrapolation of the solid phase at the melting temperature and kept constant. The $C_p$ of the liquid phase below the melting point is considered to be the extrapolation of the liquid phase above the Kauzmann temperature, and the same as the solid phase below the Kauzmann temperature. The Kauzmann temperature is introduced for the supercooled liquids and applies to the solution phase [18]. In the supercooled state, the heat capacity of the liquid is considered to be the extrapolation of the liquid phase and is higher than that of the solid phase. Therefore, when the temperature is decreasing, the entropy of the liquid phase decreases faster than the solid phase. To avoid the situation where the entropy of the liquid is lower than that of the solid phase, the Kauzmann temperature was defined as the temperature where the absolute entropy of the liquid phase reaches that of the solid phase and it was introduced in the PCM database [20,21].

### 4.5.2 Solution phase assessment

The solution phase optimization can be done manually or by the *Optisage* module. The optimization is based on all available experimental data simultaneously, including phase diagram, mixing enthalpy, enthalpy increment, activity data, etc.

In the course of optimization, thermodynamic functions of pure liquid and solid salts are remained unmodified. Their data are adopted from the commercial databases or modified during the previous optimization step and will not be modified during the next step of assessment. The main part of the work is to assess the binary interaction parameters $L_{ij}^{(v)}(T)$ in the liquid and solid phases in order to provide a better agreement between the measured and calculated values on

the phase equilibria. Generally, for the liquid solution, only two interaction parameters, $L_{ij}^{(0)}(T)$ and $L_{ij}^{(1)}(T)$, need to be optimized. The optimization was done via searching the suitable corresponding A and B in 4.16, with the high order parameters (C, D, etc.) kept at 0. In some cases, parameter C is also necessary to be added in order to get better results. The optimization of the thermodynamic parameters is carried out until there is agreement between the experimental and the predicted values. The optimization of these parameters was performed using the FactSage software [9].

For the optimization of the liquid phase in this work, pure liquid salts $Alk_2CO_3$ and AlkCl (Alk = Li, Na, K) are considered as solution components without any additional associate. The stoichiometry of carbonates was modified in accordance with Besmann and Spear [175], where the stoichiometry of the end-members is chosen in order to obtain two non-oxygen atoms per formula unit, allowing equal weighting with regard to each species ideal entropic contribution. In the present work, AlkCl remains unchanged and $Alk_2CO_3$ becomes $Alk_2CO_3$/1.5, meaning that each atom stoichiometry is divided by 1.5.

For the solid solution phase, in the case of continuous solubility, pure solid phases $Alk_2CO_3$ and AlkCl (Alk=Li, Na, K) are considered as solution components without any modification of their Gibbs energy. In this case, the interaction parameters are optimized to describe the correct equilibria between solid and liquid phases. For the limited solubility, the Gibbs energy of the dissolved compound is modified in order to reproduce the solubility limit in the phase diagram. Interaction parameters can also be added for better description of the corresponding solution phases.

# 5 Experimental results

## 5.1 $Li_2CO_3$

### 5.1.1 Phase change temperature

The melting temperature of $Li_2CO_3$ was measured by different authors [25,35,36,39–42,45,186,187] and was proposed to be in the temperature range of 993-1005 K.

The results of preliminary DTA measurements are shown in Figure 5-1a. It can be seen that during first heating up to 923 K of the raw material $Li_2CO_3$ a small peak appeared at 689 K, in the second cycle its magnitude decreased and it disappeared completely in the third cycle. This temperature (689 K) is close to the reported temperature of the solid-solid phase transition mentioned in the literature [35,37,38]. If this peak in the heating curve does reflect this solid-solid phase transition, it should be reproducible in each cycle. Therefore, the peak is not considered to be caused by a solid-solid phase transition of $Li_2CO_3$, and instead it could be attributed to the presence of some impurities, which vanish after heating. Figure 5-1b shows the DTA curves of $Li_2CO_3$ after annealing at 923 K in $CO_2$ atmosphere for 1 h, where the small peak at 689 K disappeared, that is in agreement with the experimental results reported by Janz et al. [39] and Rolin and Recapet [40]. The melting temperature was measured to be 999 K in this work.

Figure 5-2 demonstrates the 3D surface plots of the XRD signal dependence on temperature and its corresponding plan plots, where background and Cu-K$\alpha_2$ peaks were removed and the intensity is in square root scaling for clarity. The result shows that the raw material $Li_2CO_3$ contains LiOH as impurity at the initial state, indicated by the peaks occurring at 20.5 ° and 32.5 ° marked in Figure 5-2 with red LiOH. The initial LiOH content was quantified to be approx. 1 wt% and it was no longer detectable after heating to 723 K and did not reappear during cooling to room temperature. Subsequently, in the temperature range of 298-923 K, the $Li_2CO_3$ remained the same phase without solid-solid phase transformation. The corundum sample holder used for HTXRD contributes with weak characteristic $Al_2O_3$ reflections, marked with gray $Al_2O_3$ in Figure 5-2. The measured diffraction patterns match with the reported monoclinic crystal structure of $Li_2CO_3$ (space group C2/c, ICSD 100324) [188,189]. In summary, the high temperature XRD result

determines the LiOH impurity and confirms the absence of a solid-solid phase transition in the temperature range of 680-693 K, as reported elsewhere [36,40].

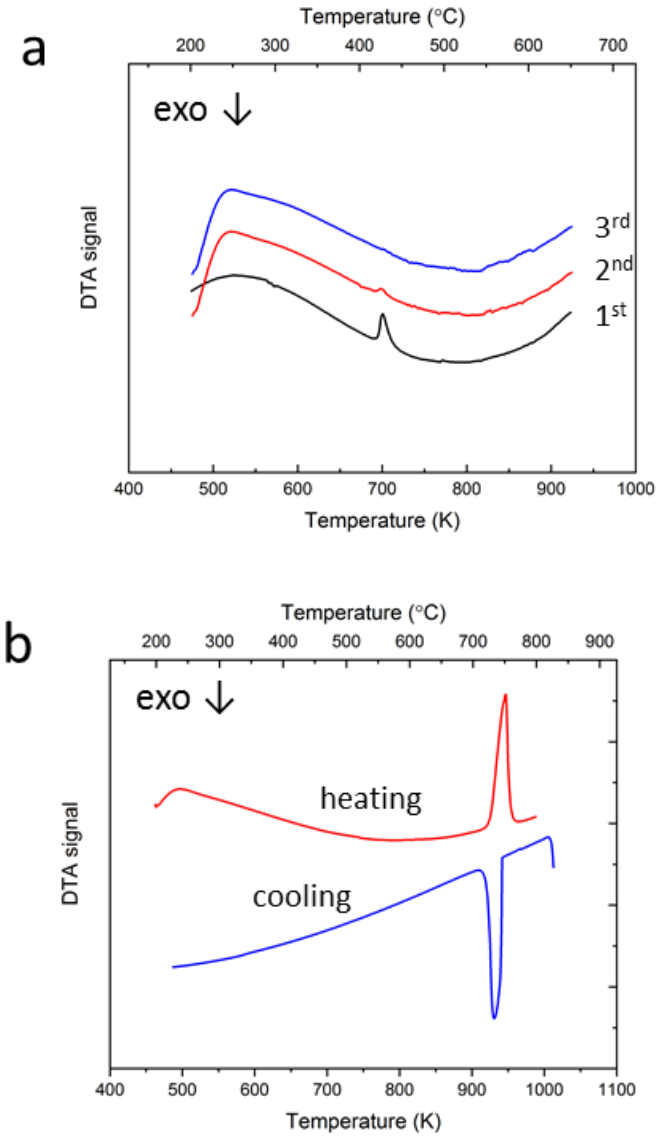


Figure 5-1. DTA curve of a) raw material $Li_2CO_3$ in open Pt crucible, b) $Li_2CO_3$ in closed Pt crucible after heating at 923 K in $CO_2$ atmosphere for 1 h.

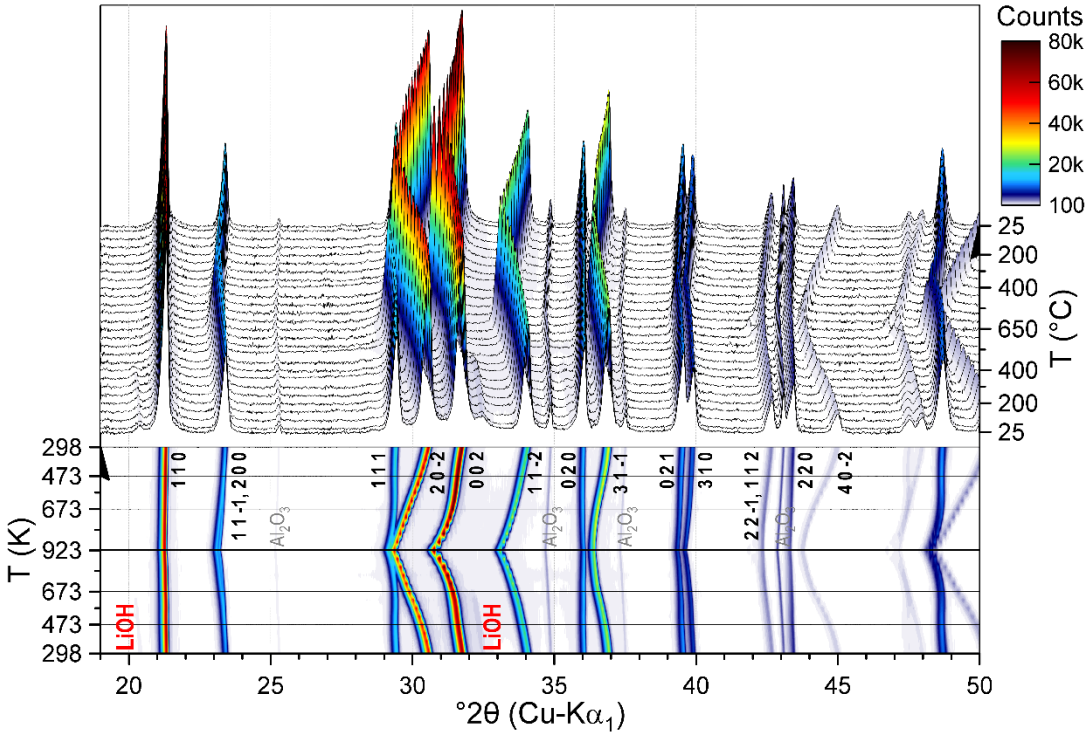


Figure 5-2. High temperature XRD of the raw material $Li_2CO_3$.

It is inferred that the reason why the presence of this impurity caused a peak at 689 K in the DTA curve is that LiOH and $Li_2CO_3$ form an eutectic, which was reported to be 692 K [190]. Disappearance of LiOH during the heating process is due to the evaporation of LiOH and the chemical reaction with $CO_2$ from air according to Eq. 5.1.

$$2LiOH + CO_2 \rightarrow H_2O + Li_2CO_3 \qquad 5.1$$

As shown in Figure 5-3a, $Li_2CO_3$ raw material loses mass when heated under Ar atmosphere, which is caused by the evaporation of LiOH. On the contrary, it gains mass when heated under $CO_2$, which is due to the reaction in Eq. 5.1. Correspondingly, the DTA peak at 689 K in Ar is larger than that under $CO_2$ gas in Figure 5-3b, which means there is less LiOH remained under $CO_2$ gas. Both the evaporation of LiOH and the reaction in Eq. 5.1 are continuous processes running over a wide temperature range and are not reflected in the DTA curve as peaks. The time required to remove LiOH depends on the holding time at high temperature and the original weight of the raw material.

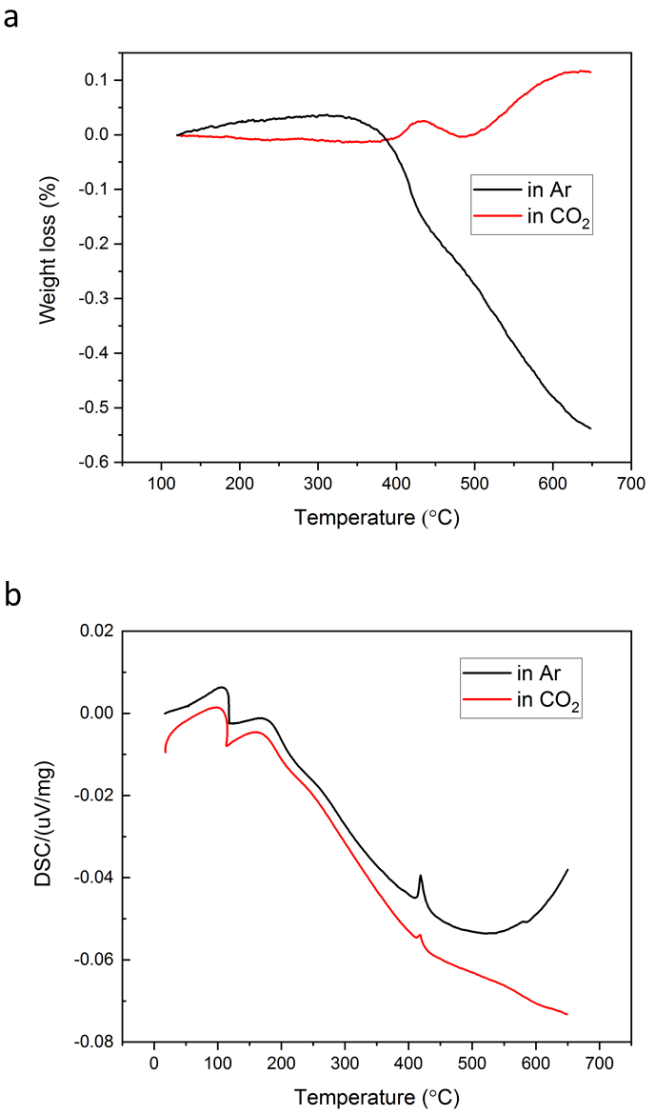


Figure 5-3. a) Comparison of the weight change of raw material $Li_2CO_3$ in Ar and $CO_2$ gas and b) corresponding DTA signal of $Li_2CO_3$ in Ar and $CO_2$ gas.

Therefore, the solid-solid phase transition detected in the previous measurements in the literature could also result from impurities. LiOH as impurity may stem from the raw material or be formed during the thermal process. For example, when $Li_2CO_3$ is heated in air above the melting temperature $Li_2O$ will be formed due to the decomposition reaction of $Li_2CO_3$, and when it is cooled down to room temperature the moisture in the air will lead to the presence of LiOH because $Li_2O$ reacts extremely easily with water. This point of view was also put forward by Smirnov et al. [191]. In their research, no peak was reported to appear at temperatures around

683 K on the DTA curve for the mixture of $Li_2CO_3$ and $Li_2O$. However, after holding the mixture under air, the peak appeared at 683-693 K due to the reaction between $Li_2O$ and $H_2O$.

As indicated by the peak shifts in the surface plots (see Figure 5-2), the temperature dependence of the $Li_2CO_3$ lattice parameters have a significant anisotropy, which is also demonstrated in Figure 5-4. Note the different scaling for *a*, *b* and *c*, where the lattice parameters *a* and *c* are changing within some tenths of an Å, while the changes of lattice parameter *b* are two orders of magnitude lower. Additionally, in contrast to the continuous increase of the lattice parameters *a* and *c* during the heating process, the lattice parameter *b* firstly increases until around 598 K and then decreases. At around 798 K, angle β also experiences this kind of change, which is considered as phase transition, as reported by Sergeev et al. [24]. Therefore, according to the present HTXRD study, solid-solid phase transitions occur at around 598 K and 798 K, respectively, while the crystal structure is kept monoclinic. The small and smooth continuous variation of lattice parameter *b* and angle β explains why the thermal effect of these solid-solid phase changes for $Li_2CO_3$ is so slight that it cannot be detected by DTA (Figure 5-1). Besides, this phase transition is different from the reported thermal effect at 623 K detected by Reisman [35] using DTA in the absence of $CO_2$, which was clarified to be caused by impurities but adopted in the thermodynamic tables of Barin [192] and used as solid-solid phase transition temperature in the NIST-JANAF tables [193] and the commercial databases SGPS [25] and FTsalt [45].

High temperature XRD of $Li_2CO_3$ was conducted by Khlapova and Kovaleva [38], and three structure modifications of $Li_2CO_3$ were claimed to be found. However, when comparing XRD pattern of these phases with the reported $Li_2CO_3$ structure (sg: C2/c, ICSD 100324) [188], it can be seen that they agree well except for some additional peaks, which may be caused by impurities.

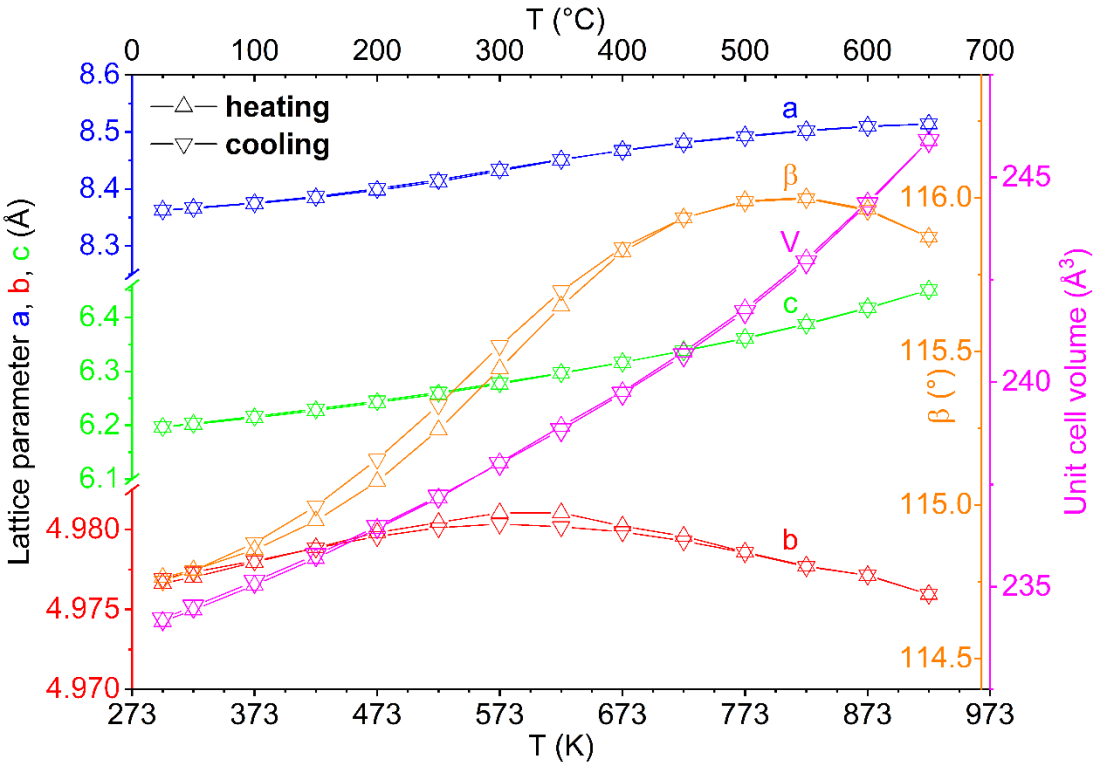


Figure 5-4. Temperature dependence of lattice parameters for $Li_2CO_3$.

### 5.1.2 Heat capacity

In the present work, the $C_p$ of $Li_2CO_3$ was measured in the temperature range of 140-923 K using three types of DSC mentioned in chapter 3 and the results are shown in Figure 5-5. The results obtained by different DSC devices agree well with each other within an error limit of ±7 J/(mol·K). Thermal effects, which were detected in the temperature range 250-300 K by Low_T DSC Netzsch, originate from the baseline of the sample holder and could not be avoided during the experiments. The absence of a peak at 689 K implies that no solid-solid phase transition occurred during heat capacity measurements in accordance with the results of Janz et al. [39]. An average value of $C_p$ was calculated based on the obtained results (black line in Figure 5-5).

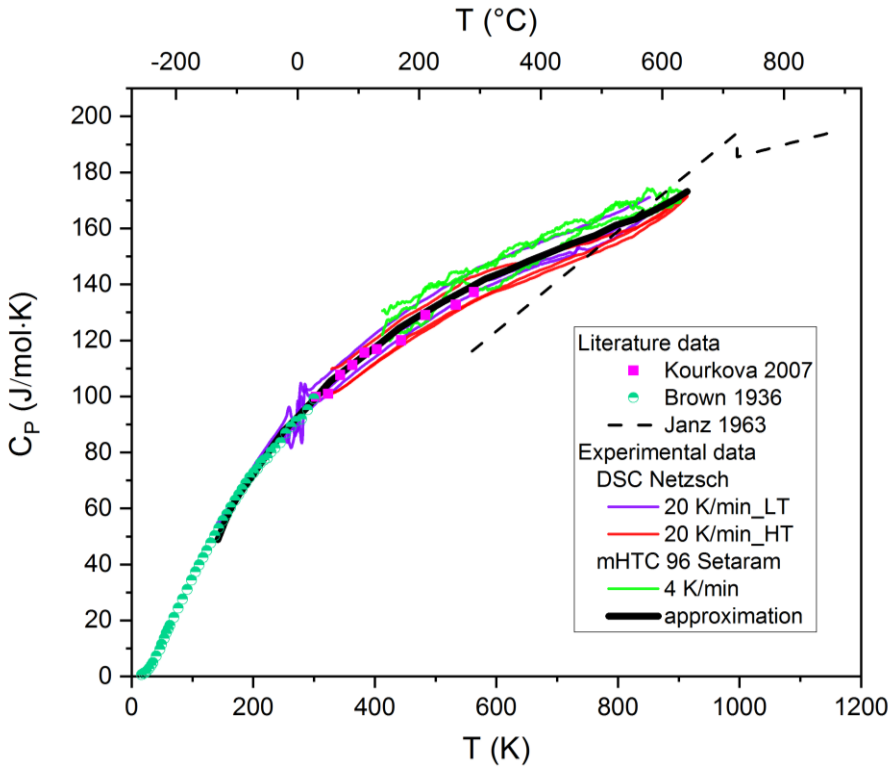


Figure 5-5. Literature values of the heat capacity of $Li_2CO_3$ and measured in this work

## 5.2 System $K_2CO_3$-KCl

As mentioned in Chapter 2, in order to verify the temperature of the eutectic temperature in the $K_2CO_3$-KCl system, the eutectic composition $0.38K_2CO_3$-0.62KCl was studied by DTA in the temperature range 100-667 °C. The measured eutectic temperature is 633 °C (Figure 5-6), which is close to the measurement of Amadori [109] (636 °C) and Bergman and Sementsova [107] (632 °C). The sharp peak in the heating and cooling curve indicate that the measured composition was quite close to the eutectic point.

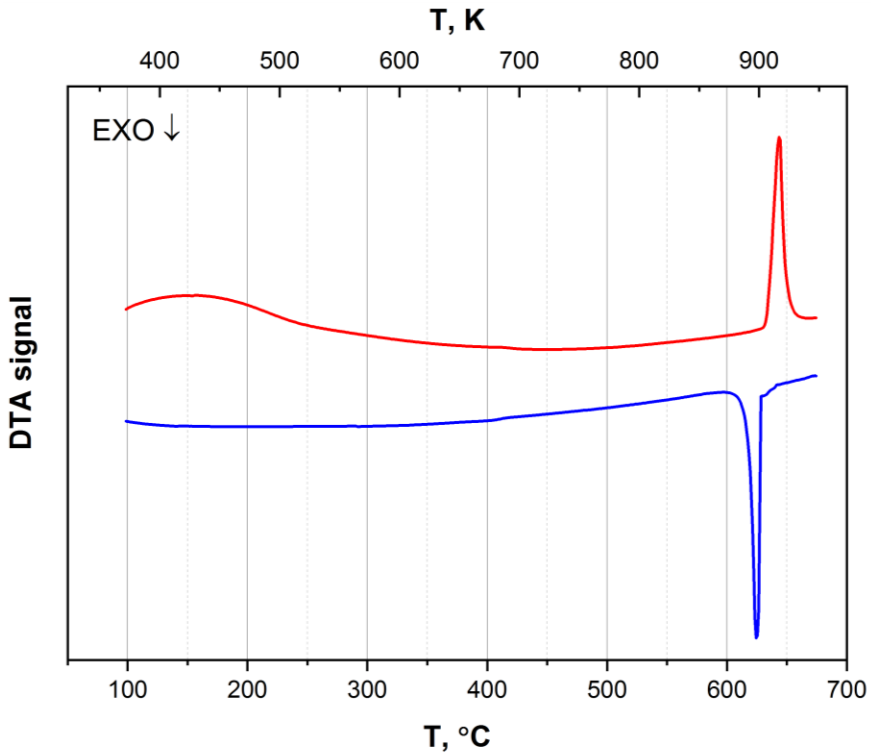


Figure 5-6. Heating and cooling DTA curve of $0.38K_2CO_3$-0.62KCl.

## 5.3 System $Na_2CO_3$-NaCl

The salt system $Na_2CO_3$-NaCl is a simple eutectic system, the phase diagram has been reported many times [108,109,114–116]. As a potential PCM material, the thermal stability of the eutectic composition of the NaCl-$Na_2CO_3$ system (0.55NaCl-0.45$Na_2CO_3$ in molar fraction) was checked by KEMS in this work. Due to the vaporization of NaCl in the measurement process, the composition of the samples changed. The activity of NaCl in the solid phase was measured for the mixture of the composition 0.47NaCl-0.53$Na_2CO_3$ at 665 °C, which is used as reference data for the thermodynamic parameter optimization in Chapter 6.

The melting temperature of the eutectic salt mixture was measured by DTA for the temperature calibration of the KEMS. The melting temperature of the eutectic mixture obtained by KEMS was 637 °C (Figure 5-7a), which is close to the result of 633 °C measured by DTA (Figure 5-7b). Therefore, the temperature uncertainty in KEMS is about ± 4 °C. Only the ion current of $NaCl^+$ was detected for the determination of the melting temperature. It is inferred that the temperature dependence of the ion current for other ions should be similar. The $NaCl^+$ ion

current increased when the sample was heated up (Figure 5-7a). There is an abrupt tipping point at the eutectic temperature. Above the eutectic temperature, 637 °C, the slope of the variation with temperature becomes larger due to the formation of the liquid phase.

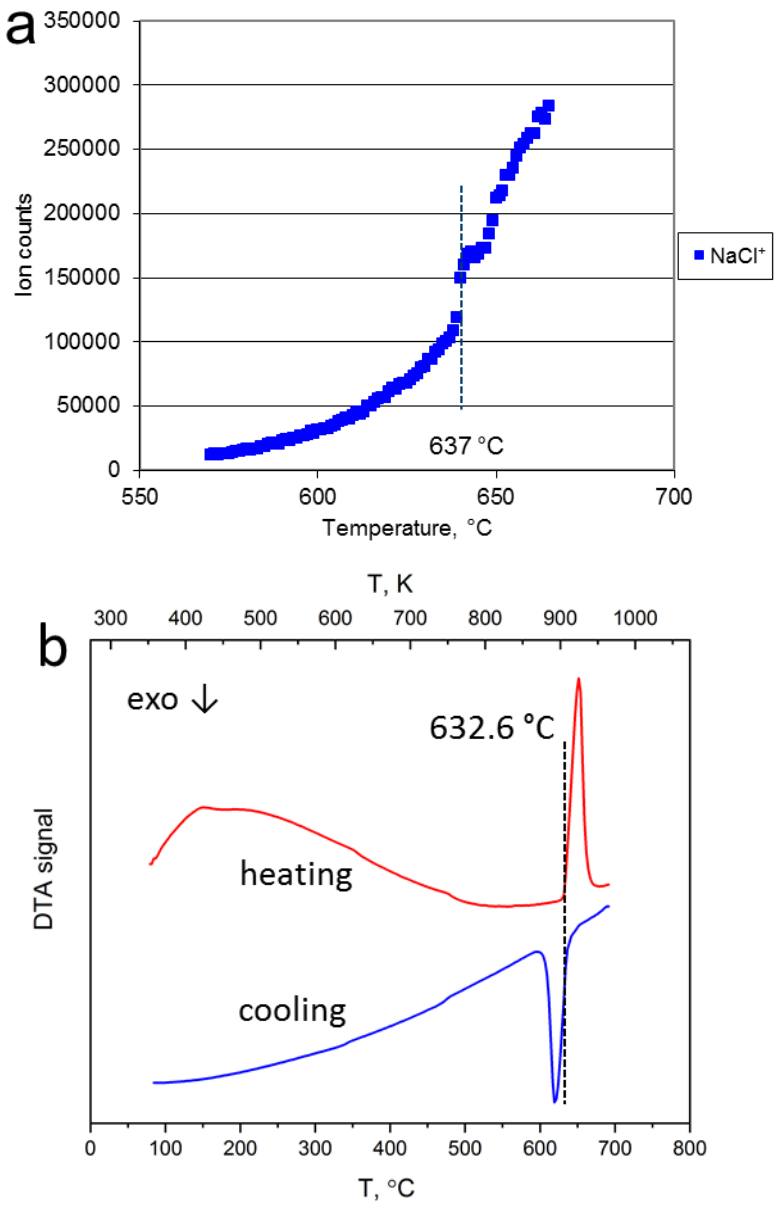


Figure 5-7. Melting temperature of the eutectic composition in the system NaCl-$Na_2CO_3$ measured by KEMS (a) and DTA (b).

For the thermal stability investigation, the types of ion species from the sample and the pure NaCl at 580 °C were determined (see Figure 5-8). The pure NaCl was taken as reference for the

measurement of the salt mixture. In Figure 5-8, it can be seen that $Na^+$ (m/z 23), $NaCl^+$ (m/z 58, 60), $Na_2Cl^+$ (m/z 81, 83) and $Na_3Cl_2^+$ (m/z 139, 141, 143) were detected at 580 °C both for NaCl and the eutectic mixture in the NaCl-$Na_2CO_3$ system, where m/z is the mass to charge ratio. The blue lines indicate the signals obtained when the samples are measured, and the pink lines represent the signals which come from the background. $CO_2^+$ (m/z 44, 45, 46) and ion species with m/z 28 (it might be $N_2$) were shown in the background signal, which stem from the environment.

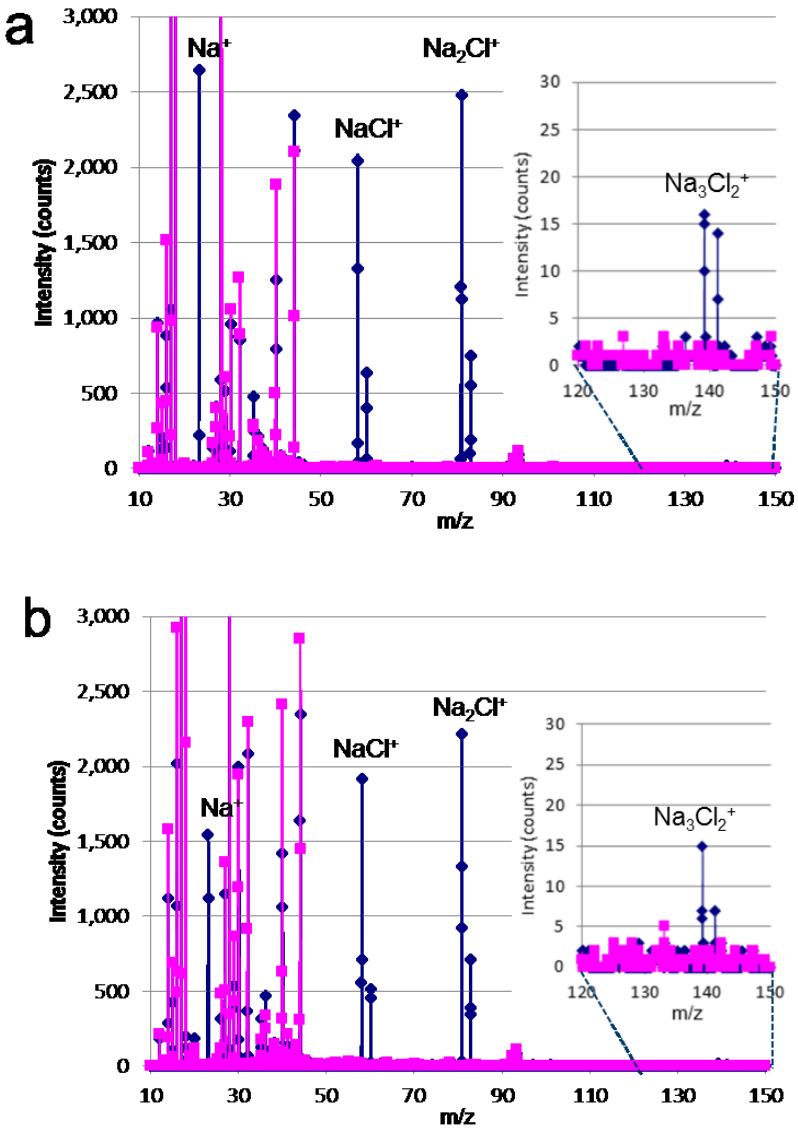


Figure 5-8. Ion species of eutectic composition in the system NaCl-$Na_2CO_3$ (a) and NaCl (b) determined by KEMS at 580 °C.

NaCl was reported to evaporate as NaCl, $Na_2Cl_2$ and $Na_3Cl_3$ molecules by Gorokhov et al. [194], while $Na_2CO_3$ was reported to be evaporated as Na, $CO_2$ and $O_2$ below 750 °C by Sergeev et al. [195], as shown in Eq. 5.2. Therefore, before the ionization, neutral gas precursors from the eutectic sample are assumed to be Na(g), NaCl(g), $Na_2Cl_2$(g), $Na_3Cl_3$(g), $O_2$(g) and $CO_2$(g). Among them Na(g) comes from the fragmentation of either $Na_2CO_3$ or NaCl.

$$Na_2CO_3 \rightarrow 2Na(g) + 1/2O_2(g) + CO_2(g) \quad 5.2$$

The ion species shown in Figure 5-8 were detected after the ionization of their neutral gas precursors. $Na^+$ was from the ionization of either Na(g) or NaCl(g), as shown in Eqs. 5.3 and 5.4. $NaCl^+$ was form the ionization of NaCl, $Na_2Cl^+$ and $Na_3Cl_2^+$ were from the ionization of $Na_2Cl_2$(g) and $Na_3Cl_3$(g) separately (Eqs. 5.6 and 5.7).

$$Na(g) + e^- \rightarrow Na^+ + 2e^- \quad 5.3$$

$$NaCl(g) + e^- \rightarrow Na^+ + Cl^* + 2e^- \quad 5.4$$

$$NaCl(g) + e^- \rightarrow NaCl^+ + 2e^- \quad 5.5$$

$$Na_2Cl_2(g) + e^- \rightarrow Na_2Cl^+ + Cl^* + 2e^- \quad 5.6$$

$$Na_3Cl_3(g) + e^- \rightarrow {Na_3Cl_2}^+ + Cl^* + 2e^- \quad 5.7$$

In Figure 5-9 the ion species of the isothermal measurement at 580 °C are indicated, after around 10 h, the signal was stable. Because the eutectic temperature of NaCl-$Na_2CO_3$ is around 638 °C, at 580 °C the eutectic sample is in solid state. NaCl and $Na_2CO_3$ coexist inside the cell, it can be seen from the comparison of Figure 5-9 (a) and (b) that the ion species in the gas phase almost stem from the vaporization of NaCl. And the amounts and ratio of different ions in the eutectic sample are similar to that in the pure NaCl. The slight difference is within the uncertainty range.

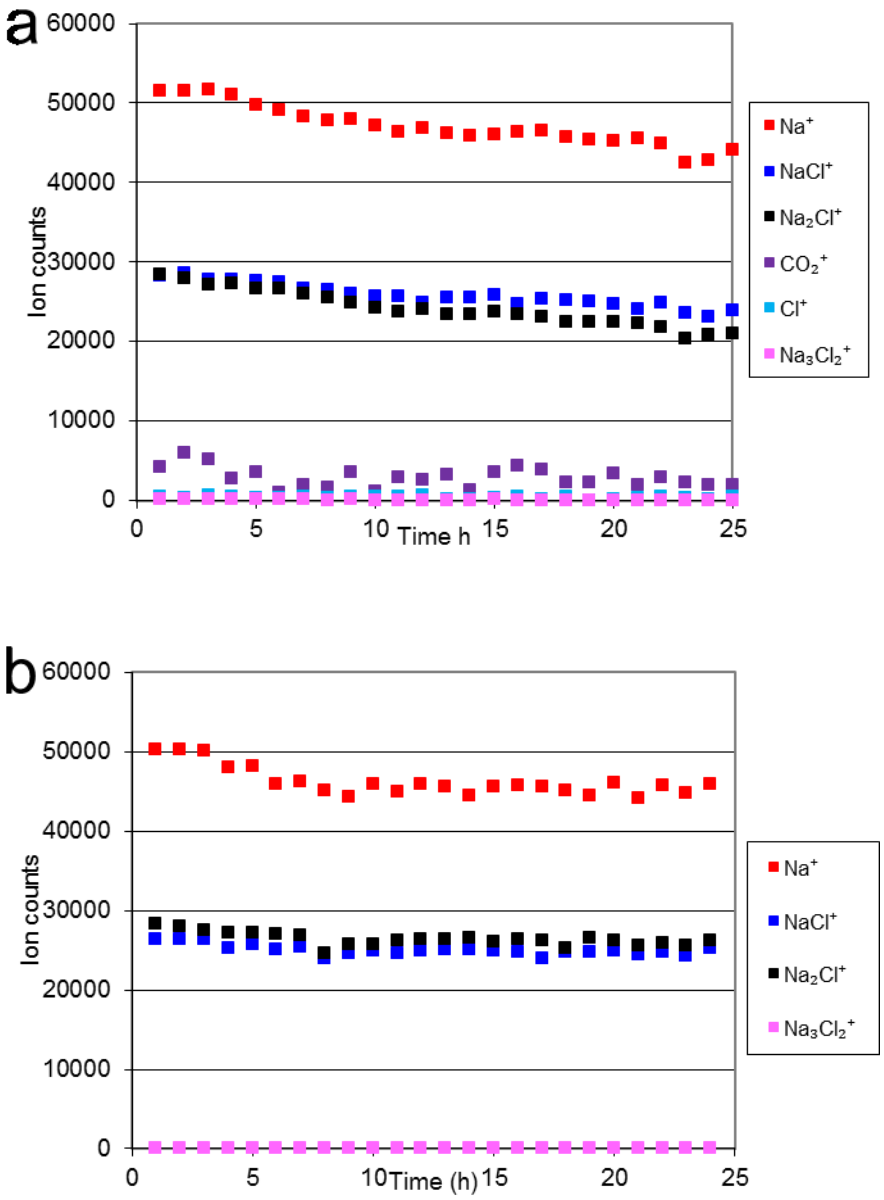


Figure 5-9. Isothermal results of ion species of eutectic composition in the NaCl-$Na_2CO_3$ (a) and NaCl (b) determined by KEMS at 580 °C.

According to the gas species activity over pure NaCl and $Na_2CO_3$ calculated with PCM and SGPS database at 580 °C and 665 °C, 5 Pa (Table 5-1), the amount of gas species Na and Cl should be much lower than that of NaCl and $Na_2Cl_2$. In the measurement, the amount of $Na^+$ is large, because the ionized NaCl partly fragmented into $Na^+$ and Cl*. According to the calculation result in Table 5-1, for the pure NaCl, the ratio of $Na_2Cl_2$ to NaCl at 665 °C (0.33) is larger than that at 580 °C (0.26). The ratio of $Na_2Cl^+$ to $NaCl^+$ calculated from the measurement is 1.4 (see Figure

5-12) and 1 at 660 °C and 580 °C, respectively. The different ratio of molecules and ions comes from the fragmentation of the molecules during the ionization in the measurement (see Eqs. 5.3-5.7).

Table 5-1. The gas species activity calculated with PCM and SGPS database at 5 Pa.

| | T, C | Activity of species in the gas phase | | | | | | |
|---|---|---|---|---|---|---|---|---|
| | | Na | Cl | NaCl | $Na_2Cl_2$ | $Na_3Cl_3$ | $CO_2$ | $O_2$ |
| NaCl | 580 | 5.65E-9 | 5.65E-9 | 6.86E-2 | 0.018 | 5.29E-5 | 0 | 0 |
| NaCl | 665 | 3.21E-7 | 3.21E-7 | 1.12 | 0.37 | 2.41E-3 | 0 | 0 |
| $Na_2CO_3$ | 580 | 4.65E-5 | 0 | 0 | 0 | 0 | 2.32E-5 | 5.81E-6 |
| $Na_2CO_3$ | 665 | 1.36E-3 | 0 | 0 | 0 | 0 | 6.81E-4 | 1.70E-4 |

An isothermal measurement of the eutectic composition in the NaCl-$Na_2CO_3$ and NaCl was carried out at 665 °C and the results were compared in Figure 5-10. It was noticed, that the signals of all species in the eutectic mixture decreased dramatically after 5 h (Figure 5-10a), while the signal of all species in the pure NaCl remained constant (Figure 5-10b). This is because after the isothermal measurement at 665 °C, the composition of the sample has changed. The vapor pressure of NaCl is much larger than that of $Na_2CO_3$, which is shown in Table 5-1 as well. Therefore, only $Na_2CO_3$ was left after the measurement. The weight change of the sample was recorded, and it showed a weight loss ratio of about 47 %. The initial mass ratio of NaCl was 41 %, which means that the NaCl was evaporated completely, and part of the $Na_2CO_3$ was also evaporated.

It is also noticed that the ratio of $Na_2Cl^+$ to $NaCl^+$ for the pure NaCl is significantly higher at 665 °C compared to the results detected at 580 °C, while in the mixture sample this ratio almost keeps the same before the dramatic decrease (see Figure 5-9 and Figure 5-10). For the pure NaCl, the different ratio between different temperatures is because the thermodynamic property of the molecules is influenced by the temperature. At higher temperature, more $Na_2Cl_2$ molecules are activated and evaporated from the solid salt. While in the mixture the NaCl is in the liquid phase, the vaporization of $Na_2Cl_2$ and $Na_3Cl_3$ molecules might be suppressed by the presence of $Na_2CO_3$.

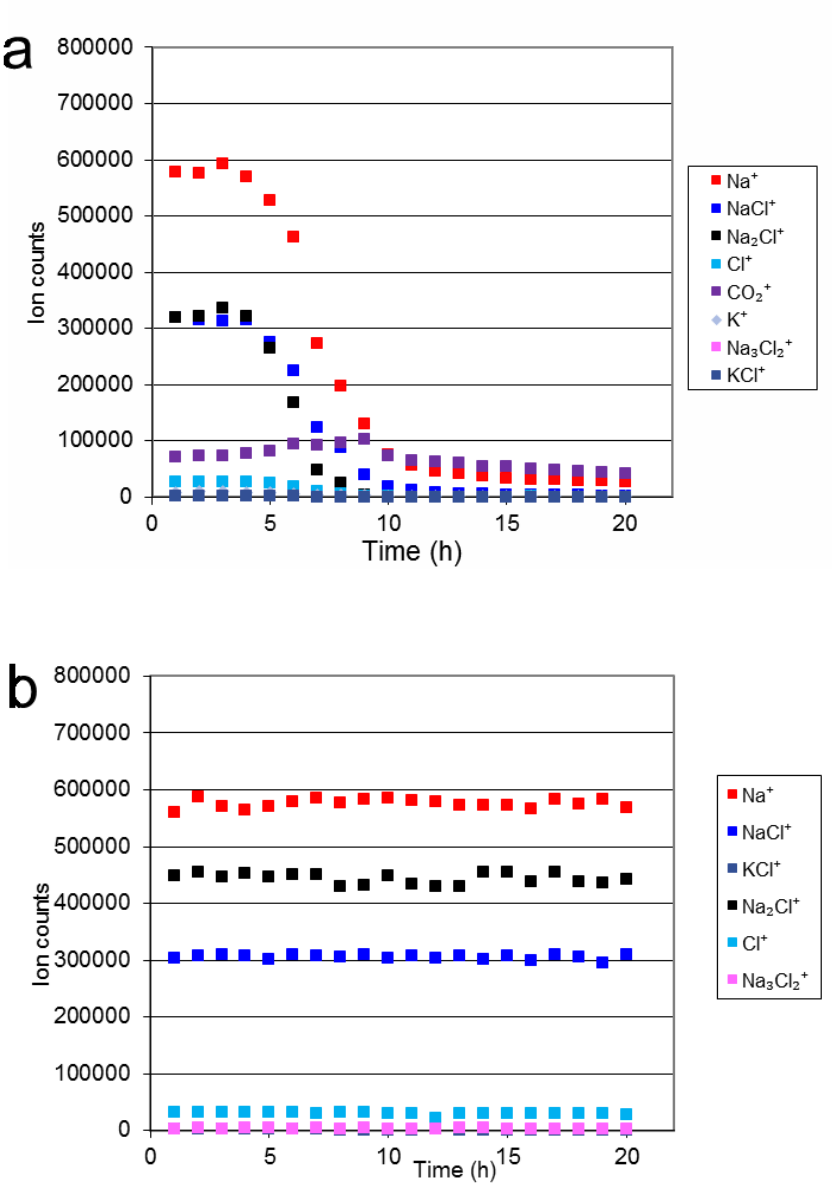


Figure 5-10. Isothermal results of ion species of eutectic composition in the NaCl-$Na_2CO_3$ (a) and NaCl (b) determined by KEMS at 665 °C.

When the temperature is kept at 665 °C, due to the continuous evaporation of NaCl, as shown in Figure 5-11, the concentration of NaCl in the whole sample changed from a to c, while the concentration of NaCl in the liquid phase changed from a to b, i.e., from the eutectic composition to 0.47NaCl-0.53$Na_2CO_3$, which is the composition at 665 °C in the liquidus line in the phase diagram.

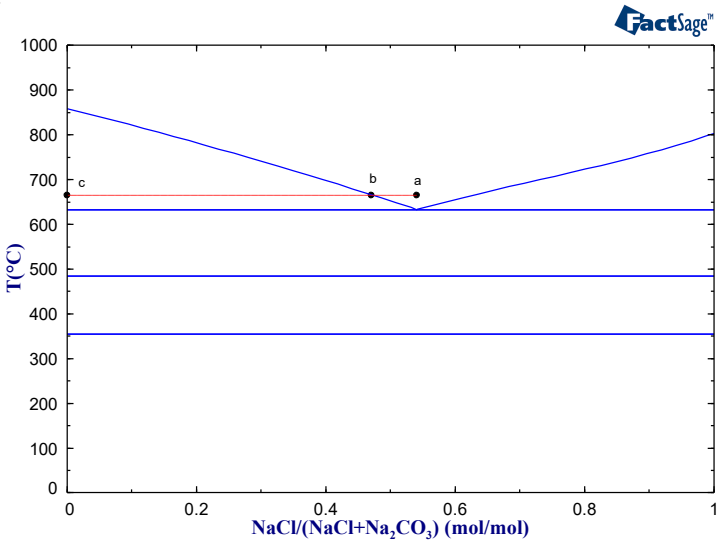


Figure 5-11. Composition change of the liquid phase demonstrated in the phase diagram.

Figure 5-12 shows the $J_{(Na_2Cl^+)}/J_{(NaCl^+)}$ and $J_{(Na_3Cl_2^+)}/J_{(NaCl^+)}$ ratios for different samples and pure NaCl, where $J_{NaCl^+}$, $J_{Na_2Cl^+}$ and $J_{Na_3Cl_2^+}$ mean the intensity of the ions detected over the eutectic mixture, while $J^o_{NaCl^+}$, $J^o_{Na_2Cl^+}$ and $J^o_{Na_3Cl_2^+}$ mean the ions intensity measured over pure NaCl. The activity of NaCl in the liquid phase at 665 °C can be further calculated according to Eqs. 5.8 and 5.9. The results from these two equations are 0.886 and 0.873 respectively, and the average value of 0.88 was taken. This activity calculated from the measurement results is taken as reference data for the modelling work in Chapter 6.

$$a = \left[\left(\frac{J_{Na_2Cl^+}}{J_{NaCl^+}}\right) / \left(\frac{J^o_{Na_2Cl^+}}{J^o_{NaCl^+}}\right)\right]^{\frac{1}{2}} = [1.1/1.4]^{\frac{1}{2}} = 0.886 \quad 5.8$$

$$a = \left[\left(\frac{J_{Na_3Cl_2^+}}{J_{NaCl^+}}\right) / \left(\frac{J^o_{Na_3Cl_2^+}}{J^o_{NaCl^+}}\right)\right]^{\frac{1}{3}} = [0.008/0.012]^{\frac{1}{3}} = 0.87356 \quad 5.9$$

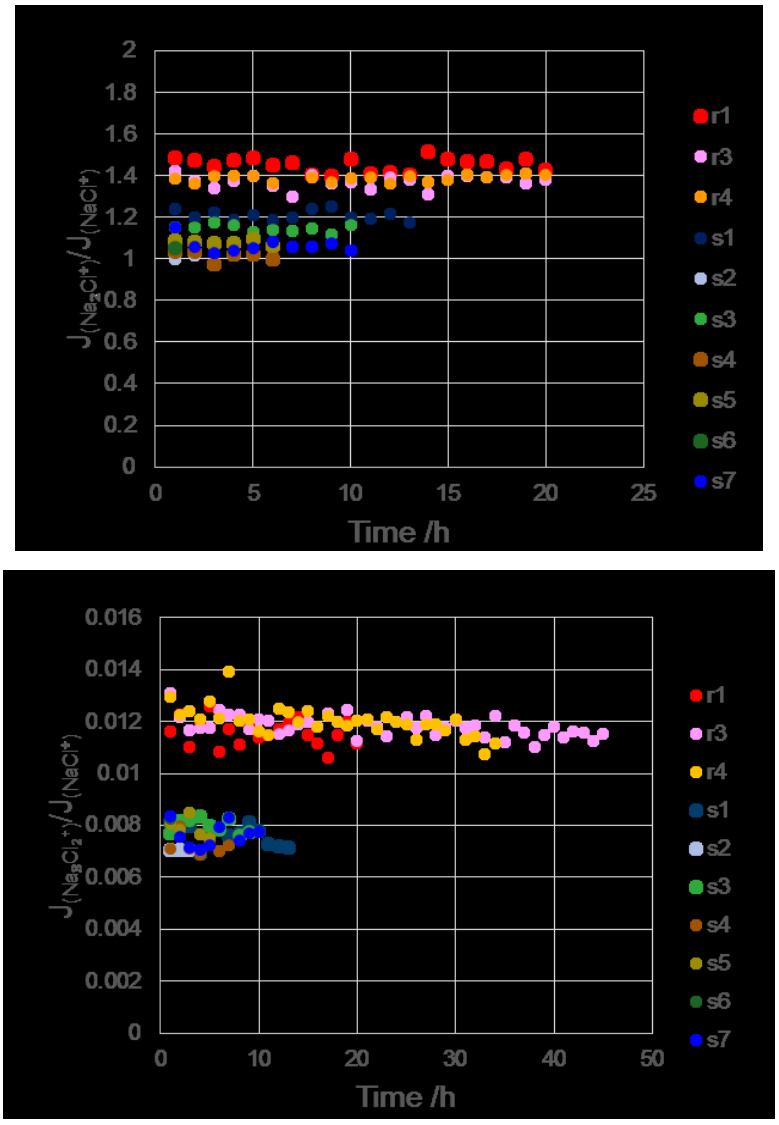


Figure 5-12. $J_{(Na_2Cl^+)}/J_{(NaCl^+)}$ at 665 °C (a) and $J_{(Na_3Cl_2^+)}/J_{(NaCl^+)}$ at 665 °C (b).

## 5.4 System $Li_2CO_3$-$Na_2CO_3$

The system $Li_2CO_3$-$Na_2CO_3$ was investigated extensively in the past [22,119–124,128–130,137]. In this work, DTA and HTXRD were used to determine the phase transition temperatures to reproduce the phase diagram (see Figure 6-17). The heat capacity of the intermediate compound $LiNaCO_3$ (sample 1 and sample 2) was measured by DSC for the determination of its Gibbs energy.

### 5.4.1 XRD/HTXRD of $LiNaCO_3$

In this work, the phase transition temperatures and crystal structures of $LiNaCO_3$ were measured by XRD/HTXRD. As mentioned in Chapter 2, this intermediate compound has been investigated many times [130,135,138–140,142,196]. The HTXRD results are shown in Figure 5-13 (Kα2 peaks and background were removed and the intensity is in square root scaling for clarity). Three solid phases with different structure from low temperature to high temperature were detected, i.e., α phase (triclinic), β phase (hexagonal) and γ phase (hexagonal), respectively. The solid-solid phase transition temperatures were 180-185 °C and 365-370 °C. When comparing our results with the experimental data from literature, it is found, that the three crystal structures and phase transition temperatures agree with those measured by Yatsenko et al. [139,140] and Zhukov et al. [141], while the structure of the low temperature α phase is different from the monoclinic structure reported by Christmann et al. [138]. The measured phase transition temperatures are also close to those reported by D'yakov et al. [135] (175 °C, 360 °C ) and Li and Zhang [142] (373 °C).

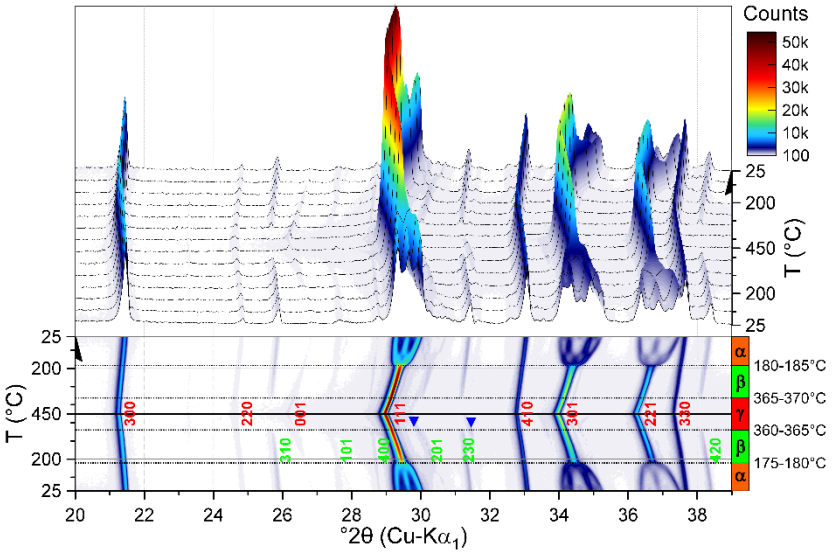


Figure 5-13. HTXRD of the composition $0.5Na_2CO_3$-$0.5Li_2CO_3$.

For the HTXRD, it can be seen that below 60 °C, a new phase seems to appear and the positions of its peaks are indicated as upward arrows in Figure 5-14. Therefore, in our work, instead of only one α phase, two phases $\alpha_1$ and $\alpha_2$ were detected coexisting in the temperature range below

60 °C, and the difference of the XRD patterns of these two phases at room temperature is shown in Figure 5-15.

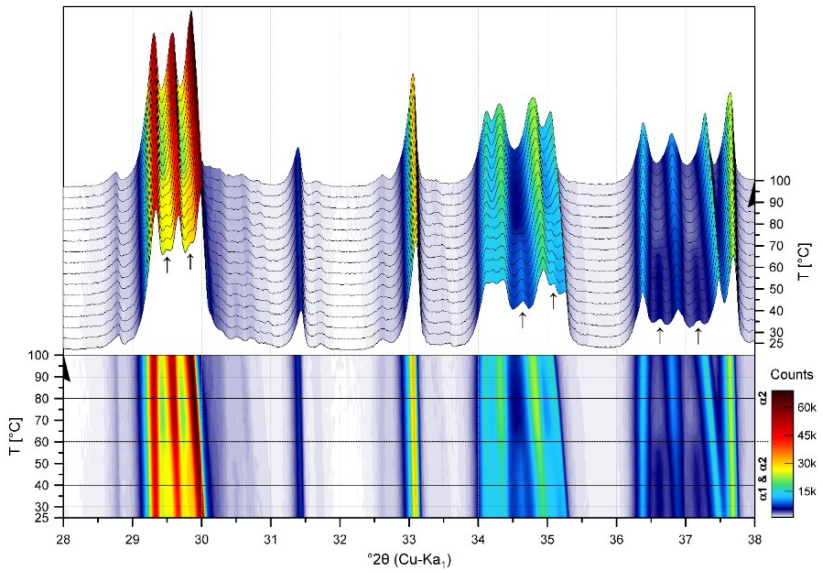


Figure 5-14. HTXRD of $LiNaCO_3$ in the temperature range of 25-100 °C.

As shown in Figure 5-15, the calculated weight ratio between $\alpha_1$ and $\alpha_2$ according to the measured XRD intensity is different in the initial state and after HTXRD. The difference of $\alpha_1$ and $\alpha_2$ can be recognized in their XRD pattern at room temperature. When 2θ is in the range of 29-30°, $\alpha_1$ has four peaks and $\alpha_2$ has three peaks. While in the range of 34-35°, the number of peaks is switched for $\alpha_1$ and $\alpha_2$. In addition, when 2θ is at 36-38°, $\alpha_1$ has five peaks and $\alpha_2$ has four peaks.

The lattice parameters of the α phase at room temperature from this work and the literature are shown in Table 5-2. The main difference between $\alpha_1$ and $\alpha_2$ is the angle α, while it is 89.2° for $\alpha_1$ and 88.4° for $\alpha_2$. It can be seen, that the phase $\alpha_2$ has the same angle α = 88.4° as the phase calculated by Ricca et al. [196] and the phase of the single crystal sample measured by Yatsenko et al. [140]. While the angle α = 89.2° in the $\alpha_1$ phase detected in this work is close to the angle α = 89.0° reported in another work of Yatsenko et al. [139], where the sample was non single crystal structure. Besides, the XRD measurement in this work shows that the weight ratio of the $\alpha_1$ phase increased after grinding. Therefore, the coexistence of $\alpha_1$ and $\alpha_2$ is assumed to be caused by kinetic effects.

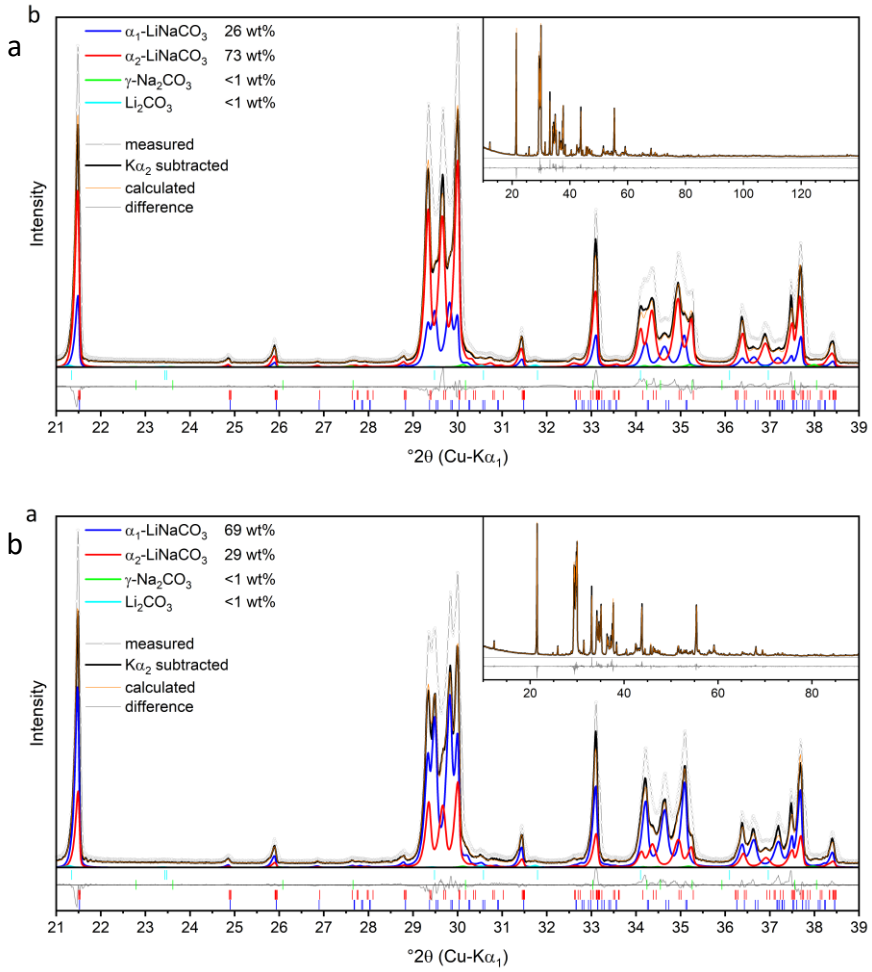


Figure 5-15. XRD patterns of $LiNaCO_3$ a) in initial state and b) after HTXRD measurement

Table 5-2. Comparison of lattice parameters of $\alpha_1$ and $\alpha_2$ at room temperature.

| Phase | a, Å | b, Å | c, Å | α, ° | β, ° | γ, ° | Reference |
|---|---|---|---|---|---|---|---|
| $\alpha_1$ | 14.30 | 14.29 | 3.31 | 89.21 | 91.66 | 119.98 | This work |
| $\alpha_2$ | 14.30 | 14.29 | 3.31 | 88.42 | 91.68 | 119.94 | This work |
| α | 14.265 | 14.261 | 3.305 | 88.41 | 91.7 | 119.95 | Ricca et al. [196] |
| α | 14.28 | 14.29 | 3.31 | 89.00 | 91.70 | 120.00 | Yatsenko et al. [139] |
| α | 14.27 | 14.27 | 3.31 | 88.41 | 91.70 | 119.95 | Yatsenko et al. [140] |

The phase transition between $\alpha_1$ and $\alpha_2$ happened at relatively low temperatures and it may be a continuous process. There might be a temperature, below which only $\alpha_1$ phase exists. However, it was not detected due to the temperature limitation of the XRD device.

The temperature dependence of the lattice parameters of different phases is shown in Figure 5-16. Here, the phase transition between different phases (180 °C and 365 °C) are illustrated obviously. While the lattice parameter of phase $\alpha_1$ and $\alpha_2$ are enlarged and shown in Figure 5-17.

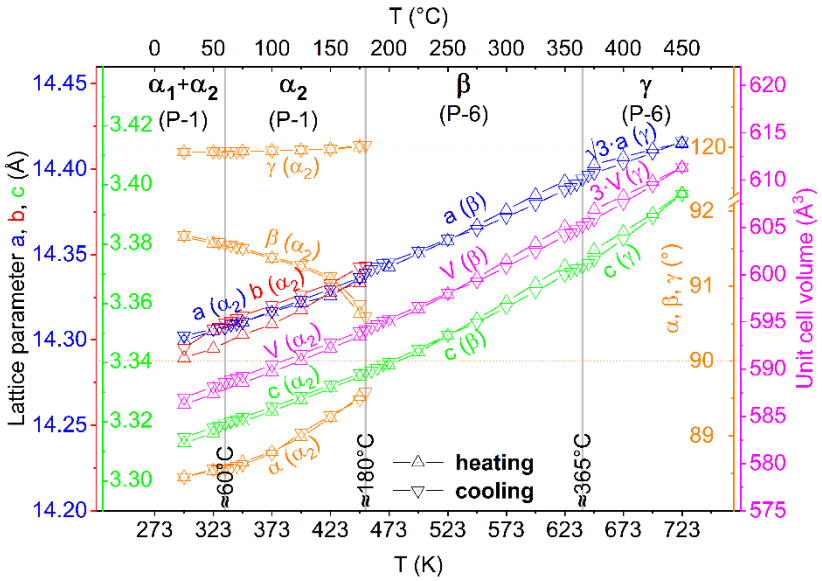


Figure 5-16. Temperature dependence of lattice parameters of $LiNaCO_3$.

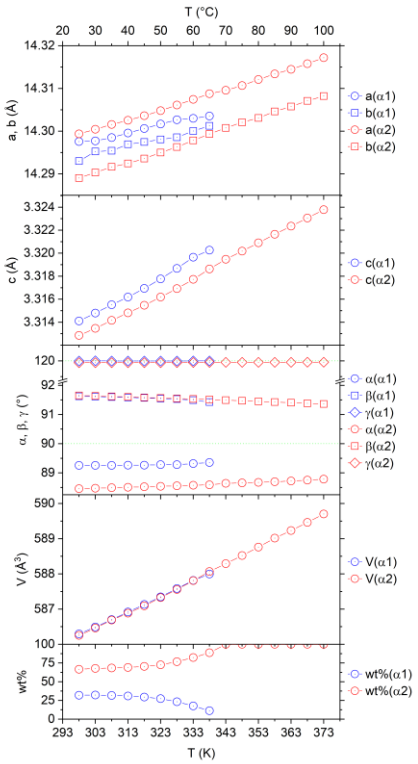


Figure 5-17. Lattice parameters of $LiNaCO_3$ in the temperature range of 25-100 °C.

### 5.4.2 HTXRD of 0.975$Na_2CO_3$-0.025$Li_2CO_3$ mixture

Figure 5-18 shows the measured diffractograms for the composition x($Na_2CO_3$) = 0.975 and it was compiled to a 3D surface plot with a corresponding plan plot for the whole investigated temperature range. Here, the presence of three solid solution phases and their structures were further confirmed. The crystal structures of the three solid phases are the same as the corresponding modifications of the pure $Na_2CO_3$. They are monoclinic γ, monoclinic β and hexagonal α from low temperature to high temperature as shown in Figure 5-18. At lower temperatures (25 - ~340 °C on heating, ~290 - 25 °C on cooling) a weak Bragg reflection at ~21.3° 2θ was measured, which is assumed to belong to $LiNaCO_3$ indicated as a pink point in Figure 5-18. Therefore, at lower temperature for the composition 0.975$Na_2CO_3$-0.025$Li_2CO_3$, the intermediate compound $LiNaCO_3$ and the solid solution phase γ coexisted. When the temperature was above 340 °C, the intermediate compound $LiNaCO_3$ disappeared. That is because when the temperature increases, the solubility of $Li_2CO_3$ in $Na_2CO_3$ becomes larger, and the intermediate compound $LiNaCO_3$ dissolved into the solid solution γ phase. The average structure (approximation) of the γ phase is isostructural to that of the β phase. Both phases have the same metric of the unit cell and very similar diffraction patterns. The main Bragg reflections of both phases are identical. The γ phase originates relatively weak additional reflections, which cannot be simulated with a standard Rietveld or Pawley/Le Bail fit. The γ-β phase transition can only be tracked by observing the formation/vanishing of the mentioned weak additional reflections, which are indicated by orange letter γ in Figure 5-18. The β-α phase transition is much easier to be tracked by observing the merging of several monoclinic reflections into one hexagonal reflection. The phase transition temperatures are collected in Table 5-3 (in section 5.4.3).

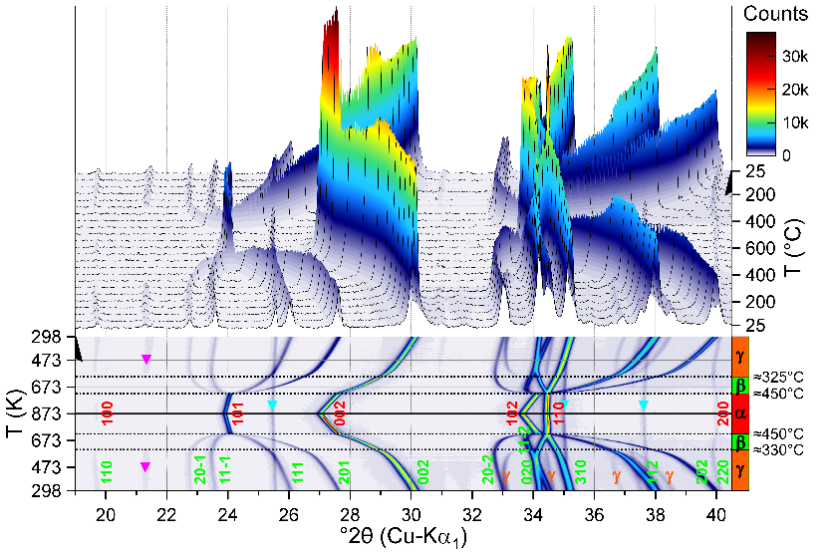


Figure 5-18. HTXRD of the composition $0.975Na_2CO_3$-$0.025Li_2CO_3$.

The lattice parameters are shown in Figure 5-19. The monoclinic lattice parameters in the diagram are recalculated for a better comparability. The high temperature hexagonal phase (called HEXAsoln, the solid solution phase based on $Na_2CO_3$ (HT)) can also be described by the lower symmetric monoclinic structures of the low temperature phases (called MONAsoln and MOLTsoln, the solid solution phases based on $Na_2CO_3$ (MT) and $Na_2CO_3$ (LT), separately). The unit cell volume $V_{UC}$ of the monoclinic structures is doubled compared to the hexagonal unit cell and the monoclinic angle beta becomes 90°. The dimensions of the lattice parameters are linked as follows: $c_{hex} = c_{mon}$, $a_{hex} = a_{mon}/\sqrt{3} = b_{mon}$, $V_{UC\,hex} = V_{UC\,mon}/2$, where hex = hexagonal and mon = monoclinic. Additionally, the lattice parameters of pure $Na_2CO_3$ reported by Sergeev et al. [24] are compared with the current result. It can be easily noticed, that the lattice parameters measured are very close to the pure substance and the crystal structure did not change, which means that the solutions are formed based on the structures of the pure substance $Na_2CO_3$. In addition, the type of the solid solutions is a substitutional solid solution, where the Li atom replaces the Na atom, which causes the difference between the solution phase and the pure substance $Na_2CO_3$. The unit cell volume of all three solid solution phases is smaller than that of the pure $Na_2CO_3$, which is because the atom size of Li is smaller than that of Na. The lattice parameters *a*, *b* and β are smaller than those of pure $Na_2CO_3$, while lattice parameter *c* is larger than that of $Na_2CO_3$, which results from the interactions between the atoms. The difference of

the lattice parameters between solid solutions and pure $Na_2CO_3$ becomes larger with increasing temperature. For the low temperature phase γ, they are very close to those of pure $Na_2CO_3$ (LT), which is due to the low solubility at this temperature. The phase change temperature of the solution phase is lower than that of the pure $Na_2CO_3$, the comparison is shown in Table 5-3 (in section 5.4.3). It can be seen that the difference of the data from DTA and HTXRD are consistent, with an error of 10 °C.

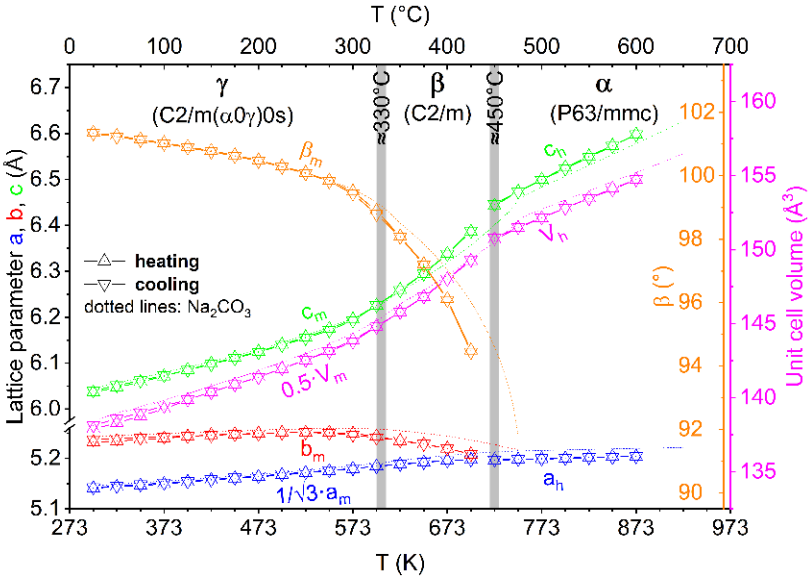


Figure 5-19. Lattice parameters and unit cell volume dependence on temperature for the composition $0.975Na_2CO_3$-$0.025Li_2CO_3$ compared with those of pure $Na_2CO_3$

### 5.4.3 DTA results

In order to check the presence of the solid solution phases, DTA measurements were performed for several samples with various compositions and the result are shown in Figure 5-20. The phase transition temperatures measured by the DTA, DSC and HTXRD are collected in Table 5-3 (Groups 1-7). The liquidus temperatures are in Group 7. The peaks indicating the solidus temperatures of the solid solution based $Na_2CO_3$ (HT) are not obvious as others but they still can be recognized from the difference between the slop of the heating curves, and are summarized as group 6. A peak was detected at around 500 °C for the compositions x($Na_2CO_3$) = 0.4, 0.5, 0.6 and 0.7. Then it shifted to lower temperature 410 °C from composition x($Na_2CO_3$) = 0.75 to 0.9. At last, it increased again to the solid-solid phase transition temperature of $Na_2CO_3$ when the

composition of $Na_2CO_3$ increases, which is shown in Group 5. This temperature change describes the bottom boundary of the solid solution phase based on $Na_2CO_3$ (HT). While in group 4, the peaks at around 400 °C were not detected at the composition $x(Na_2CO_3) = 0.4$, it was detected from the composition $x(Na_2CO_3) = 0.5$ to the composition $x(Na_2CO_3) = 0.95$ and shifted to 398 °C for the composition $x(Na_2CO_3) = 0.95$ and disappeared again for the composition $x(Na_2CO_3) = 0.975$. The peaks at around 370 °C in Group 3 were detected from $x(Na_2CO_3) = 0.4$ to $x(Na_2CO_3) = 0.85$, which is due to the solid-solid phase transition of the intermediate compound $LiNaCO_3$. When the composition moves away from $0.5Li_2CO_3$-$0.5Na_2CO_3$, the amount of $LiNaCO_3$ decreases and the peak became smaller. The peaks at around 335 °C in Group 2 was only detected at compositions $x(Na_2CO_3) \geq 0.7$. The peaks in group 2, 3 and 4 are relatively small, that is because the phase transition enthalpy is small compared to the melting and eutectic reaction. The peaks at 180 °C and 190 °C in group 1 was detected by DSC and HTXRD, it was not detected by DTA.

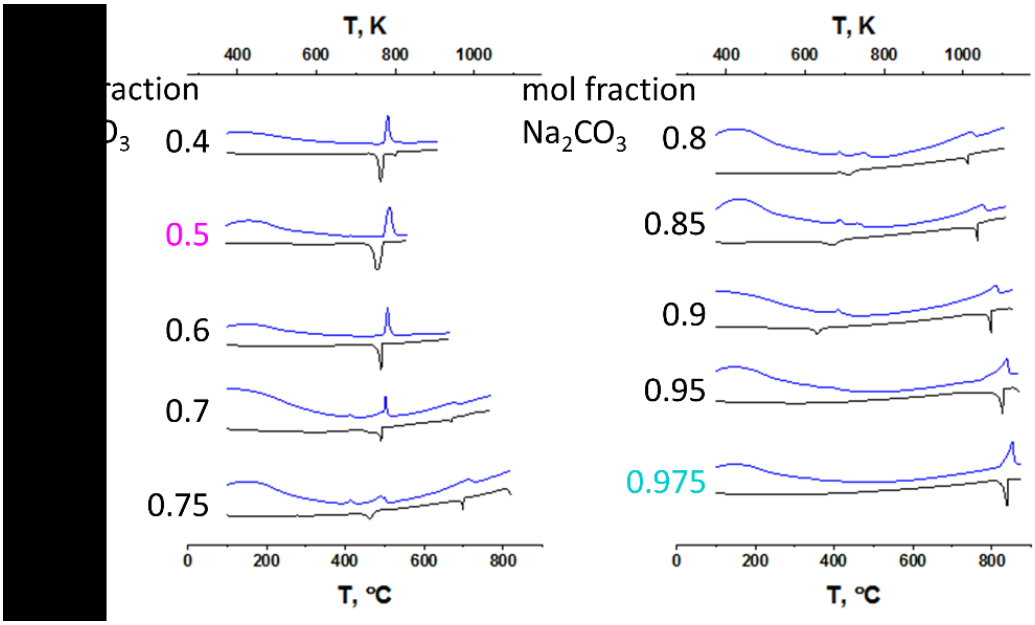


Figure 5-20. Heating DTA-curves for various compositions in the $Li_2CO_3$-$Na_2CO_3$ system

Table 5-3. Phase transition temperatures in the system $Li_2CO_3$-$Na_2CO_3$ obtained by DTA, HTXRD and DSC

| Molar fraction $Na_2CO_3$ | T, C | | | | | | | source |
|---|---|---|---|---|---|---|---|---|
| | 1 | 2 | 3 | 4 | 5 | 6 | 7 | |

| | | | | | | | | |
|---|---|---|---|---|---|---|---|---|
| 0.4 | - | - | 364 | - | 498 | - | 541 | DTA |
| 0.5 | - | - | 363 | 405 | 497 | - | - | DTA |
| | 180 | - | 365-370 | - | - | - | - | HTXRD |
| | 190 | - | 365 | - | - | - | - | DSC |
| 0.6 | - | - | 373 | 407 | 500 | - | 597 | DTA |
| 0.7 | - | 337 | 366 | 403 | 498 | - | 678 | DTA |
| 0.75 | - | - | 370 | 405 | 491 | - | 714 | DTA |
| 0.8 | - | - | 367 | 404 | 476 | 560 | 746 | DTA |
| 0.85 | - | 339 | 367 | 404 | 460 | 612 | 776 | DTA |
| 0.9 | - | 333 | - | 402 | 410 | 693 | 799 | DTA |
| 0.95 | - | 333 | - | 398 | 433 | 774 | 838 | DTA |
| 0.975 | - | 339 | - | - | 462 | 819 | 583 | DTA |
| | - | 330 | - | - | 450 | - | - | HTXRD |
| $Na_2CO_3$ | - | 354 | - | - | 484 | - | - | DTA, [24] |
| | - | 350 | - | - | 480 | - | - | HTXRD, [24] |

### 5.4.4 Heat capacity of $LiNaCO_3$

The heat capacity of intermediate compound $LiNaCO_3$ has not been reported before. In this work, it was measured by three different types of DSC mentioned in section 3.2.2. The experimental results are shown in Figure 5-21. The green line and the blue line in Figure 5-21 are the sample 1 and sample 2 (the compositions are different, see Chapter 3) measured with Netzsch_HT, and they show good agreement. Besides, the results from different devices agree well with each other, which means that our results are reproducible and reliable. Two solid-solid phase transitions were observed at 190 °C and 365 °C, respectively, in all DSC curves. The peaks in the curve measured with Netzsch_LT from -30 °C to 50 °C were not taken into consideration because they are already shown in the baseline due to some defects in the sample holder. The approximation was obtained according to the average results, which was used to find an appropriate polynomial of the $C_p$ in the new database. The uncertainty of the data is around ± 13 J/(mol·K).

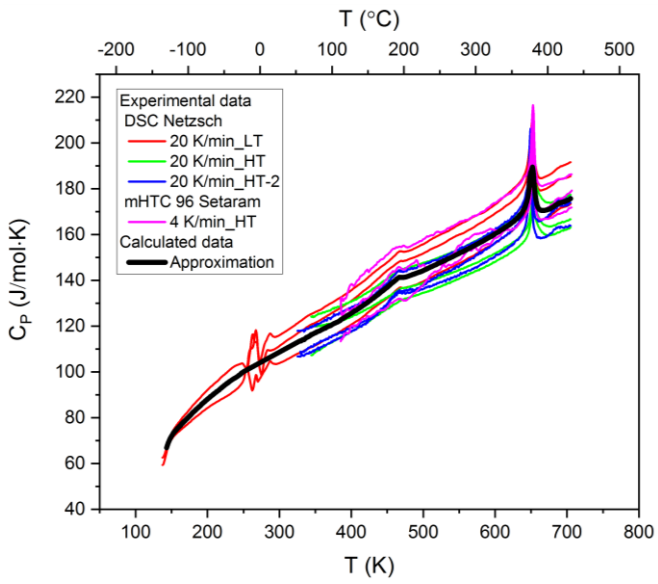


Figure 5-21. Heat capacity of $LiNaCO_3$ determined by three different types of DSC

## 5.5 System $Li_2CO_3$-$K_2CO_3$

For the system $Li_2CO_3$-$K_2CO_3$, DTA measurements were carried out at 0.85, 0.9, 0.95 molar fraction of $K_2CO_3$. They show the eutectic temperature at 496 °C for all three compositions (Figure 5-22) and the liquidus temperature decreases when the molar fraction of $K_2CO_3$ decreases from 0.95 to 0.85. The peaks at 411 °C (0.85 $K_2CO_3$), 416 °C (0.9 $K_2CO_3$) and 415 °C (0.95 $K_2CO_3$) are close to the solid-solid phase transition of $K_2CO_3$ at 421 °C.

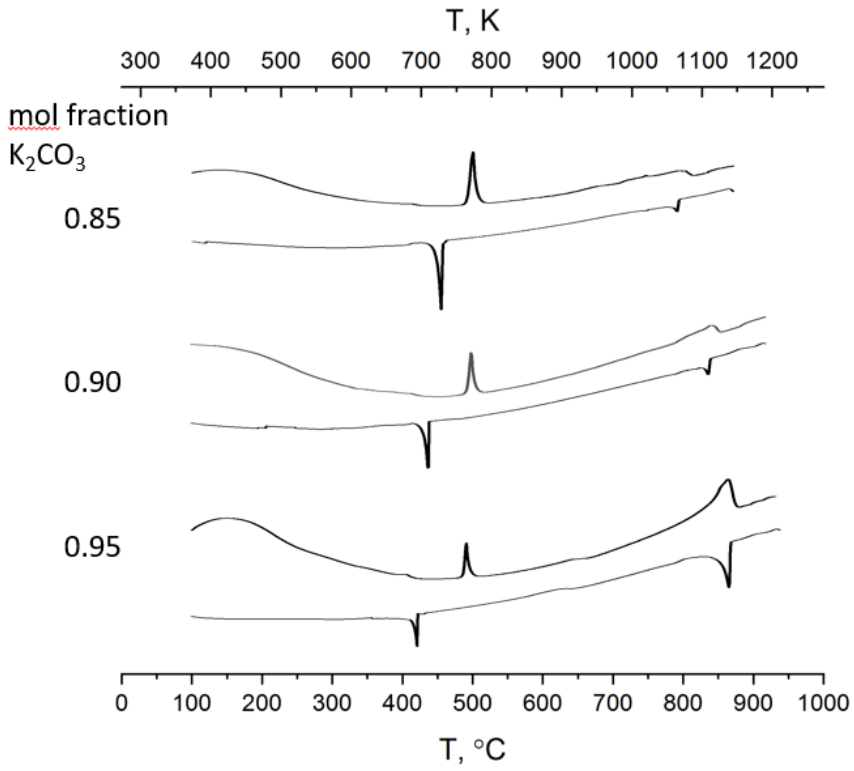


Figure 5-22. DTA results of 0.85, 0.9, 0.95 molar fraction of $K_2CO_3$ in the system $Li_2CO_3$-$K_2CO_3$.

The $C_p$ of the solid $LiKCO_3$ was measured from -130 °C to 430 °C separately by two Netzsch DSC devices and one Setaram HFDSC. It can be seen from Figure 5-23 that the results from two devices are reproducible and also in good agreement, which indicates that the present results are reliable. Peaks at 246-320 K in the curves measured with Netzsch_LT were caused by the sample holder itself because they already showed up in the baseline. One peak at 404 °C was detected, that might be caused by solid-solid phase transition, which was checked by high temperature XRD.

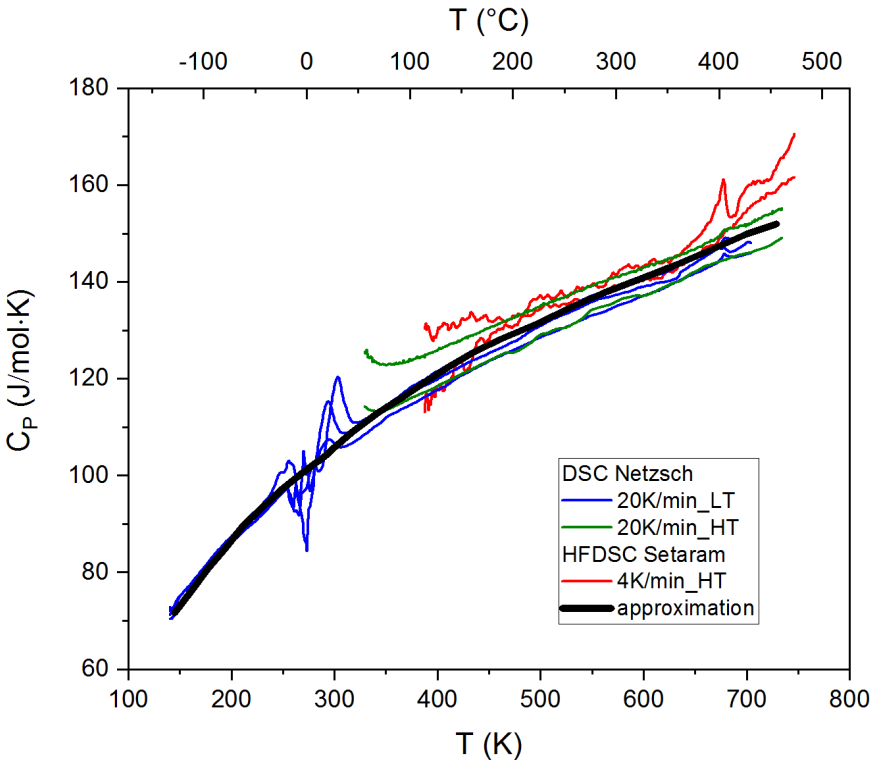


Figure 5-23. Heat capacity of $LiKCO_3$ measured by three types of DSC.

As shown in Figure 5-24, the measured diffractograms were compiled to a 3D surface plot with a corresponding plan plot for the whole investigated temperature range (Kα2 peaks and background were removed and intensity is in square root scaling for clarity). No formation of secondary phases has been observed. In agreement with literature [138,197], $LiKCO_3$ did not show a phase transformation between 25 °C and 450 °C. The temperature dependence of the lattice parameters is shown in Figure 5-25. A significant increase in crystallite size was observed during experiments. Additionally, the sample displacement parameter obtained with Rietveld refinement shows relatively strong fluctuations (Figure A-2). These effects decrease the accuracy of the lattice parameter determination, and it is reflected in the temperature range 350-400 °C (Figure 5-25). However, the crystal growth and sample displacement are not supposed to influence the thermodynamic properties and result in the peak at 404 °C in the $C_p$ curve. It is noted that this temperature is close to the solid-solid phase change temperature of $K_2CO_3$ (421 °C) [23,24], and therefore, it might be caused by the $K_2CO_3$ remained during the preparation of the sample, in which the amount was too little to be detected by XRD due to accuracy limitation of

the device. Besides, this peak is not shown in some of the curves and its intensity also changes, which could be due to the different amount of $K_2CO_3$ remained in the samples. The peak at 404 °C in the $C_p$ curve (Figure 5-23) is not caused by solid-solid phase transition of $LiKCO_3$. Therefore, this slight thermal effect is not taken into account for the optimization of $C_p$. No solid-solid phase transition of $LiKCO_3$ was reported [12] and it was not found in the HTXRD measurement in the current work.

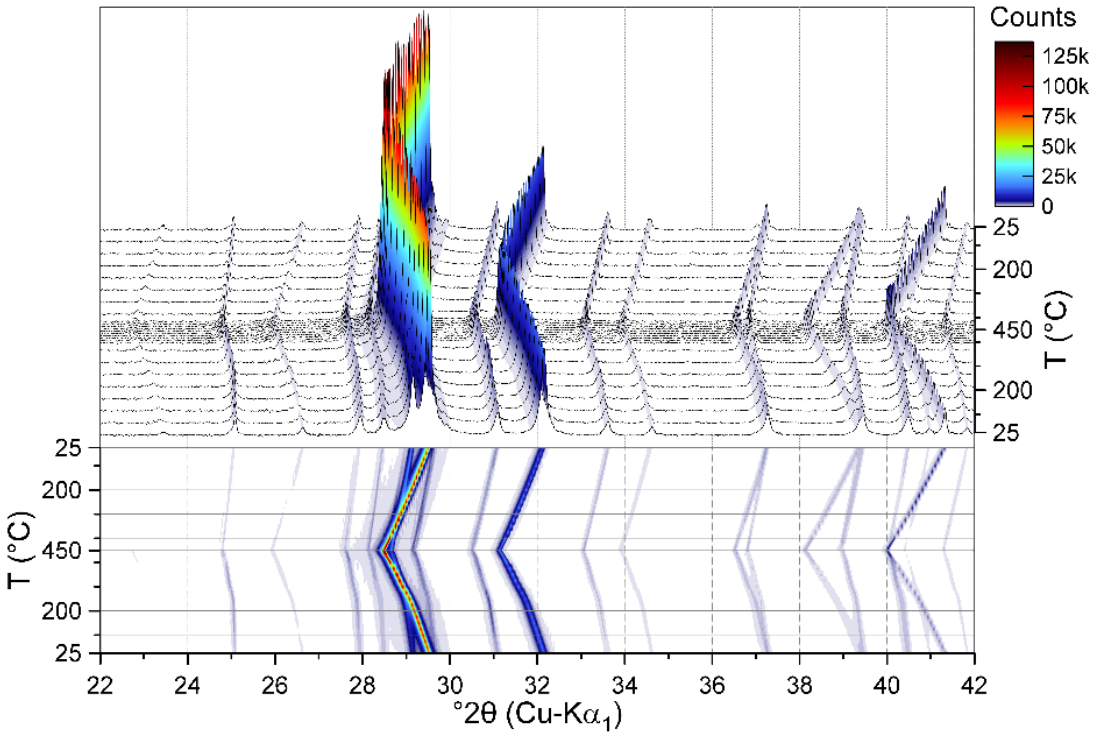


Figure 5-24. High temperature XRD of $LiKCO_3$.

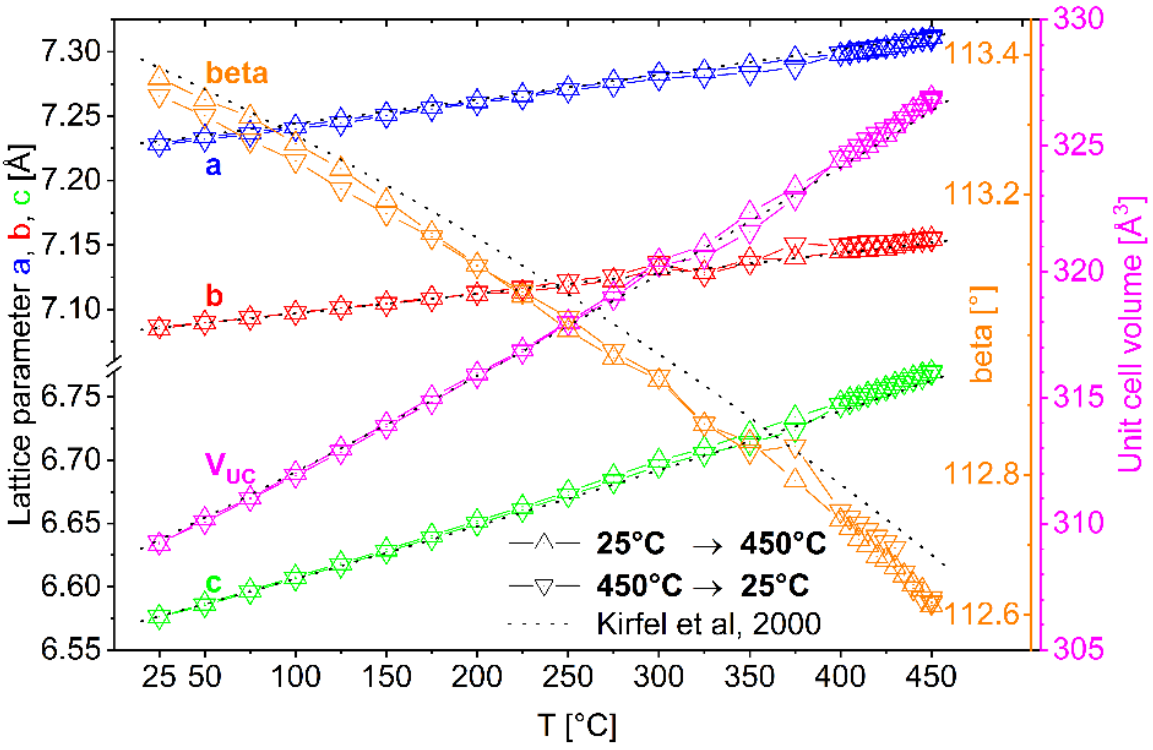


Figure 5-25. Temperature dependence of lattice parameters for $LiKCO_3$.

## 5.6 Reciprocal system $Li^+$, $K^+$ // $Cl^-$, $CO_3^{2-}$

In this work, DTA measurements were performed in a wide concentration range of the two diagonal systems in order to check the phase equilibria in the whole system.

In the $Li_2CO_3$-$(KCl)_2$ binary system, only one peak occurs in the DTA curve for the eutectic composition, which is like the peak at the melting temperature for pure substances. While near the eutectic point, the liquidus temperature is very close to the eutectic temperature in the phase diagram, which makes it difficult to distinguish them when measured with DTA, especially for the heating curve. In Figure 5-26 a) both heating curves for the compositions $x(Li_2CO_3) = 0.7$ and $x(Li_2CO_3) = 0.8$ have only one peak, which indicates that they are both close to the eutectic point. However, in Figure 5-26 b) the cooling curve of the former one shows two downward peaks while only one peak occurs for the latter one, so the composition $x(Li_2CO_3) = 0.8$ is closer to the eutectic composition.

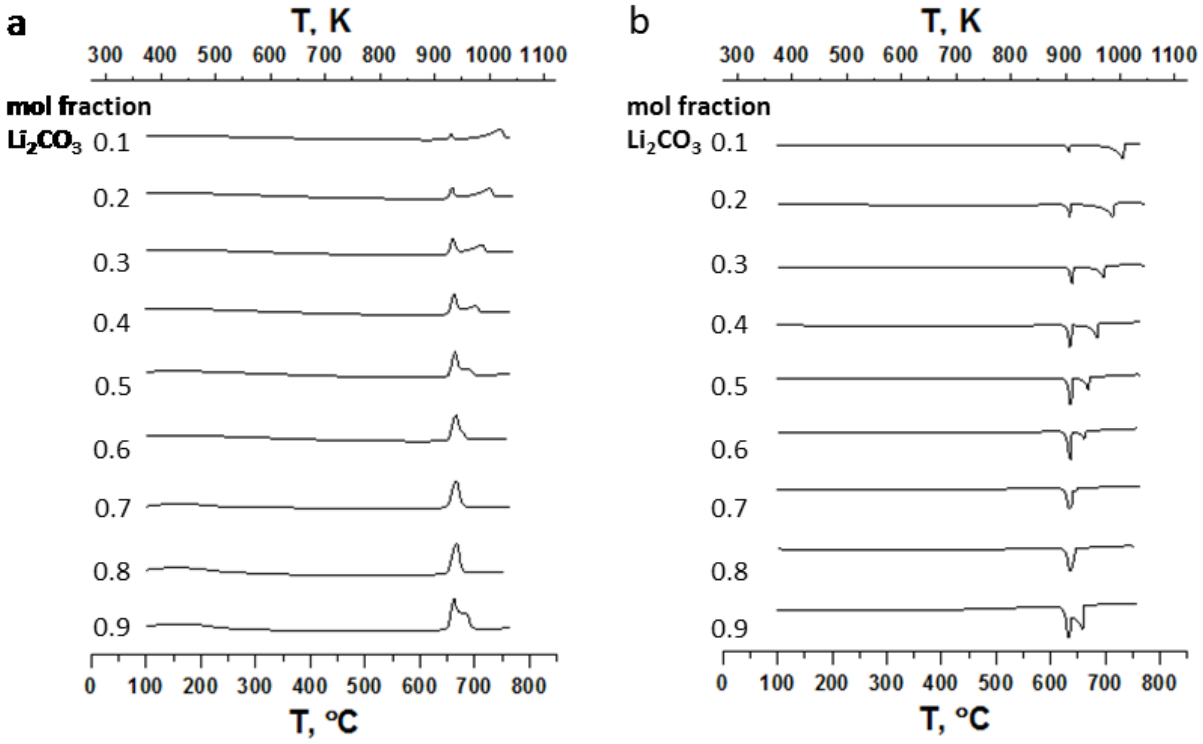


Figure 5-26. a) Heating DTA curves and b) cooling DTA curves with heating and cooling rate of 5 K/min for different compositions of the $Li_2CO_3$-$(KCl)_2$ binary system.

The phase transition temperatures of different compositions in the diagonal system $K_2CO_3$-$(LiCl)_2$ were measured by DTA (Figure 5-27). The peaks representing the liquidus temperature shifted when the composition changed. The eutectic temperature is around 468 °C in the composition range x($(LiCl)_2$) = 0-0.33, 462 °C in the composition range of x($(LiCl)_2$) = 0.33-0.5 and 345 °C in the range of x($(LiCl)_2$) = 0.5-1.

In order to verify the phase transitions, the DTA results of two samples prepared from the different salt pairs ($0.5Li_2CO_3$-$0.5(KCl)_2$ and $0.5K_2CO_3$-$0.5(LiCl)_2$) were compared with each other. Figure 5-28 shows that their DTA curves agree well, except for a small peak at 348 °C in $0.5K_2CO_3$-$0.5(LiCl)_2$. This is due to the limited accuracy of the weighing scale, which makes it difficult to give an exactly 1:1 ratio of these two substances. Here, the molar fraction of $(LiCl)_2$ is slightly higher than 0.5, so this peak appears at this temperature just like at any other composition in this system where the molar fraction of $(LiCl)_2$ is larger than 0.5.

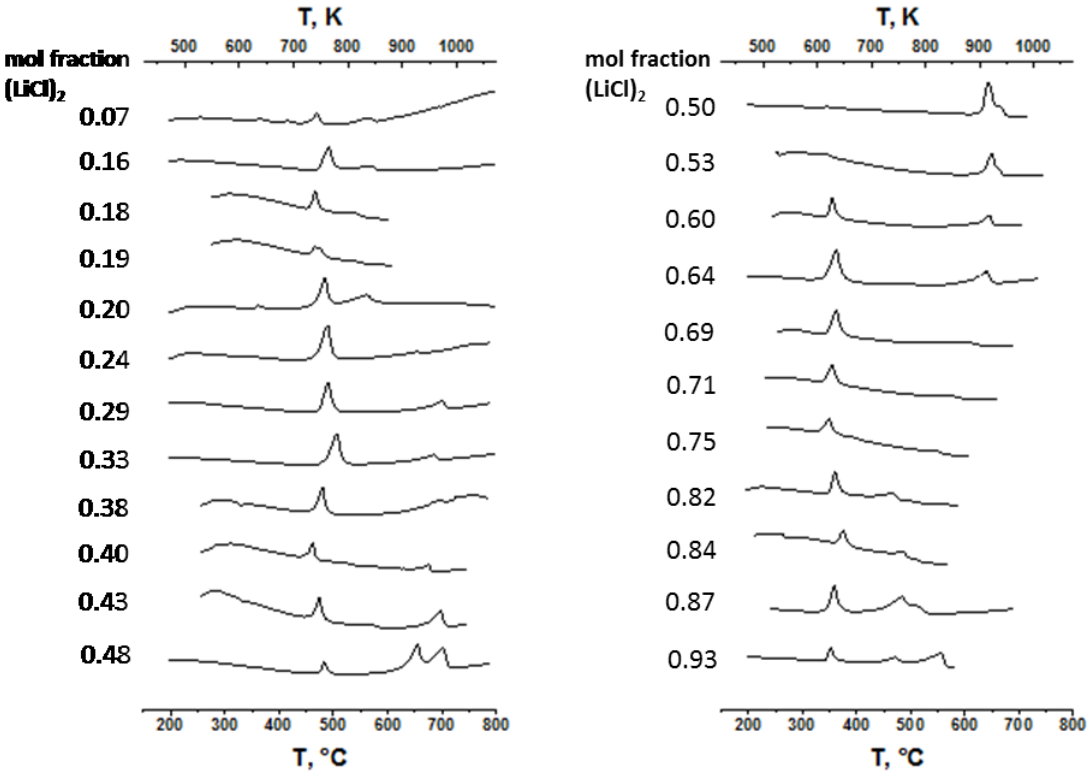


Figure 5-27. Heating DTA curves for different compositions of $K_2CO_3$-$(LiCl)_2$ binary system.

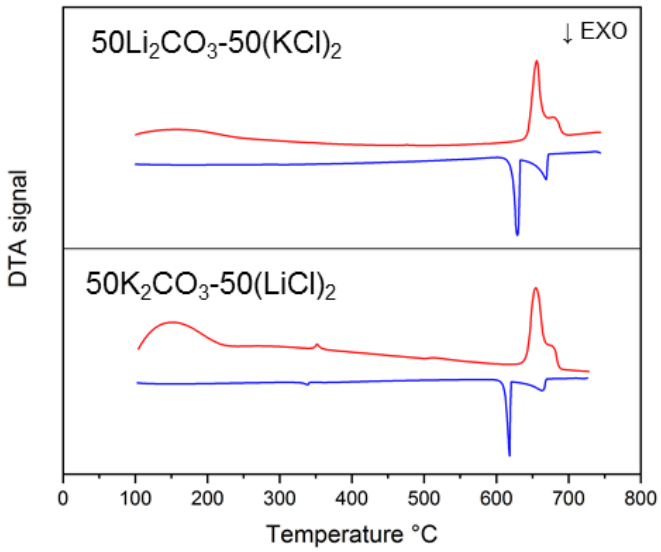


Figure 5-28. Comparison of the DTA results of the compositions $0.5Li_2CO_3$-$0.5(KCl)_2$ and $0.5K_2CO_3$-$0.5(LiCl)_2$.

## 5.7 Reciprocal system $Li^+$, $Na^+$ // $Cl^-$, $CO_3^{2-}$

In this work, DTA measurements were performed in a wide concentration range of the two diagonal systems in order to check the phase transitions in the whole system.

The DTA results of certain composition in the $Li_2CO_3$-$(NaCl)_2$ system are shown in Figure 5-29. The eutectic temperature was measured to be 622 °C and the eutectic composition is between the compositions x($Li_2CO_3$) = 0.2 and x($Li_2CO_3$) = 0.3. At the compositions x($Li_2CO_3$) = 0.7, 0.8 and 0.9, a peak shows up at 475 °C. These peaks may correspond to the solid solution of the $Li_2CO_3$-$Na_2CO_3$ or LiCl-NaCl system.

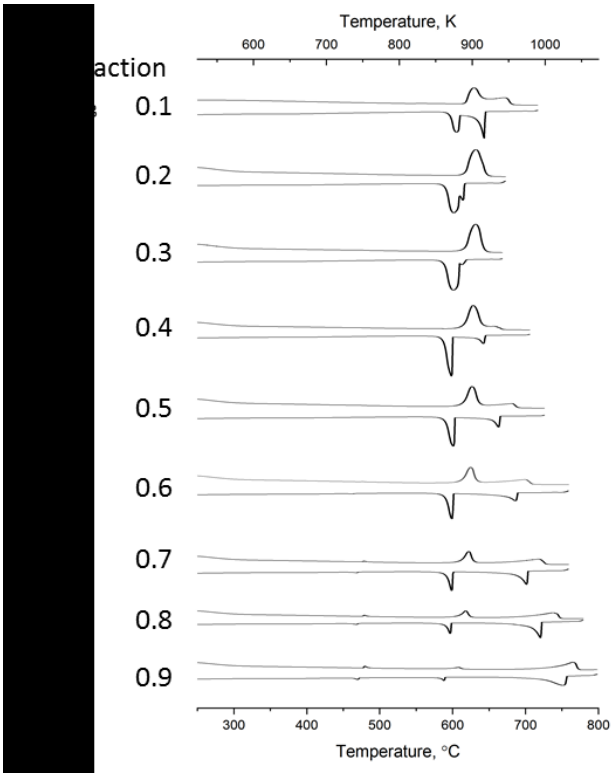


Figure 5-29. Heating and cooling DTA-curves for various compositions in the $Li_2CO_3$-$(NaCl)_2$ system

The DTA curves for compositions in the $Na_2CO_3$-$(LiCl)_2$ system (Figure 5-30) are more complicated than that for the other diagonal system. For the composition x($Na_2CO_3$) = 0.95, peaks showed at 343 °C, 404 °C and 427 °C, which is resulting from the solid solution in the $Li_2CO_3$-$Na_2CO_3$ system.

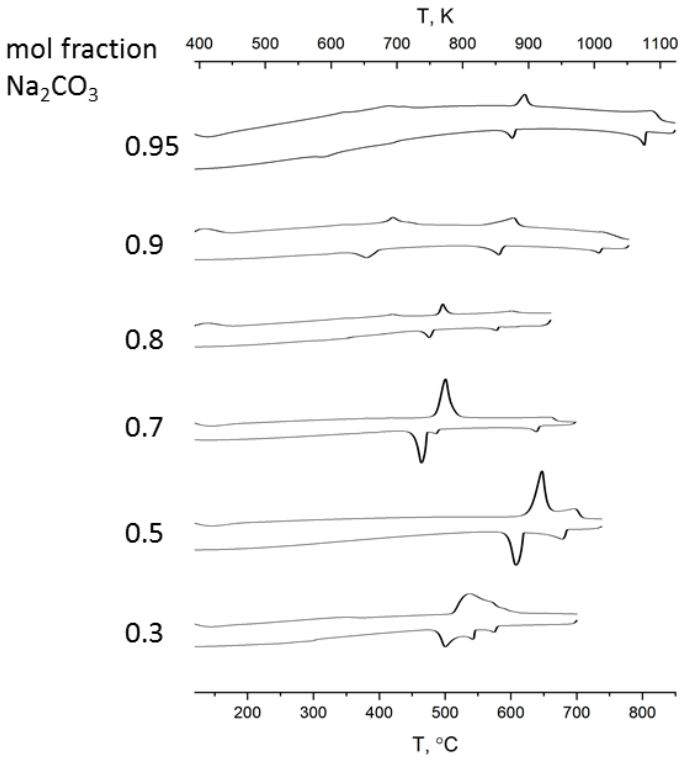


Figure 5-30. Heating and cooling DTA-curves for various compositions in the $Na_2CO_3$-$(LiCl)_2$ system

## 5.8 Reciprocal system $Na^+$, $K^+$ // $Cl^-$, $CO_3^{2-}$

In the reciprocal system $Na^+$, $K^+$ // $Cl^-$, $CO_3^{2-}$, the melting temperature of the eutectic composition (0.428KCl-0.359$Na_2CO_3$-0.213$K_2CO_3$ in molar fraction), was measured by DSC to be 569 °C (see Figure 5-31), and the melting enthalpy was 20.18±0.14 kJ/mol. This part of work has been published in the paper [159].

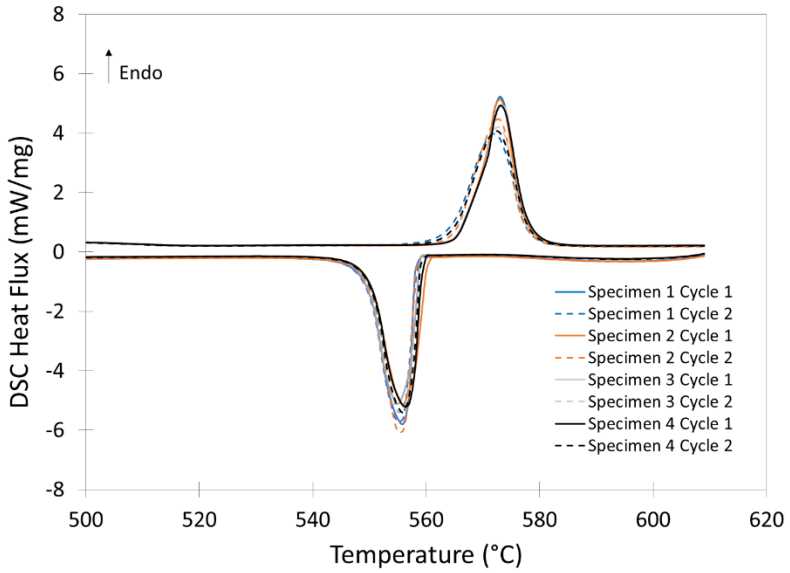


Figure 5-31. DSC measurement of the eutectic composition (0.428KCl-0.359$Na_2CO_3$-0.213$K_2CO_3$ in molar fraction) in the reciprocal system

# 6 Modelling results

## 6.1 Pure substances

### 6.1.1 $Li_2CO_3$

In the present work, the values of standard enthalpy of formation and standard entropy of lithium carbonate, i.e. $\Delta_f H^\circ_{298}$ and $S^\circ_{298}$, were adopted from reference books [192,193] without modification. The melting enthalpy determined by Janz et al. [39] is preferred over other data reported in the literature [36,40,41] in the reference databases [192,193] and in the present work. Transition temperatures and enthalpy of phase transitions (solid-solid, solid-liquid) are listed in Table 6-1.

As mentioned in Chapter 2, the presence of the solid-solid transition of $Li_2CO_3$ at 680-693 K is discussed in the literature. In the present work, no remarkable thermal effects were found neither by DTA with closed Pt crucible nor DSC studies under Helium (Chapter 5). Hence, the measured temperatures of transformation of 680-693 K mentioned in the literature [35,37] can be ascribed to the presence of impurities. On the other hand, the continuous transformation of structure of $Li_2CO_3$ accompanied by the change of the lattice parameters (Chapter 5) at around 598 K and 798 K was detected by the present HTXRD study. However, these solid-solid transitions for lithium carbonate were not detected by DTA/DSC methods because their thermal effect is too small to be detected. Therefore, it is preferred not to consider these solid-solid transitions when generating thermodynamic functions for $Li_2CO_3$ in the present study.

Table 6-1. Transition data of $Li_2CO_3$.

| Reaction | Reaction type | Temperature of transition | | | Heat of transition | |
|---|---|---|---|---|---|---|
| | | $T_{tr}$, °C (K) | method | Reference | $\Delta H_{tr}$, kJ/mol | Reference |
| $Li_2CO_3$ (LT) ↔ $Li_2CO_3$ (MT) | Solid ↔ solid* | 350 (623) | DTA (Impurities) | Reisman [35] | | |
| | | 350 (623) | Calculated | Barin [192], NIST-JANAF tables [193], SGPS [25], FTsalt [9] | 0.56 | Barin [192], NIST-JANAF tables [193], SGPS [25], FTsalt [9] |
| | | 325 (598) | HTXRD | This work | | |

| | | | | | | |
|---|---|---|---|---|---|---|
| $Li_2CO_3$ (MT) ↔ $Li_2CO_3$ (HT) | Solid ↔ solid* | 410 (683) | DTA | Reisman [35] | | |
| | | 407-420 (680-693) | DTA | Klement and Cohen [37] | | |
| | | 415 (688) | DTA | Otsubo and Yamaguchi [36] | 0.9 | Otsubo and Yamaguchi [36] |
| | | 410 (683) | Calculated | SGPS [25], FTsalt [9] | 2.24 | SGPS [25], FTsalt [9] |
| | | 416 (689) | DTA (Impurities) | This work | | |
| | | 525 (798) | HTXRD | This work | | |
| $Li_2CO_3$ (HT) ↔ liquid | melting | 732 (1005) | TA** | Amadori [186] | | |
| | | 720 (993) | DTA | Reisman [35] | | |
| | | 726 (999) | Drop calorimetry | Janz et al. [39] | 44.77 | Janz et al. [39] |
| | | 728 (1001) | DTA | Otsubo and Yamaguchi [36] | 29.96 | Otsubo and Yamaguchi [36] |
| | | 732 (1005) | DTA | Papin et al. [187] | | |
| | | 723 (986) | calorimetry | Rolin and Recapet [40] | 37.66 | Rolin and Recapet [40] |
| | | 728 (1001) | DTA, in $CO_2$ | Brown and Boryta [42] | | |
| | | 730 (1003) | DSC, XRD, in $CO_2$ | Dissanayake and Mellander [41] | 73.4 | Dissanayake and Mellander [41] |
| | | 723 (996) | In $CO_2$ | Kodama [198] | | |
| | | 732 (1005) | Calculated | SGPS [25] | 44.77 | SGPS [25], used in this work |
| | | 730 (1003) | Calculated | FTsalt [9] | 44.63 | FTsalt [9] |
| | | 726 (999) | DTA, DSC | This work | | |

* The solid-solid transitions of $Li_2CO_3$ are not included in the present database. The corresponding explanation is given in text, ** thermal analysis.

The data on heat capacity of lithium carbonate are summarized in Figure 6-1 including the reference data, ab initio calculated $C_v$ [199] and the present DSC results. In the present database, the temperature dependence of the heat capacity was generated in the temperature range from 0 K to 2000 K (Figure 6-1, Table 6-2). The $C_p$ polynomial below 298 K was modelled based on the low temperature calorimetric data of Brown and Latimer [43], which overlap with the average value from our experimental results below 298 K. The obtained polynomial provides the standard entropy of 90.22 J/mol·K by integration of the function $C_p$/T, which agrees with the measured

value (90.37 J/mol·K) in the work of Brown and Latimer [43] and the reference values (90.17 J/mol·K, e.g., in the JANAF-NIST Tables [193]).

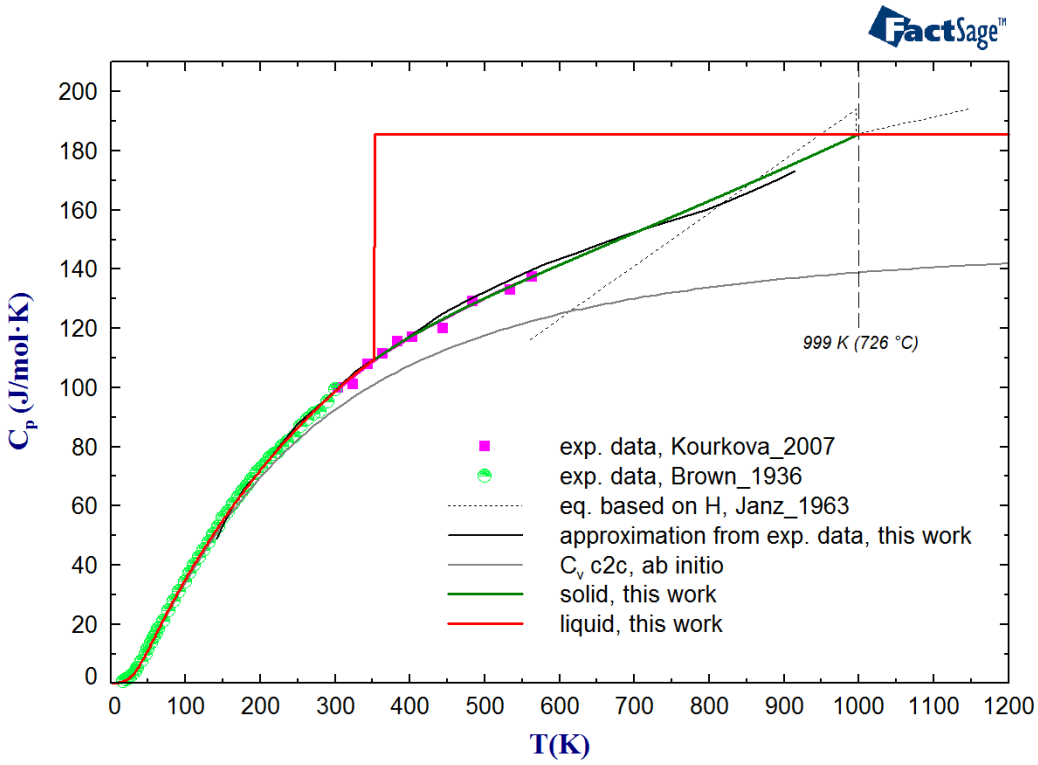


Figure 6-1. Calculated heat capacity of $Li_2CO_3$ along with the experimental and reference data (This work, Brown and Latimer [43], Janz et al. [39] and Kourkova and Sadovska [44]).

Our new data on heat capacity deviate a lot from the derived results of Janz et al. [39], which seems to be used as one of the sources of experimental data for the FTsalt database. Because of its low accuracy, the $C_p$ of the solid phase from Janz et al. [39] was not taken into account for modelling. In the present work, the temperature-dependent polynomial of heat capacity from 298 K was generated taking into account the $C_p$ data of Kourkova and Sadovska [44] along with the average $C_p$ curve obtained in the present work. This polynomial was extrapolated to the value of $C_p$ of the liquid phase (185.4 J/mol·K) used in the reference books [192,193] according to the calorimetric data by Janz et al. [39]. The $C_p$ (liq) was considered to be constant from the estimated Kauzmann temperature (351 K) and above. In the present work, the melting temperature of 999 K was determined by DTA in a closed Pt crucible, which agrees with the data reported in the literature [39,40] and is selected for the thermodynamic dataset of $Li_2CO_3$ (Table 6-2). A

comparison of the obtained $C_p$ values with theoretically calculated $C_v$ from the phonon database [199] for $Li_2CO_3$ was performed. It shows that $C_p$ and $C_v$ of $Li_2CO_3$ are very close to each other at temperatures below 150 K, which also confirms the reliability of the calculated $C_v$ values. Thermodynamic data (standard enthalpy of formation and standard entropy, $\Delta_f H^\circ_{298}$, $S^\circ_{298}$, and $C_p$(T)) for lithium carbonates are summarized in Table 6-2.

Table 6-2. Thermodynamic data of $Li_2CO_3$.

| Compound | $\Delta H^0_{298,f}$ J/mol | $S^0_{298}$ J/mol K | T (K) | $C_p$, J/mol·K | Reference |
|---|---|---|---|---|---|
| $Li_2CO_3$ (solid) | -1216038.0 | 90.171 | 1-38 | $1.0993906 \cdot 10^{-4} \cdot T^3$ | This work |
| | | | 38-298 | $6.7018903 + 0.42810052 \cdot T + 26820.101 \cdot T^{-2} - 3.6033322 \cdot 10^{-4} \cdot T^2 - 1324.4834/T$ | This work |
| | | | 298-999 | $105.68255 + 0.0518743465 \cdot T - 2282961.56206\ T^{-2} + 3.026084218 \cdot 10^{-5} \cdot T^2$ | This work |
| | | | 999-2000 | 185.435 | This work |
| $Li_2CO_3$ (liquid) | -1194857.15 | 90.289 | | solid → liquid $H_m$= 44.769 kJ/mol at 999 K (726 °C) | Janz et al. [39] |
| | | | 1-38 | $1.0993906 \cdot 10^{-4} \cdot T^3$ | This work |
| | | | 38-298 | $6.7018903 + 0.42810052 \cdot T + 26820.101 \cdot T^{-2} - 3.6033322 \cdot 10^{-4} \cdot T^2 - 1324.4834/T$ | This work |
| | | | 298-351 | $105.68255 + 0.0518743465 \cdot T - 2282961.56206\ T^{-2} + 3.026084218 \cdot 10^{-5} \cdot T^2$ | This work |
| | | | 351-2000 | 185.435 | This work |

The heat content of lithium carbonate is calculated using the new $C_p$ polynomials in agreement with the experimental values by Janz et al. [39] and Rolin and Recapet [40] (Figure 6-2). It is worth noting that the pink line [44] is overlapped by the blue line (present work) in the temperature range 303-563 K, which indicates that the present results also agree well with the data derived from the heat capacity measurements by Kourkova and Sadovska [44]. Additionally, the entropy of $Li_2CO_3$ was calculated and compared with the available data in the temperature range up to 300 K (Figure A-3).

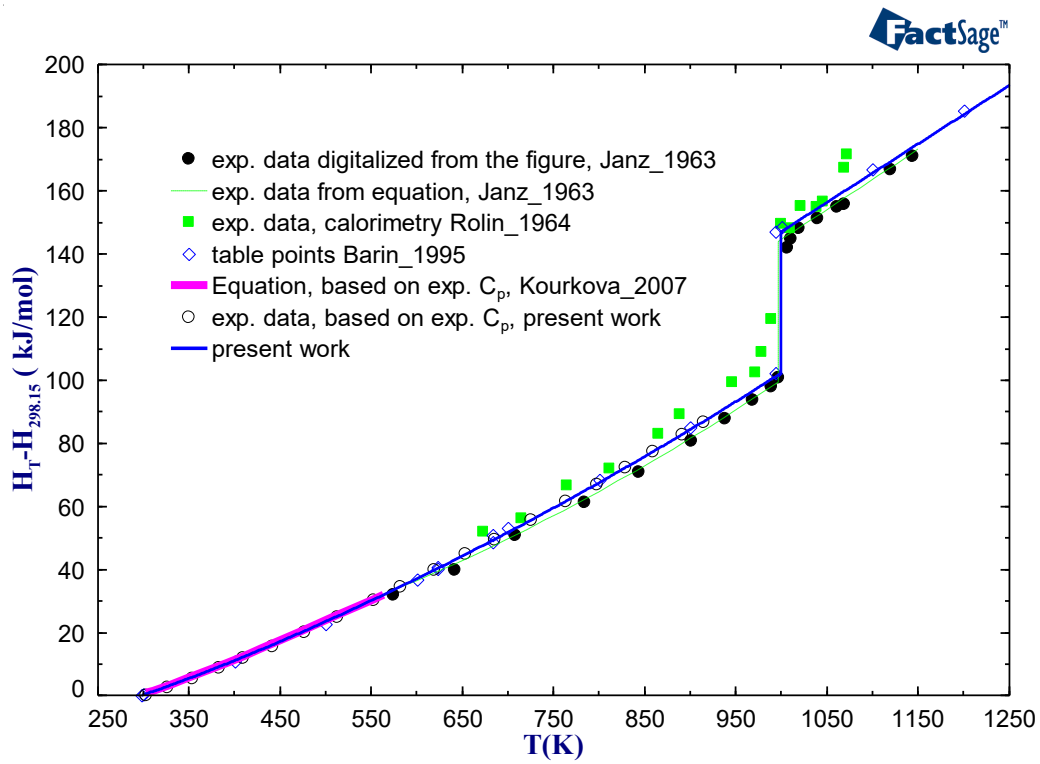


Figure 6-2. Calculated heat content of $Li_2CO_3$ along with the experimental data.

### 6.1.2 LiCl

The values of standard enthalpy of formation and standard entropy of lithium chloride, i.e. $\Delta_f H^\circ_{298}$ and $S^\circ_{298}$, were adopted from NIST-JANAF tables [193] without modifications, which were also used in the database SGPS [25] and FTsalt [9]. The melting temperatures and melting enthalpy information from literature are collected in Table 6-3. In this work, the melting temperature of LiCl was measured by DTA to be 603 °C (Figure A-4). Considering all available data in the literature, 610 °C was taken to be the melting temperature in the PCM database, which is consistent with the databases SGPS [25] and FTsalt [9]. The melting enthalpy of 19.54±0.2 kJ/mol measured by Rodigina et al. [57] was taken for the PCM database, which is within the uncertainty range considering all available data. Among them, the value 15.29 kJ/mol calculated by Zhemchuzhnui and Rambach [46] from molecular depression was not considered because it deviates too much from other experimental data.

Table 6-3. Phase transition data of LiCl.

| $T_m$, °C | Method | Reference | $\Delta H_{fusion}$, kJ/mol | Method | Reference |
|---|---|---|---|---|---|
| 610 ± 1 | calorimeter | Rodigina et al. [57] | 19.54±0.2 | Calorimeter | Rodigina et al. [57] |
| 614 | TA | Zhemchuzhnui and Rambach [46] | 15.29 | Calculated | Zhemchuzhnui and Rambach [46] |
| 606 | TA | Hüttner and Tamman [62] | | | |
| 610 | TA | Haendler et al. [56] | | | |
| 607 | Calorimeter | Douglas and Vitor [50] | 19.73±0.09 | Calorimeter | Douglas and Victor [50] |
| 598 | specific heat method | Carnelley [49] | | | |
| 606 | TA | Wartenberg and Schulz [63] | | | |
| 606 | TA | Flood et al. [52] | | | |
| 600 | TA | Guntz [54] | | | |
| 602 | TA | Sandonnini [59] | | | |
| 609 | TA | Korreng [61] | | | |
| 613 | TA | Richards and Meldrum [47] | | | |
| 605 | TA | Hachmeister [55] | | | |
| 607 | TA | Keitel [200] | | | |
| 605 | TA | Scarpa [201] | | | |
| 609 | TA | Schmitz-Dumont and Schmitz [202] | | | |
| 606 | TA | Ginnings and Phipps [53] | | | |
| 614 | | Kelley [48] | | | |
| 610 | Drop calorimeter | Dworkin and Bredig [51] | 19.92±0.4 | Drop calorimeter | Dworkin and Bredig [51] |
| 610 | Calculated | FTsalt [9], SGPS [25], NIST-JANAF tables [193] | 19.83 | Calculated | FTsalt [9], SGPS [25], NIST-JANAF tables [193] |
| 603 | DTA | This work | | | |
| 610 | Calculated | This work | 19.54 | Calculated | This work |

The data on heat capacity of lithium chloride are summarized in Table 6-4. In the temperature range 300-325 K, the data from Shirley [60] and Rodigina et al. [57] agree well with each other.

In this work, the $C_p$ below 298 K was assessed based on the measurements of Shirley [60]. Additionally, the $C_v$ of LiCl from the phonon database [199] calculated by ab initio method was taken as reference. This theoretical value of $C_v$ is in good agreement with the measured $C_p$ from Shirley [60] until 150 K. The consistency of the data confirmed the reliability of the optimization. In the temperature range of 298-883 K, the $C_p$ was optimized based on data from Rodigina et al.

[57] and Douglas and Victor [50]. These two data are in good agreement and different from the data by Kelley [48], which was not considered in the optimization. Above 883 K, the $C_p$ was assumed to be a constant value (Figure 6-3).

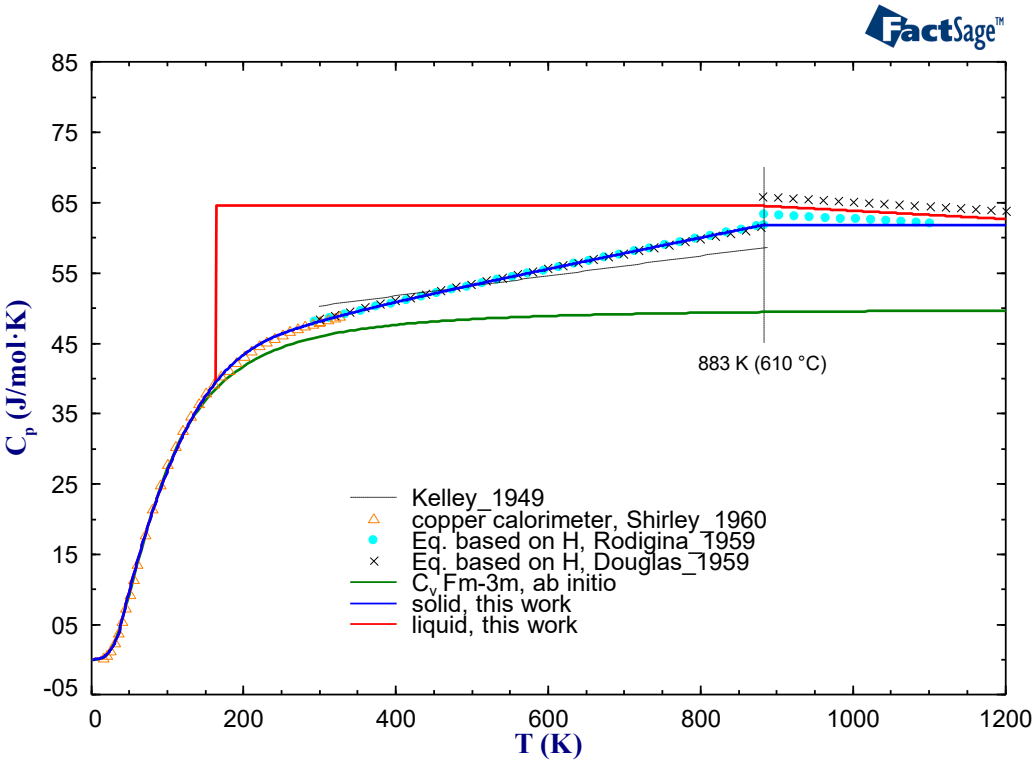


Figure 6-3. Heat capacity for solid and liquid phases of LiCl

For the liquid phase, $C_p$ above 883 K was optimized based on the average of experimental data of Rodigina et al. [57] and Douglas and Victor [50], of which both decrease with increasing temperature. As shown in Figure 6-3, the $C_p$ of the liquid phase calculated at 883 K was extrapolated to 164 K, which is the so-called Kauzmann temperature ($T_K$) as previously reported [203]. Below 164 K, the $C_p$ is the same as the solid phase. All polynomial functions of the optimized heat capacity are given in Table 6-4.

With the obtained $C_p$ polynomial, a standard entropy of 59.22 J/mol·K was calculated by integration of the function $C_p$/T, which is within the uncertainty range compared with the standard entropy of 59.30 J/mol·K in the database. This value was reported to be 59.29 ± 0.08 J/mol·K by Shirley [60]. The comparison of these entropy data of LiCl is shown in Figure A-5. The enthalpy increment is shown in Figure 6-4. The calculated results agrees well with the

experimental data from Rodigina et al. [57] and Douglas and Victor [50], which is demonstrated by the overlap of the different lines, especially in the solid phase. Rodigina et al. [57] originally measured H-$H_{293}$, here it was recalculated to H-$H_{298}$ for comparison between different data.

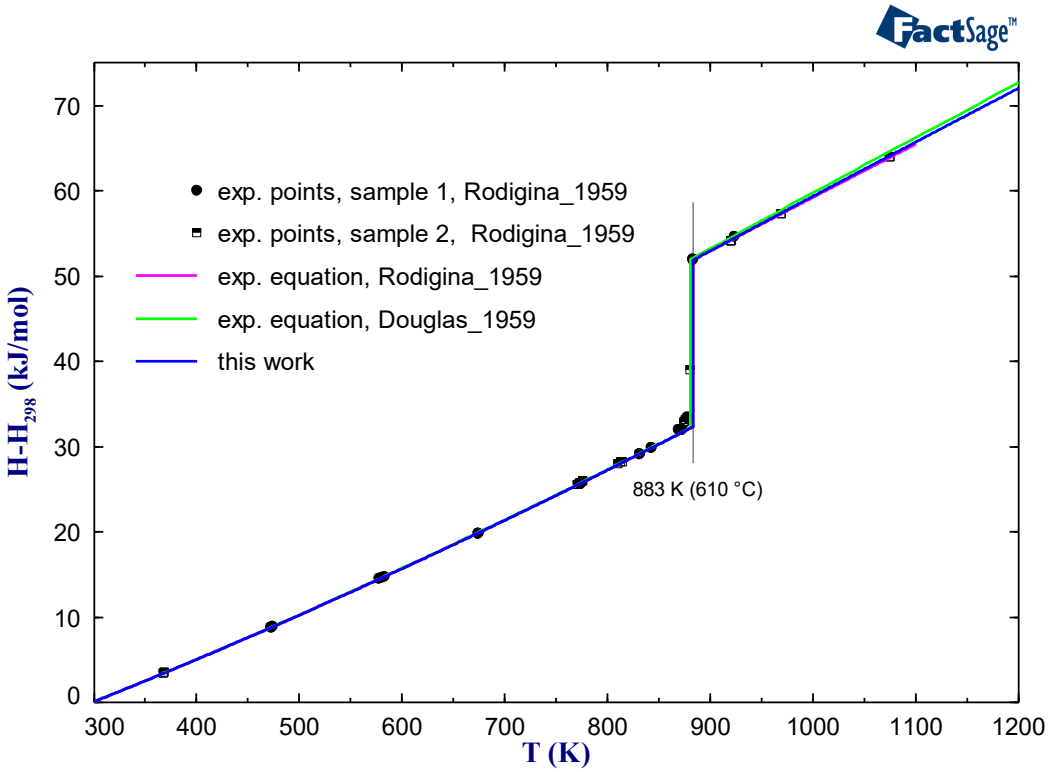


Figure 6-4. Enthalpy increment of LiCl

Table 6-4. Thermodynamic properties of LiCl.

| Compound | $\Delta H^0_{298,f}$, J/mol | $S^0_{298}$, J/mol·K | Reference | T, K | $C_p$, J/mol·K | Reference |
|---|---|---|---|---|---|---|
| LiCl (solid) | -408266.4 | 59.3 | SGPS [25] | 1-35 | $-2.65915\cdot10^{-4}\ T^2 + 7.53251\cdot10^{-5}\ T^3$ | This work |
| | | | | 35-298 | $-15.23398 + 0.59702\ T - 1.9869336\cdot10^{-3}\ T^2 + 2.336\cdot10^{-6}\ T^3$ | This work |
| | | | | 298-883 | $42.955 + 0.02152\ T - 118824.09106\ T^{-2}$ | This work |
| | | | | 883-2000 | 61.808 | This work |
| LiCl (liquid) | -394161.6 | 70.0 | This work | | solid → liquid $H_m$=19539.3 J/mol at 883 K | Rodigina et al. [57] |
| | | | | 1-35 | $-2.65915\cdot10^{-4}\ T^2 + 7.53251\cdot10^{-5}\ T^3$ | This work |
| | | | | 35-163 | $-15.23398 + 0.59702\ T - 1.9869336\cdot10^{-3}\ T^2 + 2.336\cdot10^{-6}\ T^3$ | This work |
| | | | | 163-883 | 64.5043 | This work |

| | | | | | | |
|---|---|---|---|---|---|---|
| | | | | 883-2100 | 69.714 -0.0059 T | This work |

## 6.2 Binary systems

### 6.2.1 System LiCl-KCl

Excess Gibbs energy parameters for the liquid phase in the LiCl-KCl system were assessed using phase equilibria data, mixing property, enthalpy increment of the eutectic mixture and activity of different components in the liquid phase. As shown in Figure 6-5 the phase diagram of the system LiCl-KCl was investigated extensively, and the experimental results from different research groups are in good agreement.

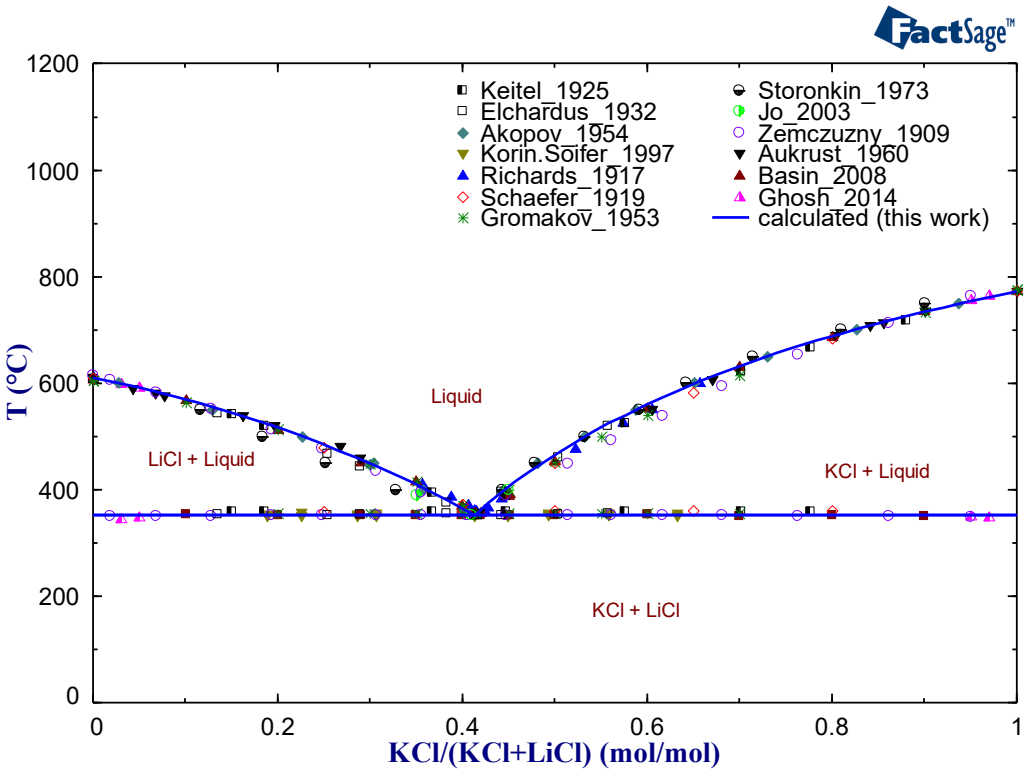


Figure 6-5. Phase diagram of the LiCl-KCl system.

As it was mentioned in chapter 2, that most of the results show that this is a eutectic system. In the assessment of Zhou and Zhang [96], the formation of solid solutions based on both chlorides with the limit of solubility of 0.05 molar fraction was suggested. It can be clearly seen in Figure 6-5 that Zhemchuzhnui and Rambach [46] measured the eutectic temperature for the composition $x_{KCl}$ = 0.018, which means that at least at this composition the solid solution phase

is absent, so that the maximum solubility is less than 0.018 (molar fraction) at KCl side. The maximum solubility is indicated less than 0.03 at the LiCl side using the data by Ghosh et al. [95]. In summary, these solid solutions are not taken into consideration for the optimization in the present work. The existing experimental and calculated eutectic composition and temperature in this system are presented in Table 6-5.

Table 6-5. Experimental and calculated eutectic points in the system LiCl-KCl.

| Reaction | Molar fraction KCl | T, °C | Method | Reference |
|---|---|---|---|---|
| Liquid ↔ LiCl + KCl | 0.415 | 361 | TA | Richards and Meldrum [47] |
| | 0.415 | 354 | TA+ visual-polythermal | Aukrust et al. [92] |
| | 0.405 | 352 | TA | Zhemchuzhnui and Rambach [46] |
| | 0.42 | 361 | TA | Schaefer [73] |
| | 0.417 | 352 | TA | Elchardus and Laffitte [94] |
| | 0.4175 | 359 | TA | Keitel [200] |
| | 0.413 | 354.4 | DSC | Korin and Soifer [93] |
| | 0.42 | 348 | Visual-polythermal | Akopov and Bergman [204] |
| | 0.43 | 352 | Visual-polythermal | Unzhakov [205] |
| | 0.418 | 352 | DTA | Basin et al. [206] |
| | 0.414 | 353 | Calculated | Zhou and Zhang [96] |
| | 0.405 | 355 | Calculated | Sangster and Pelton [89] |
| | 0.414 | 353 | Calculated | Ghosh et al. [95] |
| | 0.407 | 353 | Calculated | FTsalt [9] |
| | 0.413 | 352 | Calculated | This work |

The enthalpy increment ($H_T$-$H_{298.15}$) at the eutectic composition in the LiCl-KCl system is shown in Figure 6-6. As mentioned in chapter 2, Powers and Blalock [97] measured H-$H_{0\ °c}$ by using Bunsen ice-calorimeter, while in this work $H_T$-$H_{298}$ was obtained by subtracting $H_{298}$-$H_{273}$ calculated based on the enthalpy equation given in the temperature range of 97-351 °C. It is noticed that the experimental data points from Powers and Blalock [97] are relatively dispersed in the liquid phase and refer to the highest value. Solomons et al. [98] determined $H_T$-$H_{298}$ with cryoscopic measurement in the temperature range 592-656 K. Then, Markov et al. [99] and Clark [100] obtained their data by drop calorimetry, which agree well with each other and are taken as reference for the optimization of the liquid phase in this work. While the temperature dependence of the enthalpy increment data on the solid phase from all available investigations [97–100] are consistent. The enthalpy increment calculated with the current database agrees well the experimental results (Figure 6-6).

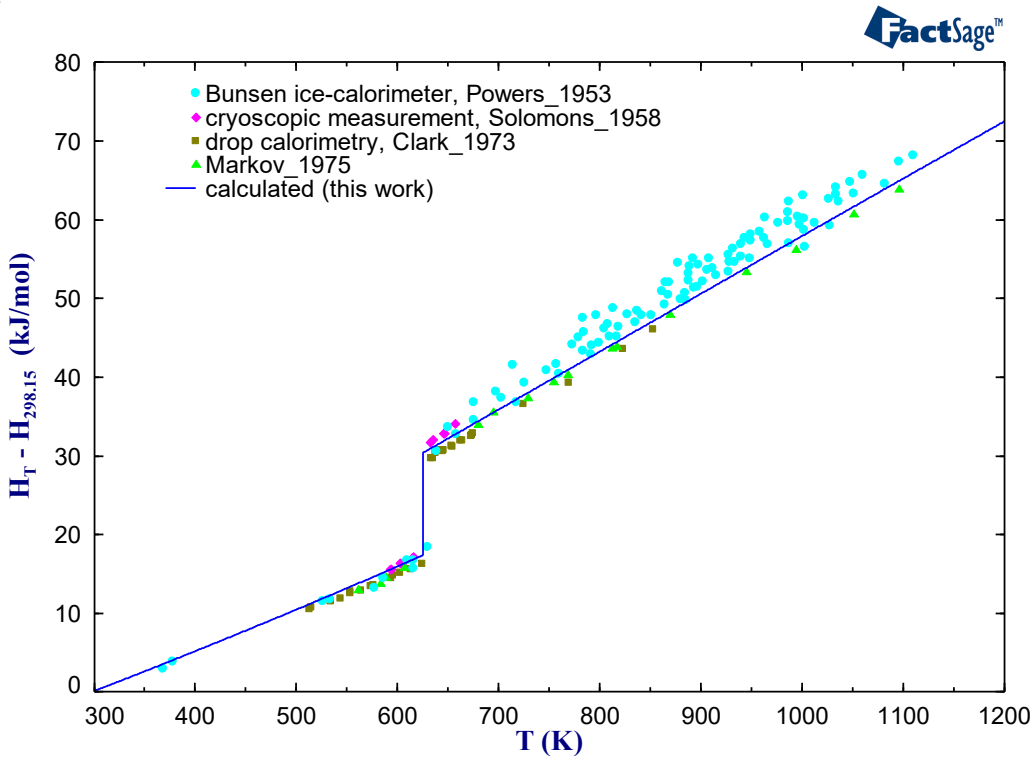


Figure 6-6. Comparison of the experimental data with the calculated enthalpy increment ($H_T$-$H_{298.15}$) of the LiCl-KCl system at the eutectic composition.

Table 6-6. Experimental and calculated melting enthalpy of the LiCl-KCl system at the eutectic composition.

| Reaction | Molar fraction KCl | Melting enthalpy, kJ/mol | Method | Reference |
|---|---|---|---|---|
| Liquid ↔ LiCl+KCl | 0.41 | 12.97±0.08 | Drop calorimetry | Clark [100] |
| | 0.41 | 14.88±2 | Bunsen ice-calorimeter | Powers and Blalock [97] |
| | 0.415 | 13.8±0.84 | Calorimeter | Aukrust et al. [92] |
| | 0.42 | 13.39±0.25 | Cryoscopic | Solomons et al. [98] |
| | 0.413 | 12.12±0.6 | DSC | Korin and Soifer [93] |
| | 0.42 | 12.34 | Drop calorimetry | Markov et al. [99] |
| | 0.407 | 14.80 | Calculated | FTsalt [9] |
| | 0.413 | 13 | Calculated | This work |

Table 6-6 presents the melting enthalpy data of the LiCl-KCl system at the eutectic composition measured by different authors including Aukrust et al. [92] and Korin and Soifer [93]. The largest value 14.88±2 kJ/mol was measured by Powers and Blalock [97], while the smallest value is 12.12±0.6 kJ/mol measured by Korin and Soifer [93] using DSC. The result calculated using FTsalt

is 14.8 kJ/mol, nearly equal to the largest value reported. The one calculated by the current database is 13.07 kJ/mol and it is close to experimental values 12.97±0.08 kJ/mol measured by Clark [100] and 13.39±0.25 kJ/mol measured by Solomons et al. [98], which have relatively smaller uncertainty and are considered to be more reliable.

The heat of solution of solid KCl in liquid LiCl at 740 °C was measured by Hersh and Kleppa [68]. It can be seen from Figure 6-7 that the present calculated results are consistent with the experimental data.

Figure 6-8 shows the calculated mixing enthalpy of liquid KCl and liquid LiCl at 740 °C, where the points are calculated using the excess enthalpy equation given by Hersh and Kleppa [68]. Markov et al. [99] measured the mixing enthalpy of the eutectic composition at 770 °C as -4.02 kJ/mol, and Aukrust et al. [92] investigated the mixing enthalpy of this system at 775 °C, the comparison of calculated and experimental results is given in Figure A-6.

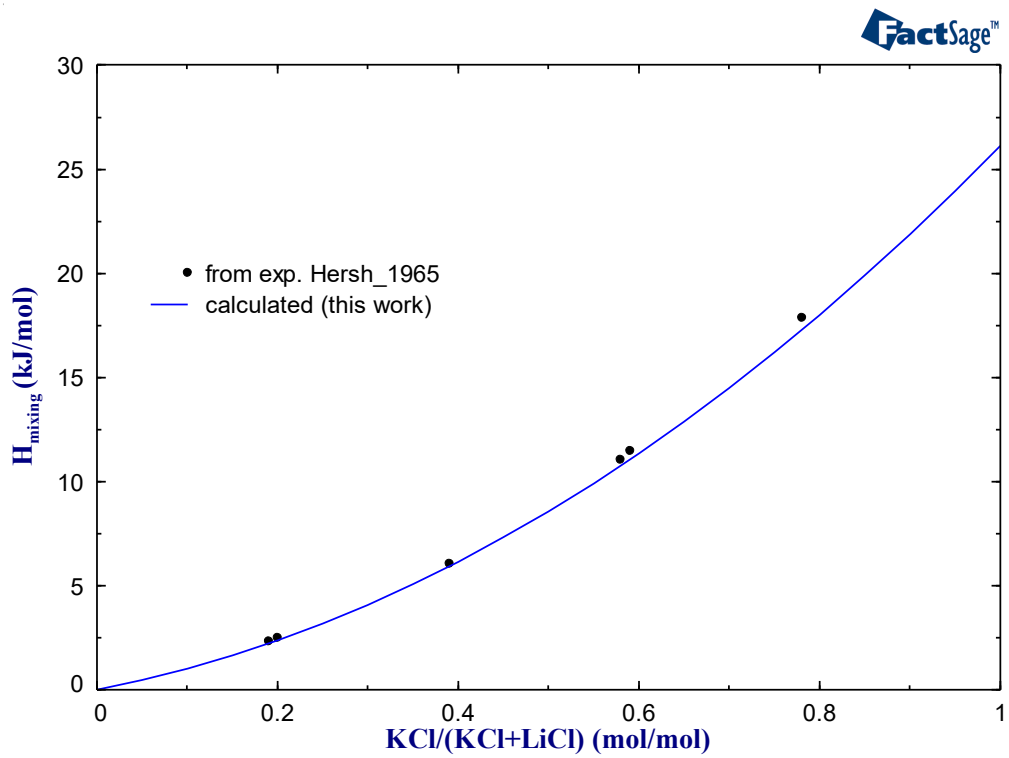


Figure 6-7. Heat of solution of solid KCl in liquid LiCl at 740 °C

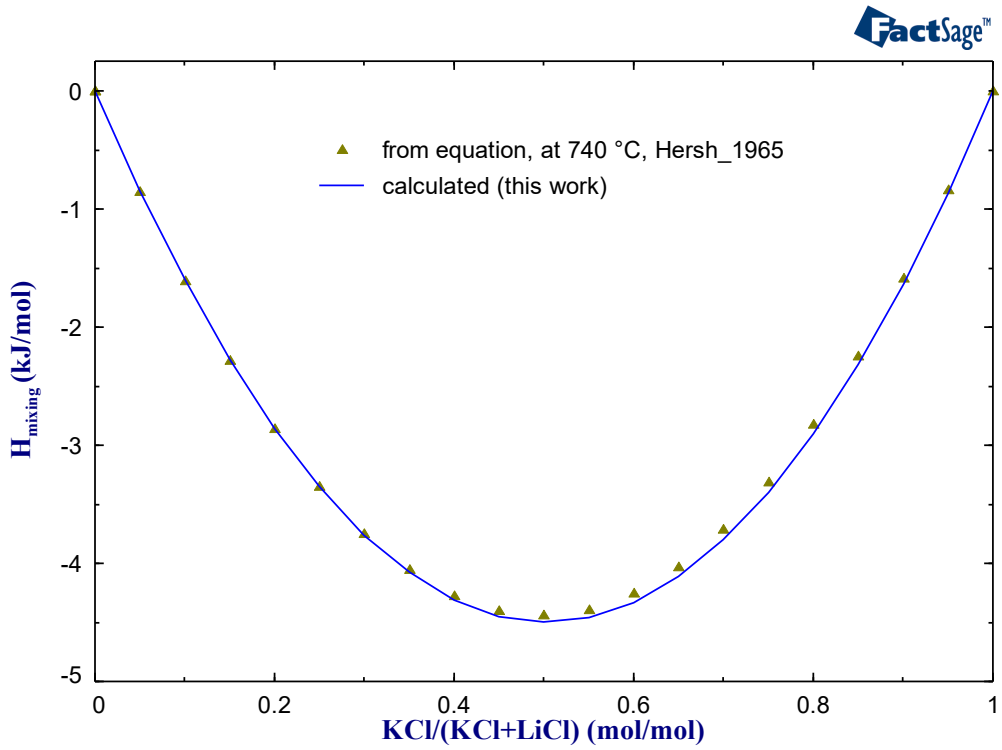


Figure 6-8. Calculated mixing enthalpy of liquid KCl and liquid LiCl at 740 °C.

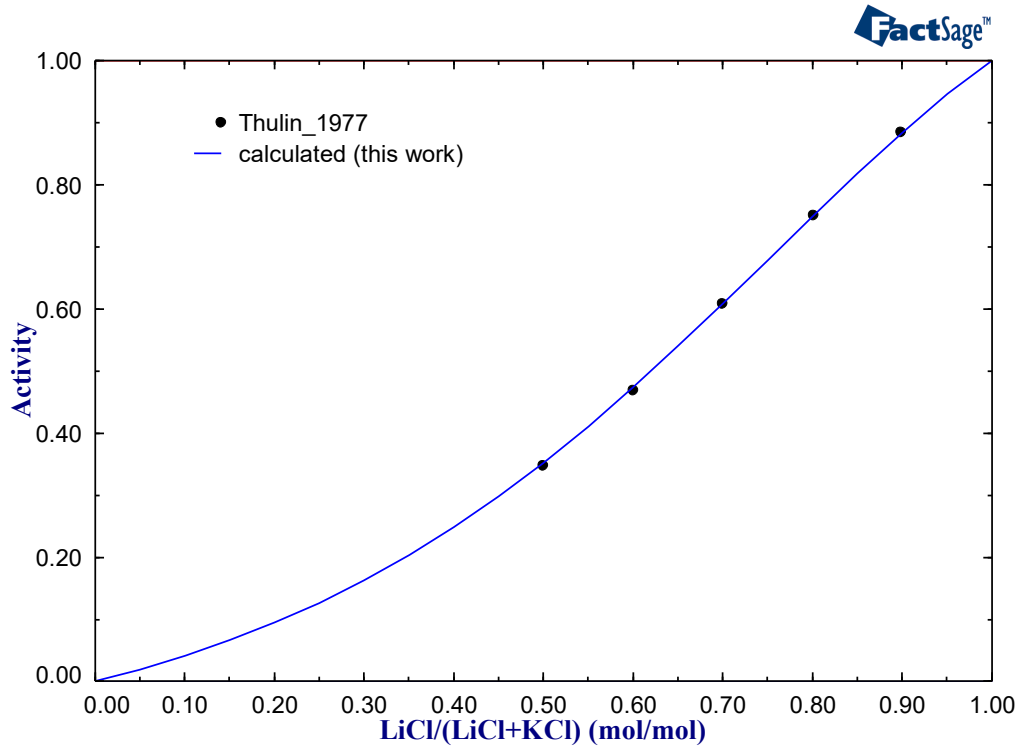


Figure 6-9. Activity of LiCl in the liquid phase at 722 °C.

The activity of LiCl in the liquid mixture at 722 °C measured by Thulin et al. [101] is taken into account for the optimization of the thermodynamic parameters. Figure 6-9 shows the experimental and calculated activity data of LiCl with good agreement. In addition, the activity data of LiCl and KCl in the liquid phase at 640 °C were measured by Behl [102] using EMF method. The comparison of the calculated and experimental results is shown in Figure A-7, where a relatively large deviation is noticed due to possible large experimental errors and more experimental activity data are therefore expected for further assessment of the present thermodynamic dataset.

The present optimized parameters for this system are given in Table 6-27 (at the end of Chapter 6). Different from the other binary systems, an additional parameter C in $L_{ij}^{(0)}(T)$ in Eq. 4.8 was introduced for the assessment of the excess Gibbs energy for the liquid of the system LiCl-KCl. Without parameter C, the calculated enthalpy increment of the eutectic composition always deviates from the reliable experimental results even if the calculated phase diagram and other thermodynamic properties agree well with the experimental data. The enthalpy increment of the eutectic composition of this system is essential, especially for the application as PCM material, and the enthalpy increment should be taken into account with a greater weight. Therefore, parameter C in $L_{ij}^{(0)}(T)$ was introduced to provide a better agreement between the calculated enthalpy data and the reliable experimental results.

### 6.2.2 System LiCl-NaCl

In this work, the binary system LiCl-NaCl was thermodynamically accessed based on the phase equilibria and the mixing enthalpy data from the literature.

As mentioned in Chapter 2, the phase diagram of the LiCl-NaCl system has been investigated many times. In this work, continuous solubility is considered between solid LiCl and NaCl (called Alk_chlorides in the present work), and a miscibility gap appears in the phase diagram at low temperature (Figure 6-10). The compounds $LiNaCl_2$ and $LiNa_2Cl_3$ reported before [80,82] are not considered in the optimization, because they were not detected in the XRD measurement by Smits et al. [91]. The solvus lines detected by Schaefer [73] and Chesnokov et al. [79] agree well

with each other, therefore, they are selected for the present assessment. The selected experimental data are shown in Table 6-7. It can be seen that our calculation agrees well with the experimental results in Figure 6-10.

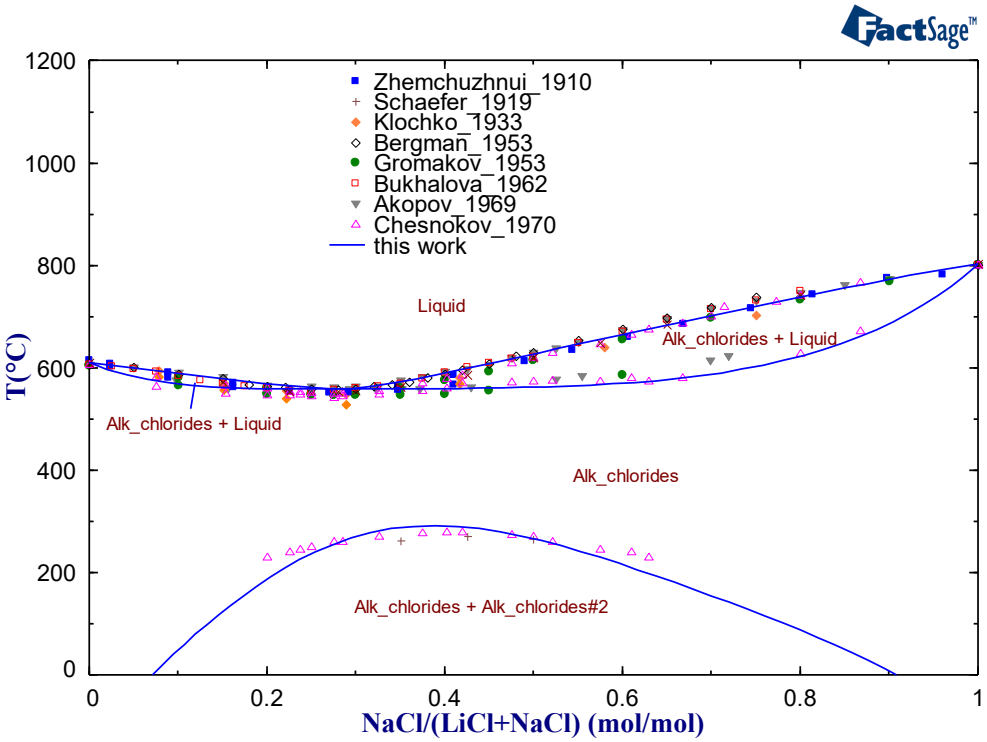


Figure 6-10. Phase diagram of the LiCl-NaCl system.

Table 6-8 presents the melting enthalpy data of the LiCl-NaCl system at the eutectic composition measured by different authors including Li et al. [143] and Tye et al. [207]. The result of 18.67 kJ/mol calculated with FTsalt is smaller than the experimental results, while the result calculated with the current database is close to the data from Tye et al. [207] and within the uncertainty range of Li et al. [143].

Meanwhile, the calculated mixing enthalpy agrees well with the experimental results from Hersh and Kleppa [68], where the mixing enthalpy was measured with liquid LiCl and solid NaCl as reference state at 740 °C at different compositions (Figure 6-11). Figure 6-12 shows the calculated mixing enthalpy with liquid NaCl and liquid LiCl as reference state at 740 °C, given as equation by Hersh and Kleppa [68]. The optimized parameters of the liquid and solid solution phases are shown in Table 6-27.

Table 6-7. Experimental and calculated invariant points in the system LiCl-NaCl.

| Reaction type | Reaction | Molar fraction NaCl | T, °C | Method | Reference |
|---|---|---|---|---|---|
| eutectic | Liquid ↔ LiCl+NaCl | 0.215 | 553 | Visual-polythermal | Bergman and Akopov [88] |
| | | 0.27 | 553 | Visual-polythermal | Akopov [87] |
| | | 0.21 | 558 | Visual-polythermal+TA | Akopov and Bergman [83] |
| | | 0.3 | 546 | Visual-polythermal | Bergman et al. [84] |
| | | 0.285 | 556 | Visual-polythermal+TA | Akopov and Korobka [77] |
| | | 0.285 | 553 | Visual-polythermal | Bortnikova et al. [82] |
| | | 0.245 | 551 | Visual-polythermal | Bukhalova and Arabadzhan [86] Arabadzhan and Bergman [85] |
| | | 0.27 | 548 | TA | Derkacheva and Gontar' [81] |
| | | 0.26 | 554 | TA | Kruglov and Prostakov [80] |
| azeotropic | Liquid ↔ Alk_chlorides | 0.27 | 552 | TA | Zhemchuzhnui and Rambach [46] |
| | | 0.28 | 553 | TA | Schaefer [73] |
| | | 0.28 | 550 | DTA | Chesnokov et al. [79] |
| | | 0.275 | 546 | TA | Gromakov and Gromakova [74] |
| | | 0.29 | 528 | Visual-polythermal | Klochko [75] |
| | | 0.25 | 555 | TA | Storonkin et al. [78] |
| | | 0.24 | 559 | TA | *Li et al. [143] |
| | | - | ≤552 | DTA | Tian et al. [76] |
| | | 0.28 | 554 | Calculated | Sangster and Pelton [89] |
| | | 0.28 | 553 | Calculated | FTsalt [9] |
| | | 0.29 | 558 | Calculated | This work |
| Maximum of solvus/ consolute | Alk_chlorides ↔ Alk_chlorides + Alk_chlorides_2 | 0.35 | 314 | TA | Zhemchuzhnui and Rambach [46] |
| | | - | 400 | Visual-polythermal | Klochko [75] |
| | | 0.43 | 271 | TA | Schaefer [73] |
| | | 0.4/0.42 | 280 | DTA | Chesnokov et al. [79] |
| | | 0.33 | 241 | Calculated | Sangster and Pelton [89] |
| | | 0.32 | 250 | Calculated | FTsalt [9] |
| | | 0.38 | 291 | Calculated | This work |

* the composition was adopted.

Table 6-8. Melting enthalpy of the azeotropic composition in the system LiCl-NaCl.

| Molar fraction NaCl | T, °C | Melting enthalpy, kJ/mol (J/g) | Method | Reference. |
|---|---|---|---|---|
| 0.24 | 559 | 21.25 ± 1.5 (460 ± 32) | TA | *Li et al. [143] |
| 0.27 | 552 | 19.68 (430) | - | *Tye et al. [207] |
| 0.28 | 553 | 18.67 | Calculated | FTsalt [9] |
| 0.29 | 558 | 19.78 | Calculated | This work |

* the composition was adopted.

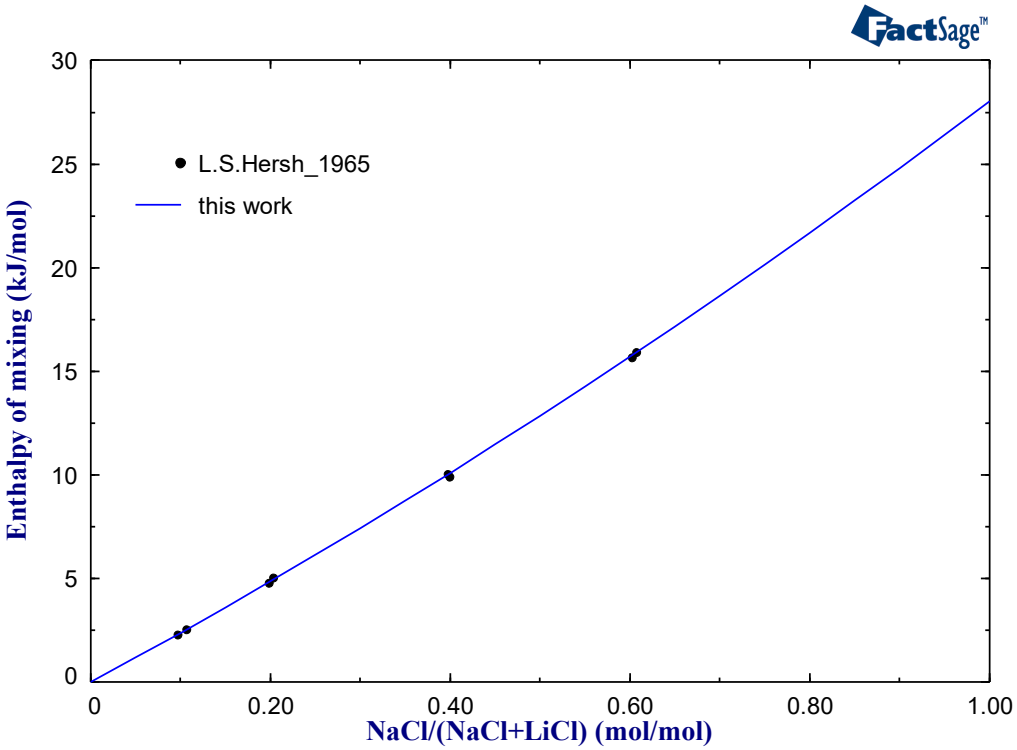


Figure 6-11. Heat of solution of solid NaCl in liquid LiCl at 740 °C.

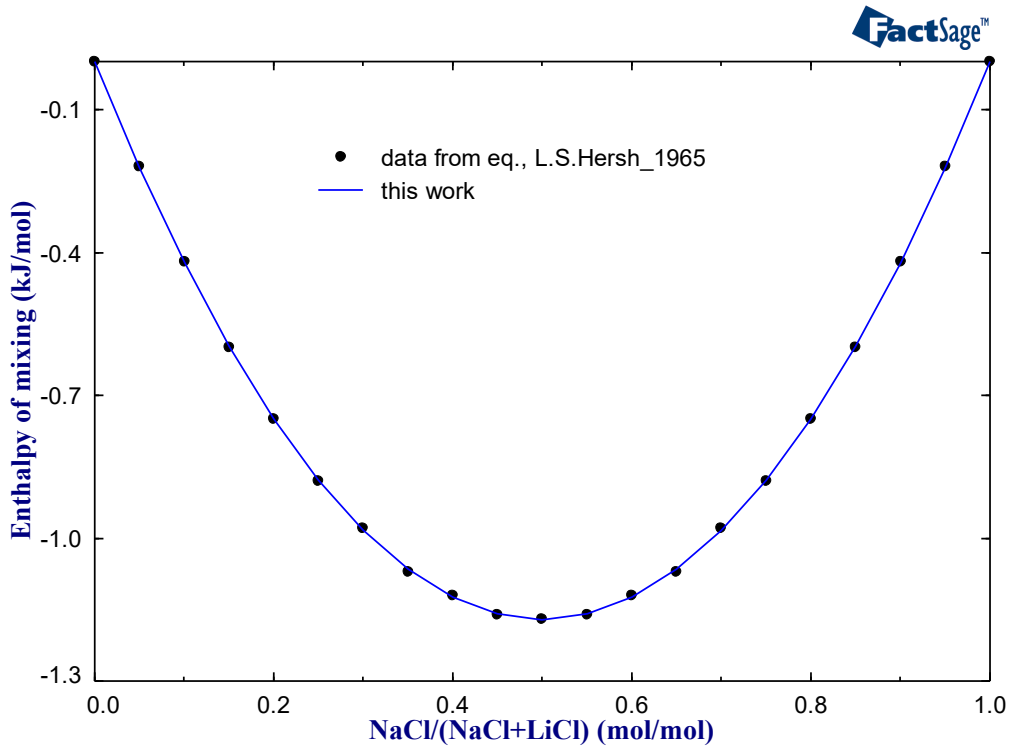


Figure 6-12. Calculated mixing enthalpy of liquid LiCl and liquid NaCl at 740 °C.

### 6.2.3 System $Li_2CO_3$-LiCl

The assessment of the $Li_2CO_3$-LiCl system in the present work was performed using the experimental results of the phase diagram from the literature.

Figure 6-13 shows the phase diagram of $Li_2CO_3$-LiCl. In the present work, the interaction parameters between lithium chloride and carbonate in the liquid phase were optimized using all the phase equilibria data from Volkov and Zakhvalinskii [103], Reshetnikov and Diogenov [104] and Levin et al. [105]. The liquidus temperatures from Volkov and Zakhvalinskii [103] and Reshetnikov and Diogenov [104] were digitalized from the projection of the reciprocal system $Li^+$, $K^+//Cl^-$, $CO_3^{2-}$ and ternary system $Li^+//Cl^-$, $CO_3^{2-}$, $SO_4^{2-}$, respectively. The liquidus line calculated using the new database shows good matching with the experimental result.

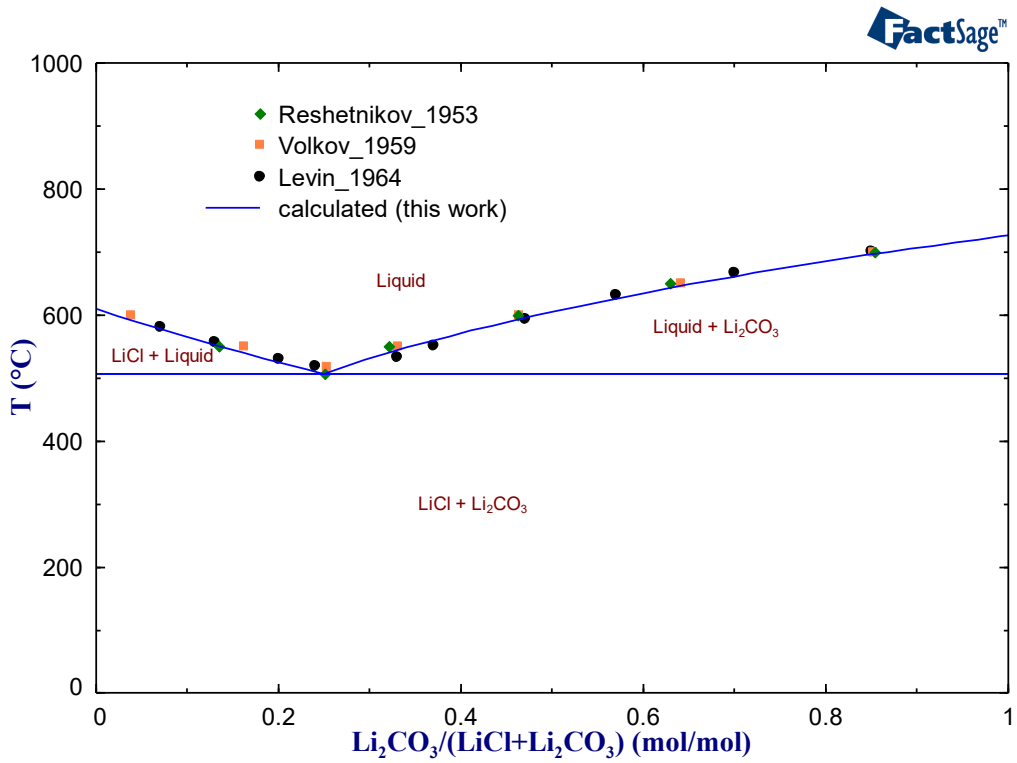


Figure 6-13. Phase diagram of the $Li_2CO_3$-LiCl system.

All experimental and calculated eutectic information in this system is collected in Table 6-9. The eutectic temperature was calculated to be 507 °C in this work, which is close to the results of Reshetnikov and Diogenov [104] (507 °C) and Levin et al. [105] (506 °C) and also the modelling

result of Dessureault et al. [106] (509 °C). While the eutectic temperature calculated with FTsalt (517 °C) is close to the data from Volkov and Zakhvalinskii [103] (518 °C). The eutectic composition calculated in this work x($Li_2CO_3$) = 0.261 is close to the average value of the experimental data. All results indicate the absence of a solid solution in this system. The optimized parameters for this system are displayed in Table 6-27.

Table 6-9. Experimental and calculated eutectic points in the system $Li_2CO_3$-LiCl.

| Reaction | Molar fraction $Li_2CO_3$ | T, °C | Method | Reference |
|---|---|---|---|---|
| Liquid ↔ $Li_2CO_3$ + LiCl | 0.28 | 506 | TA | Levin et al. [105] |
| | 0.242 | 507 | Visual-polythermal | Reshetnikov and Diogenov [104] |
| | 0.266 | 518 | Visual-polythermal | Volkov and Zakhvalinskii [103] |
| | 0.262 | 509 | Calculated | Dessureault et al. [106] |
| | 0.311 | 517 | Calculated | FTsalt [9] |
| | 0.261 | 507 | Calculated | This work |

### 6.2.4 System $Na_2CO_3$-NaCl

The optimization of the Gibbs energy of the liquid phase in the $Na_2CO_3$-NaCl system was performed based on experimental data in the literature, e.g., phase equilibrium and the activity of $Na_2CO_3$ in the solid phase.

Figure 6-14 shows the phase diagram of the $Na_2CO_3$-NaCl system. It can be seen that the calculated results agree well with the experimental results [107–109,114–116,208,209]. The eutectic information from the literature and this work are collected in Table 6-10.

The melting enthalpy information is collected in Table 6-11. It was reported to be 24.1±1.4 kJ/mol by Jiang et al. [117] and 22.5 kJ/mol by Raud et al. [26]. The melting enthalpy of 7.9 kJ/mol measured by Ye et al. [118] deviated too much from other measurements, so it was not taken for the optimization. Compared with the result 27.4 kJ/mol from FTsalt, the calculated melting enthalpy of 24.9 kJ/mol from our database is closer to the experimental data and it is within the uncertainty range by Jiang et al. [117].

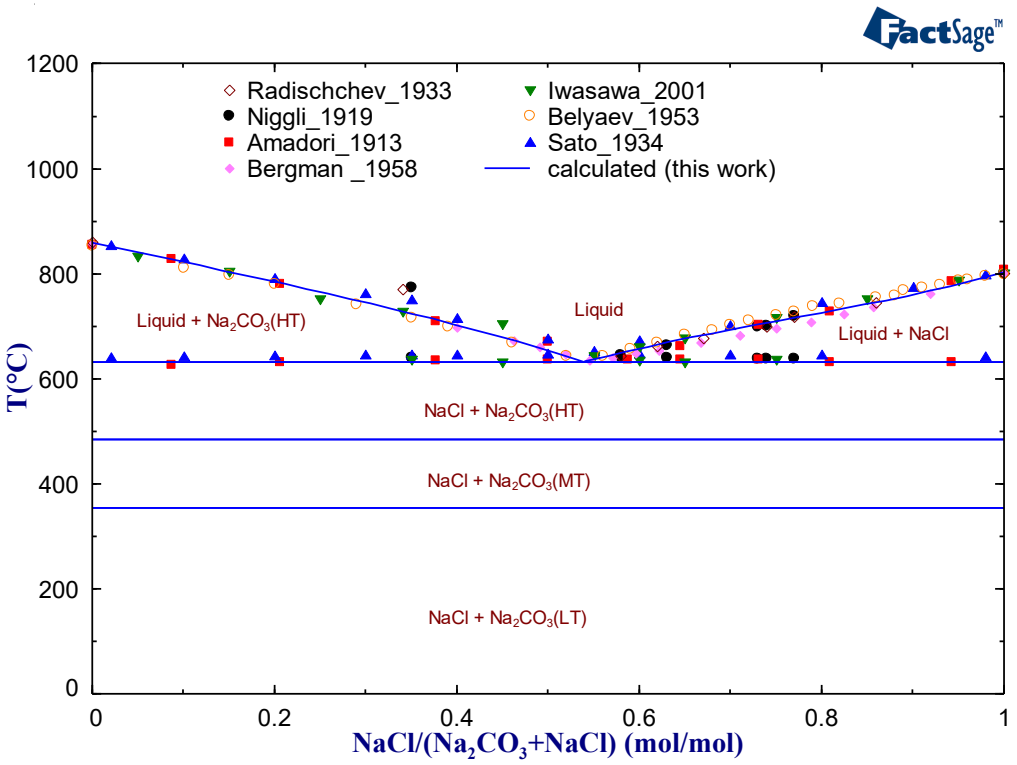


Figure 6-14. Phase diagram of $Na_2CO_3$-NaCl system.

Table 6-10. Experimental and calculated eutectic points in the system $Na_2CO_3$-NaCl.

| Molar fraction NaCl | T, °C | Method | Reference |
|---|---|---|---|
| 0.57 | 634 | Hot filament | Iwasawa et al. [116] |
| 0.59 | 638 | Visual-polythermal | Rea [209] |
| 0.55 | 632 | Visual-polythermal | Belyaev and Sholokhovich [208] |
| 0.535 | 645 | TA | Sato [115] |
| 0.53 | 638 | TA | Radishchev [108] |
| 0.545 | 634 | Visual-polythermal | Bergman and Sementsova [107] |
| 0.55 | 638 | TA | Niggli [114] |
| 0.55 | 637 | *STA | **Jiang et al. [117] |
| 0.577 | 636 | DTA | **Ye et al. [118] |
| 0.553 | 630 | DSC | **Raud et al. [26] |
| 0.59 | 636 | TA | Amadori [109] |
| 0.53 | 637 | KEMS | This work |
| 0.53 | 633 | DTA | This work |
| 0.55 | 632 | Calculated | Yaokawa et al. [113] |
| 0.55 | 632 | Calculated | FTsalt [9] |
| 0.54 | 632 | Calculated | This work |

* - simultaneous thermal analysis, ** - the composition was adopted from FTsalt [9].

Table 6-11. Melting enthalpy of eutectic composition in the $Na_2CO_3$-NaCl system.

| Molar fraction, NaCl | T, °C | Fusion enthalpy, kJ/mol (J/g) | Method | Reference |
|---|---|---|---|---|
| 0.55 | 637 | 24.1 ± 1.4 (301.8± 17.5) | STA | *Jiang et al. [117] |
| 0.577 | 636 | 7.9 (101.12) | DTA | *Ye et al. [118] |
| 0.553 | 630 | 22.5 (282) | DSC | *Raud et al. [26] |
| 0.55 | 632 | 27.4 | Calculated | FTsalt [9] |
| 0.54 | 632 | 24.9 | Calculated | This work |

* the composition was adopted from FTsalt [9].

The activity of $Na_2CO_3$ in the solid phase of the compositions x($Na_2CO_3$)=0.2, 0.4, 0.5 and 0.7 was calculated and compared with the results measured by Iwasawa et al. [116] using EMF method. As shown in Figure 6-15, they are in good agreement. All these data are taken into account when optimizing the system. Moreover, as mentioned in Chapter 5, for the composition 0.47NaCl-0.53$Na_2CO_3$, the activity of NaCl in the liquid phase at 665 °C was measured in this work by KEMS to be 0.88 according to chapter 5, and it was calculated to be 0.8 by our new database. The comparison is shown in Figure A-8. The optimized parameters of the liquid solution phase are shown in Table 6-27.

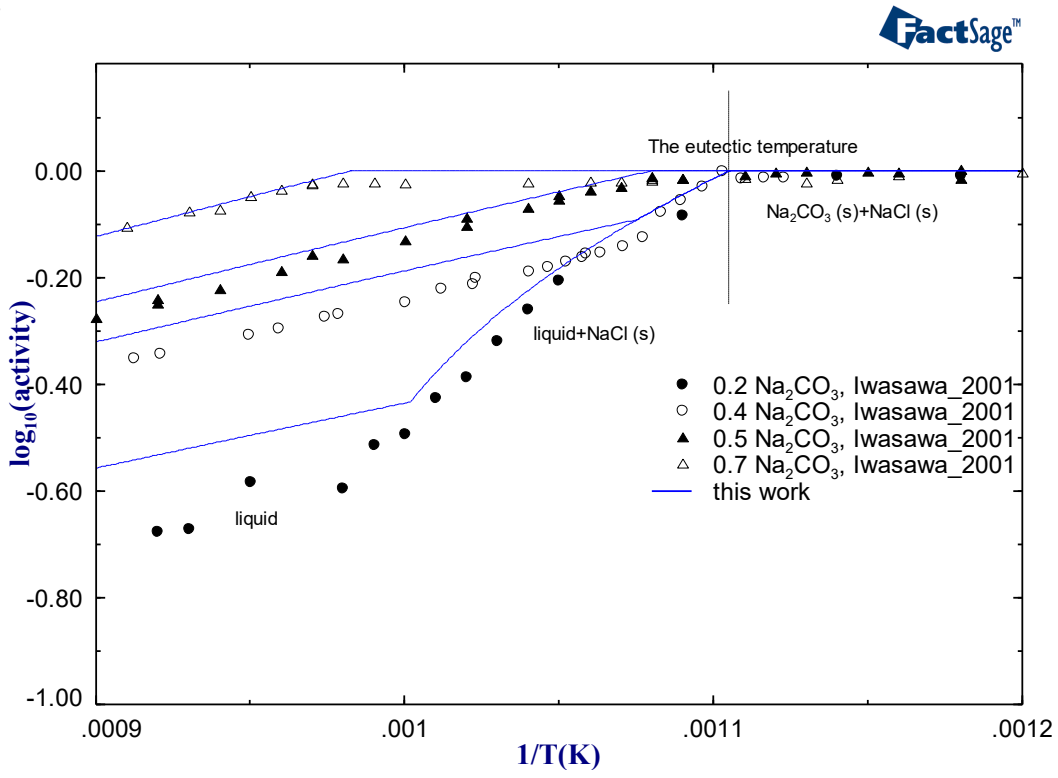


Figure 6-15. The activity of $Na_2CO_3$ in NaCl-$Na_2CO_3$ system.

### 6.2.5 System $K_2CO_3$-KCl

Excess Gibbs energy parameters for the liquid phase in the $K_2CO_3$-KCl system were assessed using the phase equilibria data. The phase diagram of the $K_2CO_3$-KCl system is shown in Figure 6-16.

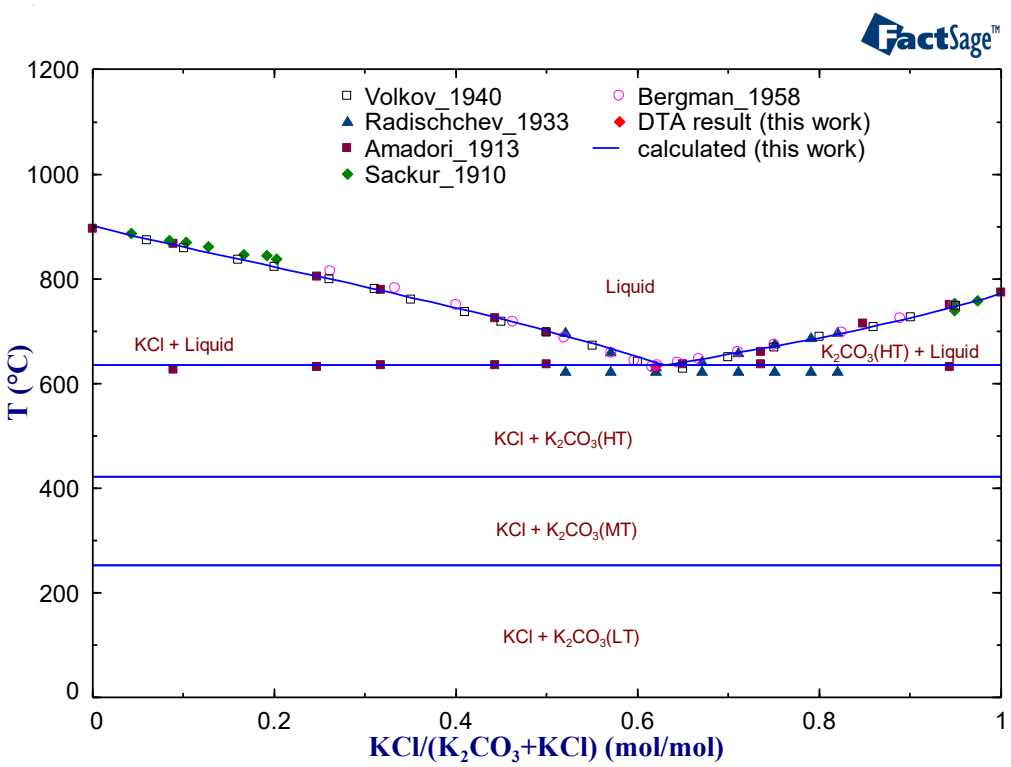


Figure 6-16. Phase diagram of the $K_2CO_3$-KCl system.

All values for the eutectic temperature and composition determined experimentally or calculated are collected in Table 6-12. The eutectic temperature obtained by Brearley and Morwood [112] of 590 °C is much lower than the other results (623-636 °C), so it was not taken into account in this optimization. The measured eutectic temperature 633 °C by DTA in our work is close to the results of Amadori [109] (636 °C) and Bergman and Sementsova [107] (632 °C). The present assessment for the $K_2CO_3$-KCl system is based on the existing liquidus data from the literature in combination with the eutectic temperature of 633 °C (present work), and a good agreement has been achieved (Figure 6-16). Beside the phase diagram, the calculated activity of $K_2CO_3$ and KCl in the liquid phase at 950 °C was compared with the predictions by Yaokawa et al.

[113] and the commercial database FTsalt, as shown in Figure A-9. The optimized parameters for this system are summarized in Table 6-27.

The melting enthalpy of the eutectic composition in this system was measured to be 27.31 kJ/mol by Raud et al. [26], which is compared with the melting enthalpy calculated by FTsalt (24.99 kJ/mol) and this work (27.26 kJ/mol) in Table 6-13.

Table 6-12. Experimental and calculated temperature and composition of the eutectic point in the system $K_2CO_3$-KCl.

| Reaction | Molar fraction KCl | T, °C | Method | Reference |
|---|---|---|---|---|
| Liquid ↔ $K_2CO_3$ + KCl | 0.65 | 636 | TA | Amadori [109] |
| | 0.62 | 590 | N/A | Brearley and Morwood [112] |
| | 0.62 | 623 | TA | Radishchev [108] |
| | 0.62 | 632 | Visual-polythermal | Bergman and Sementsova [107] |
| | 0.63 | 625 | Visual-polythermal | Volkov and Bergman [111] |
| | 0.63 | 630 | DSC | Liu et al. [159] |
| | 0.62 | 633 | DTA | *This work |
| | 0.63 | 629 | Calculated | Dessureault et al. [106] |
| | 0.62 | 623 | Calculated | Yaokawa et al. [113] |
| | 0.62 | 631 | Calculated | FTsalt [9] |
| | 0.63 | 635 | Calculated | This work |

* the composition was adopted from FTsalt [9].

Table 6-13. Melting enthalpy of the eutectic composition in the system $K_2CO_3$-KCl.

| Molar fraction KCl | T, °C | Melting enthalpy, kJ/mol | Method | Reference. |
|---|---|---|---|---|
| 0.624 | 630 | 27.31 | DSC | *Raud et al. [26] |
| 0.624 | 631 | 24.99 | Calculated | FTsalt [9] |
| 0.62 | 635 | 27.26 | Calculated | This work |

* the composition was adopted from FTsalt [9].

### 6.2.6 System $Li_2CO_3$-$Na_2CO_3$

Excess Gibbs energy parameters for the liquid phase and solid solution phases in the $Li_2CO_3$-$Na_2CO_3$ system were assessed using the phase change temperatures measured by DTA and HTXRD in this work, as well as the phase equilibrium data, mixing property, and enthalpy increment of the eutectic mixture from the literature. The Gibbs energy of the intermediate compound $LiNaCO_3$ was assessed based on the heat capacity measurements using DSC.

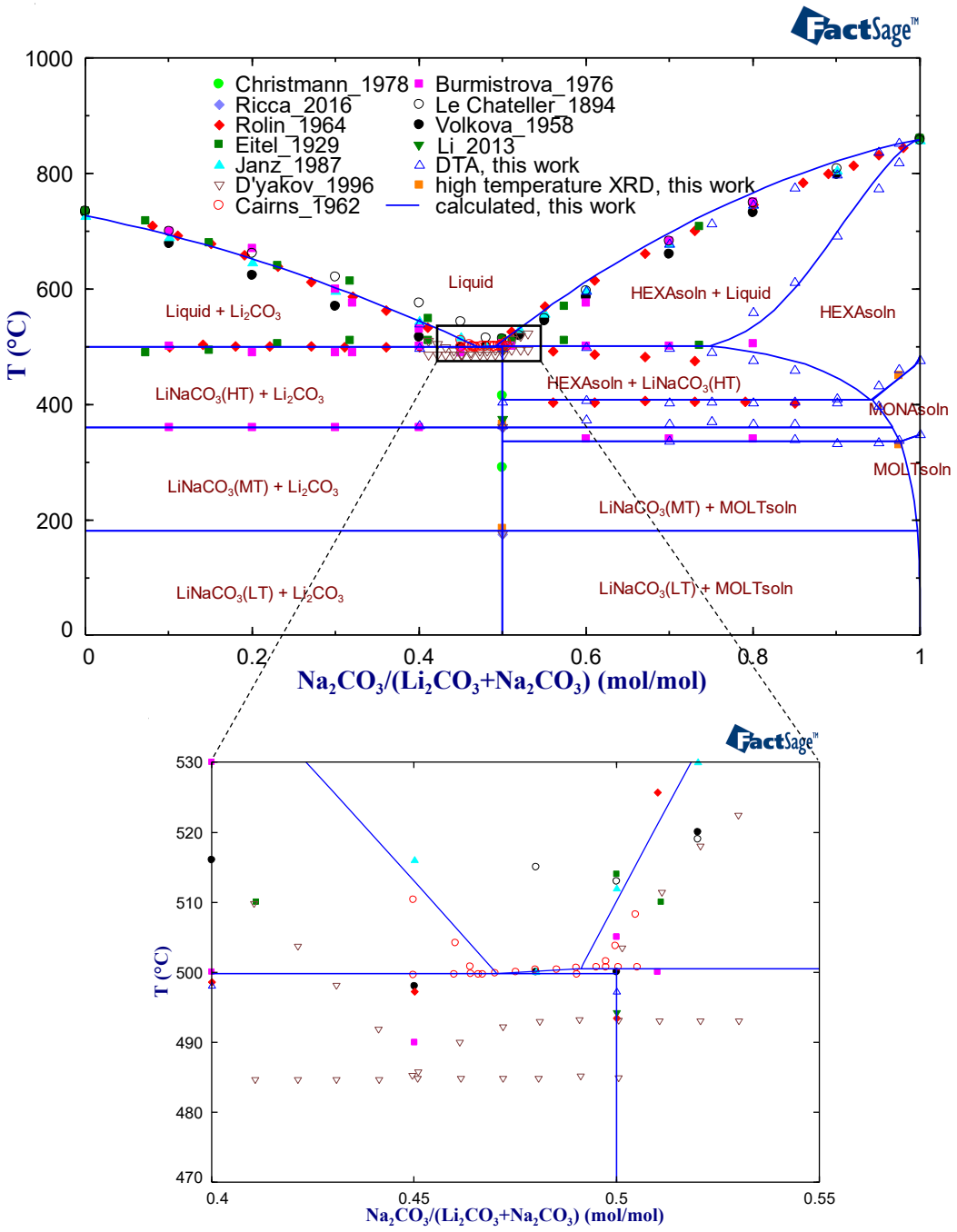


Figure 6-17. Comparison of the phase diagram calculated by the current database with experimental data in the $Li_2CO_3$-$Na_2CO_3$ system.

The comparison of the phase diagram calculated by the current database with experimental data of the $Li_2CO_3$-$Na_2CO_3$ system is shown in Figure 6-17. It can be seen that liquidus lines measured by different investigators agree well. All information on phase transitions of this phase diagram are listed in Table 6-14. As mentioned in Chapter 2, there are different opinions about

this system concerning the intermediate compound $LiNaCO_3$, i.e., 1) simple eutectic system without the intermediate compound, 2) $LiNaCO_3$ melting congruently and 3) $LiNaCO_3$ melting incongruently. After collecting and analyzing the experimental data, the intermediate compound $LiNaCO_3$ was considered to be present in this system and it was considered to be incongruently melting for the assessment. Besides, three solid solutions based on the three modifications of pure $Na_2CO_3$ (HT, MT, LT) detected by DTA and HTXRD in this work (marked as HEXAsoln, MONAsoln and MOLTsoln in Figure 6-17) were adopted for the optimization of this system.

Table 6-14. Experimental and calculated phase transitions in the system $Li_2CO_3$-$Na_2CO_3$.

| Reaction | Reaction type | Molar fraction $Na_2CO_3$ | T, °C | method | Reference |
|---|---|---|---|---|---|
| Liquid ↔ $Li_2CO_3$ + $Na_2CO_3$(HT, s3) | eutectic | 0.48 | 500 | Cryometric | Rolin and Recapet [121] |
| | | 0.48 | 500 | TA | Janz and Lorenz [120] |
| | | 0.48 | 495 | Calculated | Chen et al. [129] |
| Liquid ↔ $Li_2CO_3$ + alpha-$K_2SO_4$ | eutectic | 0.48 | 500 | Calculated | Dessureault et al. [137] |
| | | 0.48 | 502 | Calculated | FTsalt [9] |
| Liquid ↔ $Li_2CO_3$ + $LiNaCO_3$ | eutectic | 0.46 | 497 | visual-polythermal | Zakhvalinskii and Belykh [210] |
| | | 0.47 | 510 | TA | Eitel and Skaliks [130] |
| | | 0.45 | 496 | visual-polythermal | Volkov and Shvab [133] |
| | | 0.471 | 497 | visual-polythermal | Volkov and Volkova [132] |
| | | 0.467 | 499.754 ± 0.057 | Highly sensitive TA | Cairns and Macdonald [134] |
| | | 0.45 | 485 | DTA | D'yakov et al. [135] |
| | | 0.47 | 499.8 | calculated | This work |
| $LiNaCO_3$(LT) ↔ $LiNaCO_3$(MT, s2) | solid-solid | 0.5 | 175 | HTXRD | Zhukov et al. [141] |
| | | 0.5 | 175 | DTA | D'yakov et al. [135] |
| | | 0.5 | 290 | HTXRD | Christmann et al. [138] |
| | | 0.5 | 185 | HTXRD | This work |
| | | 0.5 | 170 | DSC | This work |
| | | 0.5 | 180 | calculated | This work |
| $LiNaCO_3$(MT, s2) ↔ $LiNaCO_3$(HT, s3) | solid-solid | 0.5 | 360 | HTXRD | Zhukov et al. [141] |
| | | 0.5 | 360 | DTA | D'yakov et al. [135] |
| | | 0.5 | 415 | HTXRD | Christmann et al. [138] |
| | | 0.5 | 360 | DSC | Li and Zhang [142] |
| | | 0.5 | 365 | HTXRD | This work |
| | | 0.5 | 363 | DTA | This work |
| | | 0.5 | 360 | calculated | This work |
| $LiNaCO_3$(HT, s3) ↔ liquid | congruently melting | 0.5 | 501 | visual-polythermal | Zakhvalinskii and Belykh [210] |
| | | 0.5 | 481 | DSC | Sang et al. [151] |
| | | 0.5 | 503 | visual-polythermal | Rea [209] |
| | | 0.5 | 514 | TA | Eitel and Skaliks [130] |
| $LiNaCO_3$↔ $Na_2CO_3$ + Liquid | incongruently melting | 0.5 | 500.757± 0.005 | Highly sensitive TA | Cairns and Macdonald [134] |

| | | | | | |
|---|---|---|---|---|---|
| | (peritectic point) | 0.499 | 510 | visual-polythermal | Volkov and Volkova [132] |
| | | 0.5 | 493 | DTA | D'yakov et al. [135] |
| | | 0.5 | 494.2 | DTA | Li and Zhang [142] |
| $LiNaCO_3$↔ HEXA + Liquid | incongruently melting | 0.5 | 500.5 | calculated | This work |
| Liquid ↔ $Na_2CO_3$ + $LiNaCO_3$ | eutectic | 0.51 | 501 | visual-polythermal | Zakhvalinskii and Belykh [210] |
| | | 0.52 | 510 | TA | Eitel and Skaliks [130] |
| | | 0.5 | 501 | visual-polythermal | Volkov and Shvab [133] |
| Solubility limit | - | 0.88 | | modeling | Dessureault et al. [137] |
| | | 0.84 | | calculated | FTsalt [9] |
| | | 0.75 | | calculated | This work |
| alpha-$K_2SO_4$ ↔ $Na_2CO_3$ + $Li_2CO_3$ | eutectoid | 0.92 | 287 | calculated | FTsalt [9] |
| HEXA↔ MONA + $LiNaCO_3$(HT, s3) | eutectoid | - | 404 | DTA | This work |
| | | 0.94 | 407 | calculated | This work |
| MONA ↔ MOLT + $LiNaCO_3$(MT, s2) | eutectoid | - | 334 | DTA | This work |
| | | 0.98 | 335 | calculated | This work |

As for the intermediate compound $LiNaCO_3$, even though it was reported by different authors, it was not taken into consideration in the previous assessment works [129,137] and not included in the commercial database (e.g. in FTsalt [9]). In this work, $LiNaCO_3$ is considered to be incongruently melting. Cairns and Macdonald [134] measured the eutectic temperature 499.754±0.057 °C and peritectic temperature 500.757±0.005 °C with highly sensitive TA, which is more precise than the visual-polythermal method and general TA method. Therefore, the data from Cairns and Macdonald [134] were used as the experimental basis for the assessment of the liquidus line of the $LiNaCO_3$ phase, which is illustrated in the enlarged part of Figure 6-17. It can be seen that the difference between the eutectic temperature and peritectic temperature is not easy to be detected and distinguished by the devices, therefore, it was assumed as a simple eutectic system or a congruently melting compound by other authors. D'yakov et al. [135] detected two solid-solid phase transition temperatures at 175 °C and 360 °C by DTA. Li and Zhang [142] measured one solid-solid transition temperature at 373 °C. These results are close to our experimental data and the result from Zhukov et al. [141]. On the contrary, the results from Christmann et al. [138] (290 °C and 415 °C) deviate too much from other results, therefore, it was not taken into consideration.

As mentioned in Chapter 5, the heat capacity of $LiNaCO_3$ was measured by three different DSC devices. The heat capacity equations are used to generate the Gibbs energy of this compound. The heat capacity assessment result of $LiNaCO_3$ is shown in Figure 6-18.

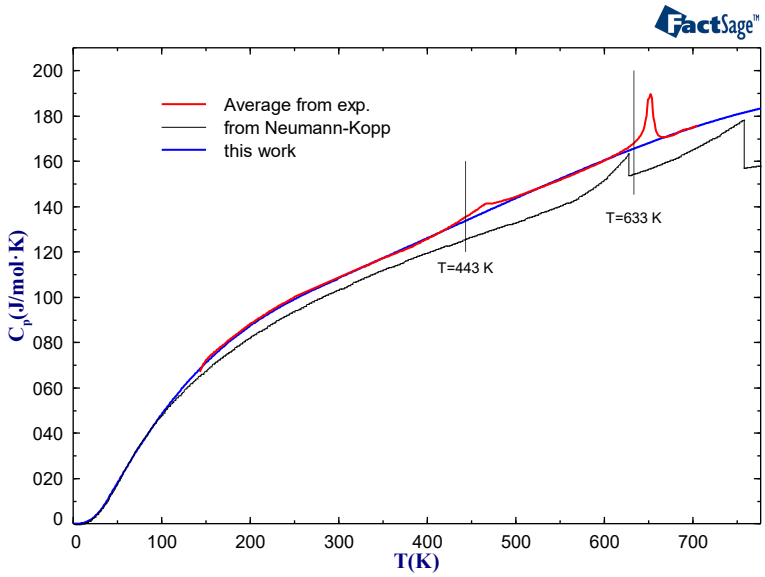


Figure 6-18. Heat capacity of the intermediate compound $LiNaCO_3$.

No experimental data about the heat capacity of $LiNaCO_3$ were reported in the literature. The heat capacity below 150 K was optimized according to data calculated by Neuman-Kopp method, while the heat capacity polynomials above 150 K were modelled using the average experimental results from the DSC measurements in the present work, which is higher than the Neuman-Kopp estimation. The heat capacity description of the three solid phases are kept identical in the PCM database. The $\Delta H^0_{298,f}$ and $S^0_{298}$ of the phase $LiNaCO_3$ (LT) are originally calculated from the pure carbonate with Neuman-Kopp method, then it was modified during the assessment of the whole system. Phase transition enthalpies at 443 K and 633 K were calculated by integrating the $C_p$ curve. The polynomials of $C_p$ for the three phases in the different temperature ranges are shown in Table 6-15.

When it comes to the solid solution phases in the $Li_2CO_3$-$Na_2CO_3$ system, one solid solution was reported in the literature by Khlapova and Elenevskaya [136]. In their work, the solubility of $Na_2CO_3$ in $LiNaCO_3$ was detected in the composition range x($Na_2CO_3$) = 0.5-0.56 through the comparison of lattice parameters of different compositions measured by XRD. However,

according to the XRD measurement of the $0.6Na_2CO_3$-$0.4Li_2CO_3$ composition at room temperature in this work, besides α1 and α2 phases of $LiNaCO_3$, 0.184 molar fraction of $Na_2CO_3$ was detected in the phase content, which is close to 0.2 molar fraction of $Na_2CO_3$ phase content calculated from the phase diagram without consideration of this solubility. In contrast, if the solubility of $Na_2CO_3$ in $LiNaCO_3$ was taken into account, the calculated phase content of $Na_2CO_3$ is 0.09 molar fraction at room temperature, which deviated too much from the experimental value. Besides, the solid-solid phase change temperature of $LiNaCO_3$ (360 °C) was detected in a large composition range, which is also against this solubility assumption, because the phase change temperature should be lower than that of pure $LiNaCO_3$. Therefore, this solid solution was excluded in the present optimization work.

Table 6-15. Thermodynamic parameters of $LiNaCO_3$.

| Phase | $\Delta H^0_{298,f}$ J/mol | $S^0_{298}$ J/mol K | T (K) | $C_p$, J/mol·K | Reference |
|---|---|---|---|---|---|
| $LiNaCO_3$ (LT, s1) | 1174149.96 | 110.4355 | 1-36 | $2.84134483\cdot10^{-4}\cdot T^3 - 2.633567945\cdot10^{-6}\cdot T^4$ | This work |
| | | | 36-298 | $-25.1235 + 0.95137\cdot T + 3607.62964\ T^{-2} - 2.46\cdot10^{-3}\cdot T^2 + 2.56407\cdot10^{-6}\cdot T^3$ | This work |
| | | | 140-776 | $98.574 - 0.04924\cdot T - 607145.59959\cdot T^{-2} - 4.38747\cdot10^{-4}\cdot T^2 - 3.00294\cdot10^{-7}\cdot T^3$ | This work |
| $LiNaCO_3$ (MT, s2) | - | - | | LT → MT $H_{tr}$ = 154 J/mol at 458 K | This work |
| | | | 1-36 | $2.84134483\cdot10^{-4}\cdot T^3 - 2.633567945\cdot10^{-6}\cdot T^4$ | This work |
| | | | 36-298 | $-25.1235 + 0.95137\cdot T + 3607.62964\ T^{-2} - 2.46\cdot10^{-3}\cdot T^2 + 2.56407\cdot10^{-6}\cdot T^3$ | This work |
| | | | 140-776 | $98.574 - 0.04924\cdot T - 607145.59959\cdot T^{-2} - 4.38747\cdot10^{-4}\cdot T^2 - 3.00294\cdot10^{-7}\cdot T^3$ | This work |
| $LiNaCO_3$ (HT, s3) | - | - | | MT → HT $H_{tr}$ = 275 J/mol at 633 K | This work |
| | | | 1-36 | $2.84134483\cdot10^{-4}\cdot T^3 - 2.633567945\cdot10^{-6}\cdot T^4$ | This work |
| | | | 36-298 | $-25.1235 + 0.95137\cdot T + 3607.62964\ T^{-2} - 2.46\cdot10^{-3}\cdot T^2 + 2.56407\cdot10^{-6}\cdot T^3$ | This work |
| | | | 140-776 | $98.574 - 0.04924\cdot T - 607145.59959\cdot T^{-2} - 4.38747\cdot10^{-4}\cdot T^2 - 3.00294\cdot10^{-7}\cdot T^3$ | This work |

The solid solution HEXAsoln (based on the HT modification of $Na_2CO_3$, hexagonal structure) was confirmed in the phase diagram (Figure 6-17). The phase transition temperature detected by the DTA measurement of this work at 500 °C did not extend over the entire composition range. Instead, lower a temperature was detected when $x(Na_2CO_3) \geq 0.75$. The larger the composition $x(Na_2CO_3)$, the lower this temperature will be. These points give the boundary of HEXAsoln, the solubility limit of $Li_2CO_3$ in $Na_2CO_3$ (HT) was determined at 0.74 molar fraction $Na_2CO_3$ and at 497 °C. In the measurement of Rolin and Recapet [121], this phase transition temperature was also observed decreasing gradually from $x(Na_2CO_3) = 0.61$.

In both measurements of Rolin and Recapet [121] and DTA results of this work, in compositions with $x(Na_2CO_3) \geq 0.5$ the phase transition at around 400 °C was detected as shown in the phase diagram (Figure 6-17). According to the FTsalt database, these data correspond to the solid-solid phase transition of pure $Li_2CO_3$, which were reported not to exist in our previous work [23] and discussed in Chapter 5.1. Besides, according to that assumption, this temperature should be detected especially at compositions where $x(Na_2CO_3) \leq 0.5$ (close to the pure $Li_2CO_3$), which contradicts both measurements. According to our new experimental results, this temperature is the eutectoid temperature of the phase HEXAsoln, which is calculated to be 407 °C with the new database, much higher than 287 °C predicted by the commercial database FTsalt.

Moreover, only one solid solution based on $Na_2CO_3$ (HT) is adopted in the FTsalt database. If this assumption was taken in this work, the eutectoid line of HEXAsoln at 400 °C should be detected in the composition range of $x(Na_2CO_3) = 0.5\text{-}1$. However, the DTA results of the composition $x(Na_2CO_3) = 0.975$ reflected in the phase diagram is opposed to it. In addition, other solid solutions (based on the low- and medium temperature modifications of $Na_2CO_3$, called MONAsoln and MOLTsoln, respectively) were detected and confirmed by HTXRD, and the phase transition temperatures are lower than the corresponding temperature for the pure $Na_2CO_3$. The eutectoid temperature of MONAsoln 334 °C was measured by DTA, which is close to the calculated result 335 °C (Figure 6-17).

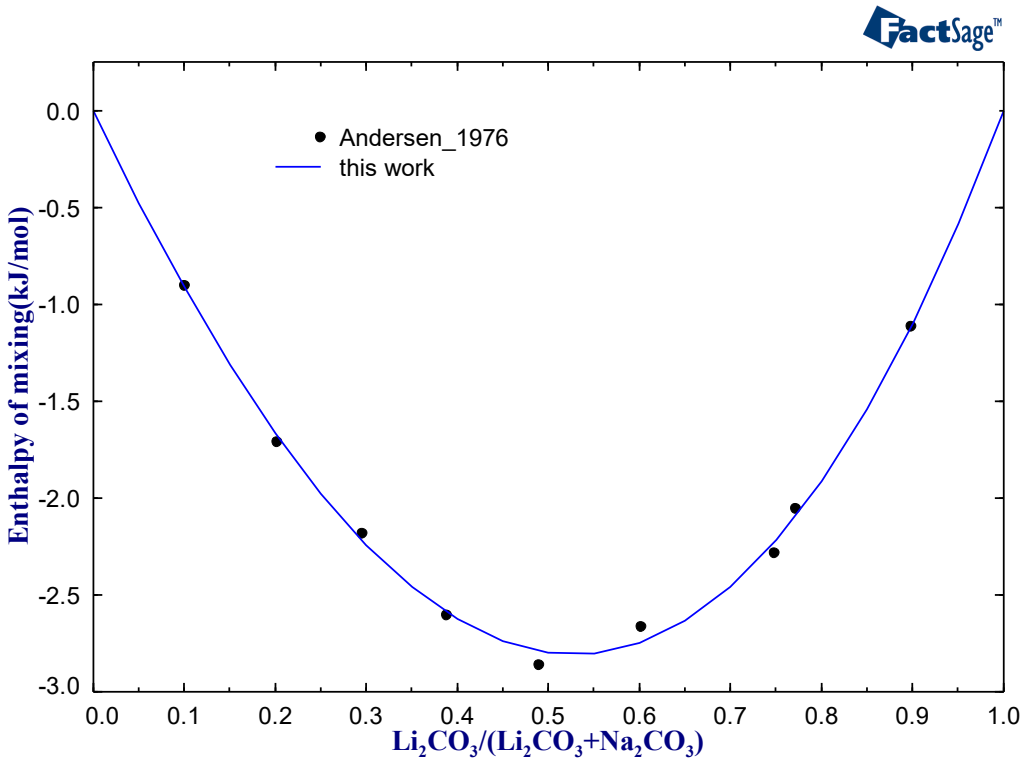


Figure 6-19. Mixing enthalpy of the $Li_2CO_3$-$Na_2CO_3$ system.

The mixing enthalpy of this system at 1178 K was investigated by Andersen and Kleppa [128] using high temperature calorimetry. It can be seen from Figure 6-19 that the results calculated by the new database are in consistence with the experimental data.

In addition, the enthalpy increment of the eutectic and 0.5:0.5 ($LiNaCO_3$) compositions were investigated by many authors, all these data are listed in Table 6-16.

Table 6-16. Melting enthalpy at certain compositions in the $Li_2CO_3$-$Na_2CO_3$ system.

| Molar fraction $Na_2CO_3$ | T, °C | Fusion enthalpy, kJ/mol (J/g) | Method | Reference |
|---|---|---|---|---|
| 0.511 | 499 | 33.5 ± 2.3 (374 ± 26) | TA | Li et al. [143] |
| 0.491 | 498 | 29.85 ± 0.05 (330.8 ± 0.6) | STA | Jiang et al. [144] |
| 0.48 | 500 | 31.56 (348.5) | DSC | Ge et al. [29] |
| 0.467 | 496 | 33.05 ± 1.65 | Drop calorimetry | Janz et al. [145] |
| 0.467 | 496 | 31.11(342) | - | Petri et al. [211] |
| 0.48 | 502 | 30.8 | Calculated | FTsalt [9] |
| 0.47 | 499.7 | 31.9 | Calculated | This work |
| 0.5 | 494 | 32.87 (365.5) | DSC | Li and Zhang [142] |
| | - | 30.3 | Calculated | FTsalt |
| | - | 31.5 | Calculated | This work |

After getting all these experimental results, the excess Gibbs energy of the liquid and solid phases (HEXAsoln, MONAsoln and MOLTsoln) in this system was optimized and the thermodynamic parameters of the liquid phase and three solid phases are collected in Table 6-27.

### 6.2.7 System $Li_2CO_3$- $K_2CO_3$

In the present work, the assessment of the $Li_2CO_3$-$K_2CO_3$ system was performed using the experimental results including the phase diagram, mixing property of the liquid phase and enthalpy increment of the intermediate compound $LiKCO_3$. The optimized parameters for this system are given in Table 6-27.

The phase diagram of the $Li_2CO_3$-$K_2CO_3$ system is shown in Figure 6-20. The experimental and calculated results in the phase diagram are listed in Table 6-17. The melting point of $K_2CO_3$ measured by Le Chatelier [123] deviates by 40 °C from the other results, so it was not taken into account for the optimization in the present work. The eutectic temperatures and melting temperatures obtained by Reshetnikov and Perfil'eva [124] are about 20 °C lower than those measured by others, which is also not used for the optimization in the present work. For the other experimental data, the eutectic between $Li_2CO_3$ and $LiKCO_3$ is measured from 482 °C to 492 °C, with an average temperature of 488 °C, while the eutectic between $K_2CO_3$ and $LiKCO_3$ is measured from 480 °C to 503 °C, with an average temperature of 496 °C. The melting temperature of $LiKCO_3$ was measured from 499 °C to 510 °C, with an average temperature of 504 °C.

No information on solid solution was reported for this system. The eutectic temperature between $Li_2CO_3$ and $LiKCO_3$ was detected at the composition $x(K_2CO_3) = 0.05$ by Jo and Banerjee [22], and the eutectic temperature (496 °C) between $K_2CO_3$ and $LiKCO_3$ was measured at the composition $x(K_2CO_3) = 0.95$ by DTA in the current work. This means, that even if solid solutions are present, the maximum solubility on both sides is less than 0.05, so that no solubility was taken into account for the optimization in this work. The calculated phase diagram after optimization agrees well with the experimental data (Figure 6-20).

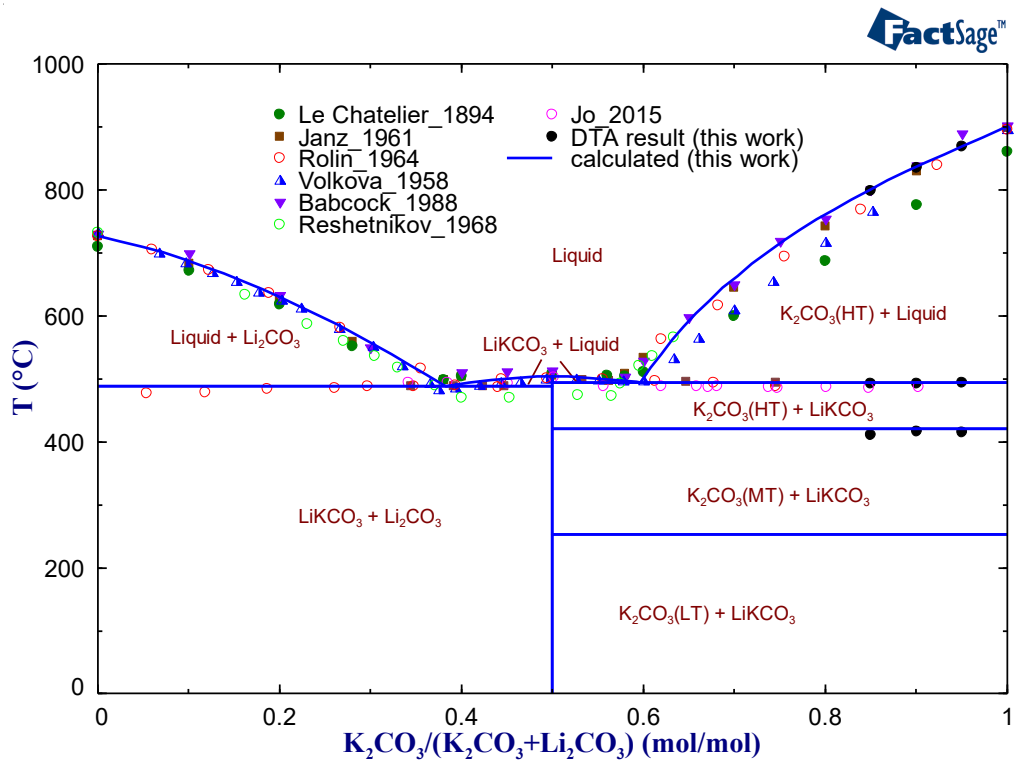


Figure 6-20. Phase diagram of the $Li_2CO_3$- $K_2CO_3$ system.

The mixing enthalpy of the $Li_2CO_3$- $K_2CO_3$ system at 905 °C is shown in Figure 6-21. The experimental results were measured by Andersen and Kleppa [128] using high temperature calorimetry under pure dry $CO_2$ atmosphere, and the weight loss of $Li_2CO_3$ was around 0.12% measured in a blank experiment. For the composition of 0.5 molar fraction of $Li_2CO_3$ the mixing enthalpy calculated with FTsalt is 840 J/mol lower than the experimental value. The calculated results of the present work agree well with the experimental results.

It can be seen from Figure 6-22 that the measured $C_p$ for the solid phase in this work is relatively higher than the results of Araki et al. [126] and Jo and Banerjee [22], and is close to the upper boundary of the scattering data points from Araki et al. [126]. At temperatures above 635 K it agrees with the results from Liu et al. [127].

Table 6-17. Experimental and calculated invariant points in the system $Li_2CO_3$- $K_2CO_3$.

| Reaction | Reaction type | Molar fraction $K_2CO_3$ | T, °C | Method | Reference |
|---|---|---|---|---|---|
| Liquid ↔ $Li_2CO_3$ + $LiKCO_3$ | eutectic | 0.37 | 491 | N/A | Le Chatelier [123] |
| | | 0.41 | 468 | Visual-polythermal | Reshetnikov and Perfil'eva [124] |
| | | 0.41 | 482 | Visual-polythermal | Volkova [119] |
| | | 0.375 | 482 | Visual-polythermal | Volkov and Shvab [212] |
| | | 0.37 | 490 | Visual-polythermal | Zakhvalinskii and Belykh [210] |
| | | - | 487 | DSC | Jo and Banerjee [22] |
| | | 0.38 | 488 | TA | Janz and Lorenz [120] |
| | | 0.395 | 490 | Cryometric | Rolin and Recapet [121] |
| | | 0.38 | 492 | Visual-polythermal | Babcock and Winnick [122] |
| | | 0.38 | 488 | Calculated | Dessureault et al. [106] |
| | | 0.398 | 480 | Calculated | FTsalt [9] |
| | | 0.385 | 490 | Calculated | This work |
| Liquid ↔ $K_2CO_3$ + $LiKCO_3$ | eutectic | 0.6 | 501 | N/A | Le Chatelier [123] |
| | | 0.56 | 472 | Visual-polythermal | Reshetnikov and Perfil'eva [124] |
| | | 0.573 | 498 | TA | Janz and Lorenz [120] |
| | | 0.555 | 500 | Cryometric | Rolin and Recapet [121] |
| | | 0.61 | 496 | Visual-polythermal | Volkova [119] |
| | | 0.56 | 492 | Visual-polythermal | Volkov and Shvab [212] |
| | | 0.58 | 500 | Visual-polythermal | Zakhvalinskii and Belykh [210] |
| | | 0.58 | 503 | Visual-polythermal | Babcock and Winnick [122] |
| | | - | 493 | DSC | Jo and Banerjee [22] |
| | | 0.573 | 480 | DSC | *Liu et al. [127] |
| | | - | 493 | DTA | This work |
| | | 0.57 | 499 | Calculated | Dessureault et al. [106] |
| | | 0.588 | 484 | Calculated | FTsalt [9] |
| | | 0.590 | 496 | Calculated | This work |
| Liquid ↔ $LiKCO_3$ | melting | 0.5 | 508 | N/A | Le Chatelier [123] |
| | | | 482 | Visual-polythermal | Reshetnikov and Perfil'eva [124] |
| | | | 505 | TA | Janz and Lorenz [120] |
| | | | 501 | Cryometric | Rolin and Recapet [121] |
| | | | 499 | Visual-polythermal | Volkova [119] |
| | | | 500 | Visual-polythermal | Volkov and Shvab [212] |
| | | | 504 | Visual-polythermal | Zakhvalinskii and Belykh [210] |
| | | | 510 | Visual-polythermal | Babcock and Winnick [122] |
| | | | 502 | DSC | Jo and Banerjee [22] |
| | | | 504 | DSC | Liu et al. [127] |
| | | | 503 | Calculated | Dessureault et al. [106] |
| | | | 503 | Calculated | FTsalt [9] |
| | | | 503 | Calculated | This work |

* the composition was adopted from Janz and Lorenz [120].

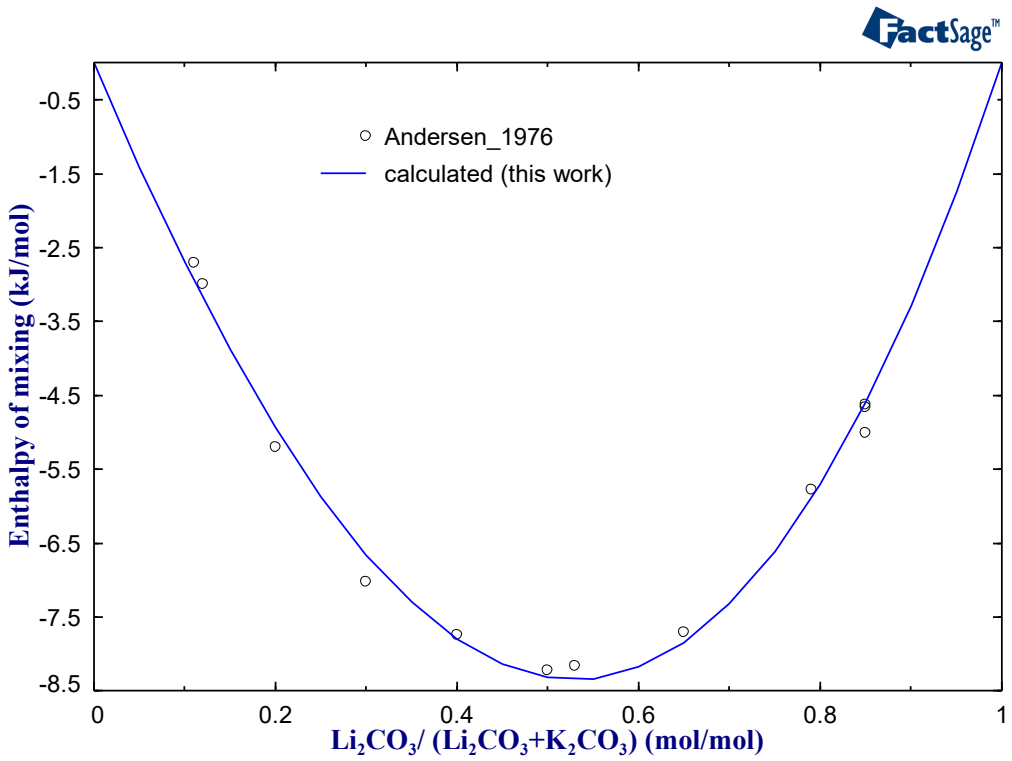


Figure 6-21. Calculated mixing enthalpy of the $Li_2CO_3$- $K_2CO_3$ system at 905 °C compared with experimental results [128].

For the assessment of the heat capacity, no experimental data are available in the temperature range 1-129 K. Therefore, the heat capacity was modeled based on the Neumann-Kopp rule with data from pure $Li_2CO_3$ and $K_2CO_3$ in the PCM database. In the temperature range of 130-776 K, the temperature-dependent polynomial of the heat capacity was modeled based on the average results obtained from the present measurements using different types of DSC devices (Figure 6-22 and Figure 5-23). The heat capacity polynomials are shown in Table 6-18. In the database, only the thermodynamic information of the solid phase for $LiKCO_3$ was described specifically, as the liquid phase of this compound can be assumed to be a mixture of $Li_2CO_3$ and $K_2CO_3$. The system can be described well without introducing the associate species $LiKCO_3$ in the liquid phase.

The comparison of the $C_p$ of the eutectic composition calculated with the database and the experimental data is shown in Figure A-10 and Figure A-11.

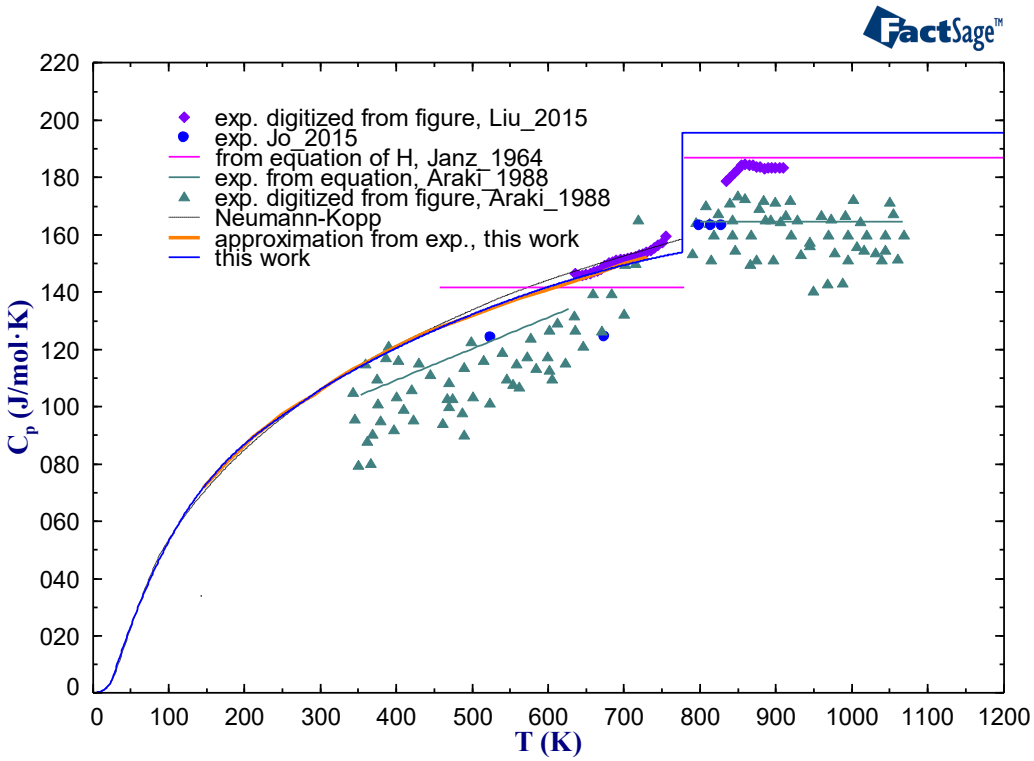


Figure 6-22. Calculated temperature dependence of the heat capacity of $LiKCO_3$ compared with several studies (Janz and Perano [125], Jo and Banerjee [22], Liu et al. [127], Araki et al. [126])

Table 6-18. Thermodynamic data of $LiKCO_3$.

| Compound | $\Delta H^0_{298,f}$ J/mol | $S^0_{298}$ J/mol K | T (K) | $C_p$, J/mol·K | Reference |
|---|---|---|---|---|---|
| $KLiCO_3$ | -1196387.4 | 113.84 | 1-25 | $0.0144717133 \cdot T + 3.37080741 \cdot 10^{-4} \cdot T^3 - 2.983406915 \cdot 10^{-6} \cdot T^4$ | This work |
| | | | 25-298 | $-18.2742 + 0.97757 \cdot T + 49.73655 \cdot T^{-2} - 3.02\ 10^{-3} \cdot T^2 + 3.80853 \cdot 10^{-6} \cdot T^3$ | This work |
| | | | 298-776 | $59.69696 + 0.19352 \cdot T - 311412.78086 \cdot T^{-2} - 9.22533 \cdot 10^{-5} \cdot T^2$ | This work |

The enthalpy increment ($H_T$-$H_{298.15}$) of $LiKCO_3$ was investigated by Janz and Perano [125]. After the generation of $C_p$ data of the solid $LiKCO_3$, the enthalpy increment of the solid calculated with the new database agrees well with the results of Janz and Perano [125] (Figure 6-23). Table 6-19 lists the experimental and calculated melting enthalpy of $LiKCO_3$. There is an obvious deviation

between different results (40±2 kJ/mol from Jo and Banerjee [22] and 31.2 kJ/mol from Liu et al. [127]). It is noted that the melting enthalpy calculated with FTsalt is 35.18 kJ/mol, whereas the calculated result of 35.63 kJ/mol using the current database is closer to the average of the experimental values and the results from Janz and Perano [125].

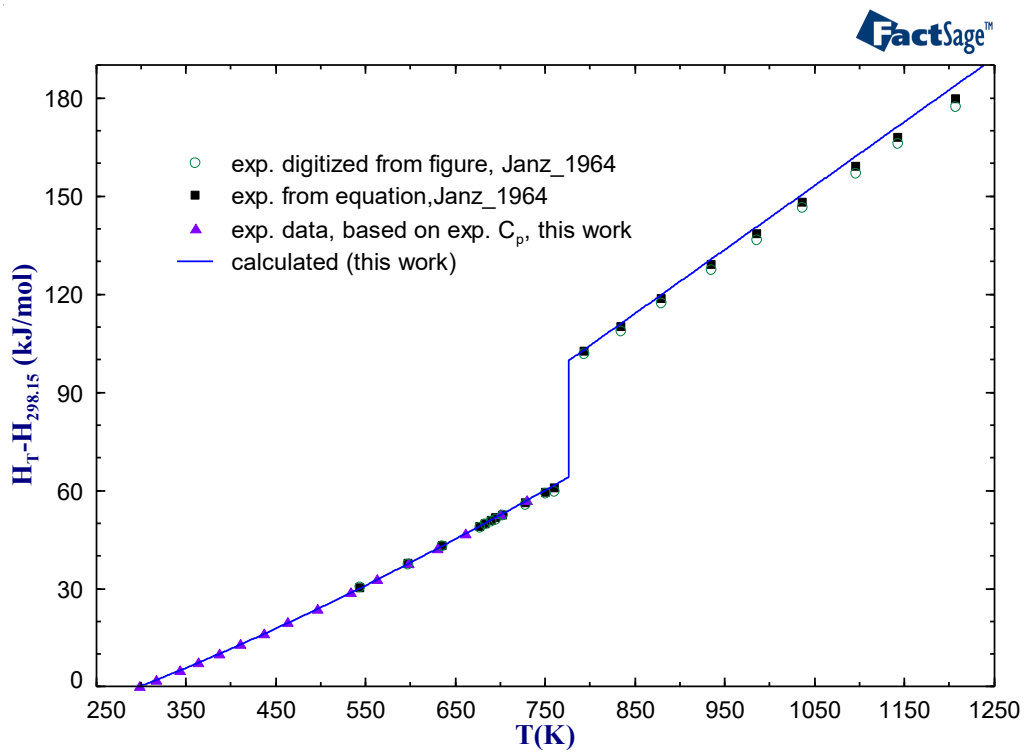


Figure 6-23. Calculated enthalpy increment ($H_T$-$H_{298.15}$) of $LiKCO_3$ compared with experimental data from Janz and Perano [125].

Table 6-19. Experimental and calculated melting enthalpy of $LiKCO_3$.

| Reaction | Melting enthalpy, kJ/mol | Method | Reference |
|---|---|---|---|
| Liquid ↔ $LiKCO_3$ | 36.4 ± 0.4 | drop calorimetry | Janz and Perano [125] |
| | 40 ± 2 | DSC | Jo and Banerjee [22] |
| | 31.27 | DSC | Liu et al. [127] |
| | 35.18 | Calculated | FTsalt [9] |
| | 35.63 | Calculated | This work |

For the assessment of the $Li_2CO_3$- $K_2CO_3$ system, the associate species $LiKCO_3$ was added as an attempt to improve the consistency between the experimental results and calculation for the phase diagram and different thermodynamic properties. However, the calculated mixing enthalpy always has a bulge at the composition x($Li_2CO_3$) = 0.5, which does not exist in the

experimental results. This inconsistency indicates that in the liquid phase this additional associate species $LiKCO_3$ should not be introduced like it was done in case of the system $Li_2CO_3$- $Na_2CO_3$ (Chapter 6.2.6).

## 6.3 Ternary systems

### 6.3.1 System LiCl-NaCl-KCl

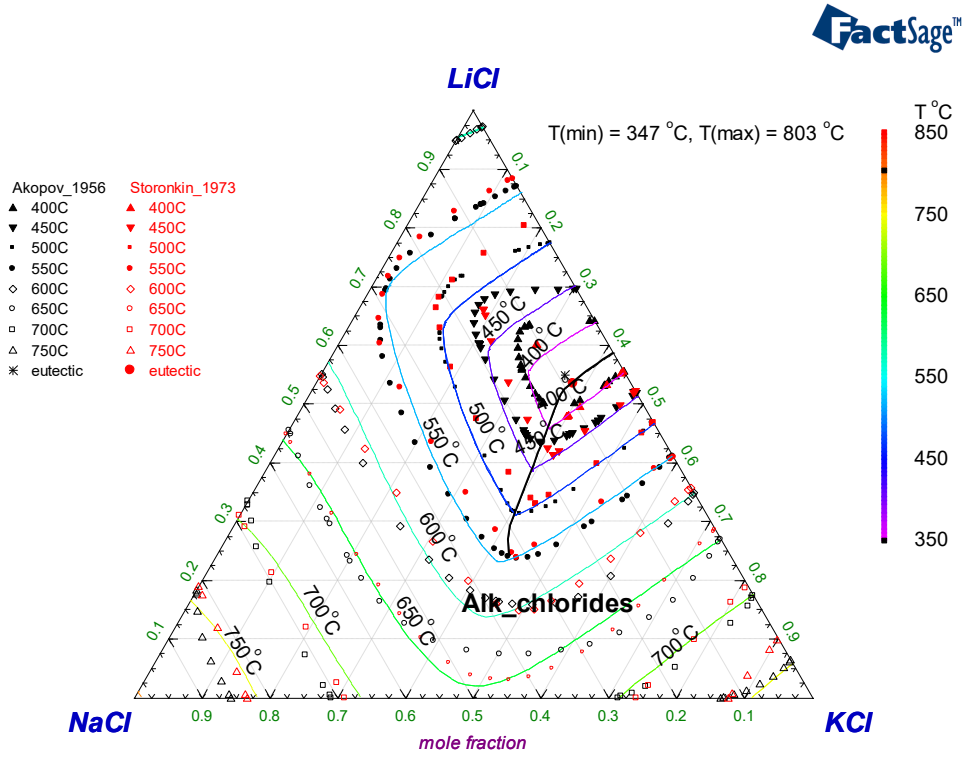


Figure 6-24. The phase diagram of the ternary system LiCl-NaCl-KCl.

The isothermal lines in the liquidus surface of the ternary system LiCl-NaCl-KCl measured by Akopov [87] and Storonkin et al. [147] were collected in Figure 6-24. The corresponding information on the eutectic in the system from the literature is summarized in Table 6-20. The calculated result agrees well with the experimental result. The thermodynamic parameters of the liquid solution phase and solid solution phase Alk_chlorides in the ternary system are shown in Table 6-27. The coefficient $L^{0,\mathrm{AlkaliCl}}_{Li^{1+},K^{1+}:Cl^{1-}}$ is introduced in the solid solution phase Alk_chlorides. It does not mean that there is a solid solubility between LiCl and KCl. It was only added for the optimization of the ternary system.

Three sections (KCl-$Na_{0.8}Li_{0.2}Cl$, NaCl-$Li_{0.6}K_{0.4}Cl$, and LiCl-$Na_{0.7}K_{0.3}Cl$) in the ternary system were calculated with the present database and compared with the experimental data as shown in Figure 6-25 (a-c).

Table 6-20. The eutectic point in the ternary system LiCl-NaCl-KCl.

| molar fraction of composition | | | T, °C | Method | Reference |
|---|---|---|---|---|---|
| LiCl | NaCl | KCl | | | |
| 0.55 | 0.09 | 0.36 | 346 | Visual-polythermal | Akopov [87] |
| 0.535 | 0.085 | 0.38 | 350 | TA | Storonkin et al. [147] |
| 0.55 | 0.09 | 0.36 | 343 | Calculated | Sangster and Pelton [148] |
| 0.55 | 0.07 | 0.38 | 347 | Calculated | FTsalt [9] |
| 0.541 | 0.078 | 0.381 | 347 | Calculated | This work |

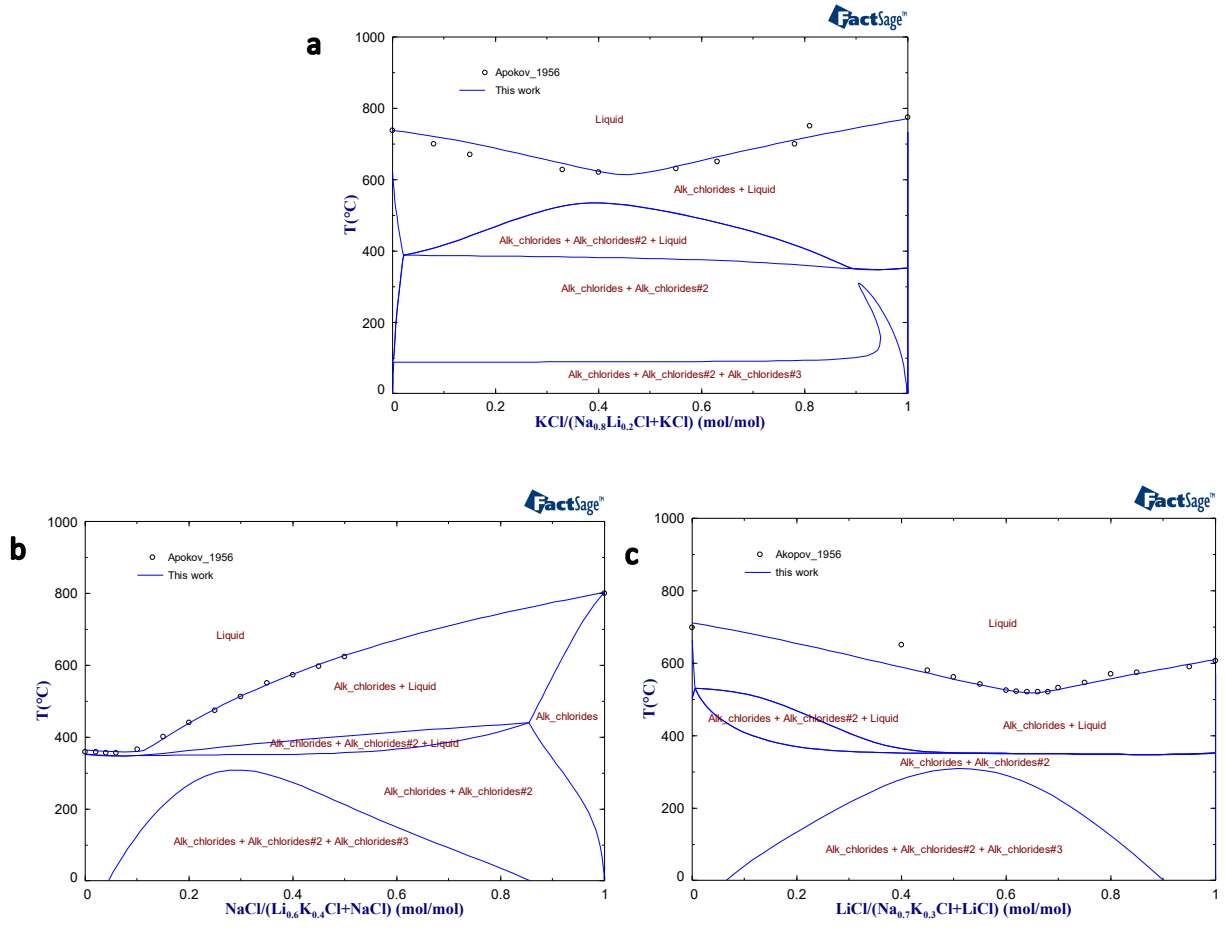


Figure 6-25. Comparison between calculated cross sections in the ternary system LiCl-NaCl-KCl with reference data [87]: a) KCl-$Na_{0.8}Li_{0.2}Cl$, b) NaCl-$Li_{0.6}K_{0.4}Cl$, and c) LiCl-$Na_{0.7}K_{0.3}Cl$.

### 6.3.2 System $Li_2CO_3$-$Na_2CO_3$-$K_2CO_3$

As mentioned in Chapter 2, the solid-liquid equilibria (liquidus surface) of the ternary system $Li_2CO_3$-$Na_2CO_3$-$K_2CO_3$ have been investigated many times. The calculated liquidus surface is shown in Figure 6-26 with five crystallization fields: $Li_2CO_3$, $LiKCO_3$, $LiNaCO_3$, HEXAsoln and HEX2soln. HEX2soln corresponds to the mentioned low temperature solid solution phase formed between $K_2CO_3$ and $Na_2CO_3$ reported by Sergeev et al. [24], as mentioned in Chapter 2.2.2.

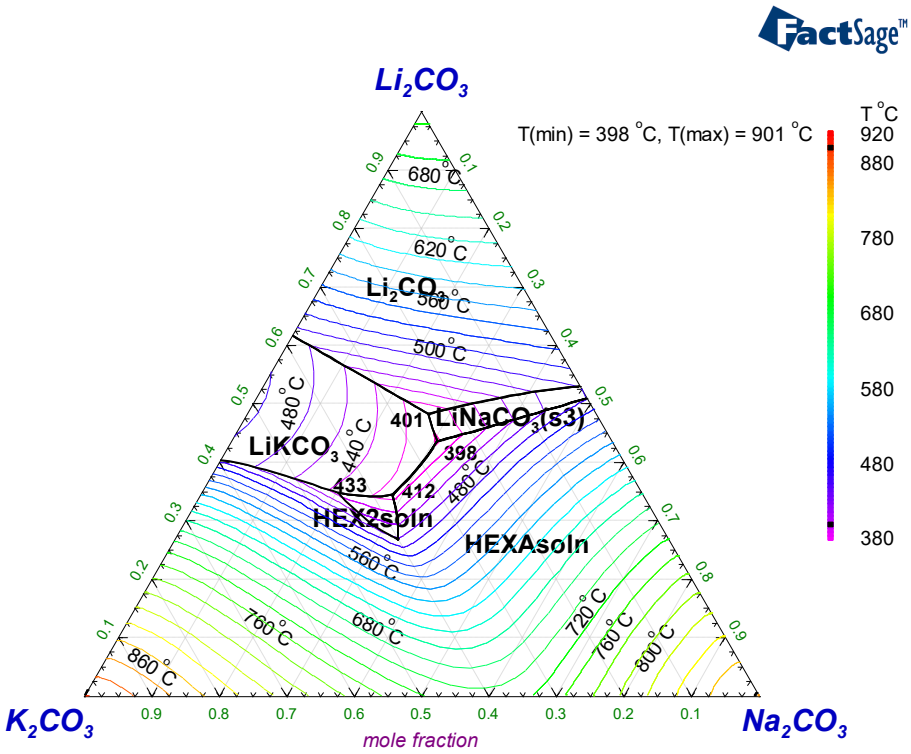


Figure 6-26. Calculated liquidus surface of the ternary system $Li_2CO_3$-$Na_2CO_3$-$K_2CO_3$.

The sections in the ternary system $Na_2CO_3$ - $Li_{1.218}K_{0.782}CO_3$, $Na_2CO_3$ - $Li_{0.862}K_{1.138}CO_3$, $Li_2CO_3$ - $Na_{1.2}K_{0.8}CO_3$, $Li_2CO_3$ - $Na_{1.446}K_{0.554}CO_3$, $K_2CO_3$ - $Li_{1.16}Na_{0.84}CO_3$ and $K_2CO_3$ - $Li_{0.974}Na_{1.026}CO_3$ are calculated and compared with the experimental data from Janz et al. [39] and the digitalized data from the liquidus surface reported by Volkova [119] as well as by Rolin and Recapet [121] in Figure 6-27 (a-f).

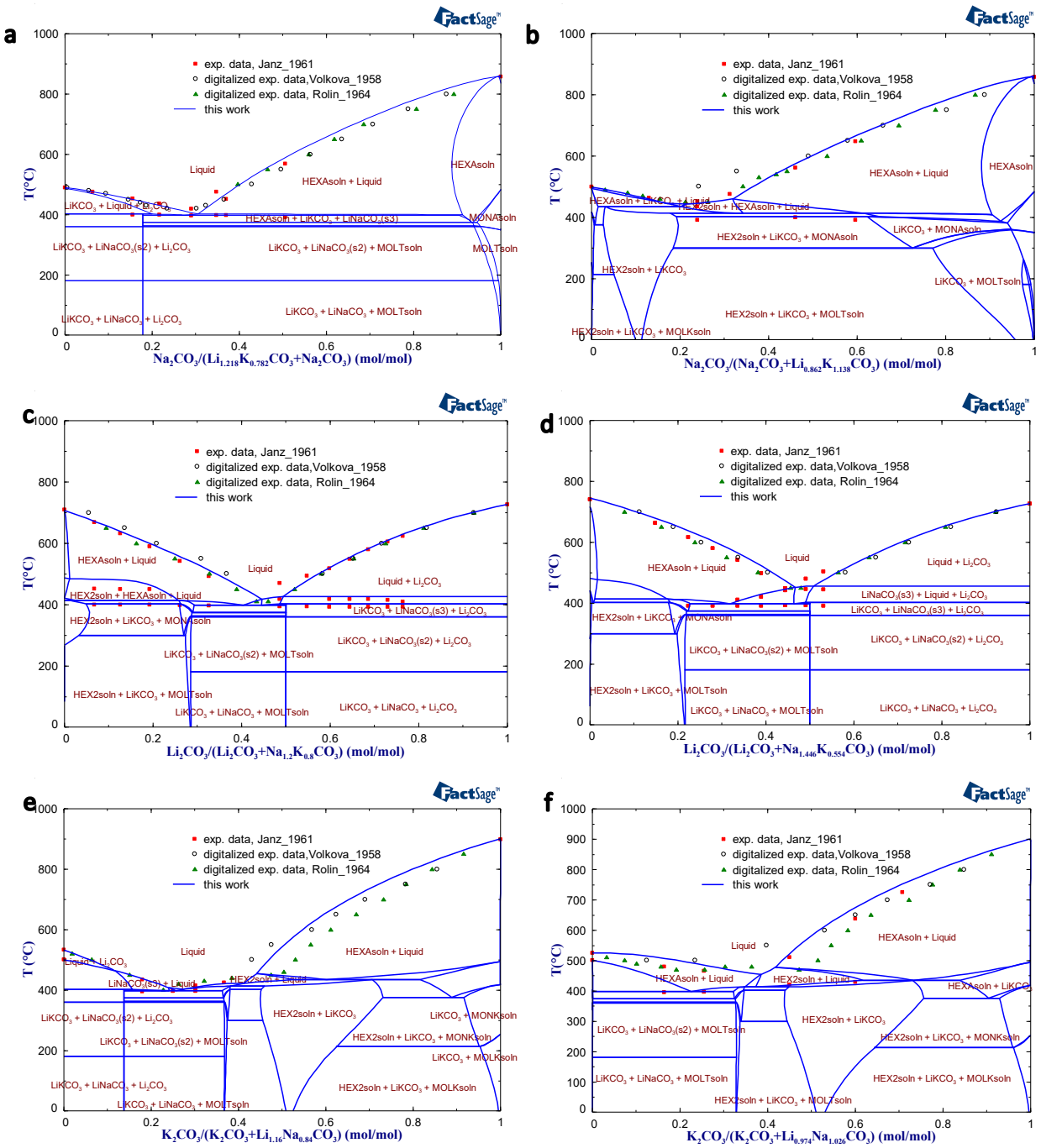


Figure 6-27. Comparison between calculated cross section in the ternary system $Li_2CO_3$-$Na_2CO_3$-$K_2CO_3$ with reference data [39]: a) $Na_2CO_3$-$Li_{1.218}K_{0.782}CO_3$, b) $Na_2CO_3$-$Li_{0.862}K_{1.138}CO_3$, c) $Li_2CO_3$-$Na_{1.2}K_{0.8}CO_3$, d) $Li_2CO_3$-$Na_{1.446}K_{0.554}CO_3$, e) $K_2CO_3$-$Li_{1.16}Na_{0.84}CO_3$ and f) $K_2CO_3$-$Li_{0.974}Na_{1.026}CO_3$.

The isothermal section at 25 °C was calculated and compared with the XRD results from Sang et al. [151]. For the composition $0.531Li_2CO_3$-$0.284K_2CO_3$-$0.185Na_2CO_3$ (in molar fraction, shown as point 1 in Figure 6-28), both the calculation and XRD measurement show three phases, namely,

$LiNaCO_3$, $LiKCO_3$ and $Li_2CO_3$. For the composition $0.5Li_2CO_3$-$0.25K_2CO_3$-$0.25Na_2CO_3$ (shown as point 2 in Figure 6-28), the calculation shows that only $LiNaCO_3$ and $LiKCO_3$ exist, while the XRD results show $LiNaCO_3$, $LiKCO_3$ and $Li_2CO_3$, which may be caused by the incomplete reaction during the preparation of the sample.

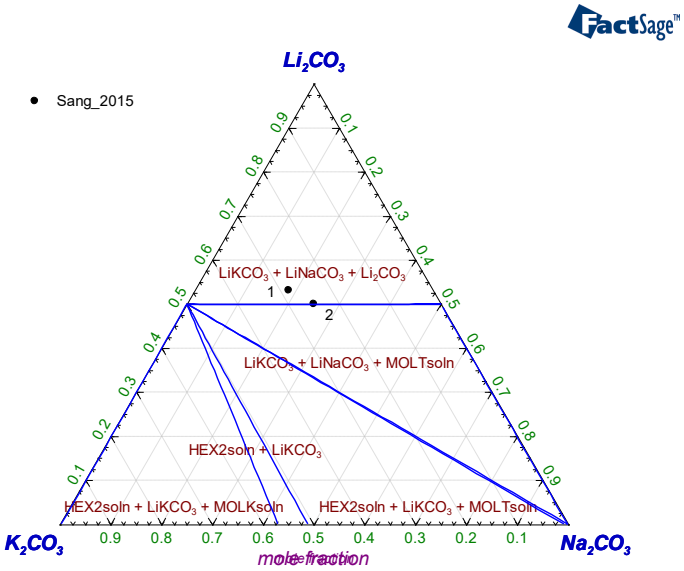


Figure 6-28. Isothermal section of the ternary system $Li_2CO_3$-$Na_2CO_3$-$K_2CO_3$ at 25 °C.

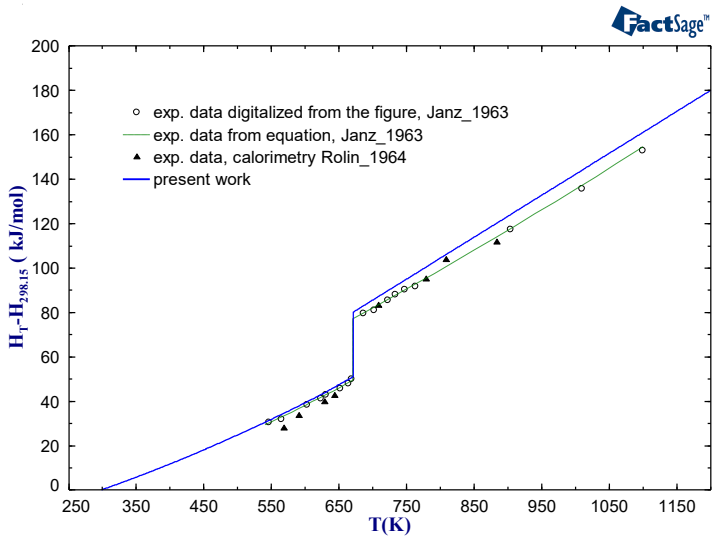


Figure 6-29. Enthalpy increment of the eutectic composition in ternary system $Li_2CO_3$-$Na_2CO_3$-$K_2CO_3$.

The calculated enthalpy increment of the eutectic composition is compared with the measurements from Janz et al. [39] and Rolin and Recapet [40] in Figure 6-29. The melting enthalpy of the eutectic mixtures was investigated many times, some other points in the system were also measured, the calculation results and the experimental results are compared in Table 6-21. The heat capacity of the eutectic composition was also measured by different researchers [39,127,153,155], and the comparison between calculation and experimental data is shown in Figure 6-30. The optimized parameters of the liquid phase of this system are shown in Table 6-27.

Table 6-21. Melting temperature and melting enthalpy of compositions in the ternary system $Li_2CO_3$-$Na_2CO_3$-$K_2CO_3$.

| Molar fraction of composition | | | T, °C | method | Melting enthalpy, kJ/mol (J/g) | Method | Reference |
|---|---|---|---|---|---|---|---|
| $Li_2CO_3$ | $Na_2CO_3$ | $K_2CO_3$ | | | | | |
| Eutectic composition | | | | | | | |
| - | - | - | 380 | - | - | - | Tamaru and Kamada [213] |
| 0.45 | 0.28 | 0.27 | 390 | Visual-polythermal | - | - | Volkova [119] |
| 0.437 | 0.305 | 0.259 | 393 | Calorimetry | 27.6 | Calorimetry | Rolin and Recapet [40] |
| 0.435 | 0.315 | 0.25 | 397 | Drop calorimetry | 27.6 ± 0.4 (275.4) | Drop calorimetry | Janz et al. [39] |
| 0.435 | 0.315 | 0.25 | 401 | DSC | 22.12 (221) | DSC | *Olivares et al. [152] |
| 0.435 | 0.315 | 0.25 | 397 | STA | 27.8 (278.2) | STA | *An et al. [153] |
| 0.435 | 0.315 | 0.25 | 393 | DSC | 26.02 (260) | DSC | *Raud et al. [26] |
| 0.434 | 0.312 | 0.254 | 397 | DSC | 27.95 (278.9) | DSC | *Liu et al. [127] |
| 0.434 | 0.312 | 0.254 | 395 | DSC | 16.0 (159.7) | DSC | *Liao et al. [155] |
| 0.44 | 0.31 | 0.26 | 397 | Calculated | - | - | Pelton et al. [149] |
| 0.42 | 0.26 | 0.32 | 397 | Calculated | - | - | Chen et al. [129] |
| 0.428 | 0.304 | 0.268 | 398 | Calculated | 29.4 | Calculated | FTsalt [9] |
| 0.436 | 0.306 | 0.258 | 398 | Calculated | 28.6 | Calculated | This work |
| Other compositions | | | | | | | |
| 0.404 | 0.349 | 0.247 | 396 | DSC | 27.76 (275) | DSC | Raud et al. [26] |
| | | | 398 | Calculated | 28.5 | Calculated | FTsalt [9] |
| | | | 398 | Calculated | 25.6 | Calculated | This work |
| 0.41 | 0.29 | 0.3 | 398 | DSC | 17.0 (166.4) | DSC | Ren et al. [214] |
| | | | 398 | DSC | 26.86 (262.9) | DSC | Yan et al. [150] |
| | | | 398 | Calculated | 29.3 | Calculated | FTsalt [9] |
| | | | 398 | Calculated | 28.3 | Calculated | This work |

* the composition was adopted from Janz et al. [39].

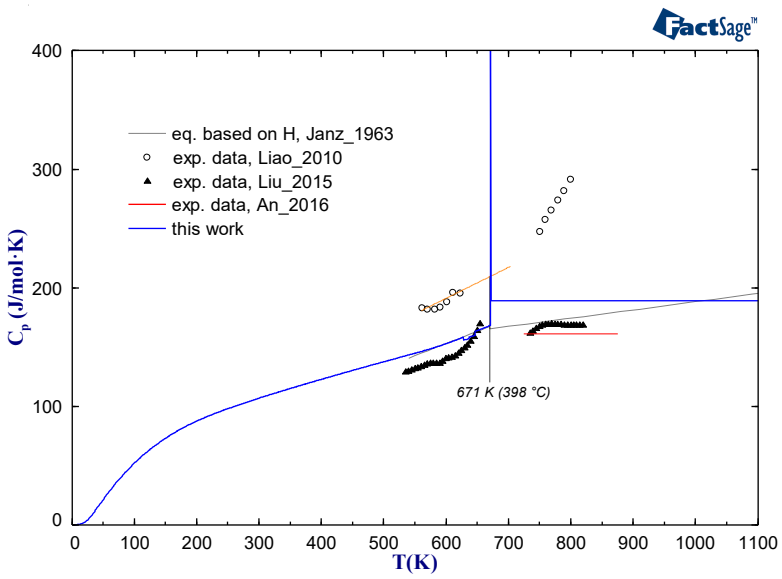


Figure 6-30. Heat capacity of eutectic composition in ternary system $Li_2CO_3$-$Na_2CO_3$-$K_2CO_3$.

## 6.4 Reciprocal systems

### 6.4.1 System $Li^+$, $Na^+$//$Cl^-$, $CO_3^{2-}$

The phase diagrams of the systems $Li_2CO_3$-$(NaCl)_2$ and $(LiCl)_2$-$Na_2CO_3$ were determined by DTA measurement in this work (Chapter 5), and the results are shown in Figure 6-31 and Figure 6-32, respectively. It is noticed that the phase diagram of $(LiCl)_2$-$Na_2CO_3$ is more complicated than the phase diagram of $Li_2CO_3$-$(NaCl)_2$ system, which means that the latter one is more stable. The reciprocal reaction of this system is shown in Eq. 6.1 and the Gibbs energy of this reaction at 298 K is calculated to be -85.36 kJ/mol.

$$Na_2CO_3 + 2LiCl \rightarrow Li_2CO_3 + 2NaCl \qquad 6.1$$

According to the experimental data of the $Li_2CO_3$-$(NaCl)_2$ system, the thermodynamic parameters were optimized for the liquid phase and shown in Table 6-27. While the optimization of the system $Li_2CO_3$-$(NaCl)_2$ (stable diagonal) is done, the optimization of the $(LiCl)_2$-$Na_2CO_3$ system was performed automatically.

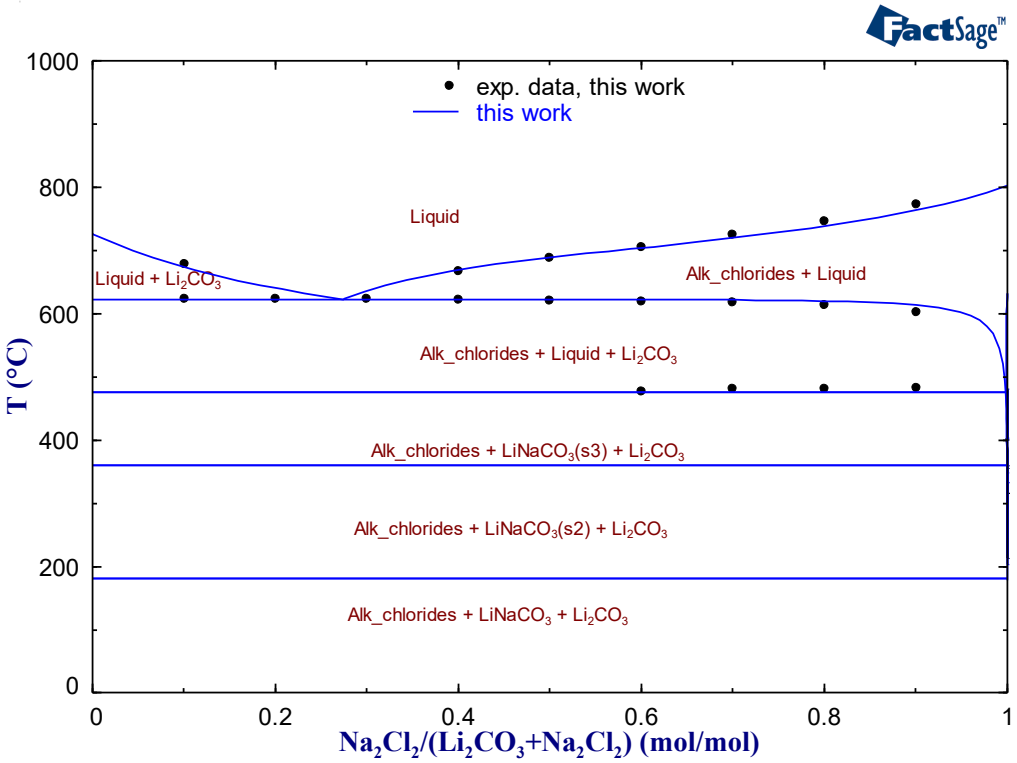


Figure 6-31. Phase diagram of the system $Li_2CO_3$-$(NaCl)_2$.

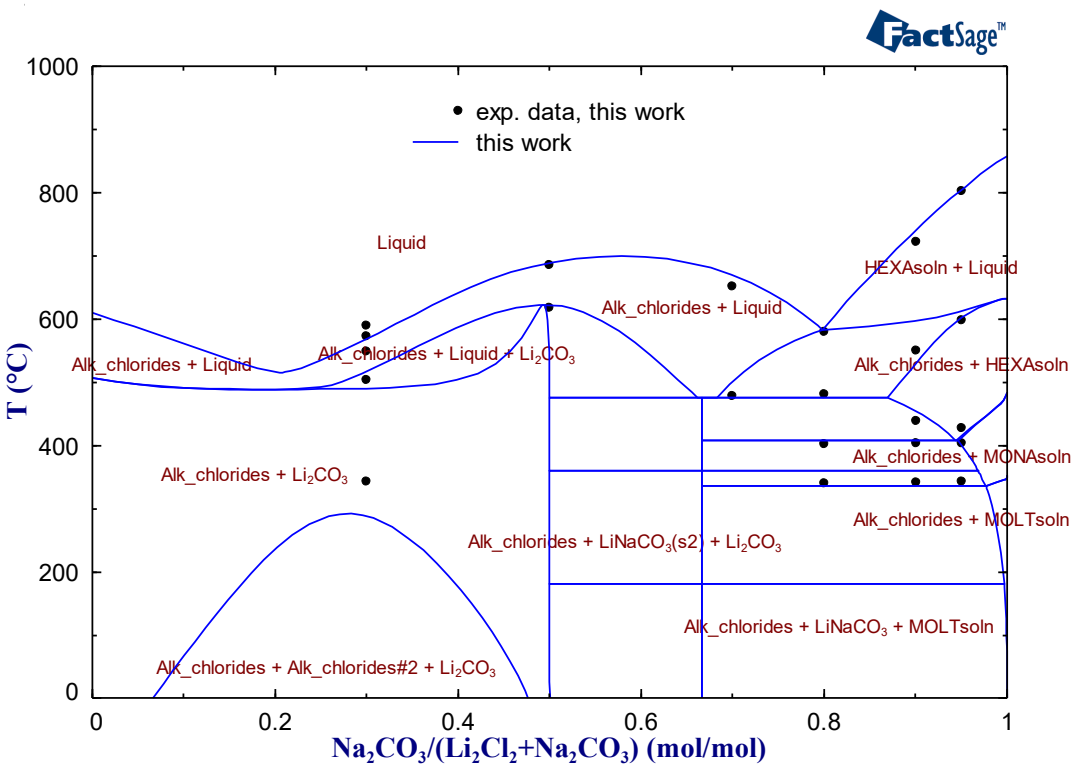


Figure 6-32.Phase diagram of the $(LiCl)_2$-$Na_2CO_3$ system.

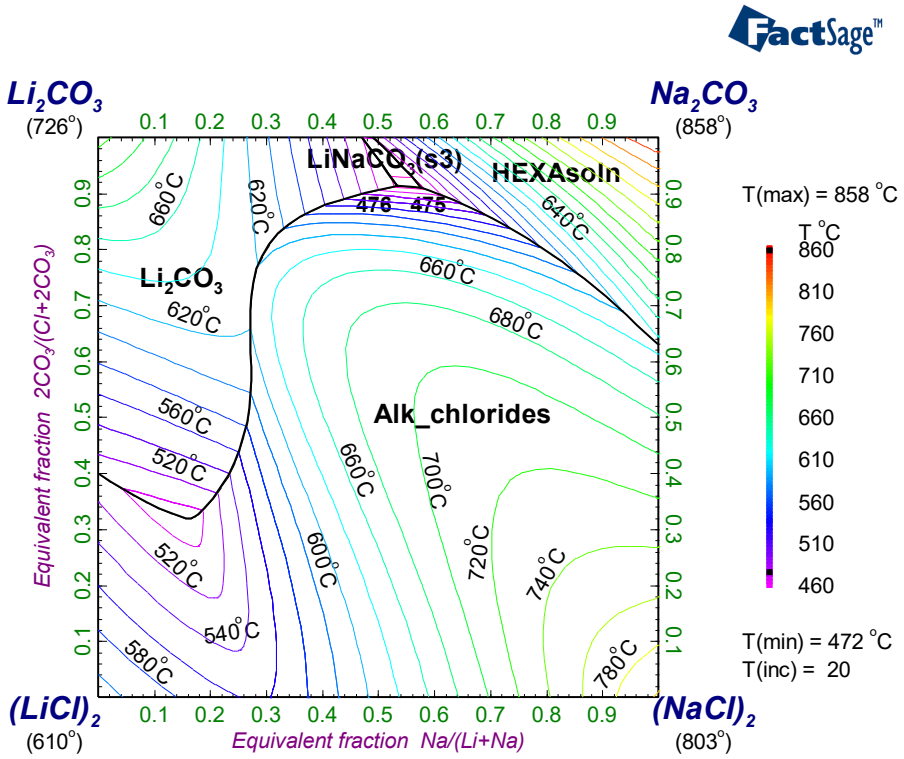


Figure 6-33. Liquidus surface of the reciprocal system $Li^+$, $Na^+//Cl^-$, $CO_3^{2-}$

The reciprocal system was calculated with the new database (see Figure 6-33). There are four crystallization fields on the liquidus surface: $Li_2CO_3$, HEXAsoln, Alk_chlorides and $LiNaCO_3$. There are two lowest temperature points in the liquid surface at 475 °C and 476 °C, the compositions are shown in Table 6-22 and compared with data from FTsalt.

Table 6-22. Information on the lowest temperatures in the liquidus surface of the reciprocal system $Li^+$, $Na^+//Cl^-$, $CO_3^{2-}$

| Reaction type | Reaction | X | Y | T, °C | Method | Reference |
|---|---|---|---|---|---|---|
| Eutectic | Liquid ↔ $Li_2CO_3$ + Rocksalt + alpha-$K_2SO_4$ | 0.551 | 0.914 | 475 | Calculated | FTsalt [9] |
| Eutectic | Liquid ↔ $Li_2CO_3$ + Alk_chlorides + $LiNaCO_3$(HT, s3) | 0.576 | 0.911 | 476 | Calculated | This work |
| Peritectic | Liquid+ HEXA ↔ Alk_chlorides + $LiNaCO_3$(HT, s3) | 0.533 | 0.912 | 475 | Calculated | This work |

X =Na/(Na+Li), Y= $2CO_3/(2CO_3+Cl)$

### 6.4.2 System $Li^+, K^+//Cl^-, CO_3^{2-}$

The liquidus surface of the reciprocal system $Li^+, K^+//Cl^-, CO_3^{2-}$ was reported by Volkov and Zakhvalinskii [103]. The phase equilibria in the reciprocal system can be predicted using the data obtained for binary systems. However, in order to make the calculated results consistent with the experimental data, the interaction parameters between $Li_2CO_3$ and $(KCl)_2$ in the liquid solution need to be optimized, which actually affects the whole reciprocal system. The optimized parameters are displayed in Table 6-27.

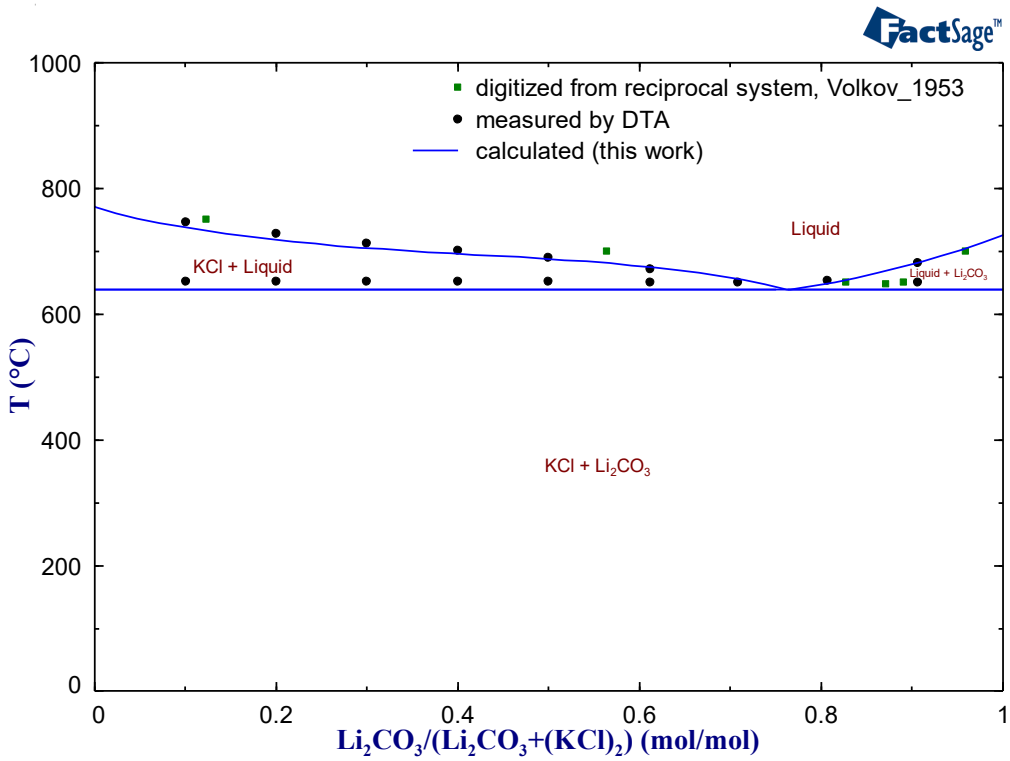


Figure 6-34. Phase diagram of the $Li_2CO_3$-$(KCl)_2$ system.

Figure 6-34 shows the phase diagram of the $Li_2CO_3$-$(KCl)_2$ system, where the calculated results are compared with the DTA measurements from this work and the data from Volkov and Zakhvalinskii [103] (digitalized from the diagonal line in the projection of the reciprocal system). The DTA results show that a eutectic reaction occurs between $Li_2CO_3$ and $(KCl)_2$ and no solid solution is present. The measured eutectic temperature is 648 °C, which is the same as the results from Volkov and Zakhvalinskii [103], while the calculated eutectic temperature in the new

database is 638 °C. During the optimization process, it is possible to improve the eutectic temperature, but at the same time, an unexpected miscibility gap will show in the liquid phase of the reciprocal system, which is near the liquid surface. To avoid this miscibility gap, the compromise was taken. Therefore, the eutectic temperature was set to 638 °C and the calculated liquidus line agrees well with own measured values of the liquidus temperature.

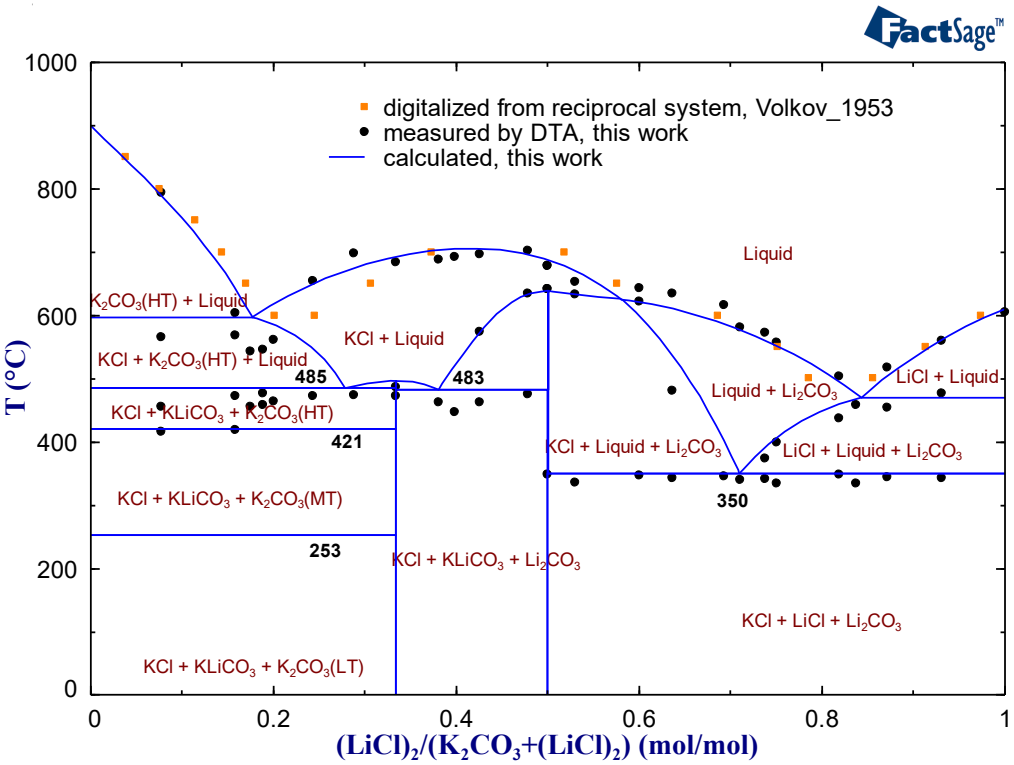


Figure 6-35. Phase diagram of the $K_2CO_3$-$(LiCl)_2$ system.

As shown in Figure 6-35, the phase diagram of the $K_2CO_3$-$(LiCl)_2$ system is more complicated, due to the reciprocal reaction in Eq. 6.2 [103]. The Gibbs energy of this reaction at 298 K is calculated to be -115.77 kJ/mol. When the molar fraction of $(LiCl)_2$ is higher than 0.5, LiCl, KCl and $Li_2CO_3$ coexist in the system, the eutectic line appears at 350 °C, which is lower than the eutectic temperature of the LiCl-KCl system of 352 °C. When it is lower than 0.33, $K_2CO_3$, KCl and $LiKCO_3$ coexist in the system, and the calculated eutectic temperature is 485°C, lower than the eutectic temperature between $K_2CO_3$ and $LiKCO_3$ of 496 °C. From 0.33 to 0.5, $Li_2CO_3$, KCl and $LiKCO_3$ coexist in the system and the calculated eutectic temperature is 483 °C, lower than the eutectic temperature between $K_2CO_3$ and $LiKCO_3$ of 490 °C.

$$K_2CO_3 + 2LiCl \rightarrow Li_2CO_3 + 2KCl \quad (6.2)$$

No additional interaction parameter is needed for the liquid phase in the $K_2CO_3$-$(LiCl)_2$ system. That is because after optimizing the four binary systems at the edges and the stable diagonal salt system, this unstable diagonal salt system is optimized automatically. The calculated liquidus line agrees well with the experimental results. Besides, the effect of the non-existent solid-solid phase transition of $Li_2CO_3$ and $LiKCO_3$ is excluded in the phase diagram.

Figure 6-36 shows the comparison of the liquidus surface projection of the reciprocal system $Li^+$, $K^+//Cl^-$, $CO_3^{2-}$ proposed by Volkov and Zakhvalinskii [103] (Figure 6-36a) and that calculated with the new dataset (Figure 6-36b). There are five primary crystallization fields in the phase diagram, four of which correspond to pure salts and the remaining one is for the intermediate compound $LiKCO_3$. According to the new dataset, the minimum temperature of the liquidus surface is 350 °C, slightly lower than 352 °C from Volkov and Zakhvalinskii [103]. All experimental and calculated information on the eutectic point in this system is collected in Table 6-23.

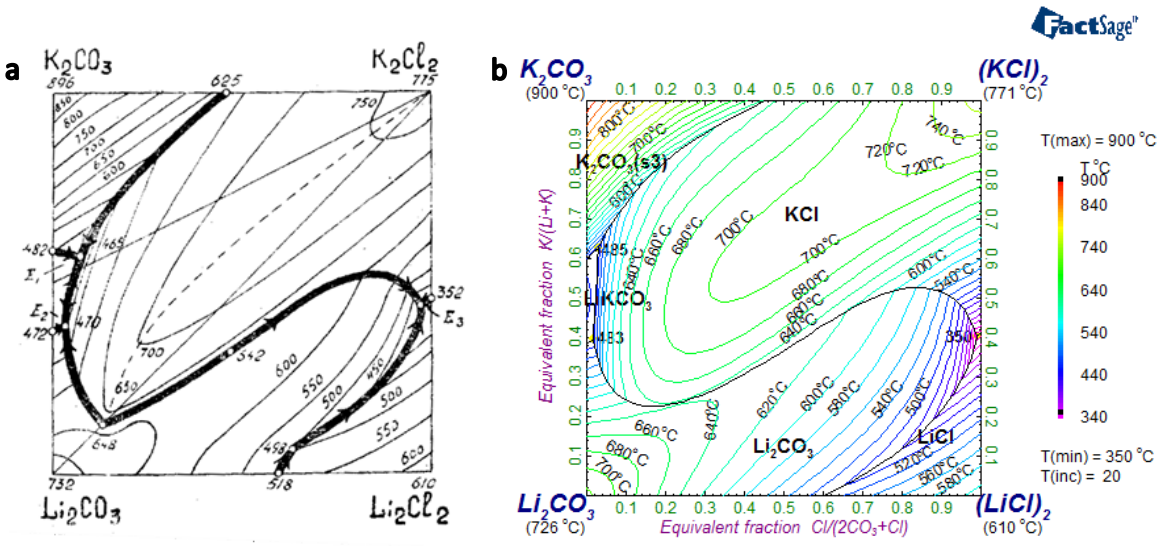


Figure 6-36. Liquidus surface of the reciprocal system $Li^+$, $K^+//Cl^-$, $CO_3^{2-}$: a) proposed by Volkov and Zakhvalinskii [103] and b) calculated with the new dataset.

Table 6-23. Experimental and calculated eutectic points in the reciprocal system $Li^+$, $K^+//Cl^-$, $CO_3^{2-}$.

| Reaction | Reaction type | X | Y | T, °C | Method | Reference |
|---|---|---|---|---|---|---|
| Liquid ↔ $K_2CO_3$ +$LiKCO_3$ + KCl | eutectic | 0.074 | 0.567 | 469 | Visual-polythermal | Volkov and Zakhvalinskii [103] |
| | | - | - | 468 | DTA | This work |
| | | 0.065 | 0.635 | 480 | Calculated | FTsalt [9] |
| | | 0.029 | 0.622 | 485 | Calculated | This work |
| Liquid ↔ $Li_2CO_3$ +$LiKCO_3$ + KCl | eutectic | 0.034 | 0.386 | 470 | Visual-polythermal | Volkov and Zakhvalinskii [103] |
| | | - | - | 462 | DTA | This work |
| | | 0.045 | 0.417 | 478 | Calculated | FTsalt [9] |
| | | 0.017 | 0.400 | 483 | Calculated | This work |
| Liquid ↔ $Li_2CO_3$ +LiCl + KCl | eutectic | 0.972 | 0.441 | 352 | Visual-polythermal | Volkov and Zakhvalinskii [103] |
| | | - | - | 345 | DTA | This work |
| | | 0.995 | 0.403 | 352 | Calculated | FTsalt [9] |
| | | 0.988 | 0.404 | 350 | Calculated | This work |

X=Cl/($2CO_3$+Cl), Y=K/(K+Li)

### 6.4.3 System $Na^+$, $K^+$//$Cl^-$, $CO_3^{2-}$

The optimization of the reciprocal system $Na^+$, $K^+$//$Cl^-$, $CO_3^{2-}$ is based on the experimental data in the literature [108,115,157–159,215].

The phase diagram of the diagonal system $(KCl)_2$-$Na_2CO_3$ was calculated and compared with the literature data, as shown in Figure 6-37. The calculated liquidus line is compared with the measurements from different authors [108,115,158,215]. The eutectic information from the measurements and calculations are shown in Table 6-24.

The phase diagram of the diagonal system $K_2CO_3$-$(NaCl)_2$ was calculated and compared with the literature data, as shown in Figure 6-38. The calculated liquidus line is compared with the measurements from different authors [108,215]. The information of two minimum points from the measurements and calculations are shown in Table 6-25.

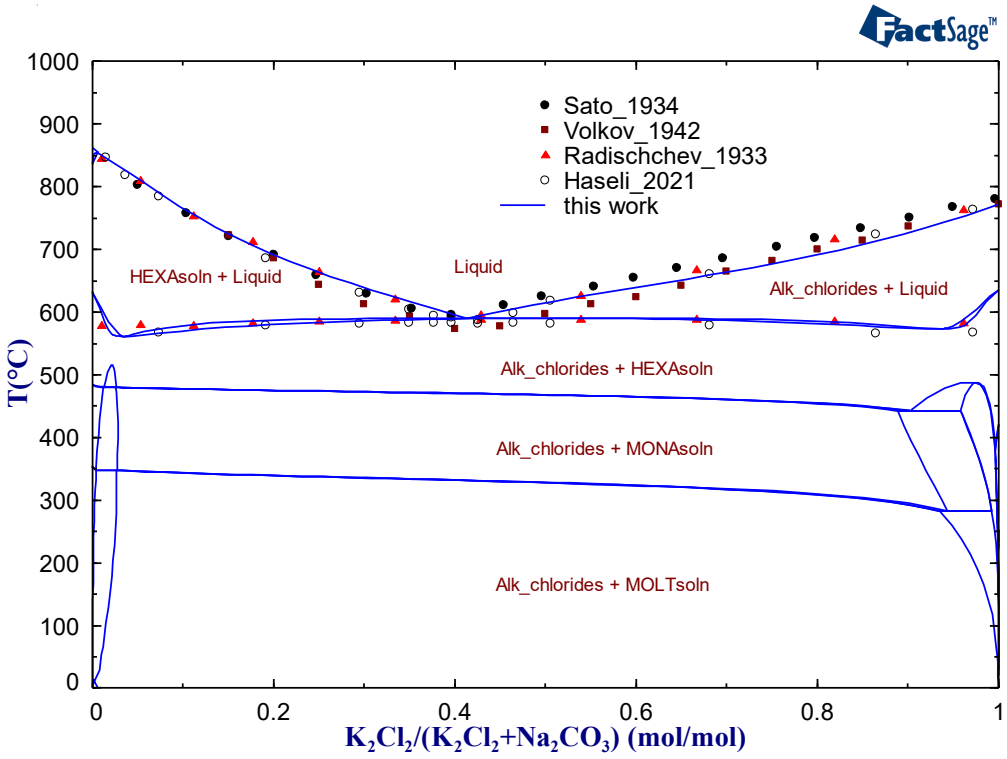


Figure 6-37. Phase diagram of the $(KCl)_2$-$Na_2CO_3$ system.

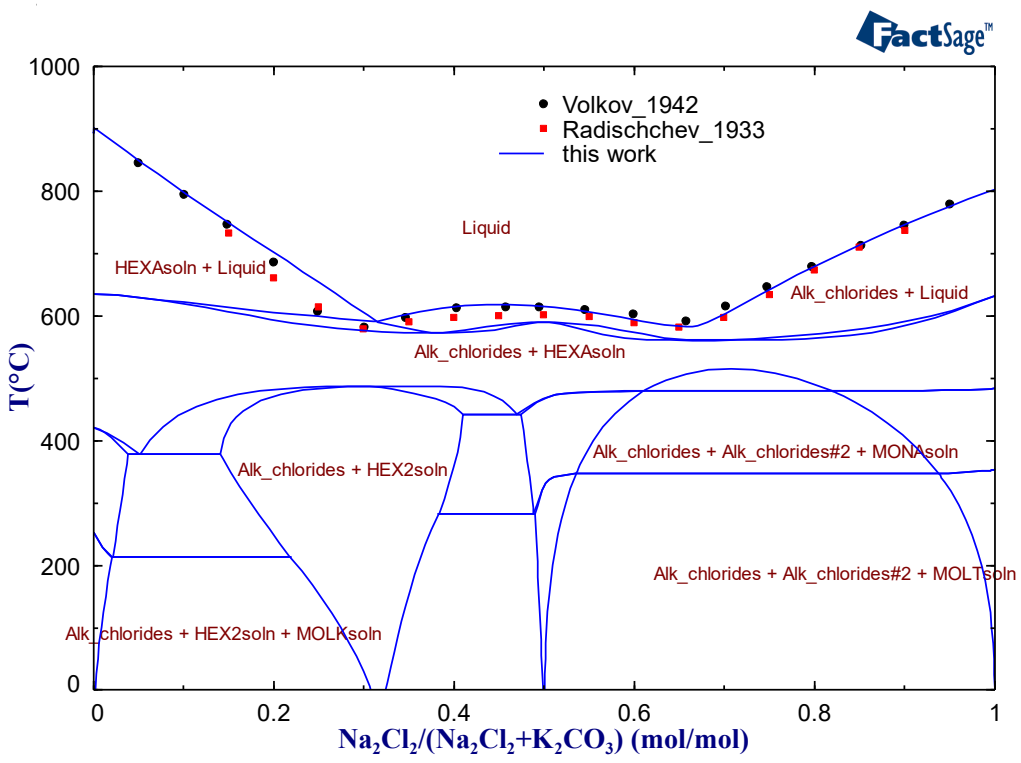


Figure 6-38. Phase diagram of the $(NaCl)_2$-$K_2CO_3$ system.

Table 6-24. Eutectic information in the $(KCl)_2$-$Na_2CO_3$ system.

| Molar fraction $(KCl)_2$ | T, °C | Method | Melting enthalpy, kJ/mol (J/g) | Method | Reference |
|---|---|---|---|---|---|
| 0.403 | 587 | Visual-polythermal | | | Rea [209] |
| 0.404 | 587 | TA | | | Sato [115] |
| 0.385 | 588 | Visual-polythermal | | | Volkov and Bergman [215] |
| 0.415 | 564 | TA | | | Radishchev [108] |
| 0.403 | 584.4 | DSC | 33 ± 0.7 (267.4±5.9) | DSC | Liu et al. [159] |
| 0.417 | 582 | DSC | 32.3 ± 1 (260.4± 8.7) | DSC | Haseli et al. [158] |
| 0.386 | 587 | Calculated | 32.07 | Calculated | FTsalt [9] |
| 0.412 | 590 | Calculated | 32.48 | Calculated | This work |

Table 6-25. Minimum in the liquidus in the $(NaCl)_2$-$K_2CO_3$ system.

| points | Molar fraction $(NaCl)_2$ | T, °C | Method | Reference |
|---|---|---|---|---|
| Minimum_1 | 0.28 | 568 | Visual-polythermal | Volkov and Bergman [215] |
| | 0.28 | 574 | TA | Radishchev [108] |
| | 0.296 | 590 | Calculated | FTsalt [9] |
| | 0.317 | 590 | Calculated | This work |
| Minimum_2 | 0.675 | 588 | Visual-polythermal | Volkov and Bergman [215] |
| | 0.66 | 576 | TA | Radishchev [108] |
| | 0.66 | 597.8 | Calculated | FTsalt [9] |
| | 0.66 | 582 | Calculated | This work |

The projection of the liquidus phase was calculated with the new database and compared with data obtained by Sato [115], Busse-Machukas et al. [157] and Radishchev [108]. Two crystallization fields are formed in the liquidus surface, i.e., HEXAsoln and Alk_chrorides. The minimum temperatures in the liquidus surface were reported in the literature and calculated by the current database (shown as red number 1 and 2 in Figure 6-39b). Besides, the melting enthalpy was measured by some authors, which was compared with the results calculated by FTsalt and the current database. It can be seen that both calculated results for the minimum_1 and miminum_2 are smaller than the measured results from Liu et al. [159] and this work. This information is collected in Table 6-26.

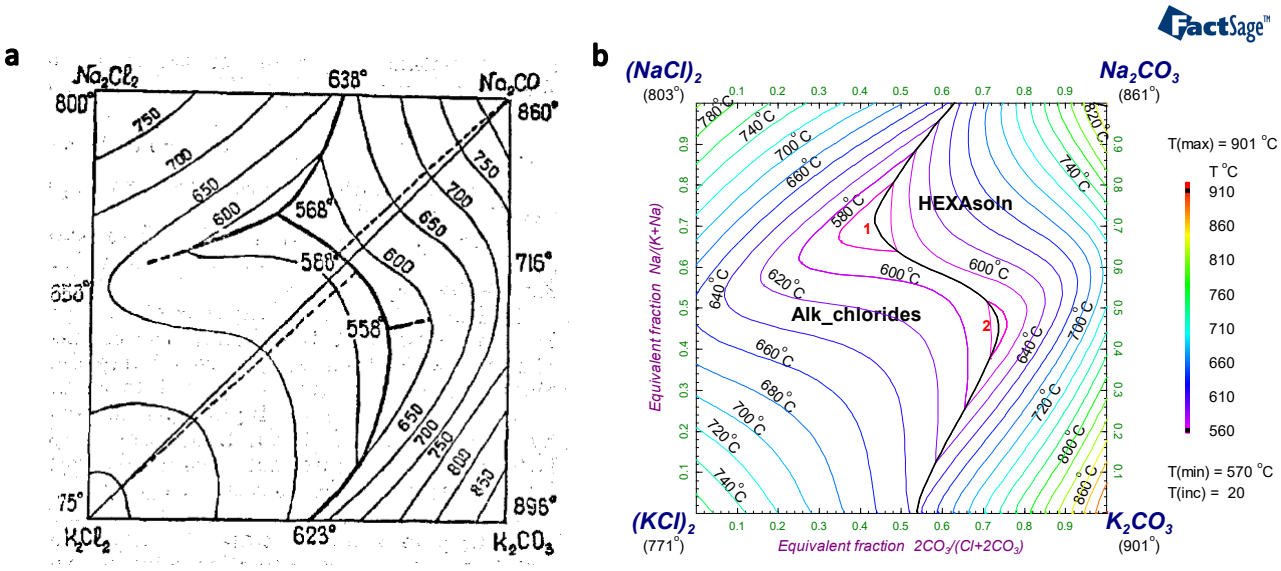


Figure 6-39. Liquidus surface of the reciprocal system $Na^+$, $K^+//Cl^-$, $CO_3^{2-}$: a) measured by Volkov and Bergman [215] and b) calculated with the new database.

Table 6-26. Experimental and calculated eutectic points or lowest temperatures in the liquidus surface in the reciprocal system $Na^+$, $K^+//Cl^-$, $CO_3^{2-}$

| Point | X | Y | T, °C | Method | Melting enthalpy, kJ/mol (J/g) | Method | Reference |
|---|---|---|---|---|---|---|---|
| Minimum_1 | 0.473 | 0.733 | 570 | DSC | 30.41(252.7) | DSC | *Liu et al. [159] |
| | 0.448 | 0.733 | - | DTA | - | - | Busse-Machukas et al. [157] |
| | 0.45 | 0.72 | 568 | Visual-polythermal | - | - | Volkov and Bergman [215] |
| | 0.45 | 0.7 | 580 | TA | - | - | Sato [115] |
| | 0.48 | 0.76 | 559 | TA | - | - | Radishchev [108] |
| | 0.473 | 0.733 | 573 | Calculated | - | - | Yaokawa et al. [113] |
| | 0.477 | 0.736 | 567 | Calculated | 34.59 | Calculated | FTsalt [9] |
| | 0.435 | 0.718 | 561 | Calculated | 29.96 | Calculated | This work |
| Minimum_2 | 0.73 | 0.45 | 558 | Visual-polythermal | - | - | Volkov and Bergman [215] |
| | 0.73 | 0.46 | 568.5 | DSC | 25.65(203.1) | DSC | *This work |
| | 0.699 | 0.461 | 585 | Calculated | - | - | Yaokawa et al. [113] |
| | 0.726 | 0.481 | 578 | Calculated | 27.96 | Calculated | FTsalt [9] |
| | 0.737 | 0.452 | 572 | Calculated | 24.39 | Calculated | This work |

X =$2CO_3/(2CO_3+Cl)$, Y= Na/(Na+K), * compositions are adopted from FTsalt [9].

## 6.5 Entire System $Li^+$, $Na^+$, $K^+//Cl^-$, $CO_3^{2-}$

The thermodynamic description of all liquid and solid solution phases in the $Li^+$, $Na^+$, $K^+//Cl^-$, $CO_3^{2-}$ system is summarized in Table 6-27.

Table 6-27. Thermodynamic description of the liquid and solid solution phases in the $Li^+$, $Na^+$, $K^+//Cl^-$, $CO_3^{2-}$ system.

| Gibbs energy data, J/mol |
|---|
| Liq: ($Li_2CO_3$/1.5, $Na_2CO_3$/1.5, $K_2CO_3$/1.5, LiCl, NaCl, KCl) |
| ${}^0G_{Li_2CO_3} = {}^0G_{Li_2CO_3(liquid)}$ |
| ${}^0G_{Na_2CO_3} = {}^0G_{Na_2CO_3(liquid)}$ |
| ${}^0G_{K_2CO_3} = {}^0G_{K_2CO_3(liquid)}$ |
| ${}^0G_{LiCl} = {}^0G_{LiCl(liquid)}$ |
| ${}^0G_{NaCl} = {}^0G_{NaCl(liquid)}$ |
| ${}^0G_{KCl} = {}^0G_{KCl(liquid)}$ |
| $L^0_{LiCl,NaCl} = -4684.03 + 3.81\,T$, $L^1_{LiCl,NaCl} = -4.38 - 2.13\,T$ |
| $L^0_{LiCl,KCl} = -39992.87 + 179.91\,T - 21.71\,Tln(T)$, $L^1_{LiCl,KCl} = -236.37 + 1.79\,T$ |
| $L^0_{LiCl,Li_2CO_3} = 1851.49$, $L^1_{LiCl,Li_2CO_3} = 712.76$ |
| $L^0_{NaCl,Na_2CO_3} = -7488.76 + 13.24\,T$, $L^1_{NaCl,Na_2CO_3} = 2963.29 - 1.62\,T$ |
| $L^0_{KCl,K_2CO_3} = 8511.27 - 2.74\,T$, $L^1_{KCl,K_2CO_3} = 4956.22 - 5.12\,T$ |
| $L^0_{Li_2CO_3,Na_2CO_3} = -7459.08 - 4.04\,T$, $L^1_{Li_2CO_3,Na_2CO_3} = -852.65 + 0.25\,T$ |
| $L^0_{Li_2CO_3,K_2CO_3} = -22194.46 + 2.80\,T$, $L^1_{Li_2CO_3,K_2CO_3} = -2668.07 - 2.22\,T$ |
| $L^{LiCl}_{LiCl,NaCl,KCl} = -25000$, $L^{NaCl}_{LiCl,NaCl,KCl} = -20475$, $L^{KCl}_{LiCl,NaCl,KCl} = -5000$ |
| $L^{Li_2CO_3}_{Li_2CO_3,Na_2CO_3,K_2CO_3} = -74075.78 + 60\,T$, $L^{K_2CO_3}_{Li_2CO_3,Na_2CO_3,K_2CO_3} = -78517.46 + 50\,T$, $L^{Na_2CO_3}_{Li_2CO_3,Na_2CO_3,K_2CO_3} = -37332.18 + 50\,T$ |
| $L^0_{NaCl,Li_2CO_3} = -20000 + 35\,T$ |
| $L^0_{KCl,Li_2CO_3} = 36918.75 - 25\,T$, $L^1_{KCl,Li_2CO_3} = 3000$ |
| $L^0_{KCl,Na_2CO_3} = -16190 + 30\,T$ |
| Alk_chlorides: ($Li^{1+}$, $Na^{1+}$, $K^{1+}$)($Cl^{1-}$) |
| ${}^0G_{LiCl} = {}^0G_{LiCl(solid)}$ |
| ${}^0G_{NaCl} = {}^0G_{NaCl(solid)}$ |
| ${}^0G_{KCl} = {}^0G_{KCl(solid)}$ |
| $L^{0,\mathrm{AlkaliCl}}_{Li^{1+},Na^{1+}:Cl^{1-}} = 4458.49 + 7.76\,T$, $L^{1,\mathrm{AlkaliCl}}_{Li^{1+},Na^{1+}:Cl^{1-}} = 984.31 - 4.50\,T$ |
| $L^{0,\mathrm{AlkaliCl}}_{Li^{1+},K^{1+}:Cl^{1-}} = 80\,T$ |
| HEXA: $(Li^{1+}, Na^{1+})_2(CO_3^{2-})_1$ |
| ${}^0G_{Na_2CO_3} = {}^0G_{Na_2CO_3(HT)}$ |
| ${}^0G_{Li_2CO_3} = {}^0G_{Li_2CO_3(solid)} + 2500$ |
| $L^{0,HEXA}_{Li^{1+},Na^{1+}:CO_3^{2-}} = 64839.27 - 50.35\,T$ |
| MONA: $(Li^{1+}, Na^{1+})_2(CO_3^{2-})_1$ |

$^{0}G_{Na_2CO_3} = {}^{0}G_{Na_2CO_3(MT)}$

$^{0}G_{Li_2CO_3} = {}^{0}G_{Li_2CO_3(solid)} + 8000$

$L^{0,MONA}_{Li^{1+},Na^{1+}:CO_3^{2-}} = 55378.68 - 45\,T$

$L^{0,MONA}_{Li^{1+},K^{1+}:CO_3^{2-}} = 80\,T$

$L^{Na_2CO_3}_{Li_2CO_3,Na_2CO_3,K_2CO_3} = 100000$

---

MOLT: $(Li^{1+}, Na^{1+})_2(CO_3^{2-})_1$

$^{0}G_{Na_2CO_3} = {}^{0}G_{Na_2CO_3(LT)}$

$^{0}G_{Li_2CO_3} = {}^{0}G_{Li_2CO_3(solid)} + 20000$

$L^{0,MOLT}_{Li^{1+},Na^{1+}:CO_3^{2-}} = 27883.6 - 20\,T$

$L^{0,MOLT}_{Li^{1+},K^{1+}:CO_3^{2-}} = 80\,T$

---

The experimental and assessment work of the pure salt $Li_2CO_3$ was published in the paper [23]. The experimental and assessment work of the pure salt LiCl, binary systems LiCl-KCl, LiCl-Li2$_C$O$_3$, KCl-$K_2CO_3$, $Li_2CO_3$-$K_2CO_3$ and the reciprocal system $Li^+$, $K^+$//$Cl^-$, $CO_3^{2-}$ was published in the paper [216].

# 7 Conclusion and outlook

In this work, a new Gibbs energy database was generated for salt system $Li^+$, $Na^+$, $K^+//Cl^-$, $CO_3^{2-}$ based on all available experimental data from the literature and the present measurements.

Experimental work for different systems was done to update the thermodynamic data. Thermodynamic properties and structure of pure $Li_2CO_3$ was investigated using various techniques. The heat capacity of $Li_2CO_3$ above room temperature was measured for the first time by different types of DSC that provides better accuracy in comparison with those data extracted from the equation of enthalpy in the literature. The thermal and structure study of $Li_2CO_3$ has shown, that previously reported solid-solid phase transition in the range of 680-693 K refers to the eutectic temperature of $Li_2CO_3$-LiOH due to undesirable impurities and $Li_2CO_3$ only has one solid phase.

The heat capacity of the intermediate compounds $LiKCO_3$ and $LiNaCO_3$ was determined by three types of DSC and the phase transitions of $LiKCO_3$ and $LiNaCO_3$ were checked by high temperature XRD. For $LiKCO_3$, the accuracy of the heat capacity data is improved compared with the previous literature data and only one phase was detected by HTXRD. For $LiNaCO_3$, its heat capacity was measured for the first time, and the three solid phases were confirmed with HTXRD. The eutectic temperature of the $K_2CO_3$-KCl system and the phase transition temperatures in the $Li_2CO_3$-$K_2CO_3$ system were measured using DTA. The phase diagram of system $Li_2CO_3$-$Na_2CO_3$was determined by DTA and high temperature XRD, three solid solution phases based on the three solid modifications of pure $Na_2CO_3$ were determined; the eutectoid temperatures were measured. Besides, DTA was used for determination of the phase transitions in the diagonal sections of the $Li^+$, $K^+//Cl^-$, $CO_3^{2-}$ reciprocal system ($Li_2CO_3$-$K_2Cl_2$ and $Li_2Cl_2$-$K_2CO_3$) and the $Li^+$, $Na^+//Cl^-$, $CO_3^{2-}$ reciprocal system ($Li_2CO_3$-$Na_2Cl_2$ and $Li_2Cl_2$-$Na_2CO_3$) to cover the lack of experimental data in the literature. The experimental results were used in the thermodynamic assessment of the focused salt system along with the literature data on phase equilibria and thermodynamic properties.

As for the modelling part, the polynomials of heat capacities of the different phases of pure $Li_2CO_3$, intermediate compounds $LiKCO_3$ and $LiNaCO_3$ were evaluated according to the new

obtained experimental data along with the data from the literature. Only one solid phase of pure $Li_2CO_3$ was described in the new database. The Gibbs energy of the three crystal modifications of $LiNaCO_3$ was generated and this is the first time their thermodynamic functions were introduced in the thermodynamic database. The Gibbs energy of LiCl (solid, liquid) was reassessed, especially the information in the temperature range below 298 K was included into the database. The solution phases in the seven binary systems $Li_2CO_3$-LiCl, $Na_2CO_3$-NaCl, $K_2CO_3$-KCl, LiCl-NaCl, LiCl-KCl, $Li_2CO_3$-$Na_2CO_3$, $Li_2CO_3$-$K_2CO_3$, two ternary systems $Li_2CO_3$-$Na_2CO_3$-$K_2CO_3$, LiCl-KCl-NaCl, and three reciprocal systems $Li^+$, $K^+$//$Cl^-$, $CO_3^{2-}$, $Li^+$, $Na^+$//$Cl^-$, $CO_3^{2-}$, $Na^+$, $K^+$//$Cl^-$, $CO_3^{2-}$ were optimized in accordance with all available experimental information in the new developed database. Three solid solutions based on the three solid modifications of pure $Na_2CO_3$ were introduced into the new database for the system $Li_2CO_3$-$Na_2CO_3$. For the whole database, the liquid solution was described by the modified associate species model, and the solid solutions were described with the sub-lattice model. Thermodynamic properties and phase diagrams of the salt systems calculated by the new database are in good agreement with the experimental data.

All in all, the obtained experimental results provided a more accurate and reliable experimental basis for the Gibbs energy description of different phases and contributed to the new database development for the salt system. Moreover, this new dataset improves the reliability and accuracy of the calculations and predictions of the properties of the salt system for the application.

Furthermore, even though the liquidus surface of the ternary and reciprocal systems is described well by the new database, the consistency of the complex solid part has not been inspected thoroughly due to the lack of corresponding experimental data. Further experimental measurements (e.g. DTA and XRD measurements on the ternary system $Li_2CO_3$-$Na_2CO_3$-$K_2CO_3$) are needed in the future.

# 8 Acknowledgement

I would like to thank Prof. Lorenz Singheiser, Prof. Ruth Schweiger Prof. Robert Spatschek and Dr. Michael Müller for offering me this opportunity to work as a PhD candidate in the institute of energy and climate research, Microstructure and Properties (IEK-2), Forschungszentrum Jülich GmgH. Then I would like to express my appreciation to all the people made this doctoral thesis possible.

I would like to present my gratitude to my supervisor Dr. Michael Müller, who has supported and helped me throughout my thesis with his excellent guidance, encouragement, and patience. I would like to thank Dr. Dmitry Sergeev for the thoughtful guidance, inspiring discussion and valuable suggestions during my experimental work. I would like to thank Dr. Elena Yazhenskikh for her patient explanation and helpful instruction during my modeling work with FactSage. I would like to thank Dr. Guixuan Wu for the interesting discussion about the thermodynamic topics and encouragement during my thesis. I would like to thank Mr. Mirko Ziegner for the high-quality XRD measurements and discussion, Mr. Ralf Küppers for the continuous vital support in the experiment set up and Mrs. Inge Dreger for the assistance during my PhD work.

I would like to take this opportunity of thanking all the colleague in the group of Michael Müller for the friendly and pleasant atmosphere they created. I would also like to thank all the scientific and nonscientific staff of IEK-2 for their help during my work period. I am very grateful to my family and friends, especially my husband Mr. Yihui Wu, for their constant attention, encouragement, and support.

This work was supported by the Federal Ministry for Economic Affairs and Climate Action on the basis of a decision by the German Bundestag within the projects PCM-Screening 1 and 2 (FKZ 03ET1441D, FKZ 03EN6005D) and by the China Scholarship Council (No. 201804910575).

# Reference


[1] Th. Brenscheidt, F. Nitschké, O. Söllner, H. Wendt, Molten carbonate fuel cell research II. Comparing the solubility and the in-cell mobility of the nickel oxide cathode material in lithium/potassium and lithium/sodium carbonate melts, Electrochim. Acta 46 (2001) 783–797. https://doi.org/10.1016/S0013-4686(00)00665-4.

[2] E. Jansen, W. Schäfer, A. Kirfel, M. Neuroth, Neutron Texture Investigation of Electrolytic $Li_2CO_3$/$KLiCO_3$ from a Molten Carbonate Fuel Cell, Mater. Sci. Forum 378-381 (2001) 718–722. https://doi.org/10.4028/www.scientific.net/MSF.378-381.718.

[3] S. Jiang, Y.Yan (Eds.), Materials for High-Temperature Fuel Cells, Wiley-VCH Verlag GmbH & Co. KGaA, Weinheim, Germany, 2013.

[4] J. Yaokawa, D. Miura, K. Anzai, Y. Yamada, H. Yoshii, Strength of Salt Core Composed of Alkali Carbonate and Alkali Chloride Mixtures Made by Casting Technique, Mater. Trans. 48 (2007) 1034–1041. https://doi.org/10.2320/matertrans.48.1034.

[5] M. Gao, Z. Chen, B. Deng, H. Yin, W. Xiao, X. Mao, D. Wang, Electrochemical Deposition of Carbon Materials in Molten Salts, ECS Trans. 80 (2017) 791–799. https://doi.org/10.1149/08010.0791ecst.

[6] J. Ge, L. Hu, Y. Song, S. Jiao, An investigation into the carbon nucleation and growth on a nickel substrate in LiCl-$Li_2CO_3$ melts, Faraday Discuss. 190 (2016) 259–268. https://doi.org/10.1039/c5fd00217f.

[7] Z. Yao, J. Li, X. Zhao, Molten salt oxidation: a versatile and promising technology for the destruction of organic-containing wastes, Chemosphere 84 (2011) 1167–1174. https://doi.org/10.1016/j.chemosphere.2011.05.061.

[8] P.D. Myers, D.Y. Goswami, Thermal energy storage using chloride salts and their eutectics, Appl. Therm. Eng. 109 (2016) 889–900. https://doi.org/10.1016/j.applthermaleng.2016.07.046.

[9] C.W. Bale, E. Bélisle, P. Chartrand, S.A. Decterov, G. Eriksson, A. E. Gheribi, K. Hack, I.-H. Jung, Y.-B. Kang, J. Melançon, A. D. Pelton, S. Petersen, C. Robelin, J. Sangster, P. Spencer, M-A. Van Ende, FactSage thermochemical software and databases, 2010–2016, Calphad 54 (2016) 35–53. https://doi.org/10.1016/j.calphad.2016.05.002.

[10] B.H. Reis, Development of a novel thermodynamic database for salt systems with potential as phase change materials, 2021. https://doi.org/10.26127/BTUOPEN-5590.

[11] M. Liu, N.H. Steven Tay, S. Bell, M. Belusko, R. Jacob, G. Will, W. Saman, F. Bruno, Review on concentrating solar power plants and new developments in high temperature thermal energy storage technologies, Renewable Sustainable Energy Rev. 53 (2016) 1411–1432. https://doi.org/10.1016/j.rser.2015.09.026.

[12] J. Stekli, L. Irwin, R. Pitchumani, Technical Challenges and Opportunities for Concentrating Solar Power With Thermal Energy Storage, J. Therm. Sci. Eng. Appl. 5 (2013). https://doi.org/10.1115/1.4024143.

[13] B. Cárdenas, N. León, High temperature latent heat thermal energy storage: Phase change materials, design considerations and performance enhancement techniques, Renewable Sustainable Energy Rev. 27 (2013) 724–737. https://doi.org/10.1016/j.rser.2013.07.028.
[14] H. Mehling, L.F. Cabeza, Heat and cold storage with PCM: An up to date introduction into basics and applications ; with 28 tables, Springer, Berlin, Heidelberg, 2008.
[15] L. Yang, X. Zhang, G. Xu, Thermal performance of a solar storage packed bed using spherical capsules filled with PCM having different melting points, Energy Build. 68 (2014) 639–646. https://doi.org/10.1016/j.enbuild.2013.09.045.
[16] J.C. Kurnia, A.P. Sasmito, S.V. Jangam, A.S. Mujumdar, Improved design for heat transfer performance of a novel phase change material (PCM) thermal energy storage (TES), Appl. Therm. Eng. 50 (2013) 896–907. https://doi.org/10.1016/j.applthermaleng.2012.08.015.
[17] R. Muren, D.A. Arias, B. Luptowski, Performance Based Cost Modeling of Phase Change Thermal Energy Storage for High Temperature Concentrating Solar Power Systems, in: pp. 193–202. https://doi.org/10.1115/IMECE2009-12848.
[18] H. Michels, R. Pitz-Paal, Cascaded latent heat storage for parabolic trough solar power plants, Sol. Energy 81 (2007) 829–837. https://doi.org/10.1016/j.solener.2006.09.008.
[19] F. Dinter, M.A. Geyer, R. Tamme (Eds.), Thermal energy storage for commercial applications: A feasibility study on economic storage systems, Springer-Verlag, Berlin, New York, 1991.
[20] B. Xu, P. Li, C. Chan, Application of phase change materials for thermal energy storage in concentrated solar thermal power plants: A review to recent developments, Appl. Energy 160 (2015) 286–307. https://doi.org/10.1016/j.apenergy.2015.09.016.
[21] K.H. Stern, High Temperature Properties and Decomposition of Inorganic Salts Part 3, Nitrates and Nitrites, J. Phys. Chem. Ref. Data 1 (1972) 747–772. https://doi.org/10.1063/1.3253104.
[22] B. Jo, D. Banerjee, Thermal properties measurement of binary carbonate salt mixtures for concentrating solar power plants, J. Renew. Sustain. Energy 7 (2015) 33121. https://doi.org/10.1063/1.4922029.
[23] J. Qi, E. Yazhenskikh, M. Ziegner, G. Wu, M. Müller, D. Sergeev, Experimental study and thermodynamic assessment of thermodynamic properties of pure $Li_2CO_3$ and $K_2CO_3$, Calphad 78 (2022) 102452. https://doi.org/10.1016/j.calphad.2022.102452.
[24] D. Sergeev, E. Yazhenskikh, P. Haseli, M Liu, M. Ziegner, F. Bruno, M. Müller, Experimental study of thermodynamic properties and phase equilibria in $Na_2CO_3$–$K_2CO_3$ system, Calphad 71 (2020) 101992. https://doi.org/10.1016/j.calphad.2020.101992.
[25] SGPS - SGTE Pure Substances database (v13.1), 2019.
[26] R. Raud, S. Bell, K. Adams, R. Lima, G. Will, T.A. Steinberg, Experimental verification of theoretically estimated composition and enthalpy of fusion of eutectic salt mixtures, Sol. Energy Mater. Sol. Cells 174 (2018) 515–522. https://doi.org/10.1016/j.solmat.2017.09.033.

[27] V.M.B. Nunes, M.J.V. Lourenço, F.J.V. Santos, C.A. Nieto de Castro, Molten alkali carbonates as alternative engineering fluids for high temperature applications, Appl. Energy 242 (2019) 1626–1633. https://doi.org/10.1016/j.apenergy.2019.03.190.
[28] D. Shin, D. Banerjee, Effects of silica nanoparticles on enhancing the specific heat capacity of carbonate salt eutectic (work in progress), Int. J. Solids. Struct. 2 (2010) 25–31.
[29] Z. Ge, F. Ye, H. Cao, G. Leng, Y. Qin, Y. Ding, Carbonate-salt-based composite materials for medium- and high-temperature thermal energy storage, Particuology 15 (2014) 77–81. https://doi.org/10.1016/j.partic.2013.09.002.
[30] Z. Zhang, Y. Yuan, L. Ouyang, H. Zhang, X. Cao, L. Sun, P.E. Phelan, Thermal properties of ternary carbonate/T-ZnOw for thermal energy storage in high-temperature concentrating solar power systems, Compos. Part A Appl. Sci. Manuf. 93 (2017) 177–184. https://doi.org/10.1016/j.compositesa.2016.11.026.
[31] S. Guo, J. Zhang, W. Wu, W. Zhou, Corrosion in the molten fluoride and chloride salts and materials development for nuclear applications, Prog. Mater. Sci. 97 (2018) 448–487. https://doi.org/10.1016/j.pmatsci.2018.05.003.
[32] A. Sheth, Y.D. Yeboah, A. Godavarty, Y. Xu, P.K. Agrawal, Catalytic gasification of coal using eutectic salts: reaction kinetics with binary and ternary eutectic catalysts, Fuel 82 (2003) 305–317. https://doi.org/10.1016/S0016-2361(02)00255-7.
[33] D. Sergeev, E. Yazhenskikh, D. Kobertz, K. Hack, M. Müller, Phase equilibria in the reciprocal NaCl–KCl–$NaNO_3$–$KNO_3$ system, Calphad 51 (2015) 111–124. https://doi.org/10.1016/j.calphad.2015.09.002.
[34] Personal communication with E. Yazhenskikh.
[35] A. Reisman, Reactions of the Group VB Pentoxides with Alkali Oxides and Carbonates. IX. A DTA Study of Alkali Metal Carbonates, J. Am. Ceram. Soc. 80 (1958) 3558–3561.
[36] Y. Otsubo, K. Yamaguchi, Thermochemical Properties and Reaction Processes of Alkali Carbonate-Ferric Oxide Systems as Investigated by Means of Differential Thermal Method. I-II. I. $Li_2CO_3$-$Fe_2O_3$ System, Nippon Kagaku Zasshi 82 (1961) 557–560. https://doi.org/10.1246/nikkashi1948.82.5_557.
[37] W. Klement, L.H. Cohen, Solid-solid and Solid-liquid Transitions in $K_2CO_3$, $Na_2CO_3$ and $Li_2CO_3$: Investigations to $\geqslant$ 5 kbar by Differential Thermal Analysis; Thermodynamics and Structural Correlations, Ber. Bunsenges. Phys. Chem. 79 (1975) 327 – 334.
[38] A.N. Khlapova, E.S. Kovaleva, Lithium carbonate polymorphism, J. Struct. Chem. 7 (1966) 559–565.
[39] G.J. Janz, E. Neuenschwander, F.J. Kelly, High-Temperature Heat Content and Related Properties for $Li_2CO_3$, $Na_2CO_3$, $K_2CO_3$, and the Ternary Eutectic Mixture, Trans. Faraday Soc. 59 (1963) 841–845.
[40] M. Rolin, J.M. Recapet, Enthalpy curves as a function of temperature and heats of fusion of $Na_2CO_3$, $Li_2CO_3$, $K_2CO_3$, and their ternary eutectic mixture, Bull. Soc. Chim. Fr. (1964) 2504–2510.

[41] M.A.K.L. Dissanayake, B.E. Mellander, Phase diagram and electrical conductivity of the $Li_2SO_4$-$Li_2CO_3$ system, Solid State Ionics 21 (1986) 279–285.
[42] P.M. Brown, D.A. Boryta, Lithium Carbonate/Sodium Sulfate Eutectic-An Additive for Improving Glass Production, J. Am. Ceram. Soc. 66 (1983) 660–663. https://doi.org/10.1111/j.1151-2916.1983.tb10617.x.
[43] O.L.I. Brown, W.M. Latimer, The Heat Capacity of Lithium Carbonate from 16 to 300°K. The Entropy and Heat of Solution of Lithium Carbonate at 298°K. The Entropy of Lithium Ion, J. Am. Chem. Soc. 58 (1936) 2228–2229.
[44] L. Kourkova, G. Sadovska, Heat capacity, enthalpy and entropy of $Li_2CO_3$ at 303.15–563.15K, Thermochim. Acta 452 (2007) 80–81. https://doi.org/10.1016/j.tca.2006.10.005.
[45] FactSage: Facility for the Analysis of Chemical Thermodynamics, Version 8, pp. 1976–2020, http://www.factsage.com/.
[46] S. Zemczuzny, F. Rambach, Schmelzen der Alkalichloride, Z. Anorg. Chem. 65 (1910) 403–428. https://doi.org/10.1002/zaac.19100650125.
[47] T.W. Richards, W.B. Meldrum, The melting points of the chlorides of lithium, rubidium and caesium, and the freezing points of binary and ternary mixtures of these salts, including also potassium and sodium chloride, J. Am. Chem. Soc. 39 (1917) 1816–1828. https://doi.org/10.1021/ja02254a004.
[48] K.K Kelley, Data on theoretical metallurgy. X. High-temperature heat-content, heat-capacity, and entropy data for inorganic compounds, Bull. - U. S., Bur. Mines, 1949.
[49] T. Carnelley, XXXI.—High melting points. Part IV, J. Chem. Soc., Trans. 33 (1878) 273–281. https://doi.org/10.1039/CT8783300273.
[50] T.B. Douglas, A.C. Victor, Preliminary report on the thermodynamic properties of lithium, beryllium, magnesium, aluminum, and their compounds with oxygen, hydrogen, fluorine, and chlorine: Chapter 3: High temperature heat content, National Bureau of Standards, Gaithersburg, MD, 1959. https://doi.org/10.6028/NBS.RPT.6297.
[51] A.S. Dworkin, M.A. Bredig, The heat of fusion of the alkali metal halides, J. Phys. Chem. 64 (1960) 269–272. https://doi.org/10.1021/j100831a023.
[52] H. Flood, O. Fykse, S. Urnes, The relation between concentration and activity in liquid salt mixtures. II, Z. Elektrochem. Angew. Phys. Chem. 59 (1955) 364–370.
[53] D.C. Ginnings, T.E. Phipps, Temperature-conductance curves of solid salts. III. Halides of lithium, J. Am. Chem. Soc. 52 (1930) 1340–1345. https://doi.org/10.1021/ja01367a006.
[54] M. Guntz, Preparation of metallic lithium, J. Chem. Soc., Abstr. 117 (1894) 732–733.
[55] K. Hachmeister, Melting, freezing and boiling phenomena of mixtures of ammonium chloride and other chlorides, Z. Anorg. Allg. Chem. 109 (1919) 145–186. https://doi.org/10.1002/zaac.19191090112.
[56] H.M. Haendler, P.S. Sennett, C.M. Wheeler, The System LiF-LiCl, LiF-NaCl, LiF-KCl, J. Electrochem. Soc. 106 (1959) 264. https://doi.org/10.1149/1.2427319.
[57] E.N. Rodigina, K.Z. Gomel'skii, V.F. Luginina, Heat content and heat capacity of lithium chloride at high temperatures, Russ. J. Inorg. Chem. 4 (1959) 442–444.

[58] F.D. Rossini, D.D. Wagmann, W.H. Evans, Selected Values of Chemical Thermodynamic Properties, U.S. Government Printing Office, 1952.
[59] C. Sandonnini, Thermal Analysis of Binary Mixtures of Chlorides of Monovalent Elements, Atti Accad. Naz. Lincei, Cl. Sci. Fis., Mat. Nat., Rend. 20 (1911) 758–764.
[60] D.A. Shirley, The Heat Capacity of Lithium Chloride from 15 to 325 Degrees Kelvin, J. Am. Ceram. Soc. 82 (1960) 3841-3843.
[61] E. Korreng, Crystallographic and thermal investigations of alkali chlorides and chlorides of divalent metals, Neues Jahrb. Mineral., Geol. Palaeontol., Abh., Abt. A 37 (1914) 50–123.
[62] K. Huettner, G. Tammann, Melting points and transition points of some salts., Z. f. anorg. Ch. 43 (1905) 215–225.
[63] H. Von Wartenberg, H. Schulz, Der Dampfdruck einiger Salze. II, Z. Elektrochem. Angew. Phys. Chem. 27 (1921) 568–573. https://doi.org/10.1002/bbpc.19210272307.
[64] D.S. Coleman, P. Lacy, The phase equilibrium diagram for the KCl-NaCl system, Mater. Res. Bull. 2 (1967) 935–938. https://doi.org/10.1016/0025-5408(67)90149-3.
[65] Yu.I. Vesnin, S.P.Zakovryashin, Decomposition of Solid Solutions KCl-NaCl, Solid State Commun. 31 (1979) 635–639. https://doi.org/10.1016/0038-1098(79)90313-2.
[66] Akopov, K.E., A.G. Bergman, Reversible-adiagonal system of sodium and potassium chlorides and sulfates, Zh. Obshch. Khim. 24 (1954) 1524–1532.
[67] A.D. Pelton, A. Gabriel, J. Sangster, Liquidus measurements and coupled thermodynamic–phase-diagram analysis of the NaCl–KCl system, J. Chem. Soc., Faraday Trans. 1 81 (1985) 1167. https://doi.org/10.1039/f19858101167.
[68] L.S. Hersh, O.J. Kleppa, Enthalpies of Mixing in Some Binary Liquid Halide Mixtures, J. Chem. Phys. 42 (1965) 1309–1322. https://doi.org/10.1063/1.1696115.
[69] D. Sergeev, D. Kobertz, M. Müller, Thermodynamics of the NaCl–KCl system, Thermochim. Acta 606 (2015) 25–33. https://doi.org/10.1016/j.tca.2015.03.003.
[70] A. Reisman, Heterogeneous equilibria in the system $K_2CO_3$ -$Na_2CO_3$, J. Am. Chem. Soc. 81 (1959) 807–811. https://doi.org/10.1021/ja01513a014.
[71] S.Z. Makarov, M.P. Shul'gina, Transformation in solid state in the system potassium carbonate-sodium carbonate, Izv. Akad. Nauk SSSR, Ser. Khim. (1940) 691–702.
[72] M. Christmann, G. Papin, Characterization of the non-stoichiometric double carbonate of sodium and potassium $(Na_xK_y)_2CO_3$, Rev. Chim. Miner. 16 (1979) 485–489.
[73] W. Schaefer, Thermal and crystallographic investigation of the ternary systems NaCl-LiCl-KCl and $CaCl_2$-$SrCl_2$-$BaCl_2$, Neues Jahrb. fur Geol. Palaontol. 43 (1919) 132–189.
[74] S.D. Gromakov, L.M. Gromakova, Several rules for the plotting of phase diagrams of binary systems, Zh. Fiz. Khim. 27 (1953) 1545–1555.
[75] M.A. Klochko, Double decomposition in the absence of a solvent. XXIV. Irreversible-reciprocal system: sodium chloride-lithium sulfate, Zh. Obshch. Khim. 3 (1933) 1026–1039.
[76] S. Tian, S. Liu, C. Zheng, Investigation on the phase diagram of the ternary system $LaCl_3$–NaCl–LiCl, J. Alloys Compd. 279 (1998) 127–131. https://doi.org/10.1016/S0925-8388(98)00654-9.

[77] E.K. Akopov, E.I. Korobka, Phase diagram of the lithium chloride-sodium chloride, Ukr. Khim. Zh. 35 (1969) 588–590.
[78] A.V. Storonkin, O.D. Grebennikova, I.V. Krivousova, I.I. Kozhina, I.V. Vasil'kova, Thermal analysis and x-ray studies of the lithium chloride-sodium chloride system, Vestn. Leningr. Univ., Ser. 4: Fiz., Khim. (1973) 70–72.
[79] A.S. Chesnokov, Kh.L. Strelets, E.F. Klyuchnikova, V.N. Veretinskii, Phase diagram, microstructure, and phase composition of the NaCl-LiCl system, Proektn. Inst. Alyum. Magnievoi Elektrodni Prom-sti.,Tr. Vses. Nauchno-Issled. 72 (1970) 90-98.
[80] A.N. Kruglov, M.E. Prostakov, Zinc chloride-sodium chloride-lithium chloride system, Zh. Neorg. Khim. 26 (1981) 1975–1976.
[81] V.N. Derkacheva, K.V. Gontar, Internal cross sections of the lithium chloride-potassium chloride-sodium chloride-barium chloride quaternary system in melts, Zh. Prikl. Khim. (S.-Peterburg, Russ. Fed.) 50 (1977) 668–671.
[82] T.P. Bortnikova, E.K. Akopov, V.A. Ocheretnyi, Ternary system of lithium, sodium, and cesium chlorides, Zh. Neorg. Khim. 19 (1974) 1066–1069.
[83] E.K. Akopov, A.G. Bergman, Li, Na, K ‖ Cl system, Zh. Neorg. Khim. 11 (1966) 1751 – 1753.
[84] A.G. Bergman, E.L. Kozachenko, S.I. Berezina, The Li, Na ‖ F, Cl system, Zh. Neorg. Khim. 9 (1964) 1214 – 1217.
[85] A.S. Arabadzhan, A.G. Bergman, Reactions of fused chlorides and bromides of lithium and sodium, Zh. Neorg. Khim. 7 (1962) 2226–2229.
[86] G.A. Bukhalova, A.S. Arabadzhan, Ternary systems of Li Na Ca--Cl, Zh. Neorg. Khim. 7 (1962) 2230–2232.
[87] E.K. Akopov, The ternary system of the chlorides of lithium, sodium, and potassium, Zh. Neorg. Khim. 1 (1956) 1019–1025.
[88] A.G. Bergman, E.K. Akopov, Reciprocal system of lithium and sodium chlorides and sulfates, Izv. Sekt. Fiz.-Khim. Anal., Inst. Obshch. Neorg. Khim., Akad. Nauk SSSR 23 (1953) 221–232.
[89] J. Sangster, A.D. Pelton, Phase Diagrams and Thermodynamic Properties of the 70 Binary Alkali Halide Systems Having Common Ions, J. Phys. Chem. Ref. Data 16 (1987) 509–561. https://doi.org/10.1063/1.555803.
[90] C. Guo, C. Li, Z. Du, Thermodynamic optimization of the NaCl–$PrCl_3$ system and the LiCl–NaCl–$PrCl_3$ system, Thermochim. Acta 540 (2012) 85–90. https://doi.org/10.1016/j.tca.2012.04.017.
[91] A. Smits, J. Elgersma, M.E. Hardenberg, A critical melting point in the solid phase of the system sodium chloride-lithium chloride, Recl. Trav. Chim. Pays-Bas, 43 (1924) 671–676.
[92] E. Aukrust, B. Björge, H. Flood, Forland. T, Activities in molten salt mixtures of potassium-lithiumhalide mixtures: a preliminary report, Ann. N. Y. Acad. Sci. 79 (1960) 830–837.

[93] E. Korin, L. Soifer, Thermal analysis of the system KCl-LiCI by differential scanning calorimetry, Bull. Soc. Chim. Fr. 50 (1997) 347–354.
[94] E. Elchardus, P. Laffitte, Thermal analysis of the systems: KCl-$BaCl_2$ and KCl-LiCl, Bull. Soc. Chim. Fr. 51 (1932) 1572–1579.
[95] S. Ghosh, R.B. Prabhakara, K. Nagarajan, K.C.H. Kumar, Experimental investigations and thermodynamic modelling of KCl–LiCl–$UCl_3$ system, Calphad 45 (2014) 11–26. https://doi.org/10.1016/j.calphad.2013.11.001.
[96] W. Zhou, J. Zhang, Thermodynamic evaluation of LiCl-KCl-$PuCl_3$ system, J. Alloys Compd. 695 (2017) 2306–2313. https://doi.org/10.1016/j.jallcom.2016.11.092.
[97] W.D. Powers, G.C. Blalock, Enthalpy and heat capacity of lithium chloride, potassium chloride eutectic, 1953. https://doi.org/10.2172/4357976.
[98] C. Solomons, J. Goodkin, H.J. Gardner, G.J. Janz, Heat of fusion, entropy of fusion and cryoscopic constant of the LiCl–KCl eutectic mixture, J. Phys. Chem. 62 (1958) 248–250.
[99] B.F. Markov, T.A. Tishura, A.N. Budarina, Thermochemical study of binary salt systems, Rev. Roum. Chim. 20 (1975) 597–602.
[100] R.P. Clark, Heats of fusion and heat capacities of lithium chloride-potassium chloride eutectic and potassium nitrate, J. Chem. Eng. Data 18 (1973) 67–70. https://doi.org/10.1021/je60056a023.
[101] L.U. Thulin, O. Wærnes, T. Østvold, Determination of Partial Gibbs Energies of Mixing of LiCl in the Alk.Cl--LiCl Mixtures from Concentration Cell Measurements, Acta Chem. Scand. 30a (1976) 731–734. https://doi.org/10.3891/acta.chem.scand.30a-0731.
[102] W. Behl, Thermodynamics of Molten Mixtures of Lithium Chloride-Potassium Chloride at 640 C, Avail.NTIS FromGovt. Rep. Announce. (U.S.), 1972.
[103] N.N. Volkov, M.N. Zakhvalinskii, Ternary reciprocal system of chlorides and carbonates of lithium and potassium, Izv. Fiz.-Khim. Nauchn.-Issled. Inst. pri Irkutskom Univ. 4 (1959) 107–110.
[104] N.A. Reshetnikov, G.G. Diogenov, Ternary system of lithium chloride, carbonate, and sulfate, Izv. Fiz.-Khim. Nauchno 2 (1953) 14–16.
[105] E.M. Levin, C.R. Robbins, H.F. McMurdie, Phase diagrams for ceramists, J. Am. Ceram. Soc., 1964.
[106] Y. Dessureault, J. Sangster, A. D. Pelton, Coupled Phase Diagram - Thermodynamic Analysis of the 24 Binary Systems, $A_2CO_3$ - AX and $A_2SO_4$ - AX Where A=Li, Na, K and X=Cl, F, $NO_3$ OH, J. Phys. Chem. Ref. Data 19 (1990) 1149–1178. https://doi.org/10.1063/1.555866.
[107] A.G. Bergman, A.K. Sementsova, The ternary systems Na ‖ Cl, $SO_4$, $CO_3$ and K ‖ Cl, $SO_4$, $CO_3$, Zh. Neorg. Khim. 3 (1958) 383–392.
[108] V.P. Radishchev, Double decomposition in the absence of a solvent. XXI. Irreversible-reciprocal system: 2NaCl + $K_2CO_3$ → 2KCl + $Na_2CO_3$, Zh. Obshch. Khim. 3 (1933) 852–864.
[109] M. Amadori, The tendency of halides and other salts of the same metal to combine fluorides, chlorides and carbonates, Atti Accad. Naz. Lincei, Cl. Sci. Fis., Mat. Nat., Rend. 22 (1913) 366-372.

[110] O. Sackur, Abnormal Molecular Weights in Fused Salts, Z. Elektrochem. Angew. Phys. Chem. 16 (1910) 649–654.
[111] N.N. Volkov, A.G. Bergman, Composition diagram of ternary systems with potassium and sodium chlorides, fluorides and carbonates, C. R. (Dokl.) Acad. Sci. URSS 27 (1940) 967–969.
[112] H. Brearley, F.C. Morwood, Erstarrungs- und Umwandlungstemperaturen von binären und ternären Salzgemischen, Landolt-Bornstein Phys. Chem. Tabl. H. W. 1 (1923) 607–608.
[113] J. Yaokawa, K. Oikawa, K. Anzai, Thermodynamic assessment of the KCl–$K_2CO_3$–NaCl–$Na_2CO_3$ system, Calphad 31 (2007) 155–163. https://doi.org/10.1016/j.calphad.2007.01.004.
[114] P. Niggli, Untersuchungen an Karbonat- und -Chloridschmelzen, Z. Anorg. Allg. Chem. 106 (1919) 126–142. https://doi.org/10.1002/zaac.19191060109.
[115] T. Sato, Equilibrium diagrams of salts for salt baths. II. Equilibrium diagram of the $Na_2CO_3$-NaCl-KCl system, Technol. Rep. Tohoku Imp. Univ. 11 (1934) 403–416.
[116] K. Iwasawa, S. Yamaguchi, M. Maeda, Phase relation and thermodynamic properties of NaCl-$Na_2CO_3$ system as a basic system for secondary fly ash in incineration processes of municipal wastes, Mater. Trans. 42 (2001) 2480–2486.
[117] Y. Jiang, Y. Sun, M. Liu, F. Bruno, S. Li, Eutectic $Na_2CO_3$–NaCl salt: A new phase change material for high temperature thermal storage, Sol. Energy Mater. Sol. Cells 152 (2016) 155–160. https://doi.org/10.1016/j.solmat.2016.04.002.
[118] L. Ye, C. Tang, Y. Chen, S. Yang, M. Tang, The thermal physical properties and stability of the eutectic composition in a $Na_2CO_3$–NaCl binary system, Thermochim. Acta 596 (2014) 14–20. https://doi.org/10.1016/j.tca.2014.07.002.
[119] L.F. Volkova, The ternary system lithium carbonate, sodium carbonate, and potassium carbonate, Izv. Sib. Otd. Akad. Nauk SSSR 7 (1958) 33–35.
[120] G.J. Janz, M.R. Lorenz, Solid-Liquid Phase Equilibria for Mixtures of Lithium, Sodium, and Potassium Carbonates, J. Chem. Eng. Data 6 (1961) 321–323.
[121] M. Rolin, J. M. Recapet, Thermodynamic properties of the alkali metal carbonates. I. The ternary diagram $Na_2CO_3$-$K_2CO_3$-$Li_2CO_3$, Bull. Soc. Chim. Fr. (1964) 2104–2110.
[122] K. Babcock, J. Winnick, Solid-liquid equilibria in the reciprocal ternary system potassium, lithium/sulfide, carbonate, J. Chem. Eng. Data 33 (1988) 96–98.
[123] H. Le Chatelier, Sur la fusibilité des mélanges de sels, C. R. Seances Acad. Sci. 118 (1894) 800–804.
[124] N.A. Reshetnikov, O.G. Perfil'eva, Phase Transformations in the K, Li// $CO_3$ OH Ternary Reciprocal System, Russ. J. Inorg. Chem. 13 (1968) 1662–1669.
[125] G.J. Janz, J.L. Perano, High-Temperature Heat Content and Fusion Properties for Binary Carbonate Mixtures: $Li_2CO_3$, $K_2CO_3$ and $Na_2CO_3$, Trans. Faraday Soc. 60 (1964) 1742–1944.
[126] N. Araki, M. Matsuura, A. Makino, T. Hirata, Y. Kato, Measurement of thermophysical properties of molten salts: Mixtures of alkaline carbonate salts, Int. J. Thermophys. 9 (1988) 1071–1080. https://doi.org/10.1007/BF01133274.
[127] M. Liu, J.C. Gomez, C.S. Turchi, N. Tay, W. Saman, F. Bruno, Determination of thermo-physical properties and stability testing of high-temperature phase-change materials for CSP

applications, Sol. Energy Mater. Sol. Cells 139 (2015) 81–87. https://doi.org/10.1016/j.solmat.2015.03.014.
[128] B.K. Andersen, O.J. Kleppa, Enthalpy of mixing in binary liquid alkali carbonate mixtures, Acta Chem. Scand., Ser. A 30 (1976) 751–758.
[129] C. Chen, T. Tran, R. Olivares, S. Wright, S. Sun, Coupled Experimental Study and Thermodynamic Modeling of Melting Point and Thermal Stability of $Li_2CO_3$-$Na_2CO_3$-$K_2CO_3$ Based Salts, J. Sol. Energy Eng. 136 (2014). https://doi.org/10.1115/1.4027264.
[130] W. Eitel, W. Skaliks, A few double carbonates of the alkalies and alkaline earths, Z. Anorg. Allg. Chem. 183 (1929) 263–286.
[131] N.P. Burmistrova, E.G. Volozhanina, DTA and Electrical conductivity study of solid phase transformations in the $Li_2CO_3$-$Na_2CO_3$ system, Russ. J. Inorg. Chem. 21 (1976) 553–555.
[132] N.N. Volkov, L.F. Volkova, Ternary reciprocal system of lithium and sodium sulfates and carbonates, Izvest. Fiz.-Khim. Nauch.-Issledovatel. Inst. Irkutsk. Univ. 2 (1953) 65–68.
[133] N. N. Volkov, T. F. Shvab, Ternary reciprocal system of lithium and sodium fluorides and carbonates, Izvest. Fiz.-Khim. Nauch.-Issledovatel. Inst., Irkutsk. Univ. 2 (1953) 60–64.
[134] E.J. Cairns, D.I. Macdonald, Sensitive thermal analysis establishing formation of the incongruently melting compound $LiNaCO_3$, Nature 194 (1962) 441–442. https://doi.org/10.1038/194441a0.
[135] V.A. D'yakov, C.A. Ebbers, M.V. Pchelkin, V.I. Pryalkin, Lithium sodium carbonate: A new nonlinear-optics crystal, J. Russ. Laser Res. 17 (1996) 489–494. https://doi.org/10.1007/BF02090628.
[136] A.N. Khlapova, V.M. Elenevskaya, The Lithium Carbonate-Sodium Carbonate System, Russ. J. Inorg. Chem. 13 (1968) 610-3.
[137] Y. Dessureault, J. Sangster, A.D. Pelton, Coupled phase diagram/thermodynamic analysis of the nine common‐ion binary systems involving the carbonates and sulfates of lithium, sodium, and potassium, J. Electrochem. Soc. 137 (1990) 2941‐2950. https://doi.org/10.1149/1.2087103.
[138] M. Christmann, N. Sadeghi, G. Papin, Crystallographic characteristics of lithium sodium carbonate and lithium potassium carbonate, Rev. Chim. Miner. 15 (1978) 312–317.
[139] A.V. Yatsenko, S.G. Zhukov, V.A. D'yakov, A. Etz, W. Molleman, H. Schenk, X-ray study of low and high symmetry phases of $LiNaCO_3$, Mater. Res. Bull. 30 (1995) 739–744. https://doi.org/10.1016/0025-5408(95)00046-1.
[140] A.V. Yatsenko, S.G. Zhukov, V.A. D'yakov, H. Schenk, Triclinic α-$LiNaCO_3$, Acta Crystallogr., Sect. C: Cryst. Struct. Commun. 52 (1996) 1–3. https://doi.org/10.1107/S0108270195010584.
[141] S.G. Zhukov, A.V. Yatsenko, V.V. Chernyshev, V.A. D'yakov, R. Le Loux, H. Schenk, X-ray high temperature powder diffraction study and computer simulation of γ-$LiNaCO_3$, Z. Kristallogr. - Cryst. Mater. 214 (1999). https://doi.org/10.1524/zkri.1999.214.5.255.
[142] Y. Li, D. Zhang, Thermal stability of $Li_2CO_3$-$Na_2CO_3$ based high-temperature phase change materials, Energy Storage Sci. Technol. 2 (2013) 369–376.

[143] Y. Li, Y. Zhang, M. Li, D. Zhang, Testing method of phase change temperature and heat of inorganic high temperature phase change materials, Exp. Therm. Fluid Sci. 44 (2013) 697–707. https://doi.org/10.1016/j.expthermflusci.2012.09.010.
[144] Y. Jiang, Y. Sun, F. Bruno, S. Li, Thermal stability of $Na_2CO_3$ -$Li_2CO_3$ as a high temperature phase change material for thermal energy storage, Thermochim. Acta 650 (2017) 88–94. https://doi.org/10.1016/j.tca.2017.01.002.
[145] G.J. Janz, C.B. Allen, N.P. Bansal, R.M. Murphy, R.P.T. Tomkins, Physical properties data compilations relevant to energy storage. II. Molten salts: data on single and multi-component salt systems, National Bureau of Standards, 1979.
[146] R.J. Petri, E.T. Ong, J. Martin, High temperature composite thermal energy storage (TES) systems for industrial applications, 1986.
[147] A.V. Storonkin, I.V. Vasil'kova, I.V. Krivousova, O.D. Grebennikova, Phase diagram of the sodium chloride-lithium chloride-potassium chloride system, Vestnik Leningradskogo Universiteta, Seriya 4: Fizika, Khimiya 16 (1973) 83–86.
[148] J.M. Sangster, A.D. Pelton, Critical coupled evaluation of phase diagrams and their thermodynamic properties of binary and ternary alkali salt systems, American Ceramic, 1987.
[149] A.D. Pelton, C.W. Bale, P.L. Lin, Calculation of phase diagrams and thermodynamic properties of 14 additive and reciprocal ternary systems containing $Li_2CO_3$, $Na_2CO_3$, $K_2CO_3$, $Li_2SO_4$, $Na_2SO_4$, $K_2SO_4$ LiOH, NaOH, and KOH, Can. J. Chem. 62 (1984) 457–474. https://doi.org/10.1139/v84-078.
[150] Q. Yan, C. Wang, C. Liu, J. Zhang, Experimental and theoretical research on the thermal properties of carbonate mixtures, IOP Conf. Ser.: Mater. Sci. Eng. 729 (2020) 12031. https://doi.org/10.1088/1757-899x/729/1/012031.
[151] L. Sang, M. Cai, Y. Zhao, N. Ren, Y. Wu, C. Burda, Mixed metal carbonates/hydroxides for concentrating solar power analyzed with DSC and XRD, Sol. Energy Mater. Sol. Cells 140 (2015) 167–173. https://doi.org/10.1016/j.solmat.2015.04.006.
[152] R.I. Olivares, C. Chen, S. Wright, The Thermal Stability of Molten Lithium–Sodium–Potassium Carbonate and the Influence of Additives on the Melting Point, J. Sol. Energy Eng. 134 (2012). https://doi.org/10.1115/1.4006895.
[153] X. An, J. Cheng, P. Zhang, Z. Tang, J. Wang, Determination and evaluation of the thermophysical properties of an alkali carbonate eutectic molten salt, Faraday Discuss. 190 (2016) 327–338. https://doi.org/10.1039/c5fd00236b.
[154] Y. Wu, S. Ming, C. Zhang, Y. Lu, Experimental research of the thermophysical properties of ternary mixed carbonate molten salts, Energy Storage Sci. Technol. 10 (2021) 1292–1296. https://doi.org/10.19799/j.cnki.2095-4239.2021.0126.
[155] M. Liao, X. Wei, J. Ding, B. Hu, Preparation and experimental investigation for LNK carbonate molten salts, Taiyangneng Xuebao/Acta Energ. Sol. Sin. 31 (2010) 863–867.
[156] R.N. Nyankovskaya, Geometric reversal in the series of reciprocal systems of halides and carbonates of sodium and potassium, Doklady Akademii Nauk SSSR 83 (1952) 419–422.

[157] V.B. Busse-Machukas, V.I. Markin, A.G. Morachevskii, E.A. Maiorova, L.N. Gerasimenko, Physicochemical properties of sodium, potassium ‖ chloride, carbonate system melts, Zh. Prikl. Khim. (S.-Peterburg, Russ. Fed.) 50 (1977) 2574 – 2576.
[158] P. Haseli, R. Jacob, M. Liu, P. Majewski, F.C. Christo, F. Bruno, Experimental phase diagram study of the binary KCl-$Na_2CO_3$ system, Thermochim. Acta 695 (2021) 178811. https://doi.org/10.1016/j.tca.2020.178811.
[159] M. Liu, E.S. Omaraa, J. Qi, P. Haseli, J. Ibrahim, D. Sergeev, M. Müller, F. Bruno, P. Majewski, Review and characterisation of high-temperature phase change material candidates between 500 C and 700°C, Renewable Sustainable Energy Rev. 150 (2021) 111528. https://doi.org/10.1016/j.rser.2021.111528.
[160] W.J. Boettinger, U.R. Kattner, K.W. Moon, J. Perepezko, NIST recommended practice guide DTA and heat-flix DSC measurements of alloy melting and freezing, Elsevier, Amsterdam, The Netherlands, 2006.
[161] R. Kasuya, T. Miki, H. Morikawa, Y. Tai, Synthesis of alkali metal platinates and their dissolution behavior in hydrochloric acid, Journal of the Ceramic Society of Japan 121 (2013) 884–890. https://doi.org/10.2109/jcersj2.121.884.
[162] E37 Committee, Test Method for Determining Specific Heat Capacity by Differential Scanning Calorimetry, ASTM International, West Conshohocken, PA.
[163] S. A. Speakman, Basics of X-ray powder diffraction, 2011, http://www.fis.unical.it/files/fl178/61731basicsofxraypowderdiffraction.pdf.
[164] A. Belsky, M. Hellenbrandt, V.L. Karen, P. Luksch, New developments in the Inorganic Crystal Structure Database (ICSD): accessibility in support of materials research and design, Acta Crystallogr. B: Struct. Sci. Cryst. Eng. Mater. 58 (2002) 364–369. https://doi.org/10.1107/s0108768102006948.
[165] T. Markus, Potential of Knudsen Effusion Mass Spectrometry (KEMS) for Thermo Chemical Studies in Materials Science, Meet. Abstr. MA2013-02 (2013) 771. https://doi.org/10.1149/ma2013-02/11/771.
[166] K. Hilpert, Potential of mass spectrometry for the analysis of inorganic high-temperature vapors, Fresenius' J. Anal. Chem. 370 (2001) 471–478. https://doi.org/10.1007/s002160100835.
[167] P.W. Atkins, J. de Paula, Atkins' Physical chemistry. Tenth edition, Oxford University Press, Oxford, New York, 2014.
[168] R.W. Cahn, P. Haasen (Eds.), Physical metallurgy. 4., rev. and enhanced ed., North-Holland, Amsterdam, 1996.
[169] B. Sundman, J. Ågren, A regular solution model for phases with several components and sublattices, suitable for computer applications, Journal of Physics and Chemistry of Solids 42 (1981) 297–301. https://doi.org/10.1016/0022-3697(81)90144-X.
[170] P. Chartrand, A.D. Pelton, The modified quasi-chemical model: Part III. Two sublattices, Metall Mater Trans A 32 (2001) 1397–1407. https://doi.org/10.1007/s11661-001-0229-0.

[171] A.D. Pelton, P. Chartrand, The modified quasi-chemical model: Part II. Multicomponent solutions, Metall Mater Trans A 32 (2001) 1355–1360. https://doi.org/10.1007/s11661-001-0226-3.
[172] A.D. Pelton, P. Chartrand, G. Eriksson, The modified quasi-chemical model: Part IV. Two-sublattice quadruplet approximation, Metall Mater Trans A 32 (2001) 1409–1416. https://doi.org/10.1007/s11661-001-0230-7.
[173] A.D. Pelton, S.A. Degterov, G. Eriksson, C. Robelin, Y. Dessureault, The modified quasichemical model I—Binary solutions, Metall Mater Trans B 31 (2000) 651–659. https://doi.org/10.1007/s11663-000-0103-2.
[174] Y. Dessureault, A.D. Pelton, Contribution to the quasichemical model of reciprocal molten salt solutions, J. Chim. Phys. 88 (1991) 1811–1830. https://doi.org/10.1051/jcp/1991881811.
[175] T.M. Besmann, K.E. Spear, Thermochemical Modeling of Oxide Glasses, J. Am. Ceram. Soc. 85 (2002) 2887–2894. https://doi.org/10.1111/j.1151-2916.2002.tb00552.x.
[176] M. L. Kapoor, M. G. Frohberg, The Second International Symposium on Metallurgical Slags and Fluxes, London, 1973.
[177] O. Redlich, A.T. Kister, Algebraic Representation of Thermodynamic Properties and the Classification of Solutions, Ind. Eng. Chem. 40 (1948) 345–348. https://doi.org/10.1021/ie50458a036.
[178] A.D. Pelton, A general “geometric” thermodynamic model for multicomponent solutions, Calphad 25 (2001) 319–328. https://doi.org/10.1016/s0364-5916(01)00052-9.
[179] M. Hillert, B. Jansson, B. Sundman, J. Ågren, A two-sublattice model for molten solutions with different tendency for ionization, MTA 16 (1985) 261–266. https://doi.org/10.1007/BF02815307.
[180] E. Yazhenskikh, T. Jantzen, K. Hack, M. Müller., A new multipurpose thermodynamic database for oxide systems, Rasplavy (2019) 116–124. https://doi.org/10.1134/s0235010619010237.
[181] L. Kaufman, H. Bernstein, Computer calculation of phase diagrams: With special reference to refractory metals, Academic Press, New York, 1970.
[182] J.-O. Andersson, T. Helander, L. Höglund, P. Shi, B. Sundman, Thermo-Calc & DICTRA, computational tools for materials science, Calphad 26 (2002) 273–312. https://doi.org/10.1016/S0364-5916(02)00037-8.
[183] S.-L. Chen, S. Daniel, F. Zhang, Y.A. Chang, X.-Y. Yan, F.-Y. Xie, R. Schmid-Fetzer, W.A. Oates, The PANDAT software package and its applications, Calphad 26 (2002) 175–188. https://doi.org/10.1016/S0364-5916(02)00034-2.
[184] K. Hack (Ed.), The SGTE casebook: Thermodynamics at work. 2. ed., CRC Press, Boca Raton, Fla., 2008.
[185] J. Leitner, P. Voňka, D. Sedmidubský, P. Svoboda, Application of Neumann–Kopp rule for the estimation of heat capacity of mixed oxides, Thermochim. Acta 497 (2010) 7–13. https://doi.org/10.1016/j.tca.2009.08.002.

[186] M. Amadori, Solubilita allo stato solido tra solfati e carbonati ad alta temperature, Atti R. Accad. dei Lincei 21(Serie Quinta) (1912) 65–71.
[187] G. Papin, M. Michaud, R. Bouaziz, Étude du Système Binaire Carbonate-Oxide de Lithium, C. R. Seances Acad. Sci., Ser. C 268 (1969) 1691-1693.
[188] H. Effenberger, J. Zemann, Verfeinerung der Kristallstruktur des Lithiumkarbonates $Li_2CO_3$, Z. Kristallogr. Cryst. Mater 150 (1979) 133–138.
[189] Y. Lin, H. Zhang, M. Zheng, The crystal structure of zabuyelite, Chin. Sci. Bull. 35 (1990) 489–492.
[190] R. Cohen-Adad, M. Michaud, J. Saied, A. P. Rollet, Alkali hydroxide-carbonate systems, Bull. Soc. Chim. Fr. (1961) 356–359.
[191] M.V. Smirnov, I.Ya. Lyubimtseva, L.A. Tsiovkina, Yu.N. Krasnov, Equilibrium Diagram of the Lithium Carbonate-Lithium Oxide system, Russ. J. Inorg. Chem. 16 (1971) 130–131.
[192] I. Barin, Thermochemical data of pure substances. 3rd edition, VCH, Weinheim, New York, Basel, op. 1995. https://doi.org/10.1002/9783527619825.
[193] Jr.M.W. Chase, NIST-JANAF thermochamical tables, Fourth Edition, Monograph 9 (Part I and Part II) (1998).
[194] L.N. Gorokhov, Y.S. Khodeev, P.A. Akishin, Mass-spectrometric investigation of the sublimation of sodium chloride, Zh. Neorg. Khim. 3 (1958) 2597–2598.
[195] D. Sergeev, E. Yazhenskikh, D. Kobertz, M. Müller, Vaporization behavior of $Na_2CO_3$ and $K_2CO_3$, Calphad 65 (2019) 42–49. https://doi.org/10.1016/j.calphad.2019.02.004.
[196] C. Ricca, A. Ringuedé, M. Cassir, C. Adamo, F. Labat, Mixed lithium-sodium ($LiNaCO_3$) and lithium-potassium ($LiKCO_3$) carbonates for low temperature electrochemical applications: Structure, electronic properties and surface reconstruction from ab-initio calculations, Surf. Sci. 647 (2016) 66–77. https://doi.org/10.1016/j.susc.2015.12.027.
[197] A. Kirfel, H. Euler, B. Barbier, E. Hägele, H. Klapper, Potassium lithium carbonate, $KLiCO_3$: single-crystal X-ray structure analysis and thermal expansion, Z. Kristallogr. Cryst. Mater. 215 (2000) 744–751. https://doi.org/10.1524/zkri.2000.215.12.744.
[198] T. Kodama, Material studies on molten carbonate fuel cell, Prog. Batteries Sol. Cells 6 (1987) 7–11.
[199] A. Jain, S.P. Ong, G. Hautier, W. Chen, W.D. Richards, S. Dacek, S. Cholia, D. Gunter, D. Skinner, G. Ceder, K.A. Persson, Commentary: The Materials Project: A materials genome approach to accelerating materials innovation, APL Mater. 1 (2013) 11002. https://doi.org/10.1063/1.4812323.
[200] H. Keitel, The ternary systems KCl-LiCl-RbCl and KCl-RbCl-CsCl, Neues Jahrb. Mineral., Geol. Palaeontol., Abh., Abt. A 52A (1925) 378-425.
[201] G. Scarpa, Thermal analysis of the mixture of the alkali hydroxides with the corresponding halides. III. Compounds of lithium, AttiAccad. Naz. Lincei, Cl. Sci. Fis., Mat. Nat., Rend. 24 (1915) 476–482.
[202] O. Schmitz-Dumont, E. Schmitz, Einfluß des Kationen- und Anionenradius auf die Bildung von Anlagerungskomplexen, untersucht an den Systemen Alkalimetavanadat-

Alkalihalogenid, Z. Anorg. Chem. 252 (1944) 329–353. https://doi.org/10.1002/zaac.19442520605.
[203] D. Sergeev, B.H. Reis, I. Dreger, M. to Baben, K. Hack, M. Müller, Thermodynamics of the $Ca(NO_3)_2$ – $NaNO_3$ system, Calphad 67 (2019) 101688. https://doi.org/10.1016/j.calphad.2019.101688.
[204] E.K. Akopov, A.G. Bergman, Complex formation in a mutual system of chlorides and sulfates of lithium and potassium, Izv. Sekt. Fiz.-Khim. Anal., Inst. Obshch. Neorg. Khim., Akad. Nauk SSSR 25 (1954) 255–262.
[205] G.M. Unzhakov, Reciprocal system of potassium and lithium hydroxides and chlorides, Dokl. Akad. Nauk SSSR 87 (1952) 791–793.
[206] A. S. Basin, A. B. Kaplun, A. B. Meshalkin, N. F. Uvarov, The LiCl-KCl binary system, Russ. J. Inorg. Chem. 53 (2008) 1509–1511. https://doi.org/10.1134/S003602360809026X.
[207] R.P. Tye, J.G. Bourne, A.O. Destarlais, thermal energy storage material thermophysical property measurement and heat transfer impact, 1976.
[208] I.N. Belyaev, M.L. Sholokhovich, Reciprocal system of sodium and barium chlorides and carbonates, Sb. Statei Obshch. Khim. 1 (1953) 134–143.
[209] R.F. Rea, Temperature measuring cones, J. Am. Ceram. Soc. 21 (1938) 98–101. https://doi.org/10.1111/j.1151-2916.1938.tb15753.x.
[210] M.N. Zakhvalinskii, P.D. Belykh, Ternary systems formed by alkali metal carbonates, Zh. Neorg. Khim. 14 (1969) 2270–2272.
[211] R.J. Petri, E.T. Ong, T.D. Claar, High-temperature salt/ceramic heat storage phase-change media, Proc. Intersoc. Energy Convers. Eng. Conf. 18 (1983) 1769–1774.
[212] N. N. Volkov, T. F. Shvab, Ternary reciprocal system of lithium and potassium fluorides and carbonates, Izvest. Fiz.-Khim. Nauch.-Issledovatel. Inst. Irkutsk. Univ. 2 (1953) 55–59.
[213] S. Tamaru, M. Kamada, Fuel cells whose working temperature lies below 600°, M., Z. Elektrochem. 41 (1935) 93–96.
[214] N. Ren, Y. Wu, T. Wang, C. Ma, Experimental study on optimized composition of mixed carbonate for phase change thermal storage in solar thermal power plant, J. Therm. Anal. Calorim. 104 (2011) 1201–1208. https://doi.org/10.1007/s10973-011-1364-5.
[215] N.N. Volkov and A.G. Bergman, Constitution diagram of reciprocal systems of fluorides and carbonates, and of chlorides and carbonates of sodium and potassium, C. R. (Dokl.) Acad. Sci. URSS 35 (1942) 47–50.
[216] J. Qi, E. Yazhenskikh, M. Ziegner, X. Zhao, G. Wu, M. Müller, D. Sergeev, Experimental study and thermochemical assessment of the reciprocal system $Li^+$, $K^+$//$Cl^-$, $CO_3^{2-}$, Calphad 83 (2023) 102603. https://doi.org/10.1016/j.calphad.2023.102603.

# Appendix

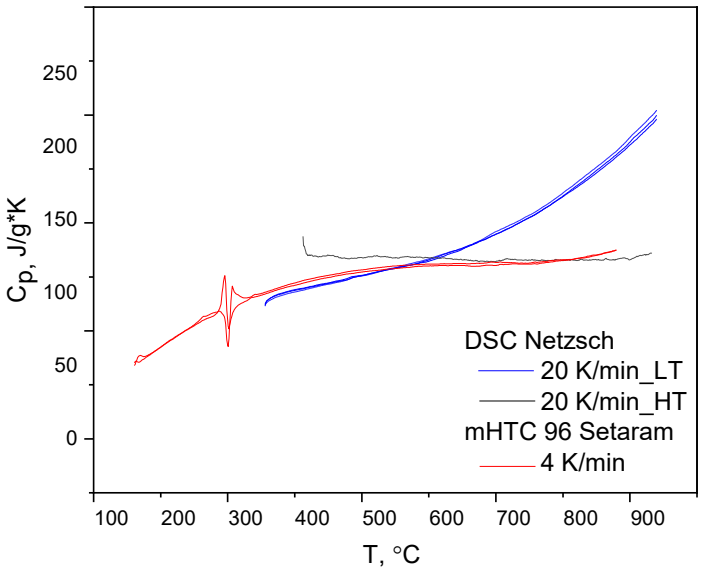


Figure A-1. Heat capacity of $Li_2CO_3$ measured with $Al_2O_3$ crucibles.

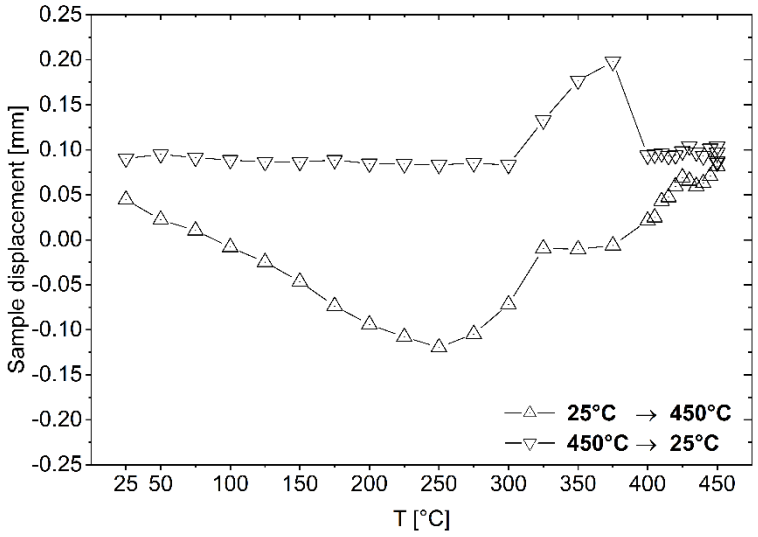


Figure A-2. Sample displacement during HTXRD measurement.

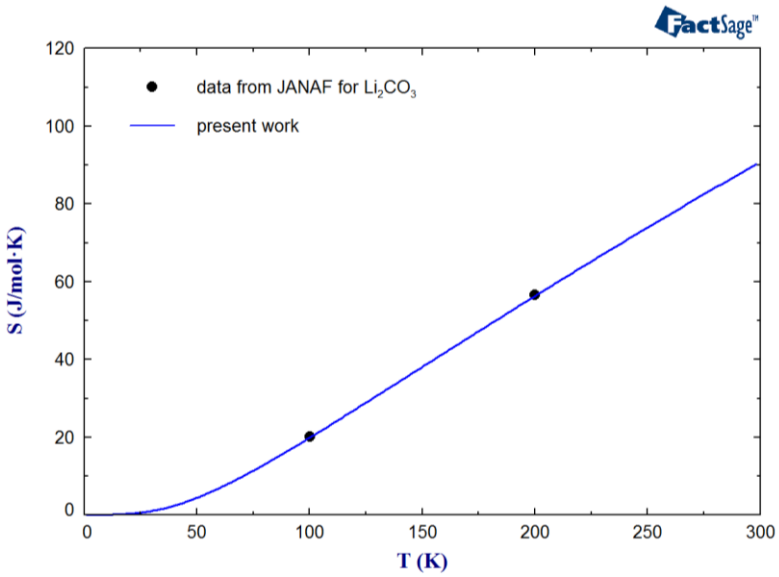


Figure A-3. Entropy for $Li_2CO_3$ at low temperatures.

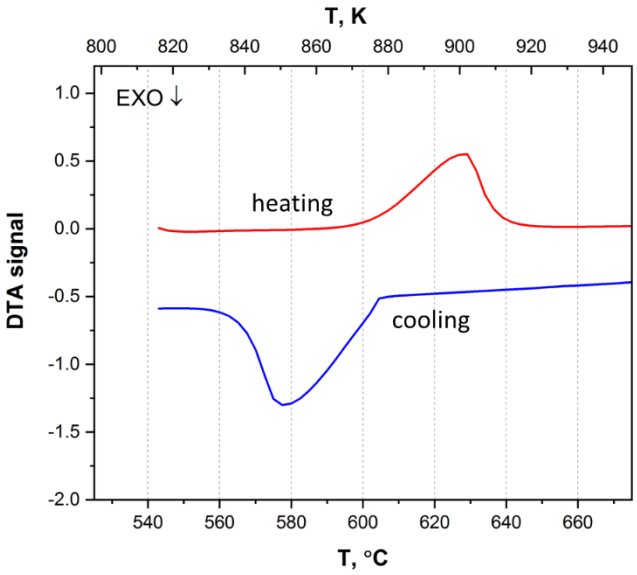


Figure A-4**.** Heating and cooling DTA curves of pure LiCl measured in this work.

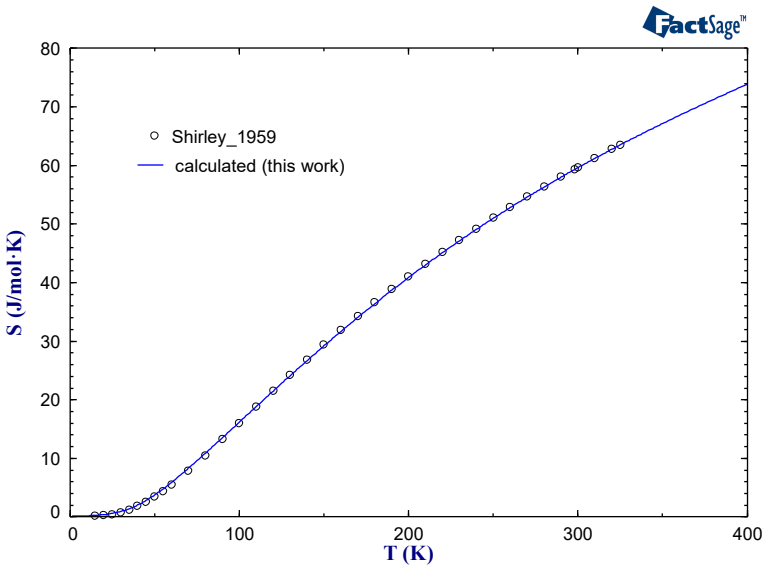


Figure A-5. Entropy of LiCl at low temperatures.

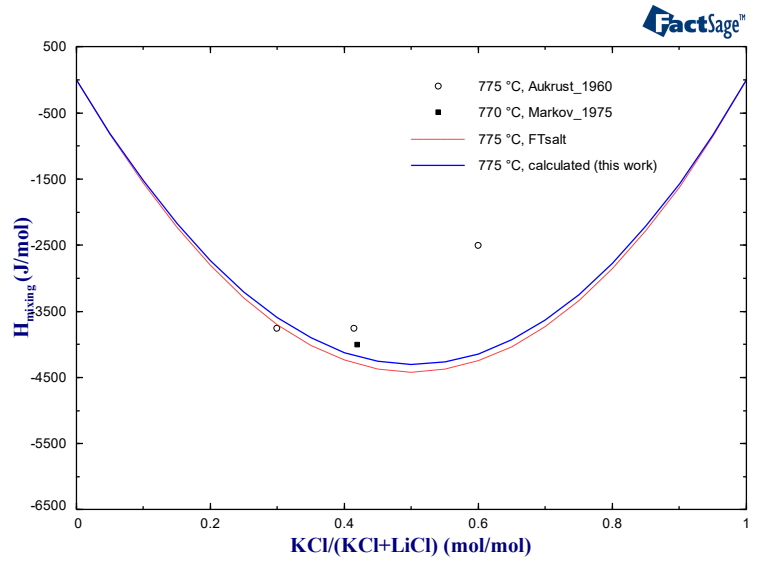


Figure A-6. Mixing enthalpy of the liquid phase in the LiCl-KCl system at 775 °C and 770 °C.

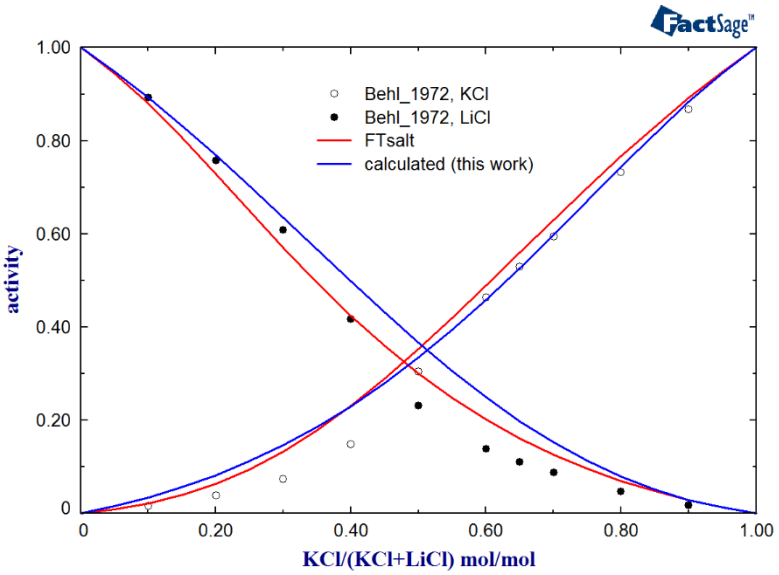


Figure A-7. Activity of LiCl and KCl in the liquid phase at 640 °C.

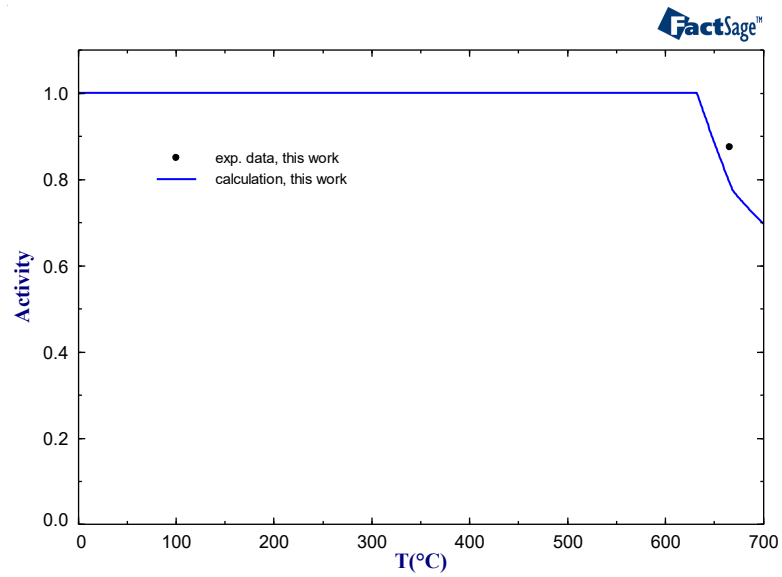


Figure A-8. Activity of NaCl in the solid phase at the composition 0.47NaCl-0.53$Na_2CO_3$.

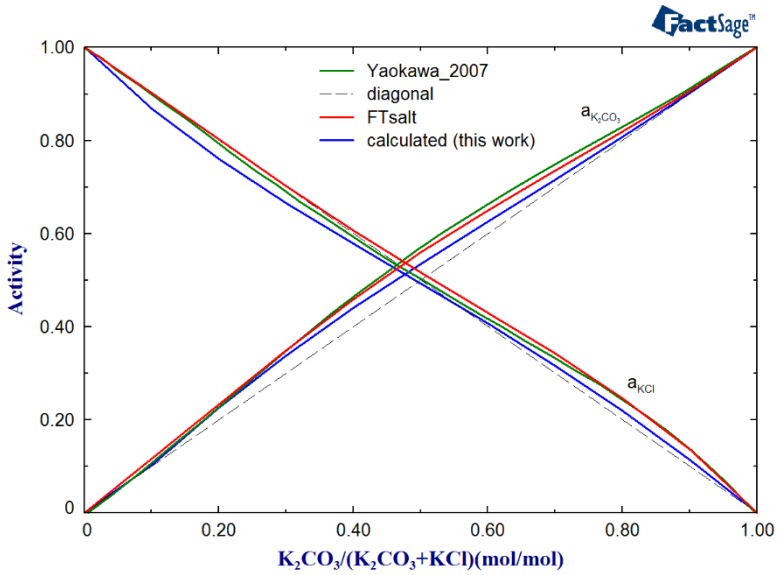


Figure A-9**.** Calculated activity of $K_2CO_3$ and KCl in the liquid phase at 950 °C in the KCl-$K_2CO_3$ system.

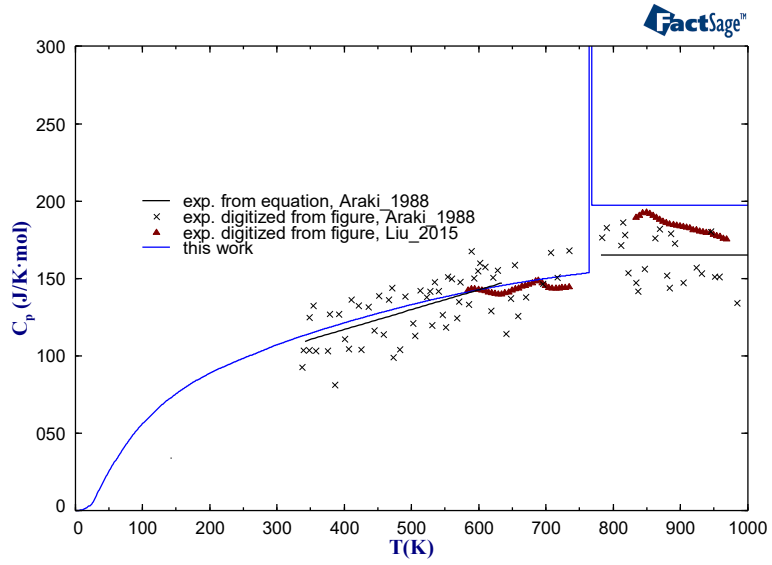


Figure A-10. Calculated temperature dependence of the heat capacity of 0.42$Li_2CO_3$-0.58$K_2CO_3$ compared with several studies (Liu et al. [92] and Araki et al. [93]).

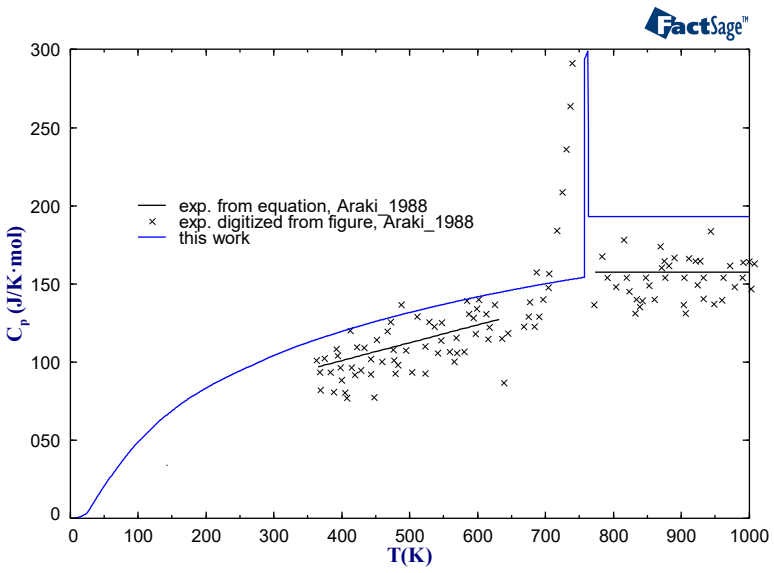


Figure A-11. Calculated temperature dependence of the heat capacity of $0.62Li_2CO_3$-$0.38K_2CO_3$ compared with data from Araki et al. [93].